

Nuclear Magnetic Resonance Measurements of
Proton Spin-Lattice Relaxation:

A Survey of Alkaloids
and
The Identification of Steric Effects on
Methyl Group Relaxation

Walter G. Chazin

A Thesis
in
The Department
of
Chemistry

Presented in Partial Fulfilment of the Requirements
for the degree of Doctor of Philosophy at
Concordia University
Montreal, Quebec, Canada

September 1983

© Walter J. Chazin, 1983

ABSTRACT

Nuclear Magnetic Resonance Measurements of
Proton Spin-Lattice Relaxation:

A Survey of Alkaloids
and
The Identification of Steric Effects on
Methyl Group Relaxation

Walter J. Chazin
Concordia University, 1983

The theory and experimental protocol whereby proton spin-lattice relaxation can be utilized for the determination of structure and stereochemistry of organic molecules are described. It is shown that for rigid, isotropically tumbling molecules, proton spin-lattice relaxation rate (R_1) and nuclear Overhauser effect (nOe) measurements can be interpreted using a relaxation pathway analysis approach. This method is based on the identification of the relative magnitudes of specific dipolar interactions between near neighbor protons and the determination of their relative contributions to the initial-slope R_1 . Interpretation of the experimental data is based on trends observed in several measurements, thereby compensating for inaccuracies associated with an analysis based on relaxation models, and experimental errors.

The methods for obtaining reliable $^1\text{H-R}_1$ and $^{-n\text{Oe}}$ data are presented, and important experimental constraints are discussed. Control experiments were carried out on a variety of organic molecules to determine the reliability, precision, and accuracy of the measurements, as well as to demonstrate several important experimental considerations.

A survey of proton spin-lattice relaxation in alkaloids is described, involving four cinchona, seven morphine, four tropane, and ten strychnos alkaloids. Using relaxation pathway analysis, the assignment of 400 MHz ^1H spectra and the determination of many features of the solution structures were possible. Previously reported ^1H chemical shifts and coupling constants for strychnine are shown to be in error. The proposed sites of substitution of three strychnine sulfonic acid derivatives, and their brucine analogues, have been verified, and the previously undetermined stereochemistry of one of them has been established.

^1H spin-lattice relaxation rates and $n\text{Oe}$ difference spectra have been measured at 400 MHz for six dimers derived from methyl-substituted 7-hydroxyindenes. Analysis of relaxation pathways has permitted assignment of all chemical shifts and identification of the relative stereochemistry at chiral centers. This analysis is consistent with the known stereochemistry of one of the compounds.

^1H spin-lattice relaxation rates have been measured at 400 MHz for a series of methyl-substituted planar aromatic compounds to determine the steric effect of adjacent substituents on the R_1 values of the methyl group. These values have been interpreted, on the basis of differences in the barriers to methyl group rotation caused by the substituent, resulting in differences in the contributions from the dipolar and spin-rotation mechanisms. ^{13}C - R_1 and $-\text{nOe}$ values have been measured at 20 MHz to aid in this analysis. A significant dynamic range of methyl ^1H - R_1 values has been observed, showing that these measurements were sensitive to the steric environment. Preliminary studies of ^1H methyl relaxation in non-planar aliphatic model systems are also reported.

DEDICATION

This thesis is dedicated to Christiane and Sara who have provided the warm home environment and daily support needed to complete such a large undertaking, and to all of my family for their spiritual support throughout the years.

ACKNOWLEDGEMENTS

I most gratefully appreciate the encouragement and guidance from Dr. L.D. Colebrook throughout the course of this research and the preparation of this thesis.

It would be impossible to thank all the individuals who have helped in the various aspects of preparing this thesis, however, I would like to personally thank the following:

Dr. A.A. Padmapriya and my wife Christiane Martel-Chazin for their ever ready guidance and assistance during the preparation of a variety of model compounds; Dr. S. Lokuge-Peiris for her assistance in learning the rudiments of experimental nmr and for time spent in discussing a variety of nmr problems; Dr. O.S. Tee for innumerable consultations and very helpful objective criticism; Dr. P.H. Bird for assistance in operation of the NRC programs to determine inter-nuclear distances from published X-ray data; Dr. Phan Viet Minh Tan for helpful discussion; Dr. R. Blair, F. Rogan, and The Centre for Research on Drug Dependence of Concordia University for collaborative studies. I would like to give special thanks to my colleague, Mr. Geoff Nesbitt, for helping to create, along with Dr. Colebrook and others, an exciting and intellectually stimulating environment for research, and for our discussions on a wide range of topics in, and related to, the nmr field.

I gratefully acknowledge the award of fellowships from the Quebec provincial government (Fonds F.C.A.C.), Canadian federal government (N.S.E.R.C.), and Concordia University.

TABLE OF CONTENTS

Chapter 1	INTRODUCTION.....	1
1.1	Organization of This Thesis.....	5
Chapter 2	THEORY.....	8
2.1.	Introduction.....	8
2.2.	Nuclear Magnetic Resonance.....	8
2.3.	A Phenomenological Description of Spin-lattice Relaxation.....	12
2.4.	General Formulation.....	17
2.4.1.	Self-relaxation.....	17
2.4.2.	Cross-relaxation.....	20
2.4.3.	Cross-correlation.....	23
2.4.4.	The Initial Slope Approximation.....	25
2.4.5.	Dipolar Spin-lattice Relaxation.....	27
2.5.	The Nuclear Overhauser Effect.....	34
2.6.	Relaxation Pathway Analysis.....	39
2.7.	Analysis of Anisotropic Overall Tumbling and Internal Motion by ^{13}C Relaxation Measurements.....	41
Chapter 3	SOME PRACTICAL CONSIDERATIONS IN MAKING ^1H - R_1 AND NOE DIFFERENCE MEASUREMENTS.....	48
3.1.	Introduction.....	48
3.2.	^1H - R_1 Experiments.....	49
3.2.1.	Procedure for Measuring R_1 Values.....	49
3.2.2.	^1H - R_1 Measurements in the Presence of Other Components.....	52
3.2.2.1.	Impurities/Minor Components.....	52
3.2.2.2.	The Presence of a Second Major Component in Solution.....	52
3.2.2.3.	^1H - R_1 Measurements in Non-degassed Solutions..	53
3.2.3.	Precision and Error.....	59
3.2.3.1.	Systematic Error- Long Term Spectrometer Instability.....	59
3.2.3.2.	Systematic Error- the Use of a Composite 180° Pulse.....	61
3.2.3.3.	Reproducibility and Precision.....	61
3.2.4.	Data Analysis.....	67
3.2.4.1.	The Use of Null-point Versus Regression Analysis.....	67
3.2.4.2.	Techniques of Regression Analysis.....	71
3.2.5.	Summary of ^1H - R_1 Discussion.....	74

3.3.	¹ H NOE Difference Experiments.....	75
3.3.1.	Procedure for Obtaining Qualitative NOE Difference Spectra.....	75
3.3.2.	Sensitivity Advantage of a Difference Spectrum.....	78
3.3.3.	Choice of Solvent.....	81
3.3.4.	Irradiation Time.....	81
3.3.5.	Saturation Efficiency Versus Selectivity.....	86
3.3.6.	Summary of ¹ H NOE Difference Experiments.....	90

Chapter 4 A SURVEY OF ¹H SPIN-LATTICE RELAXATION
IN ALKALOIDS.....91

4.1.	Introduction.....	91
4.2.	Calculation of Relaxation Parameters.....	92
4.3.	General Uses of ¹ H-R ₁ Values.....	94
4.4.	Cinchona Alkaloids.....	96
4.4.1.	Methoxy Group Conformational Preferences.....	104
4.4.2.	Other Structural Features.....	108
4.5.	Morphine Alkaloids.....	111
4.5.1.	A Preliminary Assignment of the 400-MHz ¹ H Spectrum of Morphine.....	114
4.5.2.	Refinement of Assignments and Structural Influences.....	116
4.5.3.	Conformational Preferences of Methoxy Groups.....	126
4.6.	Tropane Alkaloids.....	129
4.6.1.	Tropine.....	132
4.6.2.	Atropine.....	136
4.6.3.	Scopolamine.....	139
4.6.4.	Cocaine.....	147
4.7.	Conclusion.....	150

Chapter 5 APPLICATION OF ¹H SPIN-LATTICE RELAXATION
RATE MEASUREMENTS TO THE DETERMINATION OF
STRUCTURE AND STEREOCHEMISTRY OF SOME
STRYCHNOS ALKALOIDS.....151

5.1.	Introduction.....	151
5.2.	A Partial Reassignment of the ¹ H NMR Spectrum of Strychnine.....	153
5.3.	18-Oxostrychnine, 16-Hydroxystrychnine, and Brucine.....	167
5.4.	Strychnine Sulfonic Acids.....	173
5.4.1.	Strychnine Sulfonic Acid I.....	176
5.4.2.	Strychnine Sulfonic Acid II.....	178
5.4.3.	Strychnine Sulfonic Acid III.....	179
5.5.	Conclusion.....	183

Chapter 6	APPLICATION OF ^1H RELAXATION PATHWAY ANALYSIS TO THE DETERMINATION OF THE STRUCTURE AND STEREOCHEMISTRY OF SOME 7-HYDROXYINDENE DIMERS.....	184
6.1.	Introduction.....	184
6.2.	Results and Discussion.....	189
6.2.1.	Summary of ^1H -R ₁ Data.....	189
6.2.2.	Stereochemical Determinations.....	191
6.2.3.	Assignments in Aromatic Rings.....	199
6.3.	Conclusion.....	201
Chapter 7	STERIC EFFECTS ON SPIN-LATTICE RELAXATION OF METHYL GROUPS.....	202
7.1.	Introduction.....	202
7.2.	Methyl Group Relaxation in Substituted Aromatic Compounds.....	209
7.2.1.	Summary of Results.....	209
7.2.2.	Methyl Relaxation in Benzene Derivatives.....	217
7.2.3.	Verification of the Steric Effect in Methylanilines.....	221
7.2.4.	Methyl Relaxation in Other Aromatic Systems..	222
7.2.5.	Methyl Relaxation in Non-planar Aliphatic Systems.....	224
7.4.	Conclusion.....	233
Chapter 8	SUMMARY.....	235
Chapter 9	EXPERIMENTAL.....	241
9.1.	Materials.....	241
9.1.1.	Benzene Derivatives.....	241
9.1.2.	Preparation of 4-t-Butylcyclohexanes.....	244
9.1.3.	Preparation of 5-t-Butyl-1,3-dioxanes.....	247
9.1.4.	Alkaloids.....	248
9.2.	NMR Sample Preparation.....	249
9.3.	NMR Measurements.....	250
	REFERENCES.....	256

LIST OF FIGURES

Chapter 2

1	The Effect of Field Strength on the Difference in Energy Levels for a Spin 1/2 Nucleus.....	10
2	Motion of Spin 1/2 Nuclei in a Static Magnetic Field.....	10
3	The Variation of Spectral Density as a Function of Correlation Time.....	14
4	The Energy Level Diagram for a Spin 1/2 AX System.....	20
5	The Energy Level Diagram for a Spin 1/2 AMX System.....	20

Chapter 3

1	The Inversion-Recovery Pulse Sequence.....	51
2	Comparison of T_1 Values from Degassed and Non-degassed Solutions.....	55
3	Stack Plot of Inversion-Recovery Experiment.....	68
4	Increase in Efficiency of Data Acquisition Using the Modified Method to Obtain NOED Spectra.....	76
5	Sensitivity in Detection.....	79
6	Separation of Overlapped Resonances in NOED Spectra.....	80
7	Solvent Dependence of T_1	82
8	Solvent Dependence of NOE Acquisition Time.....	83
9	Solvent Dependence of Total Acquisition Time.....	83
10	NOE Dependence on Irradiation Time.....	85
11	Selectivity in Saturation.....	87
12	NOE Dependence on Decoupler Power.....	88
13	Incrementing Saturation Frequency and Power.....	89

Chapter 4

1	Evaluation of Relaxation Models.....	93
2	Separation of Overlapped Resonances in Partially Relaxed Spectra.....	94
3	The Structures of Cinchona Alkaloids.....	97
4	400 MHz ^1H NMR Spectrum of Quinine-HCl.....	98
5	Structures of Morphine Alkaloids.....	112
6	400 MHz ^1H NMR Spectrum of Codeine.....	113
7	Structures of Tropane Alkaloids.....	130
8	400 MHz ^1H NMR Spectrum of Cocaine.....	131
9	400 MHz ^1H NMR Spectrum of the Tropic Ester Moiety of Atropine.....	138

Chapter 5

1	400 MHz ¹ H NMR Spectrum of Strychnine.....	154
2	NOED Spectra to Determine the Assignments at C15 and C20.....	158
3	NOED Spectra to Determine the Assignments at C17 and C18, DMSO-d ₆	160
4	NOED Spectra to Determine the Assignments at C17 and C18, CDCl ₃	161
5	Assignment of the ABMX Spin System in Ring E of Strychnine, DMSO-d ₆	162
6	Assignment of the ABMX Spin System in Ring E of Strychnine, CDCl ₃	163
7	Determination of C20 Stereochemistry in SSA-III by NOED experiment.....	182

Chapter 6

1	Structures of 7-Hydroxyindene Dimers.....	185
2	400 MHz ¹ H NMR Spectrum of 7-Hydroxyindene Dimer 5.....	186
3	NOED Spectra to Determine Ring Fusion- Cis-Fused Dimers.....	193
4	NOED Spectra to Determine Ring Fusion- Trans-Fused Dimers.....	194
5	NOED Spectra to Determine C3 Stereochemistry..	195
6	NOED Spectra to Determine the C2' and C3' Stereochemistry- Trans-Fused Dimers.....	197
7	NOED Spectra to Determine the C2' and C3' Stereochemistry- Cis-Fused Dimers.....	198
8	NOED Spectra to Determine the Assignments in Aromatic Rings.....	200

Chapter 7

1	Structures of the Planar Aromatic Compounds...	210
2	Structures of the Non-planar Aliphatic Compounds.....	225
3	400 MHz ¹ H NMR Spectra of 2-t-Butyl-1,3-dioxanes.....	226
4	400 MHz ¹ H NMR Spectra of Cis- and Trans- 4-t-Butyl-1-methylcyclohexanol.....	227

Chapter 9

1	20 MHz ¹³ C NMR NOED Spectra of Methyl Carbons.....	254
---	---	-----

LIST OF TABLES

Chapter 3

1	Normalized R_1 Values Measured With and Without TMS.....	51
2	R_1 Values Measured in a Mixture and a Pure Solution.....	54
3	Comparison of ^1H - R_1 Values from Degassed Solutions to those Using the Proposed Correction Method.....	58
4	Control Experiment to Detect Long Term Instability.....	60
5	Comparison of R_1 Values Using Single and Composite 180° Pulses.....	62
6	Reproduceability- R_1 Values Determined by Linear Regression.....	64
7	Reproduceability- R_1 Values Determined by Null-Point Method.....	65
8	Comparison of R_1 Values Determined by Null-Point and Regression Analysis.....	70

Chapter 4

1	Chemical Shifts of Cinchona Alkaloids.....	100
2	^1H Spectral Parameters of Quinine-HCl.....	101
3	Normalized R_1 Values of Cinchona Alkaloids....	103
4	Selected R_1 Values for 2, 3, 4, and 5.....	105
5	NOE Enhancements of Cinchona Alkaloids.....	110
6	Chemical Shifts of Some Morphine Alkaloids....	115
7	Normalized R_1 Values of Morphine Alkaloids....	118
8	Comparison of Calculated and Observed R_1 Values in Morphine Alkaloids.....	119
9	NOE Enhancements in Morphine and Codeine.....	120
10	Complete Assignment of ^1H Spectral Parameters of Morphine-sulfate.....	122
11	Complete Assignment of ^1H Spectral Parameters of Codeine.....	123
12	Chemical Shifts of Some Tropane Alkaloids....	133
13	Normalized R_1 Values of Tropane Alkaloids....	134
14	Comparison of Calculated and Observed R_1 Values in Tropane.....	135
15	Nuclear Overhauser Effect Enhancements in Scopolamine.....	144

Chapter 5

- 1 NOE Enhancements Determined for Strychnine by the Difference Technique.....156
- 2 Revised ^1H Chemical Shifts and Coupling Constants for Strychnine.....166
- 3 Normalized R_1 Values of Strychnos Alkaloids...169
- 4 Normalized R_1 Values of the Strychnine Sulfonic Acids.....175

Chapter 6

- 1 7-Hydroxyindene Dimer ^1H Chemical Shifts.....188
- 2 7-Hydroxyindene Dimer ^1H - R_1 Values.....190
- 3 NOE Enhancements Providing Stereochemical Information.....192

Chapter 7

- 1 Normalized Methyl ^1H - R_1 Values-Substituted Aromatic Compounds.....212
- 2 ^{13}C - R_1 and -NOE Values of Substituted Aromatic Compounds.....213
- 3 Methyl Group Diffusion Constants and Rotational Barriers for Some Substituted Aromatic Compounds.....214
- 4 Normalized Methyl ^1H - R_1 Values in Conformationally Biased Cyclohexanes and 1,3-Dioxanes.....230
- 5 Normalized ^{13}C - R_1 and -NOE Values of Some 1,3-Dioxanes.....232

Chapter 9

- 1 Physical Properties of Methyl-anisoles and thioanisoles.....242
- 2 Physical Properties of t-Butylcyclohexane Derivatives.....246
- 3 Chemical Shifts for Methyl-Substituted 2-t-Butyl-1,3-dioxanes.....247

Chapter 1

INTRODUCTION

In the past ten years, nuclear magnetic resonance spectroscopy (nmr) has become one of the most powerful techniques available to the practising chemist for structural analysis of molecules. Though diffraction methods (X-ray, neutron, electron) are by far the most common methods for determining the absolute structure of a molecule, such measurements can only be carried out on crystalline material. For systems whose properties are of interest as liquids, gasses, or in solution, there remains a critical question; does the molecule retain its crystal structure? The only method available today for quantitative determination of molecular geometry of a liquid, or solute molecule in a liquid medium, is the nmr measurement of dipolar spin-lattice relaxation. The theory of dipolar spin-lattice relaxation will be presented in this thesis in a thorough and illustrative manner to facilitate a clear comprehension of the utility of the proton spin-lattice relaxation measurement.

In 1968, Vold and coworkers¹ reported on the development of a convenient method to measure spin-lattice relaxation rates (R_1 values) using a pulse Fourier transform method, but it was not until some years later that the utility of proton measurements became apparent. The major obstacle to the utilization of ^1H - R_1 measurements was the uncertainty concerning R_1 values in complex coupled systems, where the

effects of cross-relaxation and cross-correlation were presumed to be quite extensive. Finally, in 1970, Freeman, Wittekoek, and Ernst,² proposed and demonstrated that by using an "initial-slope" approximation, it was possible to define an effective R_1 for each proton in a loosely coupled spin system. The first real experimental breakthrough for the use of ^1H dipolar relaxation for structural analysis came at about the same time, when Burton, Grant, and Hall³ found that ^1H - R_1 values of a number of cis- and trans-alkenes could be correlated to their structures. In the laboratory of Dr. L.D. Hall at the University of British Columbia, proton relaxation studies were then extended to a number of complex sugar molecules.⁴ By 1976 it became apparent that ^1H - R_1 values could be utilized for the determination of structure and stereochemistry in any organic molecule. This, along with the development of the nuclear overhauser effect⁵ difference (NOED) experiment,⁶ marked the beginning of widespread use of ^1H relaxation parameters.

The theories of spin-lattice relaxation proposed by Bloembergen, Purcell, and Pound⁷, and Solomon⁸ were formulated long before any experimental methods were available to measure relaxation parameters, yet they remain today as the most useful approach for analysis of experimental parameters. Consideration of a simplified form of the relaxation rate expression for a nucleus, i , interacting in a dipolar sense with some other nucleus, j , reveals the R_1 dependence on molecular geometry:

$$(1) R_{1i} = K * t_{cij} * r_{ij}^{-6}$$

K is a series of constants, t_{cij} reflects the time scale of motion of the ij vector, and r_{ij} is the inter-nuclear distance. Clearly, if t_{cij} can be measured or approximated by an appropriate modelling scheme, the r_{ij} term can be evaluated to give the molecular geometry. If nucleus i relaxes to a number of other nuclei, the observed rate is the pairwise sum of all these interactions:

$$(2) R_{1i} = \sum_{j \neq i} R_{1ij}$$

Identification of all pairwise terms would then give a series of internuclear distances which can be correlated to provide the desired information about the geometry of the molecule. The high nmr sensitivity, high dipolar efficiency, and the great abundance of protons in organic molecules are compelling reasons for selection of this nucleus for relaxation studies; data can be obtained efficiently from all parts of the molecule.

A very important feature of proton relaxation analysis is that the dipolar relaxation interactions are mutual, eg. if proton A relaxes proton B, proton B must relax proton A. For any particular proton A, there are usually several relaxation pathways (dipolar interactions) that mediate the relaxation of A, and each of these can be evaluated to determine A's relative position. The analysis can then be

4

verified by examination of the same relaxation pathways in the opposite direction, observing relaxation contributions from A to the protons which relax A. Working in this manner, it is not necessary to rely on a single measurement for the structural analysis, hence, the reliability of the method is considerably improved. The flexibility of being able to corroborate results in either direction proves to be extremely advantageous with respect to the qualitative determination of molecular geometry, since non-quantitative experiments (eg. no time-consuming, special sample preparation) can, therefore, be utilized to rapidly determine a variety of structural features.

The potential of $^1\text{H-R}_1$ values for providing structural information has been investigated on a wide variety of molecules and reviewed in Ref. 9. Interestingly, besides the extensive amount of work in Hall's laboratory on carbohydrates, there has been only one systematic survey of $^1\text{H-R}_1$ values, that reported by Colebrook and Hall,¹⁰ on steroids. Studies of this nature are important, since the capabilities of the dipolar relaxation technique must be fully explored. A set of clearly established guidelines for interpretation must be developed, now that these experiments can be carried out in a routine manner.¹¹ Studies on natural products that originated at U.B.C. were extended by some of the research described in this thesis, in particular, the survey of $^1\text{H-R}_1$ values in alkaloids.

A survey of the literature shows that most relaxation studies have involved the analysis of ^1H - or ^{13}C - R_1 values of methine or methylene groups, whereas methyl rates have been only rarely utilized. The principal reason for this omission is that methyl relaxation is complicated by the internal methyl rotation which is superimposed on the overall tumbling of the molecule. Methyl group ^1H - R_1 values were studied in a series of model compounds to determine the dynamic range of methyl R_1 's, and to develop a basis for interpretation of these values, under normal operating conditions. The models chosen were substituted toluenes, to evaluate steric effects from the adjacent position, and conformationally-biased cyclohexanes and 1,3-dioxane analogues, to evaluate steric effects from the geminal position. A significant effect from 1,3-diaxial interactions has been previously characterized in studies by this laboratory.¹⁰

1.1. Organization of This Thesis

The relevant theory required for the relaxation analyses described in this thesis is summarized in Chapter 2. The phenomena of nmr and spin-lattice relaxation are described in an illustrative manner. Expressions for the time development of observable bulk magnetization of the isolated, AX, and AMX systems during a relaxation experiment are presented, along with a generalization to complex first order systems.

Cross-relaxation and cross-correlation terms are identified and differentiated. Explicit expressions for the dipolar relaxation of nuclei are then given, and the technique of relaxation pathway analysis as applied to the qualitative determination of molecular structure and stereochemistry is introduced. Finally, the appropriate expressions for R_1 analysis in molecules with anisotropic overall tumbling and or internal motion (eg. methyl rotation) is presented.

In Chapter 3, simple descriptions of the standard inversion-recovery R_1 , and nuclear Overhauser effect difference (nOed) experiments are given, followed by a discussion of many of the important experimental constraints. A number of control experiments are presented, establishing the reliability, precision, and relative error in the ^1H - R_1 measurements, and denoting the most important factors affecting the acquisition of qualitative multi-frequency nOed experiments.

The application of spin-lattice relaxation rate analysis to the determination of various aspects of molecular structure in alkaloids is described in Chapters 4 and 5. The survey study of cinchona, morphine, and tropane alkaloids is given in Chapter 4. This chapter contains short sections demonstrating the characteristic features of R_1 analysis, including methods for determining molecular structure by the relaxation pathway analysis technique. The application of

$^1\text{H-R}_1$ relaxation pathway analysis to the determination of structure and stereochemistry in some strychnine derivatives is described in Chapter 5. A partial reassignment of the ^1H spectrum of strychnine was made during these studies, and is also presented in Chapter 5.

The application of detailed relaxation pathway analysis, through the use of $^1\text{H-R}_1$ and nOed experiments, to the complete assignment of chemical shift, methylene proton stereochemistry, and stereochemistry at all chiral centers in six 7-hydroxyindene dimers, is presented in Chapter 6. These studies demonstrate the great power of the relaxation pathway analysis technique for the analysis of molecular structure of organic molecules.

Experiments carried out for study of methyl group relaxation are described in Chapter 7. An introduction to the difficulties involved in methyl $^1\text{H-R}_1$ analysis is followed by a discussion of the experimental protocol established for these studies. To ensure that unambiguous analysis of $^1\text{H-R}_1$ values had been made, several types of corroborative experiments- $^{13}\text{C-R}_1$, $^{13}\text{C}\{-^1\text{H}\}$ nOe, and $^1\text{H}\{-^1\text{H}\}$ nOe measurements were necessary. Calculation of the methyl rotational barriers using $^{13}\text{C-R}_1$ data and various forms of the Woessner model (described in Ref. 12) were also carried out, to provide pertinent information for the unequivocal analysis of steric factors, and are briefly described.

In Chapter 8, the research carried out for this thesis is critically summarized and future prospects are assessed.

Chapter 2

THEORY

2.1. Introduction

In this chapter, a summary of relevant spin-lattice relaxation theory will be presented. The intention here is to develop a thorough theoretical background, while presenting the material in terms that can be easily understood by the practising chemist. The accent will be placed on developing a physical understanding of the dipolar spin-lattice relaxation process in an illustrative manner, so that it is clear in what way dipolar relaxation parameters are utilized to determine structural features in organic molecules.

2.2. Nuclear Magnetic Resonance

All nuclei that possess the property of spin have a nuclear magnetic moment, proportional to the magnitude of the spin, which gives rise to observable magnetic properties. Spin is denoted by the nuclear spin angular momentum, I , and is quantized. The nuclear spin states, m_I , define the energy levels in the system, and can only take values which are $I, (I-1), \dots, -I$. For example, the proton has $I = 1/2$ and m_I values of $+1/2$ and $-1/2$.

In the presence of a static magnetic field, H_0 , the nuclear magnetic moment and field interact, causing the nuclear moment to precess about the direction of H_0 (by definition, the +z direction). The frequency of this precession, characteristic of each nucleus, is known as the Larmor frequency, w_0 , and is proportional to the strength of H_0 .*

$$(1) w_0 = \frac{\gamma_n}{2\pi} H_0$$

γ_n , the gyro-magnetic ratio, is the factor which characterizes the efficiency of the interaction between nucleus and a magnetic field. In addition to causing precession, H_0 has the effect of removing the degeneracy of the spin states. For a spin 1/2 nucleus, the energy difference between the two spin states, ΔE , is given by:

$$(2) \Delta E = \gamma_n (h/2\pi) H_0$$

where $h/2\pi$ is Planck's constant. The effect of the magnitude of H_0 on ΔE is shown in Fig. 2.1. The two spin states can be visualized as nuclei that precess either parallel ($m_I = 1/2$, α state) or anti-parallel ($m_I = -1/2$, β state) to the direction of H_0 (Fig. 2.2). In such a system, there is a resonance phenomenon possible; by supplying energy at the frequency corresponding to $\Delta E(w_0)$, transitions can be induced from one state to the other.

* The proper terminology is the magnetic inductance, B_0 , but H_0 is used here for historical reasons.

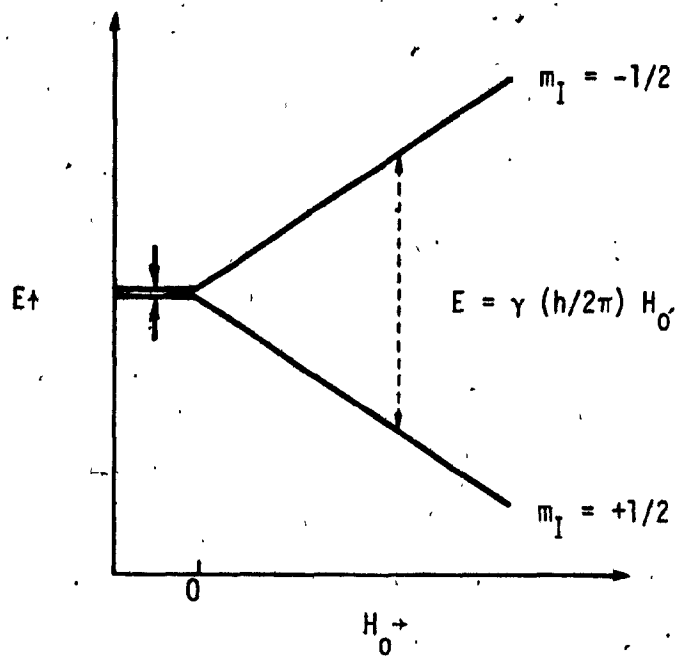


Fig. 2.1 The effect of field strength on the difference in energy levels for a spin 1/2 system.

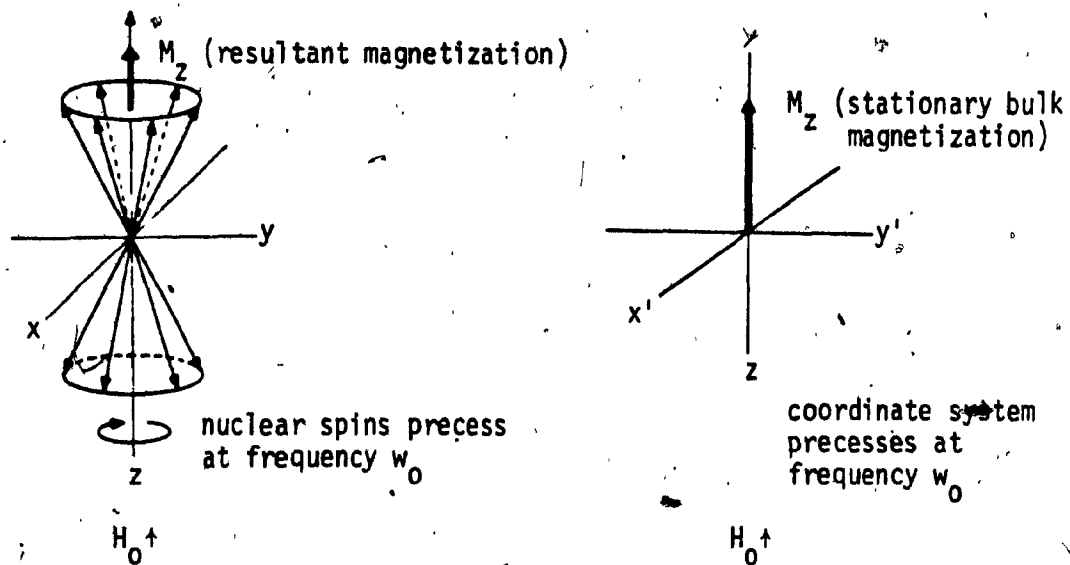


Fig. 2.2 Motion of spin 1/2 nuclei in a static magnetic field, H_0 .

Consider an ensemble of N non-interacting, spin $1/2$ nuclei in the presence of a static magnetic field, H_0 .

At equilibrium, the thermal energy in the system causes a Boltzmann distribution of spins into the α and β states:

$$(3) \frac{N_b}{N_a} = e^{-\Delta E/KT} \quad N_a + N_b = N$$

where N_a and N_b are the number of spins in the α and β states, respectively, k is the Boltzmann constant, and T is temperature.

At equilibrium, there is an excess of spins in the α state determined by the temperature and the strength of H_0 . Since the precession of the ensemble of spins is randomly phased and more spins precess in the $+z$ direction, there is a net magnetization only in the $+z$ direction; all x and y components cancel in the ensemble average at equilibrium. The bulk magnetization of the system in the H_0 field can, therefore, be represented by a vector, M_z , along the z axis (Fig. 2.2).

By supplying energy of frequency ω_0 to the system, transitions are induced. Due to the excess of α spins, the addition of energy will tend to equalize the α and β populations, giving a net absorption of energy. When the input of energy is stopped, the system will return to equilibrium by giving up this excess energy. At frequencies common to NMR, spontaneous emission is a very inefficient mechanism, energy is most often transferred to the environment (lattice) by a process known as spin-lattice relaxation.

2.3. A Phenomenological Description of Spin-lattice Relaxation

Spin-lattice relaxation is the exchange of energy between the nuclear spin and the surrounding environment. These interactions are caused by time-dependent magnetic or electric fields, $H_{loc}(t)$, which occur at the site of the nucleus. The time dependence of such fields results from random thermal motions which are present in any form of matter. For an efficient interaction to occur, the time-scale of the two interacting fields must be the same. Interactions which fluctuate either much faster or slower than the ω_0 frequency (on the order of 10^8 Hz) will not be effective in relaxing the nucleus. The most important motions for relaxation in liquids are overall molecular rotation and diffusion, and chemical exchange processes that occur on the order of 10^8 s⁻¹. These motions can be described by a Brownian model which is, in turn, applied to spin-lattice relaxation theory.

Using the Brownian motion model, three characteristics of the small, local time dependent fields, H_{loc} , can be identified:

1. The average value over time is zero.

$$\langle H_{loc}(t) \rangle = 0$$
2. The mean value of the square is non-zero.

$$\langle H_{loc}(t)^2 \rangle \neq 0$$
3. There is a characteristic average time, $t+T$, after which the value of H_{loc} is completely independent of the past value.

$$\langle H_{loc}(t) * H_{loc}(t+T) \rangle = 0$$

Note that for liquids, the value of $\langle H_{loc}(t) * H_{loc}(t+T) \rangle$ is independent of the time variable t , since t represents the experimental time scale (on the order of s) and T in liquids is on the order of 10^{-11} s. The description of the persistence of H_{loc} in a liquid is given by an auto-correlation function, $G(T)$:

$$(4) G(T) = \langle H_{loc}^2 \rangle e^{-T/t_c}$$

where T is the length of the time period, and t_c is the characteristic correlation time required for H_{loc} to lose memory of its past value.

To apply the motional model to relaxation expressions, it is necessary to transform the time-domain correlation function to the frequency domain. The resultant "spectral density" function, $J(\omega)$, gives the magnitude and frequency dependence of H_{loc} :

$$(5) J(\omega) = \langle H_{loc}^2 \rangle \frac{2t_c}{1 + \omega^2 t_c^2}$$

It is clear that the maximum value of $J(\omega)$ occurs when $\omega = 0$, that $J(\omega)$ remains constant as long as $1/t_c \ll \omega$, and that $J(\omega)$ falls off as $\omega \rightarrow 1/t_c$. These features are demonstrated in Fig. 2.3 which shows the variation of $J(\omega)$ as a function of frequency for three different values of t_c . In this diagram, note that the largest value of $J(\omega)$ at a particular frequency, ω_0 , occurs for the $1/t_c$ value closest to ω_0 , i.e. that motions on the time-scale of ω_0 are most efficient

for relaxation of ω_0 resonances. $J(\omega)$ is considerably smaller for $1/t_c$ either larger or smaller than ω_0 .

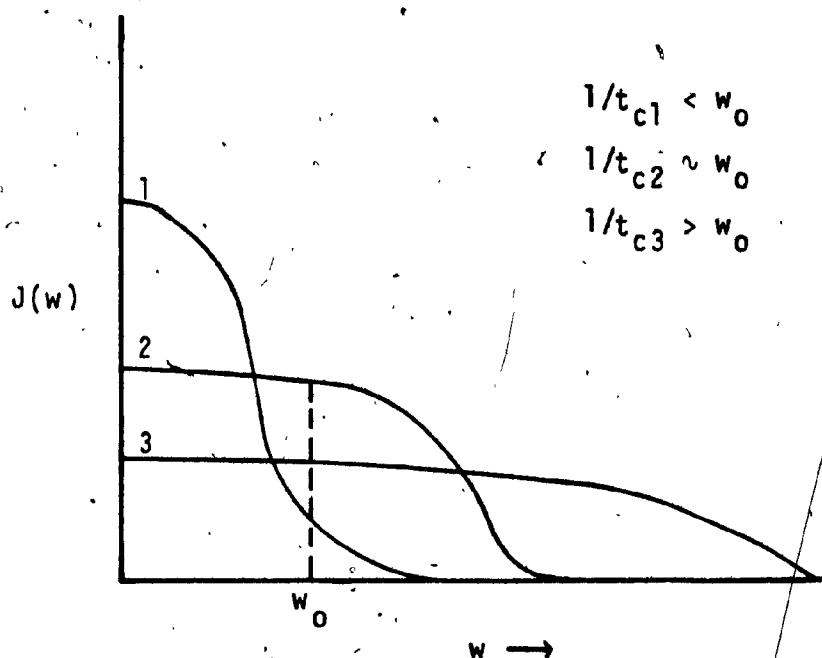


Fig. 2.3 The variation in spectral density as a function of correlation time.

The flat portions of the spectral density functions correspond to regions where $\omega_0^2 t_c^2 \ll 1$, which is called the extreme narrowing limit.¹³ In this region, the value of $J(\omega)$ will be independent of the strength of the magnetic field, so $J(\omega)$ is directly dependent on t_c :

$$(6) J(\omega) = \langle H_{loc}^2 \rangle t_c$$

Clearly, interpretation of relaxation measurements is simpler for molecules tumbling within the extreme narrowing limit.

The maximum size of a molecule which tumbles within these limits varies according to the strength of the magnetic field. At fields in common use today (1.4-11.7 T), most molecules of m.w. < 1000 d can be assumed to tumble in the extreme narrowing region. All experiments described herein have been carried out on molecules of approximately 500 d or less, so all further discussion will assume extreme narrowing conditions.

It is pertinent to consider the origin of the spin-lattice interactions in greater detail. Nuclei interact in a dipolar sense with local fields created by other magnetic nuclei or unpaired electrons. The efficiency of such interactions depends on the gyro-magnetic ratio, γ , of the interacting species. Since the γ value of an electron is 653 times greater than the γ value of ^1H , the strongest interacting nucleus, when paramagnetic species are present in any appreciable amounts, interactions of this nature dominate over the dipolar interactions between nuclei. If the nuclear interactions are of primary interest, great care must be taken in removing all paramagnetic species from the solution. The most common paramagnetic impurity is oxygen gas absorbed from the atmosphere, which must be removed by degassing the solution. The problem of the paramagnetic oxygen contribution to relaxation will be discussed in greater detail in Chapter 3.

In addition to dipolar interactions, there are several additional processes which may give rise to spin-lattice relaxation. For nuclei with a spin greater than $1/2$, interaction between nuclear moments and the quadrupole moment can often give rise to very efficient relaxation. This interaction can affect the relaxation of the quadrupolar nucleus itself, and other magnetic nuclei in reasonably close contact. Another relaxation mechanism results from changes in chemical shielding, that arise for certain nuclei, as the molecule tumbles. A fourth process which can give rise to relaxation of a nucleus occurs by a mechanism known as spin-rotation. It arises under circumstances whereby rapid rotation along a single axis in a molecule generates a local time dependent field at specific nuclei. The rapid rotation of a methyl group (relative to the overall rate of tumbling in the molecule) is an example of a spin-system where spin-rotation interactions may be important. This subject will be returned to in Chapter 7.

When proper care is taken in sample preparation, the spin-lattice relaxation of both ^1H and ^{13}C nuclei is dominated by dipolar interactions with nearby protons in the molecule. This fact can be utilized to great advantage for the analysis of structure and motion of organic molecules, as will be demonstrated further on in this thesis. The appropriate theory needed to interpret ^1H spin-lattice relaxation in terms of the dipolar mechanism, will be presented in the next few sections.

2.4. General Formulation

2.4.1 Self-relaxation

Let us return to the previously described isolated spin 1/2 system of N spins. When the system has been perturbed, it interacts with the lattice, which is a reservoir in thermal equilibrium. The rate of change of N_a can, therefore, be given by:

$$(7) \quad \frac{d N_a}{dt} = N_b W_{ba} - N_a W_{ab}$$

where W_{ab} and W_{ba} are the probabilities for transition from the α to the β state. By evaluating (7) at equilibrium and recalling (3), the relationship between the W 's and Boltzmann's law is apparent:

$$(8) \quad \text{when } \frac{d N_a}{dt} = 0, \quad \frac{N_b(0)}{N_a(0)} = \frac{W_{ab}}{W_{ba}} = e^{-\Delta E/kT}$$

Expressing N_a and N_b in terms of their sum, $N = N_t = N_a + N_b$ and their difference, $n = N_a - N_b$, the following expressions can be derived:

$$(9a) \quad \frac{dn}{dt} = -n (W_{ba} + W_{ab}) + N (W_{ba} - W_{ab})$$

$$(9b) \quad \frac{dn}{dt} = -(n - n_0) R_1$$

where n_0 is the population difference at equilibrium, and $R_1 = (W_{ab} + W_{ba})$ is the spin-lattice/relaxation rate.

By taking a macroscopic view of the system, one can translate these equations to expressions in terms of the measurable quantity, the bulk magnetic moment of the ensemble, M_z . M_z is given as the difference in population of the α and β states:

$$(10) M_z = N_a - N_b$$

The rate, R_1 , at which the system returns to equilibrium is given by:

$$(11) \frac{d M_z}{dt} = -(M_z - M_z(0)) R_1$$

$M_z(0)$ is the value of M_z at equilibrium (in the presence of H_0). The interactions of the isolated spin 1/2 system are solely influenced by the lattice, thus the R_1 value consists strictly of a term, ρ , known as the self-relaxation term:

$$(12) R_1 = \rho$$

Under non-equilibrium conditions, there are net values of M_x and M_y . The time-dependence of these components is characterized by a different relaxation rate, R_2 , since this "transverse" relaxation depends on different processes (spin-spin relaxation) in the system:

$$(13) \quad \frac{d M_x}{dt} = -M_x R_2 \qquad \frac{d M_y}{dt} = -M_y R_2$$

These expressions are given for completeness' sake, but are not necessary for the derivations of spin-lattice relaxation.

Differential equation (11) must be expanded to a form of the relationship between M_z and R_1 which can be utilized in carrying out R_1 measurements. Upon integration of (11) over time, t :

$$(14) \quad M_z(t) - M_z(0) = K e^{-tR_1}$$

The value of K is determined by the manner in which the magnetization is initially perturbed. In this form, the relaxation of the isolated nucleus is characterized by a single exponential recovery which can be determined from a plot of residual magnetization at various times, t , after the nuclei have been perturbed.

2.4.2. Cross-relaxation

In a system with more than just a single spin, the self-relaxation term is not sufficient to fully describe relaxation, since interactions between two or more spins within the system can occur. The energy diagram for a loosely coupled two-spin (AX) spin 1/2 system is shown in Fig. 2.4. The energy levels are labelled with α and β to denote the spin-state of the A and X nuclei. Transition probabilities, W_i , indicate the probability of a transition occurring between two connected states, i giving the change

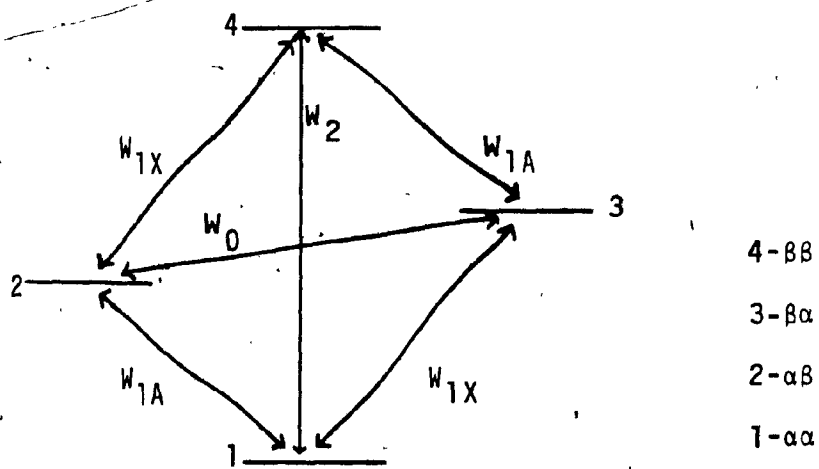


Fig. 2.4 The energy level diagram for a spin 1/2 AX spin system. Transition probabilities are indicated by W .

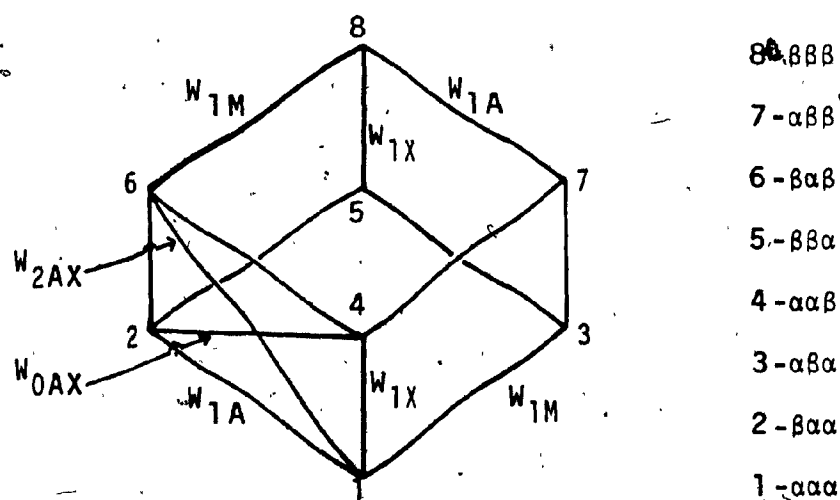


Fig. 2.5 The energy level diagram for an AMX system. Only one set of AX zero- and double-quantum transitions are shown.

in total spin during the transition. W_{1a} and W_{1x} are the allowed single quantum transitions of the A and X nuclei, respectively, which are detected in the nmr experiment.

Once the spin-states have been perturbed, spin-lattice relaxation will occur along all of the pathways shown in Fig. 2.4. In this system, there are significant probabilities not only for the standard single quantum transitions, W_{1a} and W_{1x} , but also for the zero quantum and double quantum transitions, W_0 and W_2 . Though forbidden by normal radiative selection rules, there are several non-radiative methods whereby these transitions can occur. The extremely high probability for the W_2 transition gives rise to the nuclear Overhauser effect (nOe)⁵, which will be described in more detail in section 2.5.

Analogous to the isolated spin 1/2 system, the total magnetization for each spin, M_{zi} , is given in terms of the population difference of the appropriate α and β states, for each spin. In the AX system there are two degenerate W_{1i} transitions which give rise to this magnetization. The relaxation of each spin is proportional to the perturbation of the magnetization, $M_{zi} - M_{zi}(0)$, where $M_{zi}(0)$ denotes the equilibrium magnetization, and the efficiency of the various pathways for relaxation shown in the energy diagram. The pathways available to spin A for relaxation from the β to the α state are $2W_{1a} + W_2 + W_0$ (see Fig. 2.4), with a corresponding expression for spin X. In addition, for W_2 and W_0 there is a mutual effect on the other spin so that the complete expression for relaxation of spin A is:

$$(15) \frac{dM_{za}}{dt} = -(2W_{1a} + W_2 + W_0)(M_{za} - M_{za}(0)) - (W_2 - W_0)(M_{zx} - M_{zx}(0))$$

The relaxation of A is clearly coupled to the perturbation of X, hence the formal expression for the AX system is a set of coupled differential equations:

$$(16) \frac{d}{dt} \begin{pmatrix} M_{za} \\ M_{zx} \end{pmatrix} = - \begin{pmatrix} \rho_a & \sigma \\ \sigma & \rho_x \end{pmatrix} \begin{pmatrix} M_{za} - M_{za}(0) \\ M_{zx} - M_{zx}(0) \end{pmatrix}$$

$$(17) \rho_a = 2W_{1a} + W_2 + W_0 \quad \rho_x = 2W_{1x} + W_2 + W_0 \\ \sigma_{ax} = \sigma_{xa} = \sigma = W_2 - W_0$$

Under conditions which will be specified below, the initial slope approximation can be invoked, and the set of differential equations uncouples. The measured relaxation rate for the AX system can then be expressed as the sum of the self-relaxation term, ρ_i , and the term representing the interaction between the two nuclei, σ , the cross-relaxation term:

$$(18) R_{1a} = \rho_a + \sigma \quad R_{1x} = \rho_x + \sigma$$

The efficiency of cross-relaxation is dependent on the type of mechanism that is operative. For two spins that are completely non-interactive, ie. they relax completely independently, the cross-relaxation term drops out, and only the self-relaxation terms are important. As it turns out, all mechanisms except the scalar and dipolar mechanisms cause efficient non-interactive relaxation, thus the presence of

cross-relaxation can be used to characterize the type of relaxation mechanism that is operative. For protons, the scalar mechanism is rarely significant, so cross-relaxation identifies the presence of the dipolar mechanism.

2.4.3. Cross-correlation

In addition to the cross-relaxation terms introduced in the preceding section, in any complex multi-spin system it is also necessary to account for any second order interactions between the various nuclei. Such effects would be expected to be important in systems where the various nuclei are coupled to each other. This type of interaction will be described in the simplest system, the loosely-coupled three-spin (AMX) system.

In the AMX system, there are eight energy levels and twenty-four possible transitions between these levels, as shown in Fig. 2.5. The energy levels and transition probabilities are labelled in the same manner as for the AX system. By analogy to the AX system, the time dependence of magnetization in the AMX system can be expressed in terms of population differences, related to the observable magnetization, and formulated as:

$$(19) \quad \frac{d}{dt} \begin{vmatrix} M_{za} \\ M_{zm} \\ M_{zx} \end{vmatrix} = \begin{vmatrix} \rho_a & \sigma_{am} & \sigma_{ax} \\ \sigma_{am} & \rho_m & \sigma_{mx} \\ \sigma_{ax} & \sigma_{mx} & \rho_x \end{vmatrix} \begin{vmatrix} M_{za} - M_{za}(0) \\ M_{zm} - M_{zm}(0) \\ M_{zx} - M_{zx}(0) \end{vmatrix}$$

$$(20) \quad \rho_a = W_1 + W_1' + (W_{2am} + W_{0am}) + (W_{2ax} + W_{0ax})$$

$$\sigma_{am} = W_{2am} - W_{0am} \quad \sigma_{ax} = W_{2ax} - W_{0ax}$$

The other ρ_i and σ_{ij} terms are given by permutation of subscripts. The ρ_i and σ_{ij} are the corresponding terms for self-relaxation and cross-relaxation that have been described for the AX system. Note that there are separate, pair-wise cross-relaxation terms to represent the interaction between each pair of nuclei, and that $\sigma_{ij} = \sigma_{ji}$.

Recall that relaxation depends on the random motions of the vectors between the nuclear moment and whatever local field is causing the relaxation. In a system where the relaxation of the nuclei is coupled (as identified by the presence of cross-relaxation), the vectors between different pairs of nuclei may not diffuse independently. Consider a $^1\text{H}_A-^{13}\text{C}_M-^1\text{H}_X$ methylene group. Relaxation of the ^{13}C nucleus occurs to the two ^1H nuclei, but because the protons are both bonded to the same C atom, their motions are correlated. The relaxation vectors always have a specific spatial relationship to one another, hence their relative motions are not random. These two relaxation vectors can, therefore, interact with each other, so the relaxation expressions given in (19) can not uncouple.

In all tightly spin-spin coupled systems, the effects of cross-correlation are always significant, so it is not possible to give a discrete expression for the relaxation of a particular nucleus. One very obvious sign of the presence of cross-correlation is that the various peaks of a multiplet will relax at significantly different rates, which can be observed in a partially relaxed spectrum.

Fortunately, it has been demonstrated that the effects of cross-correlations are negligible for loosely-coupled spin systems when invoking the initial-slope approximation.² The conditions for making this assumption will be described in the following section.

A clear distinction can now be made between the frequently confused terms, cross-relaxation and cross-correlation. Cross-relaxation arises from the significant probability for mutual spin flips in systems of two or more nuclei where the relaxation mechanism couples the spins. The dipolar interaction between A and M, and between A and X, is proportional to the magnitude of the relaxation vectors AM and AX, respectively, but independent of each other. Cross-correlation is an interaction between these two relaxation vectors, in the case where their motions are correlated.

2.4.4. The Initial Slope Approximation.

It follows from the coupled differential equations (16) for the AX and (19) for the AMX system, that the evolution of the longitudinal (z) magnetization of each nucleus is multi-exponential. A formal evaluation of these expressions would require a series of complex computations, even for a weakly coupled system.^{14,15} A significant theoretical breakthrough for relaxation in-coupled spin systems was reported in 1970 by Freeman, Wittekoek, and Ernst,² when

they showed that in the initial part of the magnetization recovery curve (the initial-slope region), relaxation in a loosely coupled spin system tumbling in the extreme narrowing limit can be characterized by a single exponential. Using this approximation, the dependence of M_{zi} on the state of M_{zj} , and the effects of cross-correlation are both negligible, and the relaxation expressions uncouple. It is, therefore, possible to characterize the relaxation of any nucleus in the system by a discrete relaxation rate which is the sum of self-relaxation terms (ρ_i) and pairwise interactions with the other nuclei to which i is coupled, cross-relaxation terms (σ_{ij}).

The initial-slope region was defined² in terms of transition probabilities as the period of recovery from time 0 to t s, such that $(W_{ij} - W_{ik})^2 t^2 \ll 1$, for all $j, k \neq i$. Specific transition probabilities are not usually measurable, but a practical guideline of between 0 and $1xT_1$ has been suggested¹⁶ for the initial-slope approximation, though the actual limitations will vary according to the degree to which the system is loosely coupled ($J/\Delta\delta < .1$). For systems close to this limit, the initial-slope approximation will be effective over a much more limited range. All R_1 values reported in this thesis have been calculated from sampling the magnetization well within the initial-slope region, using the interval from 0 to the null-point ($0.69xT_1$) to ensure that the initial-slope approximation was valid.

2.4.5. Dipolar Spin-lattice Relaxation

A complete derivation of relaxation by dipolar interactions requires a series of lengthy calculations, which are beyond the scope of this thesis. These calculations have been presented in various forms in a number of publications.^{8,14,17,18} A brief description of this derivation will be given in this section.

In these calculations, the probabilities for transition between two energy levels are given as a function of the auto correlation functions described in the previous section. This procedure incorporates the random molecular motions of the molecule into the relaxation model. By proper transformation, the time dependence of magnetization can then be expressed in terms of the spectral densities. The evaluation of the matrix for the dipolar interactions contains two types of spectral density functions, if there are more than two coupled spins in the system. Auto-correlation functions, $(J_{ij,ij})$ are the result of direct lattice interactions as have been described for the isolated, AX, and AMX systems. In addition to these terms, there are special spectral density functions which arise from cross-correlations $(J_{ij,ik})$ of relaxation interactions. The cross-correlation terms are not significant during the initial stages of relaxation of a loosely-coupled first order system,² so in this initial-slope region the relaxation matrix can be simplified by setting the cross-correlation elements to zero.

Using the dipolar spectral densities, the dipolar transition probabilities shown in Fig. 2.5 for the AMX system can be formulated:¹⁷

$$(21) \quad W_{1,2} = W_{1A} = 1/2 [J_{am,am}(w_a) + J_{ax,ax}(w_a) + 2J_{am,ax}(w_a)]$$

$$W_{3,5} = W_{1'A} = 1/2 [J_{am,am}(w_a) + J_{ax,ax}(w_a) - 2J_{am,ax}(w_a)]$$

$$W_{1,5} = W_{2am} = 2J_{am,am}(w_a + w_m)$$

$$W_{2,3} = W_{0am} = 1/3 [J_{am,am}(w_a - w_m)]$$

where w_1 is the Larmor frequency of spin 1. Note that in these expressions, it is assumed that there is 100% dipolar relaxation. The other nineteen transition probabilities can all be formulated from these expressions by permutation of indices indicating spin labels. To this point, the cross-correlation spectral densities $J_{am,ax}(w_a)$ in W_{1A} and $W_{1'A}$ are retained in expressions (21).

Relaxation parameters can now be formulated by substituting (21) into (18), to give:

$$(22) \quad \rho_a = J_{am,am}(w_a) + J_{ax,ax}(w_a) + J_{am,am}(w_a + w_m) + 1/3 [J_{am,am}(w_a + w_m)] + J_{ax,ax}(w_a + w_x) + 1/3 [J_{ax,ax}(w_a + w_x)] \dots$$

$$(23) \quad \sigma_{am} = 2J_{am,am}(w_a + w_m) - 1/3 [J_{am,am}(w_a + w_m)]$$

$$\sigma_{ax} = 2J_{ax,ax}(w_a + w_x) - 1/3 [J_{ax,ax}(w_a + w_x)] \dots$$

The initial-slope approximation has been incorporated to arrive at these discrete expressions for relaxation

parameters in the AMX system. Also, note that the cross-correlation terms in (21) have cancelled because W_{1A} and $W_{1'A}$ have been added, demonstrating the importance of the initial-slope approximation in multi-spin systems.

Defining a new variable, ρ_{ij} , which separates the self-relaxation mediated through interactions to each of the coupled nuclei:

$$(24) \quad \rho_{am} = J_{am,am}(w_a) + 2J_{am,am}(w_a+w_m) + 1/3\{J_{am,am}(w_a+w_m)\}$$

(20) can be recast as:

$$(25) \quad \rho_a = \rho_{am} + \rho_{ax}$$

The corresponding expressions for the other ρ terms can be obtained by permuting indices of the spin labels.

It is clear from the form of (25) that the self-relaxation rate of A is expressed in terms of the sum of independent pairwise interactions with the other protons in the system. The same statement is true for the cross-relaxation terms (σ_{ij} 's), hence the total contribution to relaxation from any particular proton is independent of the other protons in the molecule. If it is possible to separate all the contributions to R_1 , then the specific pairwise interactions can each be evaluated for the specific inter-nuclear distance, and the determination of molecular geometry is possible.

The evaluation of the spectral densities for dipolar relaxation can now be made, on the basis of the relaxation model and a description of the motion of the molecule under study. The appropriate expression for the spectral densities in the extreme narrowing limit is:¹⁷

$$(26) J_{ij,ji} = 3/10 \{ \gamma_i^2 \gamma_j^2 (h/2\pi)^2 \} t_{cij} (r_{ij})^{-6}$$

where t_{cij} is the correlation time characteristic for the ij vector, and r_{ij} is the internuclear distance. This is a dipolar auto-correlation spectral density. The cross-correlation spectral density, $J_{ij,jk}$, can also be evaluated, but is not of interest here.

The model of Brownian motion can be recalled to give a physical interpretation of the molecular motion.¹⁸ The molecule is said to tumble in a small-step Brownian diffusion process which requires many steps to complete full reorientation of the molecule, and which is characterized by a series of t_{cij} 's. Generally, a set of axes is applied to the molecule, and the motion is described by the values of t_{cij} along these axes. The most widely used motional models are the spherical, symmetric top,^{19,20} and asymmetric top models.²⁰ The spherical model is most frequently used because this model is the simplest. For this model, tumbling occurs with equal probability about all axes (all t_{cij} 's are equivalent), the molecule tumbles isotropically. Analysis of R_1 values in anisotropically tumbling systems will be discussed in section 2.5.

With motional and relaxation models, it is possible to express the self- and cross-relaxation in terms of specific quantities by substituting (26) into (22) and (23):¹⁷

$$(27) \rho_{am} = [1] \cdot \gamma_a^2 \cdot \gamma_m^2 \cdot (h/2\pi)^2 \cdot t_{cam} \cdot (r_{am})^{-6}$$

$$(28) \sigma_{am} = [0.5] \cdot \gamma_a^2 \cdot \gamma_m^2 \cdot (h/2\pi)^2 \cdot t_{cam} \cdot (r_{am})^{-6} = 1/2 (\rho_{am})$$

The corresponding expressions for the other σ and ρ values in the AMX system can be formulated by permuting spin labels. Anisotropic motion can be easily incorporated into these expressions by appropriate choice of t_c values.

The relationship between the ρ and σ terms as shown in (25) and (26), has several important consequences:

1. Explanation of the so-called 3/2 effect. As will be shown below, the observed relaxation rate is the sum of ρ and σ terms, hence a factor of 3/2 is present for all systems of two or more spins.
2. The ratio of the non-selective R_1 value ($\rho + \sigma$) to the single selective value (ρ only) is 1.5 in systems which relax only via the dipolar or scalar mechanisms.
3. The maximum value of the nOe in any homonuclear system is 50%.

Selective R_1 ²¹ and nOe experiments are the two principal methods for measuring specific self-relaxation and cross-relaxation terms. In proton systems, selective R_1 values have been shown to be superior to the nOe measurement for detailed quantitative analysis,* but for technical reasons, have not become nearly as common as the nOe experiment.

* Selective $^1\text{H-R}_1$ values have been utilized for accurate determination of molecular geometries of a number of carbohydrates in solution.^{16,22}

For the qualitative studies described in this thesis, measurements of the nOe by the highly sensitive difference method²³ were sufficient. The nOe will be discussed in greater detail in section 2.5.

With expressions (25) and (26) available, there remains only to determine the final form of the relaxation equations which relate these expressions to the observable magnetization. It has been shown that the general form for an AMX system (18) is a set of coupled differential equations, whose solution would be non-exponential. In the initial-slope region, however, the equations behave as if they were not coupled, and in addition, the effects of cross-correlation on data for weakly coupled spin systems are negligible. It is clear, therefore, that the magnetization for each nucleus can be characterized by a single exponential when the initial-slope approximation is valid. The general expression for any loosely-coupled spin system is given by:

$$(29) \quad M_i(t) = M_i(\infty) + \{M_i(0) - M_i(\infty)\}e^{-R_1 t}$$

where for any spin i (eg. $i = A, M, X$), $M_i(t)$ is restricted to the initial-slope region. Note that though (29) has been derived for an AMX system, it is valid for any loosely-coupled spin system. The measured rate of relaxation of a resonance can now be formulated in terms of specific self-relaxation and cross-relaxation components:

$$(30) R_{1i} = \sum_j (\rho_{ij} + \sigma_{ij}) \quad j \neq i$$

Substituting into (30) with (27) and (28), and making the assumption of isotropic tumbling, for an AMX system of protons relaxed by intra-molecular dipolar interactions, the relaxation rate of proton A is given by:

$$(31) R_{1A} = 3/2 \{ \gamma_H^4 (h/2\pi)^2 t_c \} \sum_j (r_{Aj})^{-6}$$

This expression can be generalized for any multispin proton system, which is at least pseudo first order. The relaxation of any proton i in such a system is given by:

$$(32) R_{1i} = 3/2 \{ \gamma_H^4 (h/2\pi)^2 t_c \} \sum_j (r_{ij})^{-6}$$

Thus, for any loosely coupled proton in an isotropically tumbling molecule, the observed relaxation rate is directly dependent on the rate at which the molecule tumbles, and the number of, and distances to, the other protons in the molecule.

The inverse sixth power dependence on internuclear distance implies that relaxation contributions are significant only for the nearest neighbors of a particular proton. In consequence, R_1 values (and nOe enhancement factors) are extremely sensitive to local structure and stereochemistry, and can be utilized for the determination of specific structural features of a wide range of organic molecules.

2.5. The Nuclear Overhauser Effect

In many instances, structure analysis requires more detailed characterization of specific dipolar interactions than is possible by simple R_1 analysis. It is, therefore, necessary to utilize some other technique such as selective R_1 experiments^{21,22} or nOe measurements⁵ to characterize relaxation contributions from specific protons. The most widely used method today is to measure nOe enhancements in the difference mode.²³ A description of the the procedure and some practical considerations for the nOe difference (pOed) experiment are given in Chapter 3.

The nOe enhancement is a measure of the cross-relaxation term and is, therefore, in ^1H systems, indicative of dipolar coupling between two nuclei. It is observed as an enhancement of signal intensity of a resonance, upon pre-saturation of another resonance. The magnitude of the enhancement is proportional to the extent to which the saturated signal contributes to the dipolar relaxation of the enhanced signal. The origin of the nOe can be explained in a qualitative sense by a simplified example of the nOe in a hypothetical AX system. The energy diagram for the AX system was given in Fig. 2.4.

Signal intensities in any spin system depend on the relative populations of the spin states involved. In the AX model system, let there be a total number of N spins, and assume that at equilibrium, $1/4$ of them will populate the two intermediate energy states, $\alpha\beta$ and $\beta\alpha$. The $\beta\beta$ state, which has a slightly higher energy, will have a slightly lower population. The amount by which the population is lower will be called Δ , thus the population of the $\beta\beta$ state is $(N/4) - \Delta$. Using similar logic, the population of $\alpha\alpha$ must be $(N/4) + \Delta$. The intensity of all observable (single quantum) transitions will be equivalent, because the population differences are all equal to Δ .

Consider the effect on A of irradiating X transitions until the populations of the appropriate spin states are equalized (saturated). In addition, recall that in a system where there is dipolar coupling, double quantum transitions of the W_2 type are very efficient. As a result, the Boltzman distribution between the $\alpha\alpha$ and $\beta\beta$ states is maintained. Since these two processes are simultaneously effective, the population of the state $\alpha\beta$ must be equal to that of the $\alpha\alpha$ state $(N/4) + \Delta$. The states $\beta\alpha$ and $\beta\beta$ also have equivalent populations $(N/4) - \Delta$. The population difference for the spin A transitions is, therefore, 2Δ instead of Δ , so a two-fold enhancement of the intensity of resonance A is predicted by this simple model.

With this qualitative sense of the nOe , a summary of the more rigorous mathematical treatment can be presented.

Recalling (16):

$$(16) \frac{dM_{za}}{dt} = -\rho_a(M_{za} - M_{za}(0)) - \sigma(M_{zx} - M_{zx}(0))$$

which gives the rate equation for the magnetization of spin A in an AX system, it is possible to consider the effect of saturation of the X transitions. Under conditions of saturation, the magnetization of the saturated spin is zero, so (16) reduces to:

$$(33) \frac{dM_{za}}{dt} = -\rho_a(M_{za} - M_{za}(0)) + \sigma(M_{zx}(0))$$

Under steady-state conditions:

$$(34) \frac{dM_{za}}{dt} = 0, \text{ so } \rho_a(M_{za} - M_{za}(0)) = \sigma(M_{zx}(0))$$

Noting the simple equality, $M_{za}(0)/M_{zx}(0) = \gamma_a/\gamma_x$,

(32) becomes:

$$(35) M_{za} - M_{za}(0) = \frac{\sigma}{\rho_a} \frac{\gamma_x}{\gamma_a} M_{za}(0)$$

Taking the ratio of the A magnetization under conditions of X saturation to the A magnetization without saturation, the concept of enhancement of signal intensity can be introduced:

$$(36) \frac{M_{za}}{M_{za}(0)} = 1 + \frac{\sigma}{\rho_a} \frac{\gamma_x}{\gamma_a} = 1 + n$$

where n is defined as the nOe enhancement factor.

From equations (27) and (28), if the spin system is completely relaxed by internal dipolar interactions the ratio $\sigma/\rho_a = 0.5$, so the generalized expression for the nOe enhancement is:

$$(37) n = 0.5 \frac{\gamma_x}{\rho_a}$$

The dependence on γ values has very important consequences for sensitivity enhancement in heteronuclear systems involving 1H and low abundance, low γ nuclei. The most common example is the sensitivity enhancement of ^{13}C signals by broadband proton irradiation, where there is a three-fold gain in signal intensity. In any homo-nuclear system, $\gamma_a = \gamma_x$, so the maximum enhancement is 50%.

Recalling that relaxation in the initial-slope region can be characterized by the summation of discrete pairwise interactions for loosely coupled spin systems, the nOe in a multi-spin proton system can be expressed as the ratio of the specific cross-relaxation rate to the total self-relaxation rate:

$$(38) n_{i \leftarrow \{j\}} = \frac{\sigma_{ij}}{\rho_i}$$

Using (27) and (28) and assuming isotropic motion, (38) can be expressed as the following:

$$(39) \quad n_{i \leftarrow \{j\}} = 1/2 \frac{(r_{ij})^{-6}}{\sum_k (r_{ik})^{-6}} \quad k \neq i$$

This latter expression reveals the great power of the $^1\text{H-nOe}$ as a probe of molecular geometry in organic molecules. The magnitude of the nOe is a measure of the relative relaxation contribution of the saturated proton to the enhanced proton (36), and can be directly correlated to the relative distance between the two protons (37). In a qualitative measurement, the nOe is a means of determining whether the two protons are near to or far away from each other. The principal advantage of the nOe experiment over the non-selective R_1 is this specificity in the characterization of a relaxation pathway between two protons, whereas the R_1 value reflects the summation of all relaxation pathways. To determine a full set of relaxation pathways in a complex molecule by this technique would, however, require many experiments, thus nOed spectroscopy is usually used as a complement to determine specific features of interest, after R_1 values have been analyzed.

2.6. Relaxation Pathway Analysis

In the generalized relaxation expression (32), each term in the summation constitutes a specific dipolar relaxation pathway. Due to the unique location of each proton in the molecule, there is a unique set of relaxation pathways which characterize each proton. In many instances, the various relaxation pathways to and from a particular proton can be found, through the use of nOe and R_1 experiments, thereby establishing its identity.

Relaxation pathways may be evaluated semi-quantitatively for any molecule, assuming that the molecule tumbles somewhat isotropically, and using internuclear distances measured on Dreiding molecular models, or from crystal coordinates determined by diffraction methods. Simultaneous evaluation of (32) for two protons j and k gives:

$$(40) \quad \frac{R_{1j}}{R_{1k}} = \frac{\sum_i (1/r_{ij})^6 \quad i \neq j}{\sum_i (1/r_{ik})^6 \quad i \neq k}$$

Relative R_1 values can be calculated directly from (40).

nOe enhancements, n , can be predicted in a similar manner by evaluating each $(1/r_{ij})^6$ term using (39).

Though these calculations serve as an invaluable aid in the interpretation of the experimental data, their limitations are obvious. Fortunately, interpretation of the experimental data is based not on a single measurement,

but on trends seen in several measurements. The use of several observations to obtain information on a single site compensates for inaccuracies associated with calculations based on a model, and for experimental errors.

Using relaxation pathway analysis, in conjunction with a simple mathematical model which enables the prediction of relative relaxation rates, it is possible to obtain structural and stereochemical information on complex organic molecules. The experiments may be carried out easily and rapidly, using a modern, high field spectrometer. Sample preparation does not require degassing if only qualitative information is desired. In the first level of analysis (R_1 measurements) there is a high information content in that the relaxation rates of all protons are obtained in a single experiment. If necessary, specific information on relaxation pathways (ie. on relationships to near neighbors of a particular proton) may then be obtained by the more time-consuming, but more selective and sensitive NOE difference experiment.

Applications of relaxation pathway analysis are given in three separate chapters. In Chapters 4 and 5, structural features will be analyzed for a variety of alkaloid molecules, to demonstrate the applicability of this technique for structure analysis. An in-depth analysis of relaxation pathways will be utilized in Chapter 6 to make some rather difficult chemical shift assignments, and to analyze the the complex stereochemistry in some 7-hydroxyindene dimers.

2.7. Analysis of Anisotropic Overall Tumbling and Internal Motion by ^{13}C Relaxation Measurements

To describe the motion of a molecule by the rotational diffusion model, the symmetry (or shape factor) in the molecule will serve to characterize the relationship between the values of t_{cij} along various axes of the molecule. A molecule with cubic symmetry tumbles isotropically and is characterized by a single rotational diffusion constant, D , which is related to t_{cij} by:²⁰

$$(41) \quad t_{cij} = \frac{1}{6D}$$

If the molecule under consideration tumbles anisotropically, an effective correlation time, t_{eff} , must be defined, in terms of the composite effect of several direction-dependent diffusion constants. In the general case, the motion can be described in terms of a rigid ellipsoid tumbling at different rates about three axes (asymmetric top),^{19,20} each with a unique diffusion coefficient, $D_1 \neq D_2 \neq D_3$. An analysis by this method would be extremely laborious, so certain assumptions are usually made to simplify this description. For many molecules, it is possible to assume that the molecule tumbles as a symmetrical rigid ellipsoid (symmetric top),²⁰ with equivalent diffusion coefficients about two of the axes, $D_1 \neq D_2 = D_3$. The corresponding expression for the effective t_c is:

$$(42) t_{\text{eff}} = \frac{A}{6D_2} + \frac{B}{5D_2+D_1} + \frac{C}{2D_2+4D_1}$$

where A, B, and C are geometric coefficients reflecting the angle, Δ , between the relaxation vector of any two nuclei, and the principal axis of the ellipsoid:²⁰

$$(43) A = \frac{1}{4}(3\cos^2\Delta-1)^2 \quad B = \frac{3}{4}(\sin^2 2\Delta) \quad C = \frac{3}{4}(\sin^4\Delta)$$

To carry out motional analysis, it is necessary to determine the R_1 values of specific relaxation vectors. In organic molecules, ^{13}C - R_1 measurements are uniquely suited to such an analysis, for two principal reasons:

1. The relaxation of protonated ^{13}C nuclei is invariably dominated by interactions with directly bonded protons.
2. ^{13}C is present in low natural abundance, there is no interaction with other directly bonded ^{13}C atoms or ^{13}C -H relaxation vectors.

The ^{13}C - ^1H system is essentially magnetically isolated and the inter-nuclear distances are known to a high degree of confidence, the exact requirements for a straightforward calculation of t_{eff} using (27), (28), and (30):

$$(44) R_1^{13\text{C}} = n \cdot (h/2\pi)^2 \cdot \gamma_{\text{C}}^2 \cdot \gamma_{\text{H}}^2 \cdot (r_{\text{C-H}})^{-6} \cdot t_c$$

where n is the number of directly bonded protons and all the other symbols have their standard meaning.

To analyze (42) for D_1 and D_2 , $^{13}\text{C}-R_1$ values are measured for two relaxation vectors for which the Δ values are different. This, of course, requires that Δ values are known or can be estimated. If these angles are not known, then a technique such as the iteration method of Platzer²⁴ is necessary. This approach involves calculating R_1 values for as many protonated C atoms as possible, while systematically varying Δ values, until a "best fit" is found for all the experimental data. A simpler method of analysis is possible when the R_1 for a specific relaxation vector which is parallel to the principal rotation axis can be measured. For this vector, $\Delta = 0$, $B = C = 0$, $A = 1$, and $t_{\text{eff}} = 1/6D_2$, hence D_2 can be readily determined using (44).

In the course of studies of methyl group ^1H relaxation (Chapter 7), it was necessary to carry out a number of additional experiments to corroborate the proposed steric nature of the observed effects. An estimation of methyl rotation barriers was made using $^{13}\text{C}-R_1$ values.¹² This requires a specific model to characterize the effective motion arising from the superimposition of overall molecular tumbling and internal methyl rotation. Internal motion is usually independent of overall tumbling, and so it can be characterized by an independent diffusion coefficient, D_i . The simplest case occurs when the axis of internal rotation coincides with the principal diffusion axis (eg. in toluene); it is only necessary to add the D_i term to D_1 .²⁰ The generalized expression for the symmetric top model is:

$$(45) t_{\text{eff}} = \frac{A}{6D_2} + \frac{B}{5D_2 + D_1 + aD_1} + \frac{C}{2D_2 + 4D_1 + amD_1}$$

The values of a and m vary according to the model used to represent the superimposed internal motion. If the motion is assumed to occur by stochastic diffusion (independent small step diffusion approaching continuous motion), then $D_{1,\text{eff}} = D_1 + D_1$, therefore, $a = 1$ and $m = 4$. If the motion is described by instantaneous jumps between preferred conformations, then $D_{1,\text{eff}}$ in the C term for t_{eff} is reduced by $1/4$, therefore, $a = r/2$ and $m = 1$. The value of r represents the number of degenerate preferred conformations (eg. six for a six-fold methyl rotation barrier and three for a three-fold barrier). Expression (45) is also valid in the limit of isotropic motion ($D_1 = D_2$). The preference for either the stochastic or methyl-jump models is a matter of continuing controversy,¹² and will be discussed in Chapter 7.

Most determinations of D_1 reported in the literature have assumed overall isotropic tumbling in the molecule, in order to use simplified forms of (44) and (45). In such studies, D is calculated using R_1 values and C-H bond lengths of the protonated C atoms in the molecular framework, then D_1 is directly calculated using the R_1 value and C-H bond length of the methyl group. Two studies have been published^{24,25} where anisotropic symmetric top

motion has been assumed. In these studies, either D_1 , D_2 , and D_i values are simultaneously optimized to fit all the relaxation data, or D_1 and D_2 are optimized separately to the R_1 values of ring protons, then D_i is calculated directly, using the methyl R_1 , and (44) and (45).

In the general case where the axis of internal motion does not coincide with the principal diffusion axis, the expression for t_{eff} is much more complex. Woessner introduced the necessary formulation in 1969,²⁶ allowing for an angle α between the internal axis of motion and the principal diffusion axis:

$$(46) \quad t_{\text{eff}} = \frac{1}{2} \left(\frac{A_1}{6D_2} + \frac{A_2}{6D_2 + aD_i} + \frac{A_3}{6D_2 + aD_i} \right. \\ \left. + \frac{B_1}{D_1 + 5D_2} + \frac{B_2}{D_1 + 5D_2 + aD_i} + \frac{B_3}{D_1 + 5D_2 + aD_i} \right. \\ \left. + \frac{C_1}{4D_1 + 2D_2} + \frac{C_2}{4D_1 + 2D_2 + aD_i} + \frac{C_3}{4D_1 + 2D_2 + aD_i} \right)$$

$$(47) \quad A_1 = 1/8 (1 - 3\cos^2\alpha)^2 (3\cos^2\Delta - 1)^2 \\ A_2 = 9/16 \sin^2 2\alpha \sin^2 2\Delta \\ A_3 = 9/16 \sin^4 \alpha \sin^4 \Delta \\ B_1 = 3/8 \sin^2 2\alpha (3\cos^2\Delta - 1)^2 \\ B_2 = 3/4 (\cos^2 2\alpha + \cos^2 \alpha) \sin^2 2\Delta \\ B_3 = 3/4 (\sin^2 \alpha + 1/4 \sin^2 2\alpha) \sin^4 \Delta \\ C_1 = 3/8 \sin^4 \alpha (3\cos^2\Delta - 1)^2 \\ C_2 = 3/4 (\sin^2 \alpha + 1/4 \sin^2 2\alpha) \sin^2 2\Delta \\ C_3 = 3/16 [(1 + \cos^2 \alpha)^2 + 4\cos^2 \alpha] \sin^4 \Delta$$

If $\alpha \neq 0$, but is known, the calculation using (46) is carried out after determination of the diffusion constants for overall molecular tumbling, as has been outlined above. When the value of α is not known, it can be included as a parameter in an iterative analysis of relaxation data, or estimated by a computer simulation of the moments of inertia in the molecule and a subsequent analysis of anisotropic tumbling. Interestingly, in studies in which the more complex analyses have been carried out,^{24,25} there appears to be no significant difference in the value of D_i from that calculated by assuming isotropic overall tumbling and on-[principal]-axis internal motion. Most of the results reported in Chapter 7 have been calculated assuming isotropic motion and on-axis internal rotation. A selected number of comparative calculations utilizing the more complex methods have been carried out, to verify that the simplified calculations were accurate.

The calculated values of diffusion constants for internal motion can be used to estimate the activation energy for the methyl rotation. For a quantitative determination, an Arrhenius plot of D_i would be necessary. The energy barrier, V , at a particular temperature can, however, be estimated directly from the value of D_i using:²⁷

$$(48) V = RT * (\ln \frac{D_i}{D_{i0}})$$

where R and T have their standard definitions. D_{10} for a methyl group is the rotational diffusion coefficient for a free rotor at the specified temperature. Grant and coworkers²⁸ have calculated the following value:

$$(49) D_{10} = (kT/I)^{1/2} = 0.89 \times 10^{13} \text{ s}^{-1} \quad (40^\circ)$$

where I is the moment of inertia of the methyl group.

The analysis of $^{13}\text{C-R}_1$ data to derive values for methyl rotational diffusion rates and barriers is a useful method of obtaining information needed for the interpretation of ^1H relaxation rates, and will be utilized in the study of steric effects on methyl $^1\text{H-R}_1$ values in Chapter 7.

Chapter 3

SOME PRACTICAL CONSIDERATIONS IN MAKING $^1\text{H-R}_1$ AND NOE DIFFERENCE MEASUREMENTS*

3.1. Introduction

There are several important experimental constraints that must be accounted for in the course of measuring relaxation parameters. Accurate and reliable methods must be utilized for both acquisition and analysis of experimental data. In this chapter, some of the important practical considerations will be discussed, based on experience accumulated with a variety of organic molecules. Emphasis will be placed on specific technical aspects which have not been sufficiently covered in the literature.

A series of $^1\text{H-R}_1$ control experiments have been carried out to evaluate:

1. Preferred methods of data analysis
2. The effects of additional components in solution
3. The magnitude of errors arising from spectrometer instability
4. The reproducibility and precision of measurements

A description of methods for obtaining reliable $^1\text{H-R}_1$ results in an efficient manner, according to the complexity of the molecule under study and the kind of information required, will be presented.

* Parts of this chapter have been presented at the 22nd ($^1\text{H-R}_1$ discussion) and 23rd ($^1\text{H-nOe}$ discussion) Experimental NMR Conferences in Madison, Wisconsin, April, 1982, and Asilomar, California, April, 1983.

The experimental aspects of ^1H - $n\text{Oe}$ difference measurements that will be discussed are:

1. Sensitivity
2. Choice of solvent (influence on acquisition time)
3. Irradiation Period
4. Saturation efficiency versus selectivity

A protocol which optimizes the efficiency of acquisition of qualitative multifrequency $n\text{Oe}$ d experiments, developed in the course of these studies, will also be presented.

3.2. ^1H - R_1 Experiments

3.2.1. Procedure for Measuring R_1 Values

A large number of methods have been proposed to measure spin-lattice relaxation rates, though it has only been since the advent of pulse Fourier transform nmr that R_1 values have become widely accessible and applied to a range of chemical problems. By far the most popular technique is that of inversion-recovery, originally proposed by Waugh and coworkers.¹ This method is generally recognized as the most accurate method for R_1 determination, and so has been utilized for all experiments presented in this thesis. A description of other methods can be found in most nmr texts, eg. Ref. 29.

The standard version of the experiment utilizes the following pulse sequence:

$$(1) \{P - 180^\circ - t - 90^\circ - \text{Acq.}\}_n \quad P > 5T_1$$

The experiment can be best visualized by considering the behavior of the bulk magnetization vector (see Fig. 3.1). The equilibrium magnetization is initially inverted by the 180° pulse. During the variable time period, t , the magnetization vector will shrink as the system relaxes back toward equilibrium. If a long enough t period is used the magnetization will go through a null and return to the positive z direction. After the time t , a 90° pulse is applied to the system, to tip the magnetization into the x, y plane where it can be detected. The experiment is then repeated for the desired number of times (depending on required S/N), ensuring that a sufficient preparation period, $P > 5T_1$, is allowed for equilibrium to be reestablished.

The change in magnetization as a function of t is given by the general relaxation expression (2.14), where $K = 2$ for the inversion recovery experiment. The intensity of the detected signal can be utilized to follow the change in magnetization,* so this equation can be expressed as:

$$(2) I(t) = I(0) * (1 - 2e^{-R_1 t})$$

R_1 values are determined by evaluating this expression by regression analysis of the data points or by the null-point method, as will be described in section 3.2.4.

* For many nuclei, including ^1H , peak heights can be used instead of peak areas, without loss of accuracy.

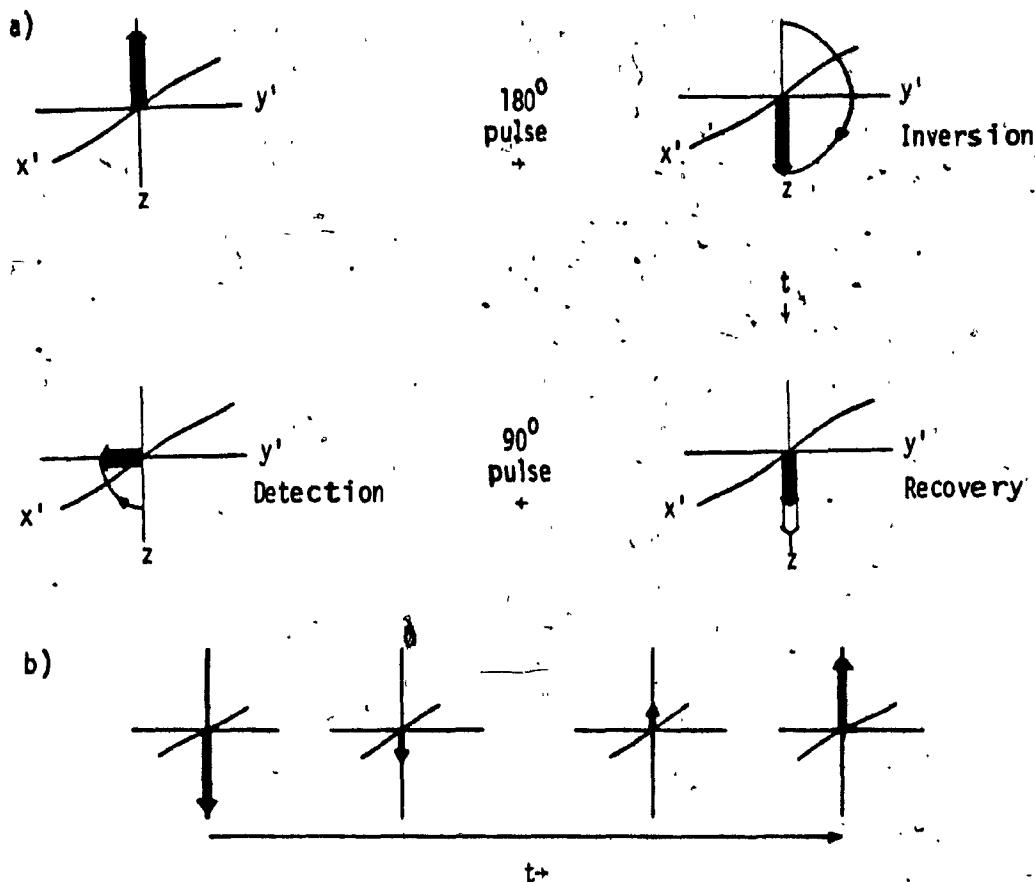


Fig. 3.1 The inversion-recovery experiment: a) the effect of the pulse sequence on the bulk magnetization, b) the recovering magnetization with increasing delay time, t .

Table 3.1

Normalized R_1 Values Measured With and Without TMS¹

<u>Proton</u>	<u>Normalized $R_1$²</u>	
	<u>With TMS</u>	<u>Without TMS</u>
Methyls-1,3	1.58	1.57
Methyl-2	1.44	1.42
Methyl-5	1.52	1.54

1. Experiments on 0.1 M 1,2,3,5-Tetramethylbenzene in $CDCl_3$ at ambient temperature.

2. R_1 values determined by two parameter, non-linear regression analysis to a precision of 0.003 s^{-1} or better, then normalized to H4/H6.

3.2.2. $^1\text{H-R}_1$ Measurements in the Presence of Other Components

The measurement of $^1\text{H-R}_1$ values is often carried out in solutions which contain more than just a single component. It is, therefore, important to know whether the measurement is affected by the presence of the other components in the solution.

3.2.2.1 Impurities Minor/Components

The presence of minute quantities of impurity from both solute and solvent is inevitable, unless the sample has been prepared under fastidious conditions. In many cases, a minor component is desirable, for example, TMS for chemical shift reference. Results from experiments to determine if the presence of TMS in solution had any effect on measured R_1 values are given in Table 3.1. It is clear from these data that the presence of TMS in solution at a concentration of 0.1% does not affect the R_1 measurement.

3.2.2.2. The Presence of a Second Major Component in Solution

A series of control experiments have been carried out to determine if R_1 values can be accurately measured in solutions which contain more than a single major component. This is an important consideration with respect to using R_1 values for structural analysis of compounds which are available only in impure form due to extreme separation problems, or limits in the quantity of compound that can be obtained.

In Table 3.2, the results of a series of $^1\text{H-R}_1$ experiments are given on solutions of the cis- and trans-isomers of 4-t-butyl-1-methylcyclohexanol. These data show that, within experimental error, the R_1 values are the same whether measured in a solution of the mixture of isomers or a solution of one isomer only, firmly establishing that the presence of a second, non-paramagnetic component in solution will not affect the R_1 measurement.

3.2.2.3 $^1\text{H-R}_1$ Measurements in Non-degassed Solutions

The presence of paramagnetic impurities in solution will have one of two possible effects on the measured R_1 values. If the paramagnetic species interacts with the molecule of interest in a specific manner, then the effect on the R_1 's will be selective, eg. some R_1 values will be very greatly affected, whereas others will be affected only slightly, if at all. If the interaction is non-specific, then the effect will be approximately equivalent for all protons in solution. Paramagnetic interactions can be used advantageously, for example, as an aid in establishing sites of molecular association, or as relaxation reagents to increase the rate at which spectra can be accumulated. Removal of paramagnetic species (often carried by dust) is desirable to ensure that there are no specific effects. Note that the effect of the paramagnetic

Table 3.2

R₁ Values Measured¹ in a Mixture and a Pure Solution
Cis- and Trans-4-t-Butyl-1-methylcyclohexanol

<u>Proton</u>	<u>Normalized R₁²</u>	
	<u>Pure Solution</u>	<u>50:50 Mixture</u>
<u>Trans</u>		
2,4a	.80	.77
2,4e	.84	.81
3,5a	.88	.88
3,5e	.93	-
4	.70	.72
Me(e)	.88	.87
t-bu	(.62)	(.60)
<u>Cis</u>		
2,4a	.88	.88
2,4e	.82	.80
3,5a	.88	.86
3,5e	1.00	1.02
4	.71	.69
Me(a)	.89	.91
t-bu	(.65)	(.63)

1. Measured from 0.1 M CDCl₃ solutions at ambient probe temperature.

2. R₁ values determined by the null-point method to an estimated precision of ± 0.03 s⁻¹ or better, then normalized to the t-butyl whose R₁ (s⁻¹) is given in parentheses ().

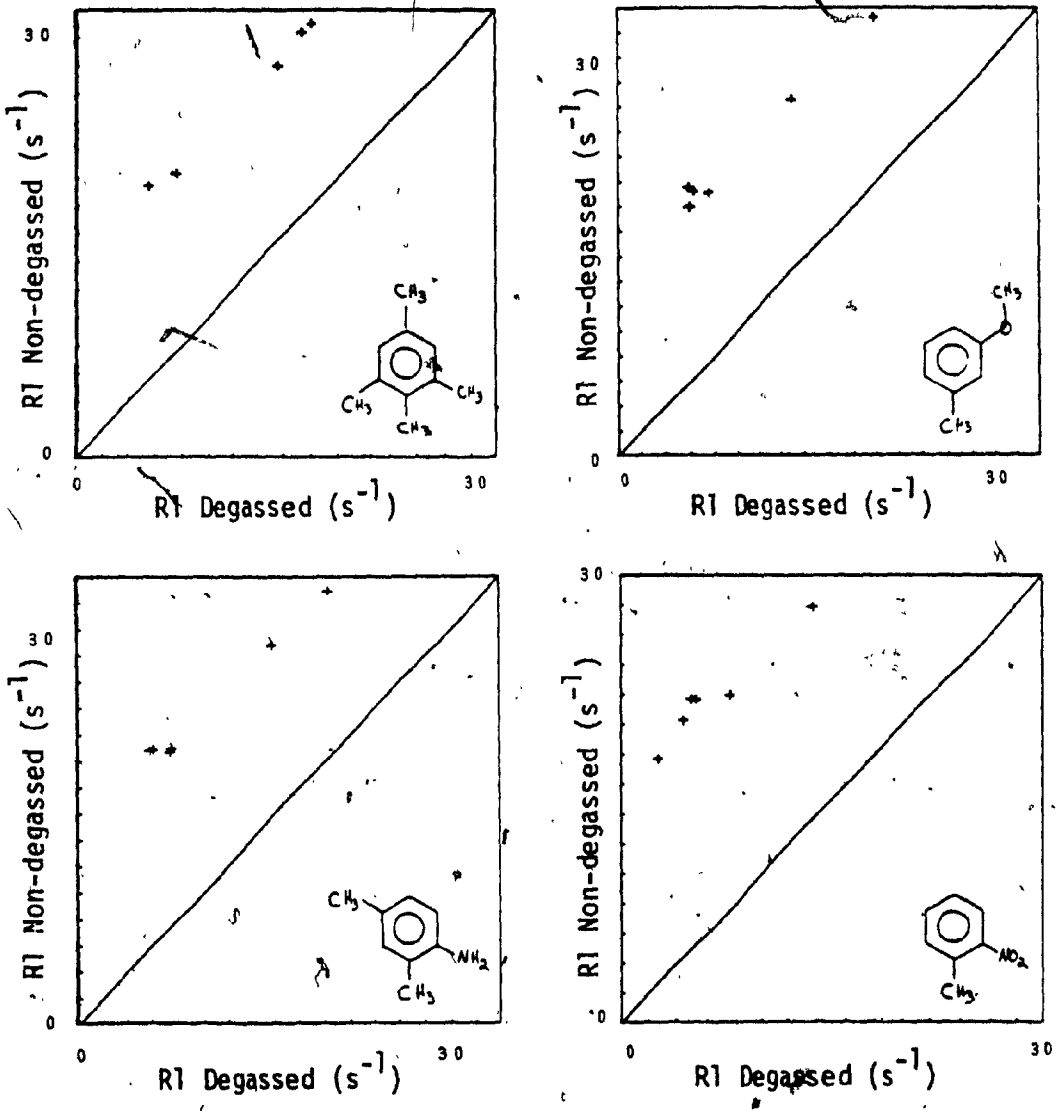


Fig. 3.2 Comparison of R_1 values from degassed and non-degassed solutions exhibiting the approximate equivalence of the R_1 contributions from dissolved oxygen.

species can be observed for very low relative concentrations, and so, as the working concentration is lowered, greater precautions are necessary for the removal of trace paramagnetic impurities, particularly in commercial solvents.

The most prevalent of paramagnetic impurities is dissolved oxygen gas, which can be removed by any standard degassing technique. Studies carried out by Colebrook and Hall,¹¹ have shown that the oxygen interacts in a non-specific manner, as evidenced by the equivalence of the contributions to different protons in a molecule. This means that for studies where accurate quantitative R_1 values are not needed, it is not necessary to degas the solution. These studies were carried out on an alkaloid of similar size to the alkaloids in this thesis, thus it was deemed not necessary to carry out additional control experiments on alkaloids. Most of the model compounds used in the methyl study were, however, considerably smaller than alkaloids, so a set of control experiments on a representative number of these compounds was obtained.

The comparative results of R_1 values measured in non-degassed and degassed solutions are given in Fig. 3.2. The equivalence of the oxygen contribution is demonstrated by the fact that the non-degassed R_1 values fall along a straight line parallel to the main diagonal. These experiments were required, because the contribution from oxygen in a non-degassed solution is a very large percentage of the measured R_1 for a slowly relaxing proton.

Nonetheless, the oxygen contribution can be easily accounted for in R_1 analysis, and so reliable qualitative information can be drawn from the R_1 values of non-degassed solutions of small molecules. This implies, of course, a considerable time saving with respect to sample preparation, and data acquisition time.

If accurate quantitative R_{1d} values are required, degassing is necessary. During the course of these studies, a rapid method for determining these "degassed" values has been developed and tested. The method relies on the non-specific nature of the oxygen interaction. An accurate value for the R_1 of TMS from non-oxygen sources at the operating temperature of the spectrometer can be determined from experiments on degassed samples. In the range 291-295°K, the R_1 of TMS in $CDCl_3$ in degassed samples was $0.075 \pm 0.005 \text{ s}^{-1}$ ($0.075 \pm 0.002 \text{ s}^{-1}$ at 293°K). This number can then be used to determine the oxygen contribution of observed R_1 values of protons in any non-degassed sample, as long as the measurements are made in the specified temperature range. The oxygen contribution is simply subtracted from the measured R_1 values of the non-degassed solution, giving the R_1 contributions to dipolar and other mechanisms. This approximation works quite well, even for the extremely slowly relaxing molecules listed in Table 3.3. For these molecules, the measured R_1 value in a non-degassed solution can have up to an 80% contribution from dissolved oxygen, yet a reasonable approximation of the R_1 value can be made

by the proposed method. Though this method is considerably less accurate than the measurement of R_1 values from a degassed sample, it is useful for obtaining approximate values of R_{1d} and offers a very considerable time-saving over the traditional degassing method.

Table 3.3

Comparison of $^1\text{H-R}_1$ Values from Degassed Solutions to those Using the Proposed Correction Method.

<u>Proton</u>	<u>R_1 (s^{-1})</u>	
	<u>Corrected</u> ²	<u>Degassed</u> ³
<u>o-Nitrotoluene</u>		
H3	0.03	0.029
H4,6	0.06	0.053
H5	0.06	0.047
Me	0.14	0.154
<u>1,2,3,5-Tetramethylbenzene</u>		
H4,6	0.06	0.066
Me-1,3	0.18	0.182
Me-2	0.15	0.152
Me-5	0.17	0.176

1. Experiments on 0.1 M CDCl_3 solutions, at ambient probe temperature.

2. Estimated precision of $\pm 0.01 \text{ s}^{-1}$.

3. R_1 's determined by 2-parameter, non-linear regression analysis to a precision of $\pm 0.003 \text{ s}^{-1}$ or better.

3.2.3. Precision and Error

The determination of the precision and error in measurements is an important aspect in the analysis of the reliability and, therefore, utility of any physical method. A series of control experiments have been carried out to determine the precision of the $^1\text{H-R}_1$ measurements reported in this thesis, and the confidence limits within which these measurements may be considered reliable.

3.2.3.1. Systematic Error- Long Term Spectrometer Instability

There are two specific parameters which are somewhat sensitive in the I-R relaxation experiment, and which can be monitored by control experiments. A series of control experiments to verify that the pulse width can be properly adjusted to give accurate and consistent 180° inverting pulses will be described in section 3.2.3.2. A second series of control experiments was carried out to determine the effects of long-term spectrometer instability, and will be described here.

Any long-term drift in the spectrometer would manifest itself as a systematic error in the measured R_1 , causing larger R_1 values. This error can be detected by varying the order of recovery delays (t); instead of using a sequentially varying delay list (ie., .1, .3, .5, ..s), a randomly alternating sequence is used (ie., .1, 3.5, 1.9, ..s).

Listed in Table 3.4 are typical results of R_1 measurements in successive experiments using a normal and an alternating delay sequence. No significant error was detected but it was observed that R_1 values calculated from the alternating sequence experiment exhibited a slightly lower precision.

Table 3.4

Control Experiment to Detect Long Term Instability
-The Effect of an Alternating Sequence-

<u>Proton</u>	<u>R_1 (s^{-1})</u>	
	<u>Control ($\pm .003$)</u>	<u>Alternating ($\pm .004$)</u>
TMS	0.238	0.236
H6	0.219	0.219
H5	0.229	0.229
H4	0.202	0.202
H2	0.194	0.193
Methyl	0.310	0.309

1. Experiments on 0.1M m-iodotoluene in $CDCl_3$ at $292^\circ K$.

2. R_1 's determined by 2-parameter, non-linear regression analysis to the precision reported in parenthesis.

3.2.3.2. Systematic Pulse Error- the Use of a Composite 180° Pulse

Freeman and Levitt³⁰ suggested the use of a composite 180° pulse to nullify errors that arise from missettings of the pulse width. The composite 180° pulse consists of three pulses ($90^\circ_x-180^\circ_y-90^\circ_x$), in place of the single 180°_x in the standard I-R sequence. A representative example of the results of control experiments comparing R_1 values measured using single and composite 180° pulses is given in Table 3.5 for the alkaloid quinine.

The differences in these values are within the expected error of 5-10% normally quoted for R_1 values. If some significant error in pulse width were present, the composite pulse R_1 's would be systematically different from those determined with a single 180° pulse. The agreement of these data implies that pulse widths can be set sufficiently accurately, hence, composite 180° pulses are not necessary.

3.2.3.3. Reproducibility and Precision

Control experiments were carried out to determine the reproducibility and precision of the $^1\text{H-R}_1$ measurements for each of the three types of systems studied: small molecules, non-degassed solution, regression analysis; small molecules, degassed solution, regression analysis; alkaloids, non-degassed solution, null-point method. The results are listed in Tables 3.6 and 3.7, respectively.

Table 3.5

Comparison of R_1 Values Using Single and Composite 180° Pulses

<u>Proton</u>	<u>R_1 (s^{-1})</u>	
	<u>Single</u>	<u>Composite</u>
2c	5.5	5.5
2t	6.7	6.6
3	2.4	2.4
4	2.8	2.8
5ex	4.7	4.8
5en	4.6	4.6
6ex	7.7	7.5
6en	5.8	5.5
7ex	4.7	4.8
7en	4.6	4.6
8	3.5	3.4
9	3.8	3.8
10	1.2	1.3
11c	1.5	1.5
11t	1.3	1.3
2'	.90	.87
3'	1.4	1.4
5'	2.7	2.7
6'-OMe	1.9	1.8
7'	.63	.64
8'	.70	.68

1. Experiments on 0.1 M Quinine-HCl in DMSO- d_6 at ambient probe temperature. R_1 values determined by the null-point method to a precision of $\pm 0.1 s^{-1}$ or better, and are the average of two experiments each.

Short-term reproducibility was verified by successive or interleaved experiments. Long-term reproducibility was verified by repeating experiments over a period of two months, with careful adjustment of experimental conditions. All data were analyzed completely independently to minimize bias in the results, e.g. in the determination of null-points.

Simple error analysis was carried out to determine precision and standard errors, using the following equations:

$$(3) S = \left[\frac{1}{n} \sum_i \left(m_i - \frac{\sum m_i}{n} \right)^2 \right]^{1/2}$$

$$(4) E = S/(n)^{1/2}$$

where n is the number of experiments, and m_i are the measured quantities, S is the standard deviation, and E is standard error.

The molecules chosen for control experiments were selected to typify both the experimental systems and problems usually encountered in making $^1\text{H-R}_1$ measurements, thus the spectra contain several protons with well resolved resonances over a wide range of R_1 values and, in addition, protons which demonstrate typical problems with overlapped and/or tightly coupled resonances.

Table 3.6

Reproducibility- R_1 Determined by Linear Regression¹

\bar{H}	Experiment							\bar{M} (s^{-1})	\bar{S} (s^{-1})	\bar{E} (%)
	1	2	3	4	5	6	7			
<u>m-Iodotoluene, non-degassed, successive experiments</u>										
2	.192	.192	.192	.193	.194	-	-	.193	.0008	0.2
4	.202	.201	.202	.202	.202	-	-	.202	.0004	0.1
5	.228	.227	.228	.229	.229	-	-	.228	.0008	0.2
6	.217	.218	.219	.219	.219	-	-	.218	.0009	0.2
<u>o-Nitrotoluene, degassed, experiments over a two month period</u>										
1	.153	.153	.155	-	-	-	.154	.154	.0010	0.3
3	.028	.029	.029	.029	.028	.029	.029	.029	.0005	0.6
4/6 ²	.054	.053	.054	.053	.053	.053	.054	.053	.0005	0.4
5	.048	.047	.048	.046	.047	.047	.048	.047	.0008	0.6

1. All experiments on 0.1 M $CDCl_3$ solutions, at 292°K. R_1 values determined by 2-parameter, non-linear regression analysis.
 \bar{M} = mean R_1 value, \bar{S} = standard deviation, \bar{E} = % standard error.

2. H4 and H6 are tightly-coupled and overlapped.

Table 3.7
 Reproducibility of R_1 Values- Null-Point Determinations¹

quinine-HCl				cinchonine-HCl			
\bar{H}	M (s)	S (s)	E (%)	\bar{H}	M (s)	S (s)	E (%)
2c	.125	.000	0.0	2c	.135	.000	0.0
2t	.103	.003	1.0	2t	.115	.000	0.0
3	.285	.000	0.0	3	.292	.003	0.4
4	.245	.000	0.0	4	.310	.000	0.0
5ex	.147	.003	0.7	5ex ²	.148	.003	0.7
5en	.150	.000	0.0	5en			
6ex	.090	.000	0.0	6ex	.113	.003	0.9
6en	.120	.000	0.0	6en	.120	.005	1.5
7ex ²	.147	.003	0.7	7ex	.150	.000	0.0
7en				7en	.140	.000	0.0
8	.197	.008	1.4	8	.205	.000	0.0
9	.183	.003	0.6	9	.190	.000	0.0
10	.567	.011	0.7	10	.610	.000	0.0
11c	.448	.010	0.8	11c	.540	.000	0.0
11t	.533	.006	0.4	11t	.650	.000	0.0
2'	.770	.000	0.0	2'	.850	.000	0.0
3'	.487	.011	0.8	3'	.550	.000	0.0
5'	.260	.000	0.0	5'	.285	.000	0.0
6'	.370	.000	0.0	6'	.570	.000	0.0
7'	1.090	.020	0.6	7'	.740	.000	0.0
8'	.980	.000	0.0	8'	1.117	.006	0.2
Avg.			0.4	Avg.			0.2

1. Experiments on 0.1 M DMSO-d₆ solutions at 293°K. Null-points measured in three successive experiments.

M = mean null-point; S = standard deviation, E = % standard error.

2. Null-point cannot be measured to due to tight-coupling and overlap.

The data in Tables 3.6 and 3.7 clearly indicate the high precision of the $^1\text{H-R}_1$ measurement on a modern spectrometer. The overall percentage error, taken to be twice the largest percentage standard error, was 2.8% for quinine-HCl and 3.0% for cinchonine-HCl, where R_1 values determined by the null-point method. For m-iodotoluene and o-nitrotoluene (degassed) the values were 0.4% and 1.3%, respectively, where R_1 values were determined by regression analysis.

Two important conclusions can be drawn from these data. First, though the precision of the regression analysis method is far superior, the null-point method gave $^1\text{H-R}_1$ values well within the usual estimated limits ($\pm 5\%$) for the absolute accuracy of R_1 by the I-R method. Second, though the absolute accuracy of the $^1\text{H-R}_1$ is indeterminate, high precision implies that relative R_1 values from a single experiment are accurate, and can be used with confidence for qualitative studies of molecular structure.

3.2.4. Data Analysis

3.2.4.1. The Use of Null-point Versus Regression Analysis

The data measured from a series of I-R experiments must be analyzed to determine the R_1 value. As mentioned previously, the variation of intensity, I , of a resonance is described by (2). R_1 can be determined by either the null-point or regression analysis methods. The null-point method involves an explicit evaluation of (2) at the time when $I(t) = 0$, giving R_1 directly: $R_1 = 0.69/t_{\text{null}}$. The time value of $I(t) = 0$ is interpolated from a stack plot of a series of I-R experiments (Fig. 3.3). Alternatively, the measured data can be fitted to (2) by iterative regression analysis on a computer. The regression analysis been carried out using a variety of regression methods, a few of which will be discussed further in the next section.

It is clear that the null-point method, if null-points can be accurately evaluated, is a much faster method of R_1 determination than computer regression analysis. The relative accuracy of the methods must, therefore, be carefully evaluated, before deciding which of the methods is preferable. Certainly, in the case where the R_1 values of only a few well separated resonances are of interest, regression analysis will not be particularly time consuming, and would give more accurate results. If a large number of

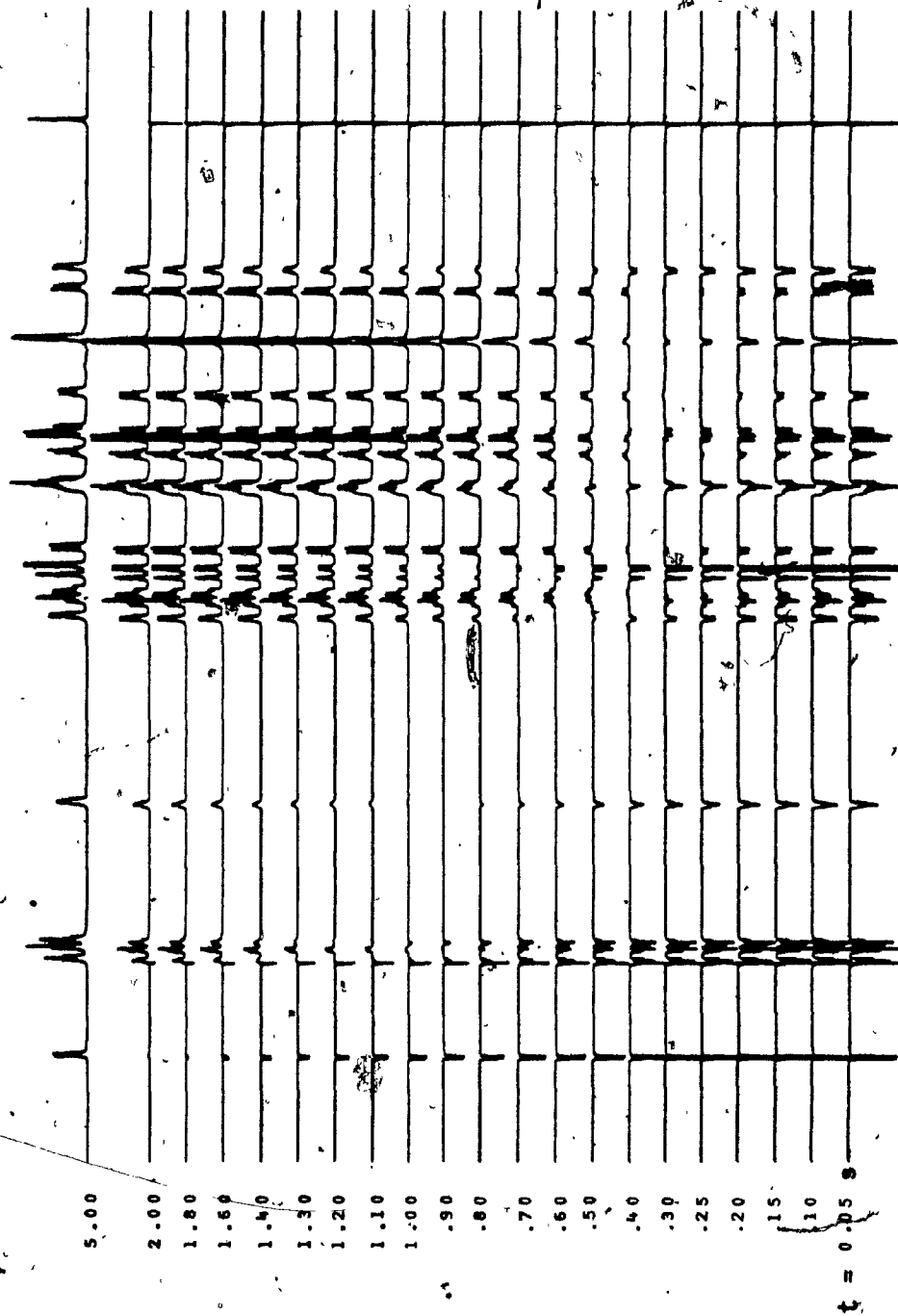


Fig. 3.3 Stack plot of 400 MHz ^1H nmr inversion-recovery experiments from a 0.1 M CDCl_3 solution of strychnine.

R_1 values are to be measured, or if the resonances of interest severely overlap, then regression analysis may not be feasible, thus it is important to determine how reliable the null-point method is, by carrying out a series of control experiments. Hall and Colebrook¹¹ have briefly reported the results of such comparative studies, on the alkaloid vindoline. A number of control experiments have been carried out during the course of this thesis, two examples are given in Table 3.8.

The data in this table typify the excellent agreement that was generally found in the analysis of R_1 values by the two different techniques. It must be pointed out that the precision of the regression analysis is inherently much better than the null-point method, and therefore, when it can be carried out conveniently, it is the method of choice. The null-point method is nonetheless quite accurate (to the quoted precision), as is evidenced by the agreement of the data. It has been suggested by Freeman and Levitt³⁰ that, when utilizing the null-point method, a composite inverting pulse (180° pulse) should be used to reduce errors resulting from errors in this pulse. This subject has been taken up in section 3.2.3.2, where it has been shown that such precautions were not necessary for the studies described herein.

Table 3.8

Comparison of R_1 Values Determined by
Null-Point and Regression Analysis

<u>Proton</u>	<u>R_1 (s^{-1})</u>	
	<u>Null-Point</u> ²	<u>Regression Analysis</u> ³
<u>Small Molecule- Caffeine</u> ¹		
TMS	0.23	0.222
H	0.23	0.221
Methyl-1	0.49	0.494
Methyl-3	0.44	0.446
Methyl-7	0.45	0.452
<u>Large Molecule- Hexamethyl-7-hydroxyindene dimer #3</u> ¹		
Me-1	1.54	1.52
H2	.95	.90
H3	.89	.92
Me-3	1.33	1.36
Me-4	.76	.76
H5	.43	.412
H6	.37	.373
Me-1'	.87	1.87
H2'	2.17	2.16
H2'	1.69	1.70
H3'	.71	.71
Me-3'	1.28	1.32
Me-4'	.79	.80
H5'	.43	.409
H6'	.33	.334

1. Experiments on 0.1 M $CDCl_3$ solutions at ambient probe temperature. See Fig. 6.1³ for structure of indene dimer.

2. Estimated precision of $\pm 0.01 s^{-1}$ for caffeine, and $\pm 0.03 s^{-1}$ for indene dimer.

3. Determined by 2-parameter, non-linear regression analysis to a precision of $\pm 0.003 s^{-1}$ or better for caffeine, and $\pm 0.01 s^{-1}$ or better for indene dimer.

3.2.4.2. Techniques of Regression Analysis

The selection of what method to use for regression analysis of R_1 data has been a subject of considerable controversy in the past ten years. In this thesis, all ^1H - R_1 values calculated by computer fitting of relaxation data, were carried out by a two-parameter non-linear regression analysis. ^{13}C - R_1 values were calculated by three-parameter non-linear regression. The preference for non-linear over linear regression has been thoroughly discussed by Leipert and Marquardt,³¹ and will not be taken up here. The selection of two- or three-parameter fitting remains somewhat more controversial, so a short description of the advantages and limitations of each will follow.

Equation (2) has two variable parameters, $I(0)$ and R_1 , but has been derived assuming an ideal inverting pulse (exactly 180° inversion). A third parameter can be included, one which allows for imperfection in this pulse. The formula is thereby expanded to:

$$(3) I(t) = \{I_\infty - (I_\infty - I(0))\} e^{-R_1 t}$$

The term $(I_\infty - I(0))$ allows for error in the inverting pulse.

Leipert and Marquardt³¹ have shown that the separate estimation of the two parameters I_∞ and $I(0)$ is not necessary, thus an experiment to measure I_∞ specifically is not required, since it can be estimated from the value of $I(0)$. It must be pointed out, however, that it is important

to have data points with $t > T_1$, in order to get an accurate three-parameter iteration. Such points are much less critical for two-parameter fitting, an important aspect which will be returned to shortly. Assuming that accurate data can be obtained for a wide range of t values, the principal difference between two- and three-parameter fitting reduces to a question of sensitivity of the iteration to errors in the inverting pulse. It has been clearly demonstrated³² that the R_1 value determined by non-linear regression analysis is insensitive to pulse width errors of up to $\pm 10\%$. Since the 180° pulse width can be very accurately determined on modern spectrometers, (within a few %), it is clear that three-parameter fitting is not an absolute necessity. In addition, Leipert and Marquardt³¹ have carried out statistical analyses on a series of control experiments, which show that two-parameter fitting gives consistently better fits to the relaxation data. The principal problem associated with the three-parameter fit is that, with an additional variable parameter, the variance of error is almost always greater, since errors in the iteration to both intensity parameters, will be propagated to the R_1 parameter. For example, the pulse width may be very carefully adjusted, but due to spectrometer instability, there are fluctuations in the intensity data. The iteration will attempt to compensate for these errors by adjusting all parameters, even though the pulse width is very accurate. This results in an erroneous R_1 value in the three-parameter analysis.

For the calculation of ^1H - R_1 values in particular, the presence of cross-correlation effects will have a serious effect on the accuracy of R_1 values calculated by three-parameter fitting. The three-parameter fit requires data points to describe the curvature of the recovery curve well beyond the initial slope region. Since data points beyond the initial slope region are inaccurate when cross-correlation is effective, the three-parameter fit will be correspondingly inaccurate. As a result, two parameter fitting of ^1H relaxation data is superior for measurement of ^1H - R_1 values of CH_2 and CH_3 groups, for which cross-correlation is known to be significant, and has been used here for all ^1H measurements. For the measurement of ^{13}C relaxation data under conditions of broad-band proton decoupling, the effects of cross-correlation are usually not significant. Using a modern spectrometer, these data are inevitably of very high quality (data are fitted rapidly and with high precision) and can be acquired over a wide range of t values, thus three-parameter fitting would be the method of choice because of its ability to better compensate for small pulse errors.

3.2.5. Summary of $^1\text{H-R}_1$ Discussion

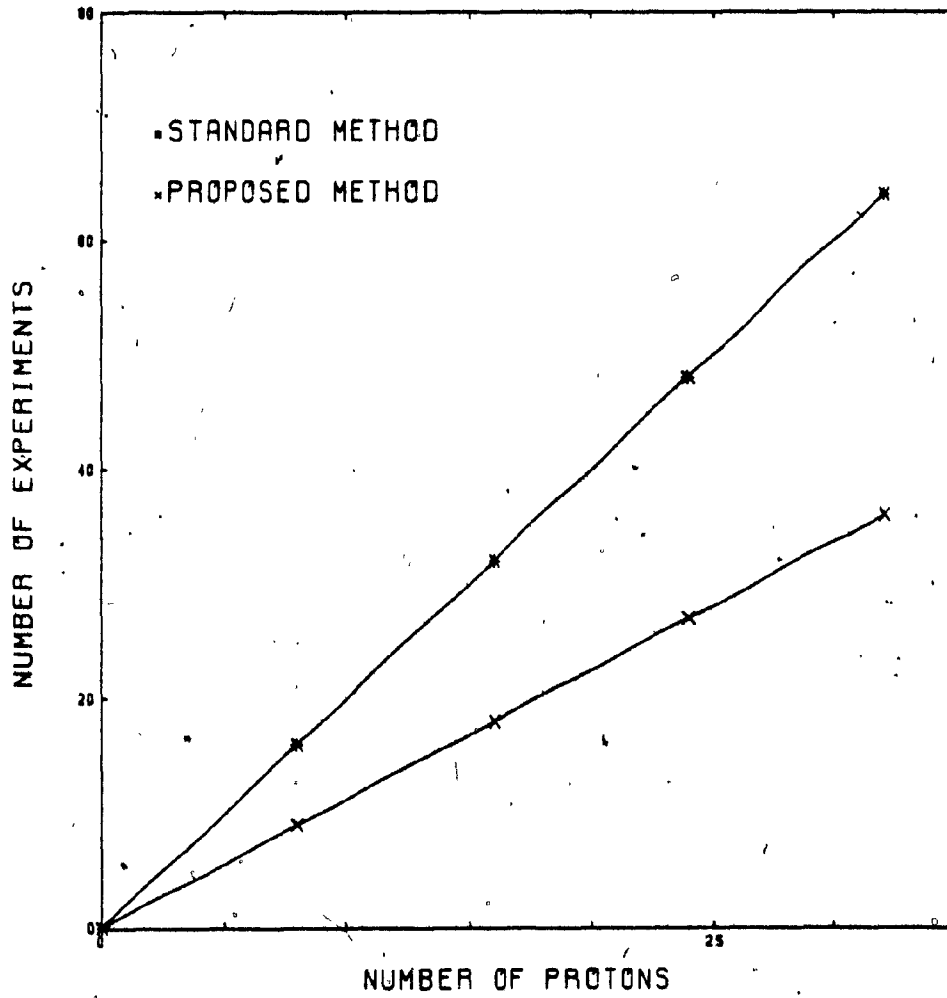
Some of the more critical aspects of measuring $^1\text{H-R}_1$ values reliably and efficiently have now been presented, leaving the question, "How rapidly can reliable results be obtained?". This is of great practical importance when considering the usefulness of an nmr technique. The answer, in part, depends on how accurate the results must be.

For qualitative studies, it is suggested that samples be prepared in the normal manner (0.1 M) without degassing. The experiments can be carried out at ambient temperature, and with the WH-400 spectrometer, acquisition of four scans per experiment into 16K data blocks over the typical 4000 Hz (10 ppm) spectral window is sufficient. The R_1 's can be reliably determined from stack plots by the null-point method. In this manner, the complete preparation, data acquisition, and analysis of reliable $^1\text{H-R}_1$'s requires only 1.5-2 hours. For more accurate results, better S/N and digitization is required, so acquisition of eight scans into 32K data blocks, and R_1 determination by regression analysis is suggested. The more refined analysis will require at least double the amount of time to obtain the data. Of course, for quantitative measurements, degassing would be required.

3.3. ^1H NOE Difference Experiments

3.3.1. Procedure for Obtaining Qualitative NOE Difference Spectra

Steady-state nOe difference spectra were obtained using a slightly modified version of the method of Hall and Sanders,³³ who acquired nOe spectra for four chemical shifts, with a single control. Our method is designed for efficient qualitative studies (see Fig. 3.4), emphasizing acquisition of an entire set of nOed spectra for the molecule under study. Difference spectra were obtained for up to eight different chemical shifts (on-resonance acquisitions), using only a single control (off-resonance acquisition). The acquisition of eight fids rather than four³³ after the equilibration period further improves efficiency by reducing the number of these equilibration periods by half. With these modification, and computer control of the decoupler, a complete set of nOe spectra could be obtained in a single overnight run (about 10 hrs.). It should be noted that this method requires that drift be kept to a minimum for clean subtraction, so that the high stability of a super-conducting magnet is necessary. Irradiation times were about $5XT_1$, although reliable data can be acquired with significantly smaller irradiation periods.



INCREASE IN EFFICIENCY OF DATA ACQUISITION

Fig. 3.4

The nOe difference spectra were then produced by subtraction of the reference free induction decay from the decay containing the nOe information. Both data sets were subjected to exponential multiplication corresponding to line broadening of 0.8-1.5 Hz, before Fourier transformation. Substantial line broadening optimized the quality of the difference spectra, particularly for tall, narrow lines. The resultant nulling of unenhanced signals was very satisfactory, as had been reported previously by Hall and Sanders.^{23,24} These workers also suggested the use of subsaturating power levels to achieve frequency selectivity. This proved to be satisfactory for most experiments. When complete selectivity could not be achieved, the approach taken was to acquire additional experiments in which incremental changes in the decoupler power or frequency were made.³⁴ By correlating the effects on enhancements to the changes in experimental conditions, the origin of observed enhancements could usually be determined. Occasionally, the observation of negative nOe enhancements (see Fig. 5.2) arising from three-spin effects* was also helpful in analyzing nOe enhancements in experiments where complete selectivity was not possible.

* For an explanation and example of three-spin effects, see Ref. 13.

The procedure is given in Chapter 9, and can be summarized by the following:

Acquisition

1. Pre-equilibration ($10XT_1$)
2. Acquisition of eight scans with $n0e$
3. Up to 3 additional on-resonance experiments (repeating 1 and 2)
4. Move saturation far off resonance and repeat 1 and 2
5. Up to 4 additional on-resonance cycles (repeating 1-4)
6. Recycle until sufficient S/N (25-100 times)

Data Processing

7. Exponential multiplication (1-2 Hz), all fids
8. Subtract control fid from fid with $n0e$
9. Fourier transform

3.3.2. Sensitivity Advantage of a Difference Spectrum

Conventional measurement of $n0e$ enhancements by integration of full peak areas is subject to large inherent errors, particularly for small enhancements or in crowded spectra. The subtraction of a carefully acquired control spectrum from the spectrum with the $n0e$ enhancements greatly enhances the sensitivity of the $n0e$ experiment (Fig. 3.5).

The high sensitivity of the difference technique can often be used to great advantage as a means of identifying the component resonances in a crowded region of the spectrum, as demonstrated in Fig. 3.6 for the overlapping H15a, H17b, and H22a resonances in neo-strychnine.

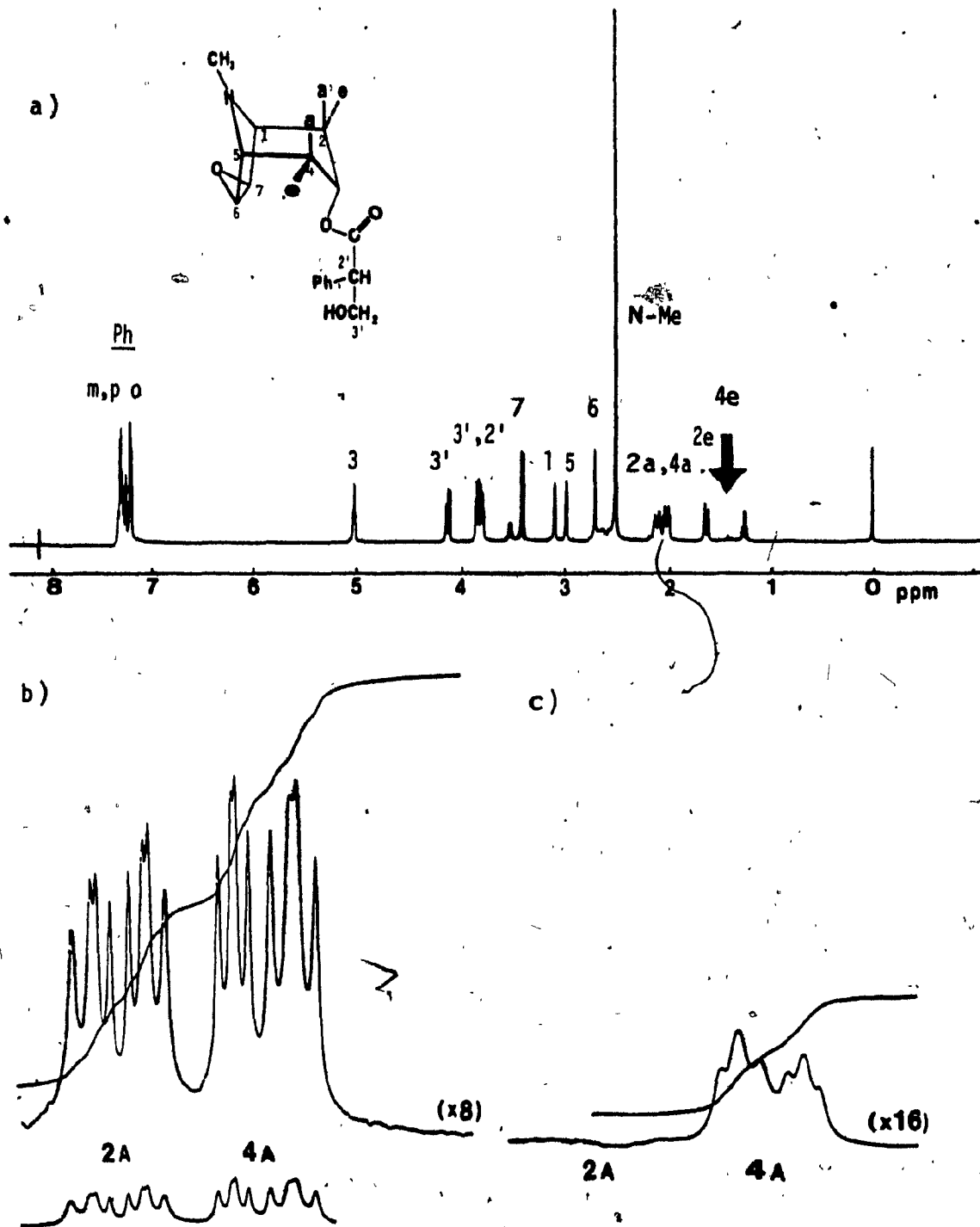


Fig. 3.5 400 MHz nmr spectra of scopolamine (0.1 M CDCl_3) with saturation of H4e: a) full spectrum, b) expansion of H2a/H4a region, c) same as b) from the difference spectrum.

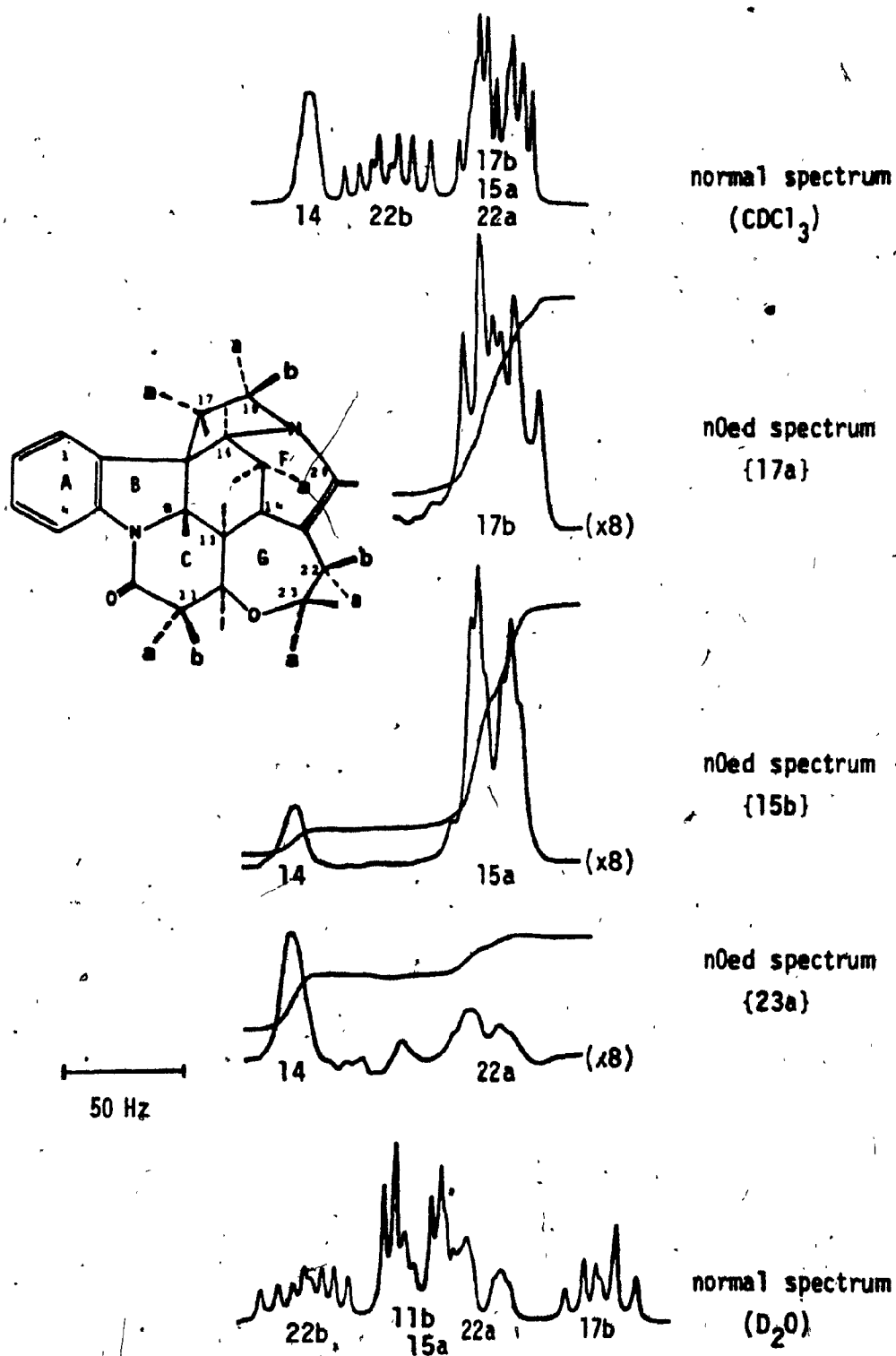


Fig. 3.6 Partial 400 MHz ^1H spectra of neo-strychnine demonstrating the use of nOed spectra to reveal the component resonances of highly overlapped regions of the normal spectrum.

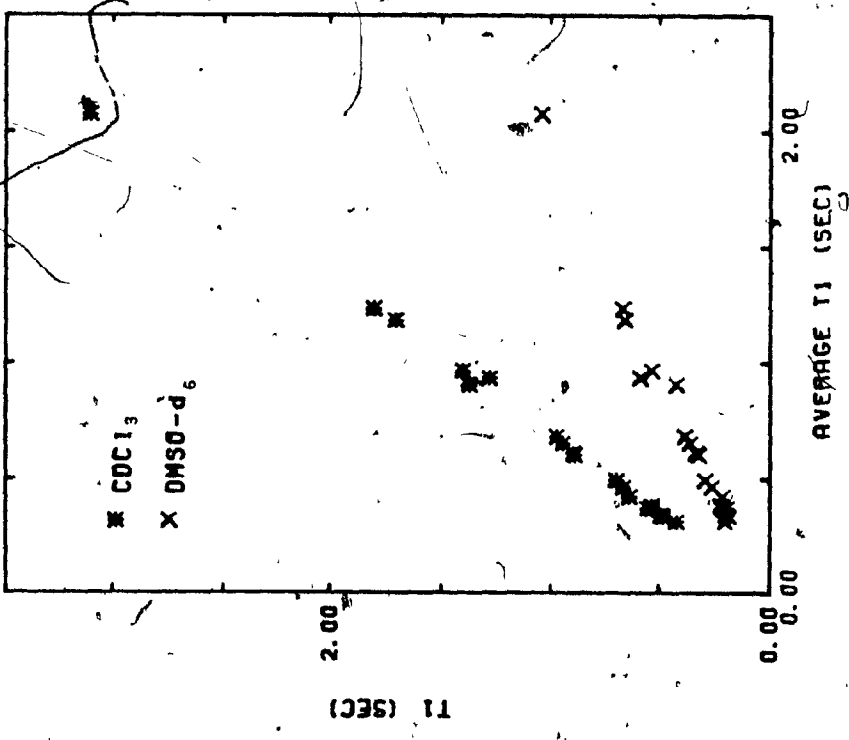
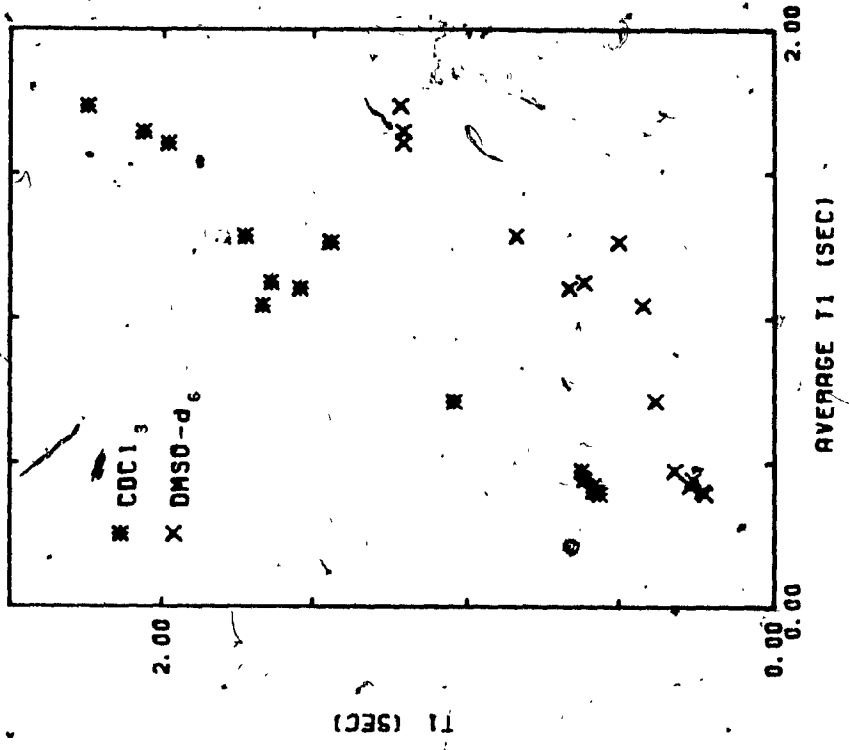
3.3.3. Choice of Solvent

Presuming that the interaction between solute and solvent is non-specific, a solvent with higher viscosity will be preferred, since relaxation times will be lower. This effect is demonstrated in Fig. 3.7 for CDCl_3 and DMSO-d_6 solutions of strychnine and codeine. Shorter T_1 values will mean shorter pre-equilibration and irradiation periods, and correspondingly shorter times to acquire the nOe enhanced spectrum. The relationship between relaxation time and the time required for acquisition of 400 scans with nOe for a single proton in a typical experiment is shown in Fig. 3.8. The resultant solvent dependence of total acquisition time for all the protons in codeine and strychnine is shown in Fig. 3.9.

3.3.4. Irradiation Time

A critical constraint in the nOe experiment is the time of irradiation. Ideally, the full nOe enhancement will be obtained when the proton under study has been saturated for a time $D \gg T_1$, typically $D = 5X(T_1)$. In practice, there are several complicating factors, which suggest the use of shorter periods [$D = (2-3)X(T_1)$].

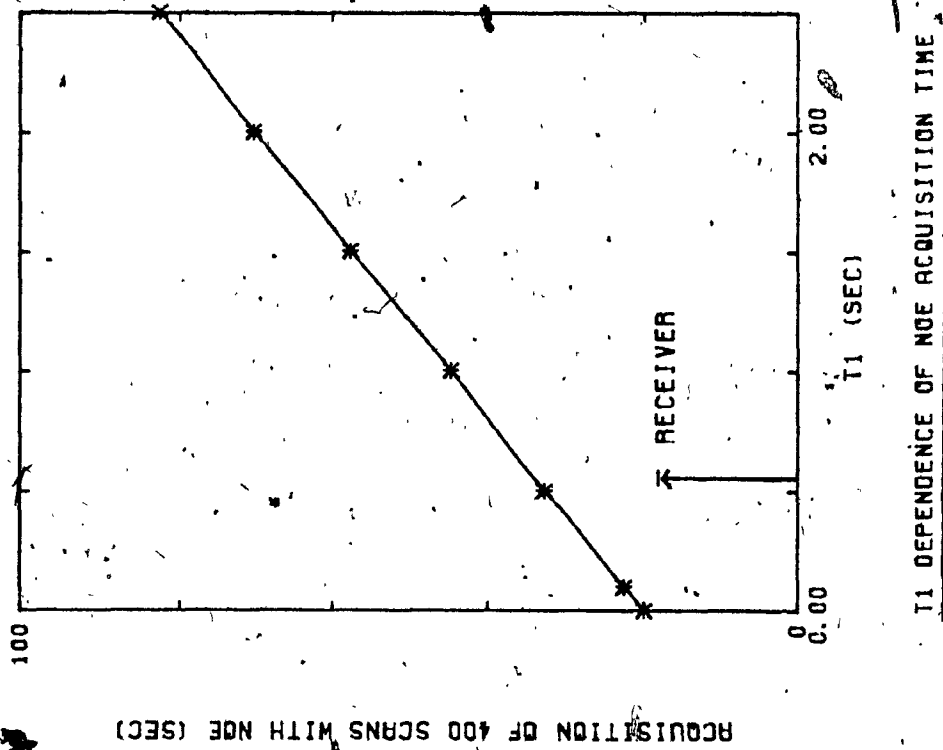
The presence of three-spin effects,^{5,35} which give rise to negative enhancements, will prevent the accurate determination of specific nOe enhancements. The three-spin effect depends on the presence of a specific negative enhancement, which develops more slowly than a normal nOe .



SOLVENT DEPENDENCE OF T1 - CODEINE

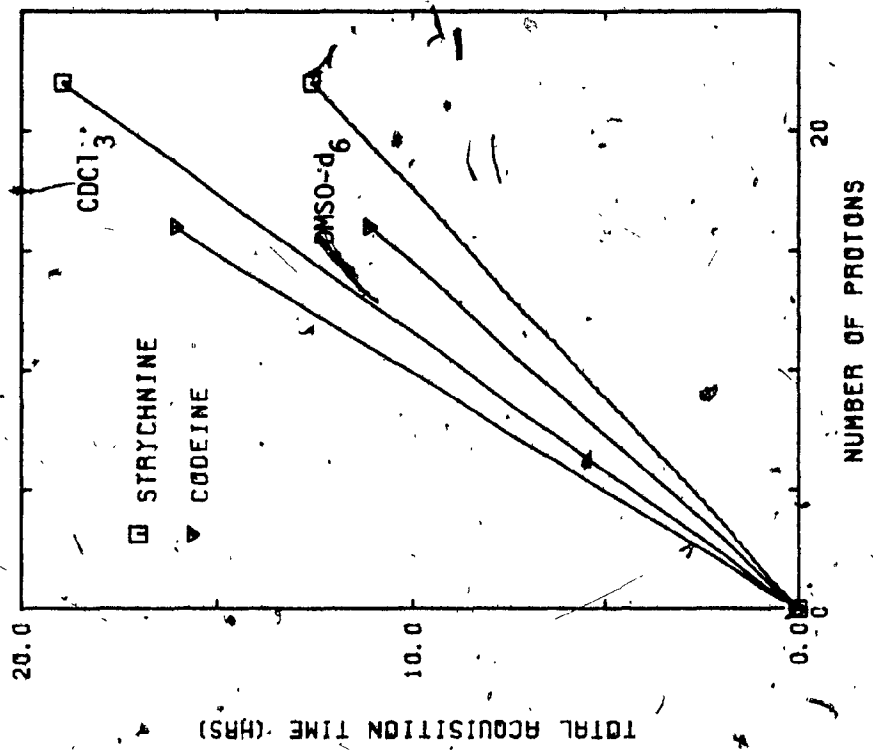
SOLVENT DEPENDENCE OF T1 - STRYCHNINE

Fig. 3.7



T1 DEPENDENCE OF NOE ACQUISITION TIME

Fig. 3.8



SOLVENT DEPENDENCE OF TOTAL ACQUISITION TIME

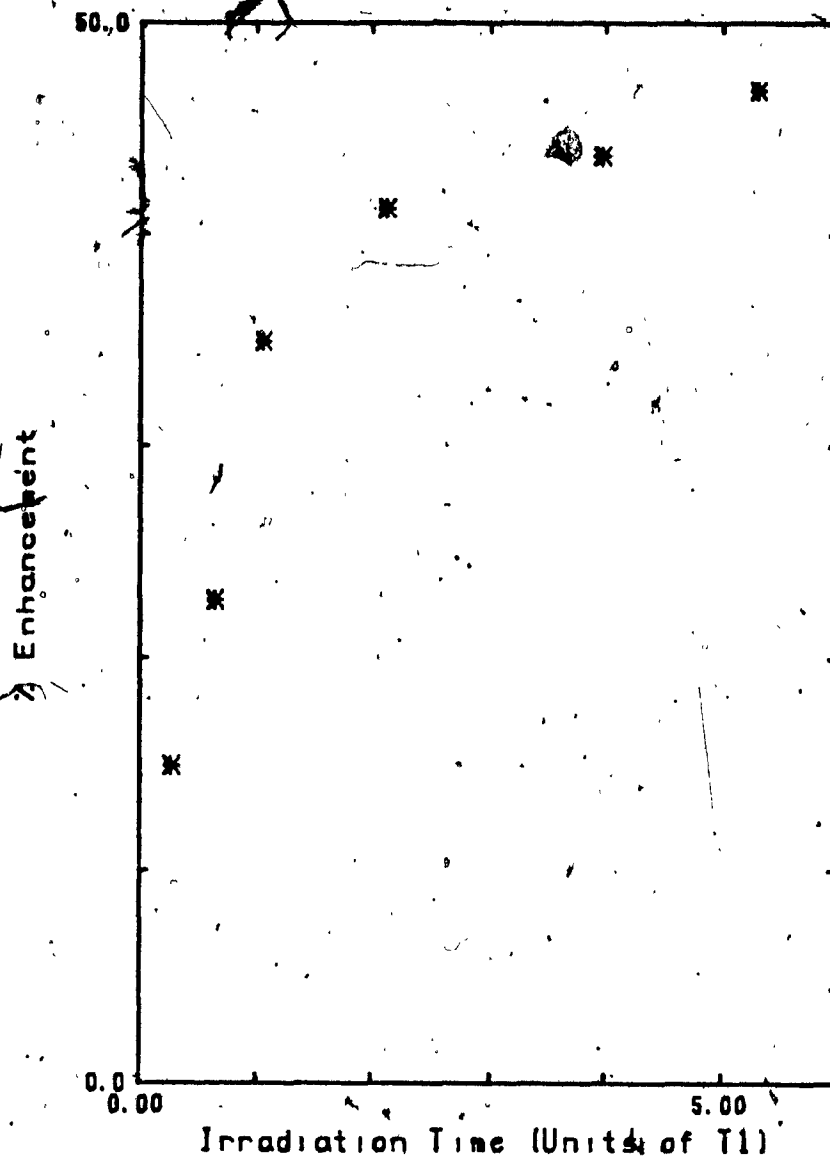
Fig. 3.9

Utilization of short irradiation times will, therefore, prevent the three-spin effect from becoming significant. The three-spin effect can, however, be extremely useful for the determination of dipolar connectivities which are difficult to observe under normal experimental conditions.³⁵

The principal benefit from using short irradiation periods is that the overall efficiency of the experiment is improved; sufficient S/N is acquired in a shorter period of time. The bulk of the nOe enhancement builds up in the initial part of the $5X(T_1)$ saturation period, thus a considerable time saving is realized using the $2-3X(T_1)$ period, without a great loss in the magnitude of the observed of the enhancement. The dependence of the magnitude of the nOe enhancement on the length of the irradiation period is demonstrated in Fig. 3.10.

When short irradiation periods are used, the full nOe enhancement cannot be observed. However, this is not a particular problem, since:

1. In most molecules, full enhancement is not observable due to tight-coupling or three-spin effects.
2. Full enhancements are not necessary for most qualitative studies.



NOE DEPENDENCE ON IRRADIATION TIME

Fig. 3.10 Observation of the NOE enhancement of H4/6 in 1,2,3,5-tetramethylbenzene (0.1 M CDCl_3 , degassed) upon saturation of Me-1/3 and Me-5.

3.3.5. Saturation Efficiency Versus Selectivity

The ability to selectively saturate a specific resonance in any region of the spectrum is by far the most critical technical problem associated with any 1-D measurement of the nOe . The selectivity criterion is demonstrated for the saturation of H_{2e} and H_{4e} in scopolamine in Fig. 3.11.

By reducing the decoupler power to successively lower levels, the desired selectivity can often be obtained, but in many cases, at the expense of the magnitude of the observed enhancement. The dependence of the magnitude of the observed nOe on the power of the saturating field is shown for H_2/H_4 in 1,2,3,5-tetramethylbenzene in Fig. 3.12.*

For small enhancements, this is a critical problem.

The alternative is to reduce the saturation power just enough to achieve a certain degree of selectivity, then to increment the decoupler frequency through the region of interest. This procedure can also be utilized by incrementing the saturation power. Often, the two methods are combined, and upon correlation of the data, unambiguous results are obtained. In Fig. 3.13, an example of this approach is demonstrated for the two overlapped Me-3b and Me-3!a doublets in a hexamethyl 7-hydroxyindene dimer.

* The resonances of Me-1/3 and Me-5 are so close in the spectrum that they can be saturated simultaneously and a nearly full nOe is observed.

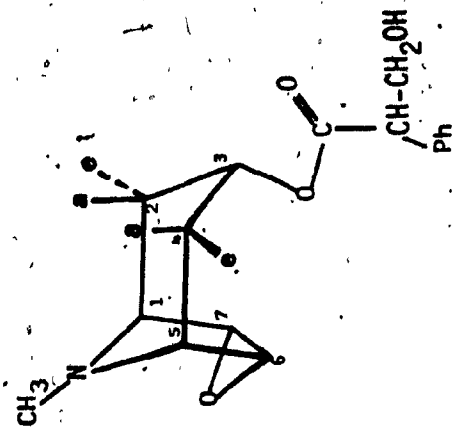
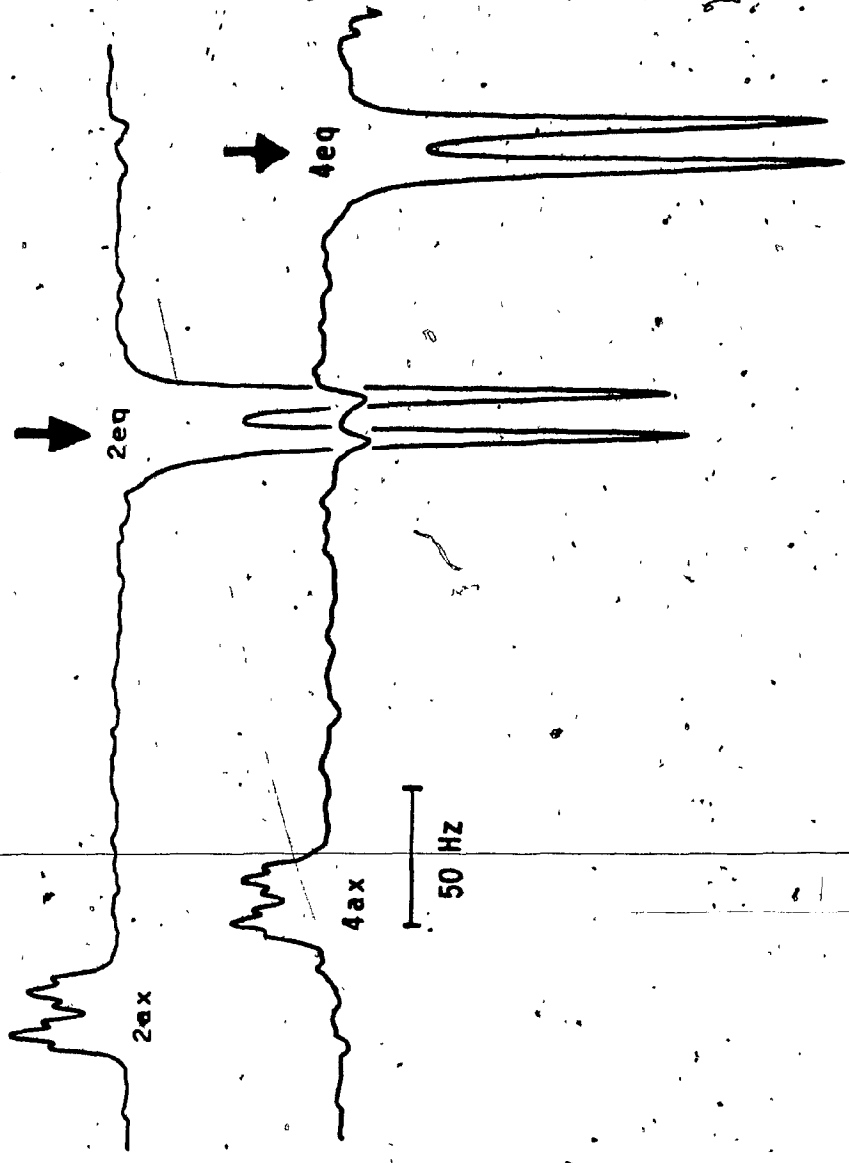


Fig. 3.11 400 MHz ¹H nmr difference spectra from a 0.1 M CDCl₃ solution of scopolamine demonstrating selectivity in saturation.

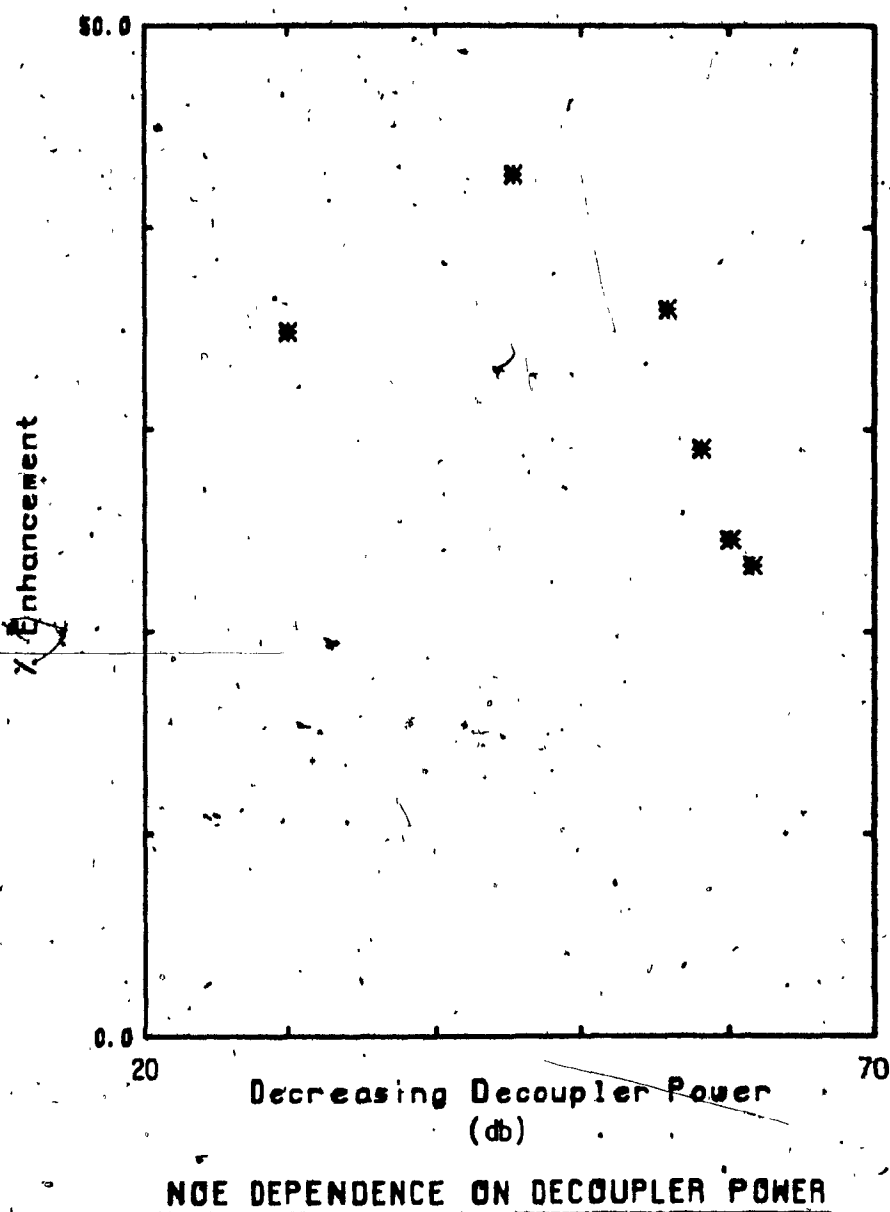


Fig. 3.12. Observation of the NOE enhancement of H_{4/6} in 1,2,3,5-tetramethylbenzene (0.1 M CDCl₃, degassed) upon saturation of Me-1/3 and Me-5.

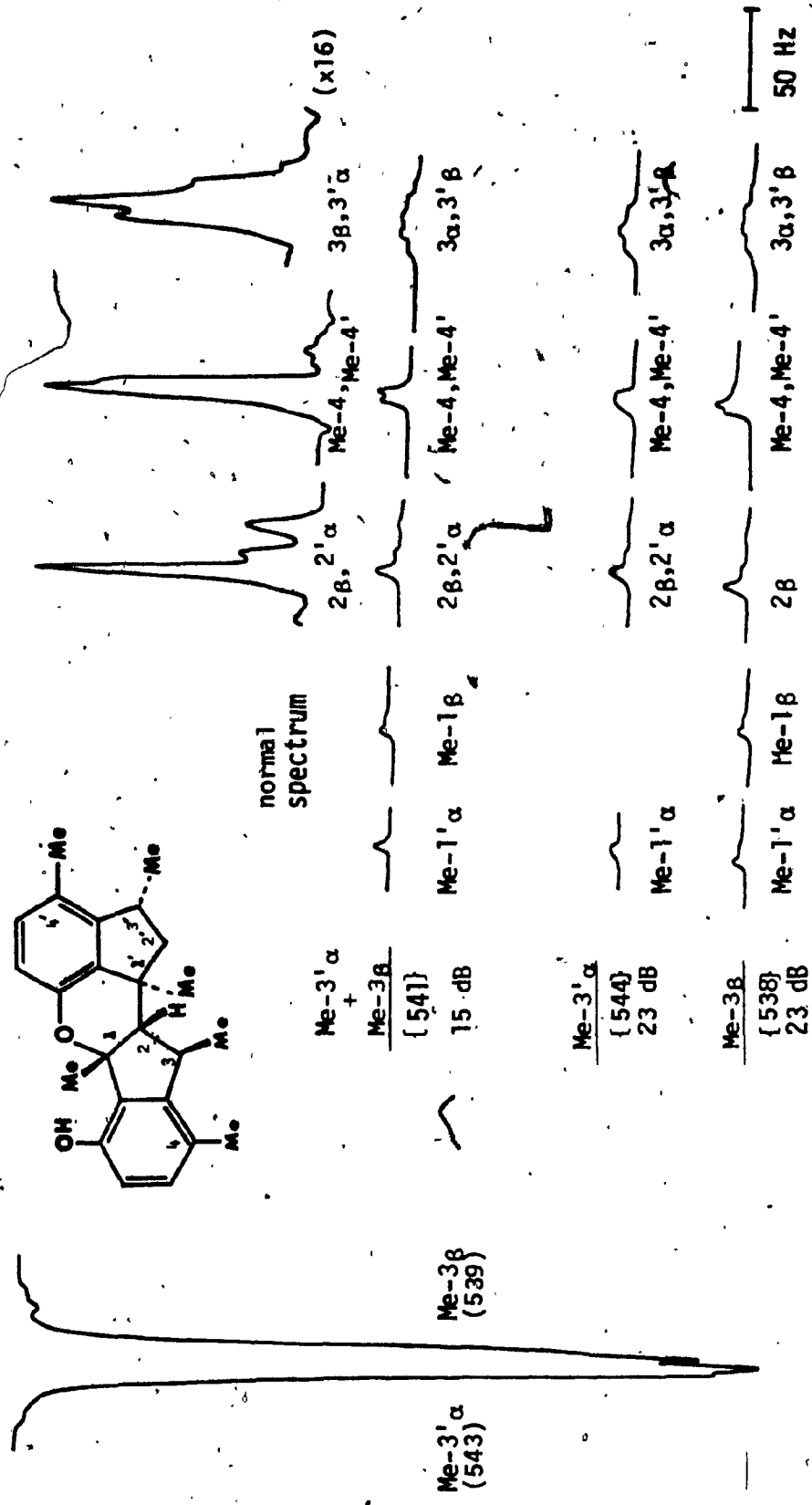


Fig. 3.13 Partial 400 MHz ¹H nmr spectra of 7-Hydroxyindene dimer 5 (0.1 M CDCl₃) demonstrating the technique of incrementing decoupler power and frequency to determine the origin of nOe enhancements which cannot be observed due to problems associated with saturation selectivity.

3.3.6. Summary of ^1H -NOE Difference Experiments

The determination of the precision and accuracy in the measurement of the nOe enhancement becomes increasingly complex with an increase in the number of protons in the molecule. The principal advantage of the difference technique is the higher selectivity and sensitivity in detection of the nOe. In all studies, the relative nOe enhancements within a single difference experiment can be taken to be quite reliable. The comparison of enhancements measured in different experiments must, however, be avoided in qualitative studies, due to the often incomplete saturation of resonances. All of the factors that have been discussed above will affect the accuracy of the measured enhancement in a standard or difference nOe spectrum, but it is clear that the precision of nOe measurement in complex spectra will, invariably, be superior to the standard measurement.

Chapter 4

A SURVEY OF ^1H SPIN-LATTICE RELAXATION IN ALKALOIDS

4.1. Introduction

In this and the following chapter, $^1\text{H-R}_1$ values measured for four cinchona, four tropane, seven morphine, and ten strychnos alkaloids will be presented and analyzed. These four classes have been selected because they are representative of the variety of structures encountered in the alkaloid family. Within each group, the compounds were chosen to be rather similar in structure, so that an evaluation of the sensitivity of $^1\text{H-R}_1$ measurements to specific structural features could be made. In addition, the molecules were selected on the basis of availability and chemical interest, with respect to their structure, nmr spectra, and biological activity. It is of interest to note that these are the first high field nmr studies of almost all of the molecules.

It is intended to show here how $^1\text{H-R}_1$ analysis can be utilized to obtain specific insights into the solution structures of alkaloids. In certain instances, it is possible to make an unambiguous structural assignment on the basis of R_1 data alone, but frequently it is necessary to rely on other sources of information to corroborate the analyzed R_1 data. The measurement of nOe enhancements has proven to be particularly valuable in this respect, as will become apparent in these chapters. In fact, the nOe

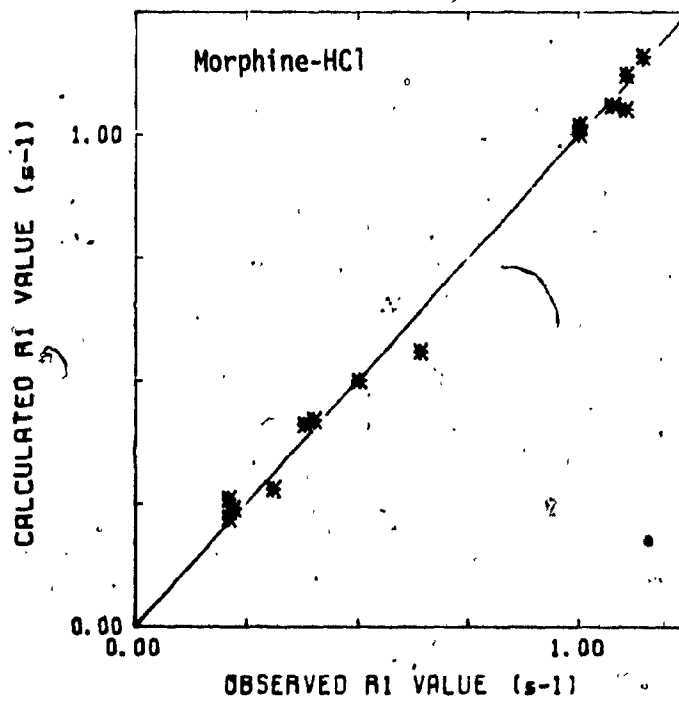
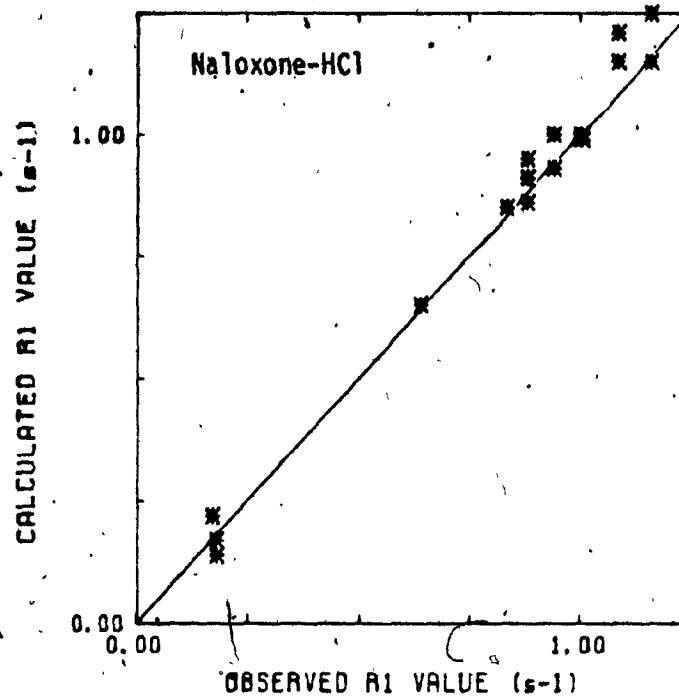
Analysis is sometimes much more effective than R_1 analysis. It is rarely advisable, however, to attempt nOe measurements before determining R_1 values, since the latter can be obtained with a substantially smaller investment of machine time, and are useful in guiding the selection of relevant nOe experiments.

4.2. Calculation of Relaxation Parameters

In any R_1 analysis of a complex molecule, some form of modelling is invariably required to aid in interpretation of the data. As pointed out in Chapter 2, calculations of both R_1 (2.40) and nOe enhancements (2.39) can be carried out using a simple mathematical model for dipolar relaxation, by assuming a completely first order spin system(s) and isotropic overall tumbling of the molecule. The required inter-proton distances can be measured on Dreiding molecular models, or calculated using crystal coordinates determined by X-ray or neutron diffraction.* The advantages of the crystal coordinate method are:

1. No cumbersome measurements on a molecular model.
2. All calculations are carried out by computer.
3. Direct comparisons between crystal and solution structure are possible, once the solution structure has been refined.

* Since the coordinates of H atoms cannot normally be determined to a high degree of confidence from X-ray studies, the H positions are calculated assuming standard C-H, N-H, and O-H bond lengths and angles.



EVALUATION OF RELAXATION MODEL

Fig. 4.1

An indication of the quality of the modelling scheme can be obtained by comparing the fit of calculated and observed R_1 values in an isotropically tumbling molecule that has a considerable range of structural features and R_1 values. Some comparative data for two morphine alkaloids are given in Fig. 4.1. In general, there is excellent agreement between calculated and observed data. The calculated relaxation pathways can, therefore, be utilized with confidence for the analysis of experimental data.

4.3. General Uses of ^1H - R_1 Values

Relaxation data for complex molecules can be used in a variety of ways. The simplest example is the identification of two or more overlapped resonances in partially relaxed spectra (Fig. 4.2).

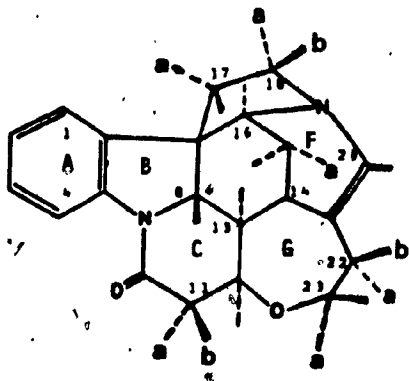
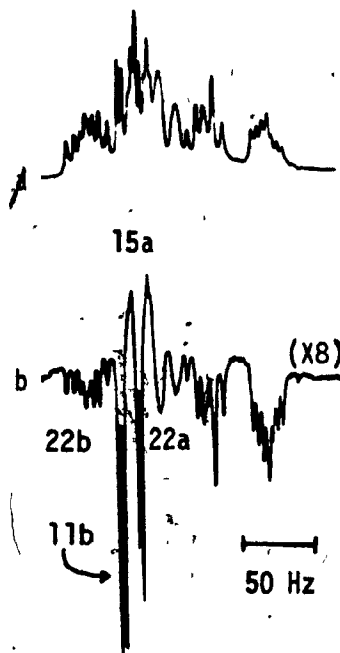


Fig. 4.2. Partial 400 MHz inversion-recovery ^1H nmr spectra:
a) $t = 0.44$ s, b) $t = 0.20$ s.



Due to the extreme dependence on inter-proton distance, $^1\text{H-R}_1$ values provide a fast and reliable means of differentiating those protons which have efficient relaxation pathways from those that do not. It is usually possible to rapidly distinguish three separate groups of protons in the spectrum by their $^1\text{H-R}_1$ values:

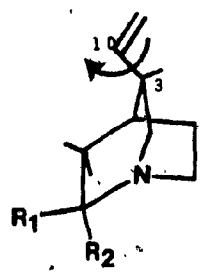
1. Methylene protons- relax rapidly due to the close proximity of the geminal partner.
2. Aliphatic methine protons- relax in an intermediate range.
3. Aromatic and other isolated protons- relax more slowly than aliphatic methines, because they have fewer vicinal neighbors and no trans-diaxial interactions.

It is important to note that these divisions are by no means absolute. In certain molecules, the ranges of R_1 values will overlap; and in some instances, specific structural features may substantially raise or lower a specific R_1 value, relative to the other protons in its group.*

$^1\text{H-R}_1$ values can also give an indication of additional degrees of motional freedom which may be available to certain parts of a molecule. The specific case of methyl rotation will be discussed in detail in Chapter 7. In addition to methyl rotation, there are various types of segmental motion possible in side chains of the molecule.

* Frequently, it is just these unusual resonances which prove to be of vital importance in the analysis of the solution structure.

The increase in the rate of motion will have the effect of reducing t_c and the R_1 value, hence, uncharacteristically small R_1 values are an indication of additional motional freedom. For example, the 11c and 11t methylene protons in cinchona alkaloids, I, relax considerably slower ($1.1-1.5 \text{ s}^{-1}$) than all other methylene pairs ($4.5-7.3 \text{ s}^{-1}$), the aliphatic methine protons ($2.2-4.0 \text{ s}^{-1}$), and far lower than the rate predicted by calculation. These very low R_1 values reflect the freedom of the vinyl group to rotate about the C3-C10 bond.



4.4. Cinchona Alkaloids

The antimalarial activity of cinchona alkaloids, in particular quinine, has been the subject of study for a number of years.³⁶ More recently, quinidine has been shown to have potent antiarrhythmic activity.³⁷ The basic molecular structure of cinchona alkaloids consists of two parts, a quinoline ring and a quinuclidine ring, bridged by a single C atom (C9), as shown in Fig. 4.3. Four structurally similar compounds were utilized for nmr

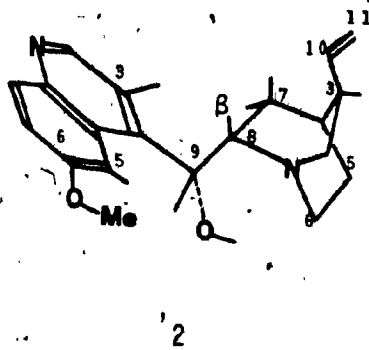
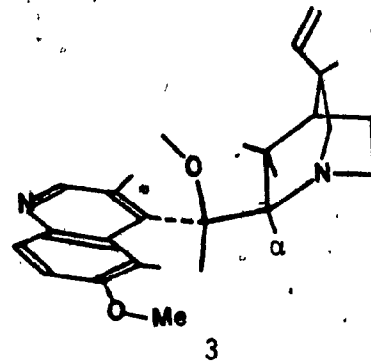
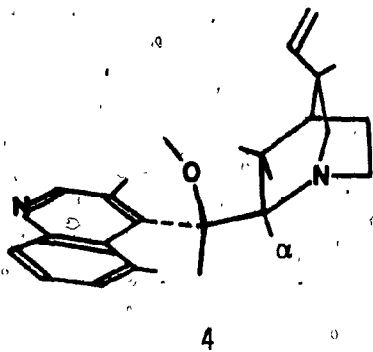
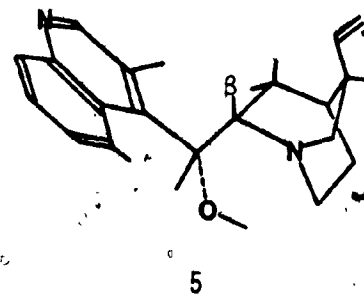
2
quinine3
quinidine4
cinchonine5
cinchonidine

Fig. 4.3 Structures of the cinchona alkaloids.

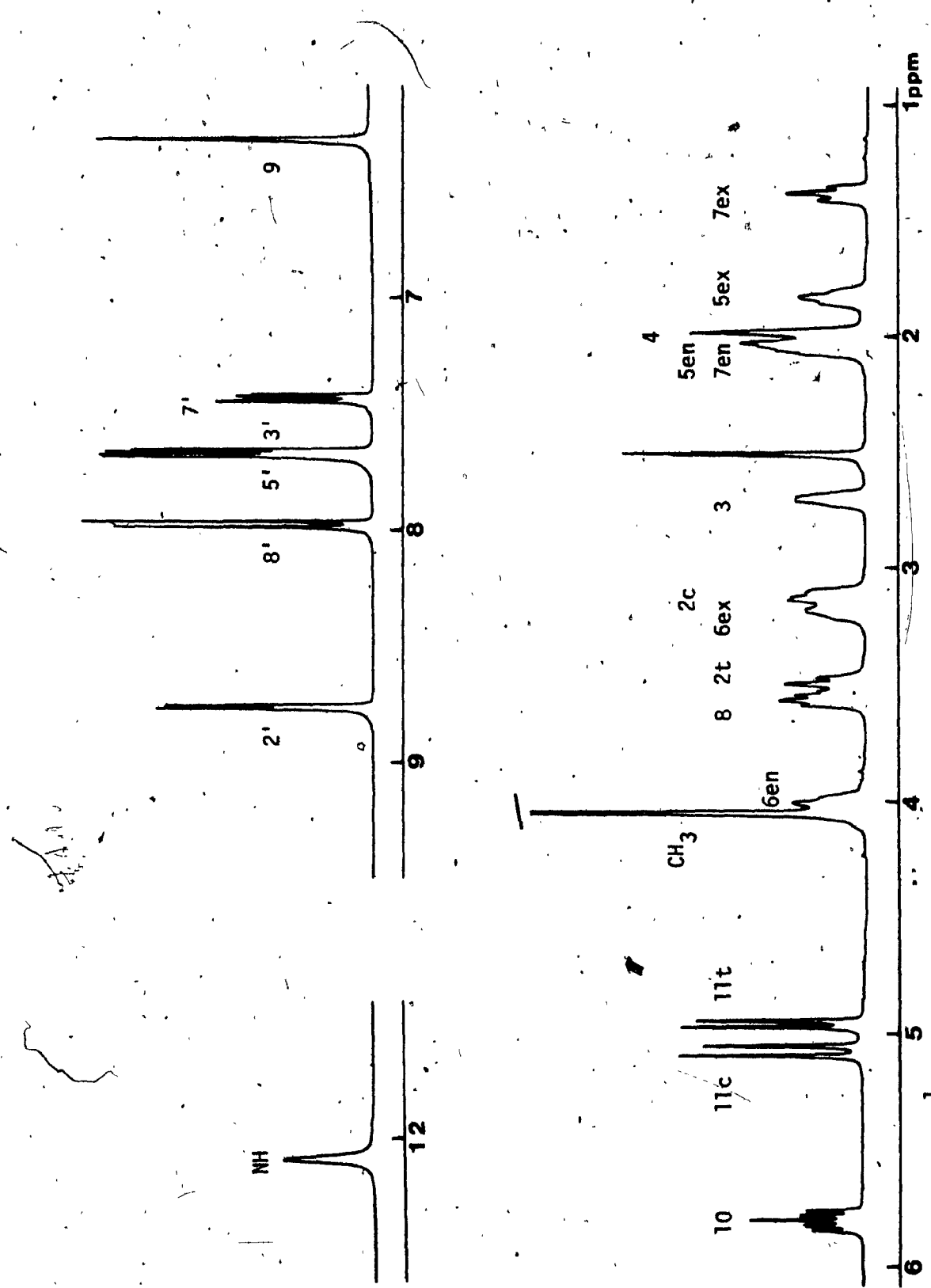


Fig. 4.4 400 MHz ^1H nmr spectrum of quinine-HCl, 0.1 M DMSO-d_6 .

studies- quinine, quinidine, cinchonine, and cinchonidine. The primary structures of these molecules differ only at C6', where quinine and quinidine have a methoxy group. Cinchonine and cinchonidine are isomeric at C8 and C9, as are quinine and quinidine. Note that it is cinchonine and quinidine, not quinine, that have the same 8_g,9_S configuration.

The 400 MHz ¹H spectral parameters reported here result from the first high field studies of cinchona alkaloids. The spectrum of quinine-HCl is shown in Fig. 4.4. Assignments of all resonances for these four compounds are given in Table 4.1. Spin-spin coupling constants have been assigned with the aid of computerized resolution enhancement.⁶⁶ Typical values are given in Table 4.2. The assignments have been made with the aid of molecular models on the basis of standard methods of analysis (theoretical considerations, decoupling experiments, and computer simulations) and relaxation data. There will be no further discussion of the assignments of cinchona alkaloids, since the technique will be described for other alkaloids whose assignments were more difficult to make.

Upon consideration of molecular models, several important structural features of cinchona alkaloids are evident. Both the quinoline and quinuclidine rings are rigid structures, and since they are bridged by a single atom, there is very little motional freedom about the bonds

Table 4.1

Chemical Shifts of Cinchona Alkaloids

	<u>quinine</u>	<u>quinidine</u>	<u>cinchonine</u>	<u>cinchonidine</u>
2'	8.76	8.75	8.93	8.92
3'	7.66	7.64	7.69	7.69
5'	7.68	7.66	8.54	8.65
6'	-	-	7.69	7.66
6'-OMe	4.04	4.03	-	-
7'	7.43'	7.42	7.81	7.80
8'	7.98	7.97	8.09	8.07
2c	3.11	3.99	3.98	3.09
2t	3.49	3.41	3.42	3.49
3	2.70	2.65	2.65	2.69
4	1.97	1.91	1.91	1.98
5ex	1.82			1.82
5en	2.03 ⁺	1.77*	1.77*	2.05 ⁺
6ex	3.17	3.16	3.19	3.19
6en	4.00	3.38	3.34	3.97
7ex	1.38	2.32	2.32	1.41
7en	2.03 ⁺	1.11	1.14	2.05 ⁺
8	3.56	3.52	3.49	3.55
9	6.32	6.51	6.49	6.29
10	5.82	6.06	6.06	5.79
11c	5.07	5.22	5.22	5.07
11t	4.95	5.21	5.21	4.95
NH	12.09	12.07	11.75	11.83

1. Measured from 0.1 M DMSO-d₆ solutions of the HCl salts, referenced to 0.1% internal TMS. Values in ppm. "*" = tight coupling, "+" = severe overlap.

Table 4.2

¹H Spectral Parameters of Quinine-HCl¹

H	δ (ppm) ²	J (Hz) ²
2'	8.758	2',3' = 4.5
3'	7.659	
5'	7.681	5',7' = 2.7
6'-OMe	4.044	
7'	7.432	7',8' = 9.0
8'	7.975	
2c	3.108	2c,2t = 13.5
2t	3.489	2t,3 = 10.5
3	2.695	3,4 = 7
		3,11t = 0.9
4	1.973	4,5en = 2
		4,7en = 1
5ex	1.824	5ex,5en = 12
		5ex,7ex = 3.6
5en	2.03	5en,6ex = 5.7
6ex	3.172	6ex,6en = 11.6
6en	4.000	
7ex	1.378	7ex,7en = 13.5
7en	2.03	7en,8 = 7.0
8	3.558	8,9 = 1.0
10	5.824	10,11c = 17.0
11c	5.071	11c,11t = 1.2
11t	4.954	
NH	12.09	
		2c,6en = 2
		3,10 = 7
		3,11c = 0.9
		4,7ex = 2
		5ex,6ex = 11.6
		5en,6en = 11.4
		7ex,8 = 10.5
		10,11t = 10.5

1. Measurements made from a 0.1 M solution in DMSO-d₆ at ambient probe temperature (20°C), with 0.1% TMS as internal reference.

2. The precision of measurement was ± 0.003 ppm in chemical shifts (δ) and ± 0.2 Hz in coupling constants (J), unless indicated by a smaller number of significant figures. The signs of J values have not been determined.

in the bridge due to adverse steric interactions. This implies that the entire molecule tumbles as a single unit, except for the pendant substituents at C6' and C3, thereby simplifying R_1 analysis.

The determination of structural features by relaxation parameters required both $^1\text{H-R}_1$ and $-n\text{Oe}$ measurements. The great similarity in primary and secondary structure of these four molecules is reflected in the remarkable consistency of the $^1\text{H-R}_1$ values (Table 4.3). Analysis of relaxation pathways by calculation using the crystal coordinate method indicates that the effective proton environments (and, therefore, the $^1\text{H-R}_1$ values) for protons at 2', 8', 2t, 3, 4, 5ex, 6ex, 10, 11c, and 11t should be completely unaffected by the structural differences. These calculations also lead to predictions of several important inter-ring relaxation pathways, which were subsequently characterized by $n\text{Oe}$ enhancements. In addition, detailed relaxation pathway analysis was utilized for determination of the stereochemistry at C8. The determination of the conformation of the 6'- OCH_3 group in quinine and quinidine was possible by $^1\text{H-R}_1$ analysis alone.

Table 4.3

Normalized R_1 Values of Cinchona Alkaloids

	<u>quinine</u>	<u>quinidine</u>	<u>cinchonine</u>	<u>cinchonidine</u>
2'	.17	.13	.16	.13
3'	.27	.27	.25	.28
5'	.54	.56	.51	.50
6'	-	-	.25	.23
6'-OMe	.39	.39	-	-
7'	.13	.13	.19	.20
8'	.13	.12	.12	.13
2c	1.07	1.00	1.00	1.07
2t	1.32	1.08	1.29	1.12
3	.48	.51	.49	.47
4	.58	.47	.47	.54
5ex	(4.78)	(5.1)*	(5.1)*	(4.78)
5en	.9 ⁺	1.0*	1.0*	1.0 ⁺
6ex	1.53	1.12	1.23	1.21
6en	1.12	1.12	1.17	1.12
7ex	.97	1.00	.93	1.00
7en	.9 ⁺	1.04	1.00	1.0 ⁺
8	.71	.70	.73	.72
9	.74	.68	.77	.76
10	.24	.24	.23	.24
11c	.30	.27	.25	.32
11t	.26	.23	.21	.27

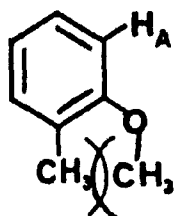
1. All values measured from 0.1 M DMSO- d_6 solutions of the HCl salts, and normalized to the R_1 (in parentheses ()) of H5ex.

"*" = tight coupling, "+" = overlap problem.

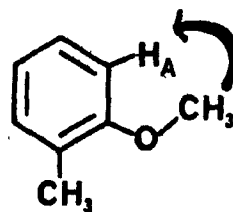
4.4.1. Methoxy Group Conformational Preferences

A series of recent publications has demonstrated how spin-lattice relaxation techniques can be applied to the detection of methoxy group conformational preferences in a variety of molecules.^{38,39,40} Sanders and coworkers⁴¹ have outlined the basis for interpretation of relaxation parameters, but have concentrated on analysis of nOe enhancements. A new method, utilizing $^1\text{H-R}_1$ measurements for this conformational analysis, will be described and demonstrated in this section.

Conformational bias of the methoxy group in simple compounds such as o-methylanisole is well characterized.^{42,43}



A



B

The R_1 value of H_A in conformation A is predicted to be significantly lower than that of all other ring protons, because the methoxyl protons are rather distant and, therefore, less efficient than a ring proton in causing H_A to relax. In conformation B, the H_A R_1 value would be higher than the other ring protons, because the methoxyl protons would be quite close to H_A , and the relaxation pathway

would be efficient. The experimentally observed 50% elevation of the $^1\text{H-R}_1$ value of H_A indicates a preference for conformation B.⁴⁴ The interpretation of R_1 values in more complex systems may require additional selective- R_1 or nOe measurements, however, in many aromatic systems, it appears that conformational bias is clear-cut³⁸ and other experiments are not necessary. This method of analyzing methoxyl conformations can be applied to the cinchona alkaloids, quinine, 2, and quinidine, 3. The pertinent $^1\text{H-R}_1$ values are given in Table 4.4. The corresponding data for 6'-H analogues cinchonidine, 5, and cinchonine, 4, respectively, are included for comparison.

Table 4.4

Selected R_1 Values for 2, 3, 4, and 5

	R_1 (s^{-1})			
<u>H</u>	<u>2</u>	<u>3</u>	<u>4</u>	<u>5</u>
5'	.54	.50	.57	.51
7'	.13	.20	.13	.19
8'	.13	.13	.12	.12

1. All measurements on 0.1M solutions of HCl salts in DMSO-d_6 at 20°C . R_1 values normalized to H5-ex.

Consider, first, the effects on the R_1 of H7'. This proton, rather isolated from the rest of the molecule, is relaxed primarily by protons at the 6' and 8' positions, with a much smaller contribution from protons at 5'. In 2 and 3, where there is a methoxy group at 6', R_1 values for H7' are expected to be substantially different from those in 4 and 5, when the methoxy groups has a definite conformational preference. In the 7'-cis orientation, the relaxation pathway from the methoxy group to H7' will be very efficient, so the H7' R_1 values should be higher than the corresponding values in 5 and 4. Alternatively, if the 5'-cis orientation is greatly preferred, the H7' R_1 values should be lower than those in 5 and 4. The observed R_1 values indicate a bias of the methoxy group towards H5' in compounds 2 and 3.

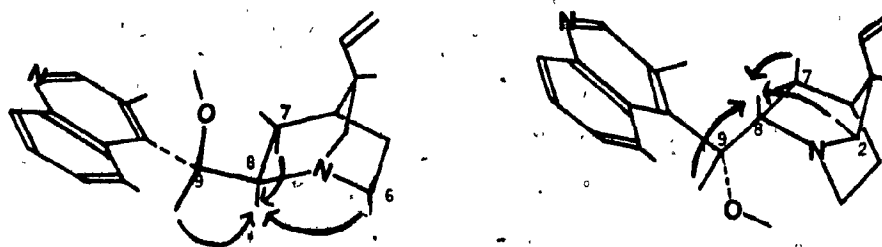
This deduction is further corroborated by comparison of H7' R_1 values to those of H8'. H8' is relaxed almost exclusively (>90%) by interaction with H7' in all four compounds, so the observed similarity in H8' R_1 values is expected. In 4 and 5, H7' has a higher R_1 value than H8' because it is relaxed not only by H8', but also H6' (about 49% each). Note that there are no other major contributors to H7' relaxation. The near equivalence of H7' and H8' R_1 values in 2 and 3 must, therefore, reflect the loss of a major relaxation pathway, implying that these two protons are equally isolated (they are relaxing only to each other), hence, the methoxy group must be strongly favoring the 5'-cis orientation.

If the methoxy group prefers the 5'-cis orientation, an increase in the R_1 of H5' is expected. The magnitude of this effect should, however, be much smaller than that felt at H7', because H5' has several efficient relaxation pathways from protons outside the quinoline ring (eg. H8, H9). The much larger H5' R_1 values, relative to those for the other quinoline ring protons in all four compounds, provide clear indications of these additional relaxation pathways. Calculations of the various contributions to H5' relaxation indicate that the maximum methoxy group contribution (when the methoxy group is locked in the 5'-cis orientation) is 30%. The observed +10% difference in the H5' R_1 value in 2 and 3, relative to the 6'-H analogues (5 and 4, respectively), is only consistent with a definite 5'-cis methoxyl conformational preference.

The R_1 data are completely consistent in their indication of a very significant 5'-cis conformational bias for the methoxy group in 2 and 3. It is of interest to note that this conformation is observed in the crystal state, as determined by X-ray diffraction analysis.⁴⁵ As a check on the R_1 data, the nOe method as outlined by Sanders, et.al.⁴¹ was utilized to determine the presence or absence of specific methoxyl conformational preference. The ratio of H5' to H7' nOe upon pre-saturation of OMe-6' was calculated to be 6 for the 5'-cis orientation, whereas the corresponding ratio for a 1:1 equilibrium of (5'-cis:7'-cis) was 0.5. The observed ratio of 7 was unambiguous corroborative evidence of the strong preference for the 5'-cis orientation.

4.4.2. Other Structural Features

The first step in the determination of C8 configuration from relaxation parameters is to determine significant relaxation pathways and the projected differences in R_1 values for the α - and β -linked isomers. When H8 is in the α position (β linkage), relaxation of H8 is dominated by interactions with H9, H7en, and H6en. When H8 is in the β position (α linkage), relaxation is dominated by interaction with H9, H7ex, and H2c. The total effect of major

 β linked

(III)

 α linked

contributors to H8 relaxation is effectively equivalent, so no differences in $^1\text{H-R}_1$ values are expected or observed. A second approach, was to determine if the relaxation of nearby protons would be affected by the difference in C8 stereochemistry. The contributions of H8 to nearby methylene protons (C2, C6, C8) are too small to result in a significant effect on their R_1 values. The only methine proton with a substantial contribution from

H8 is H9, but the accompanying change in C9 configuration compensates for the change at C8, thus, the inter-proton distance and relaxation contribution are essentially unchanged. In summary, the determination of C8 configuration is not possible solely from $^1\text{H-R}_1$ values.

The specific relaxation pathways mentioned above can, however, be characterized by nOe enhancements (Table 4.5). The large enhancement of H8 upon presaturation of one of the C7 protons clearly distinguishes between H8a and H8b. Other key nOe's which were identified were those from H8 to the corresponding C7 proton and a nOe in quinidine from H6en to H8.

The relative orientations of the quinoline and the quinuclidine rings could also be determined by the detection of nOe enhancements. Inter-ring relaxation pathways between H7ex and H7en, and H3', H5', and H8 imply that these protons are reasonably close to each other. This serves to unambiguously assign the relative orientations of quinoline and quinuclidine rings as shown in Fig. 4.3.

Though there is a possibility for a number of widely differing relative orientations of the quinoline and quinuclidine rings, the ^1H relaxation experiments indicate that steric factors prohibit most orientations, as had been predicted by inspection of the molecular models of these compounds. A great similarity is evident in the crystal and solution geometries of the cinchona alkaloids studied.

Table 4.5

NOE Enhancements of Cinchona Alkaloids¹

<u>[]</u>	<u>Key enhancements</u>	<u>Other enhancements</u>
3'	7en, 9	2'
5'	8, 9	6'
6'-Me	5' > 7'	
2c	3'	2t, 7ex, 10, 11c, 11t
6en	8	6ex, 5en
7ex	3', 8b	4, 7en, 10
7en	3', 8a	4, 7ex
8a	5', 7en	9
8b	5', 7ex	9 ₁
9	3', 5'	8

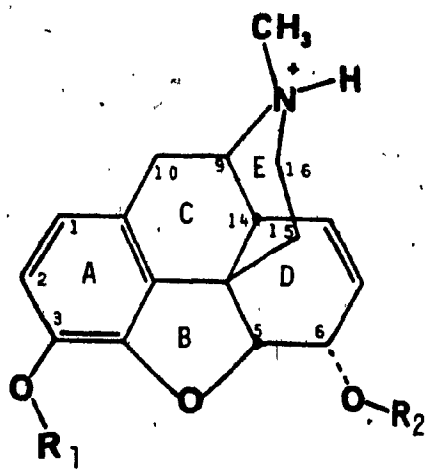
1. Cumulative results obtained at ambient temperature on 0.1 M CDCl₃ or DMSO-d₆ solutions of the four cinchona alkaloids.³ The choice of free-base or HCl salt and of solvent was made on the basis of maximizing chemical shift dispersion in the spectrum.

4.5. Morphine Alkaloids

Morphine alkaloids are well known for their extremely potent analgesic activity, and have been under study by a wide range of scientists for a number of years.⁴⁶ A number of synthetic morphine derivatives, such as nalorphine,⁴⁷ naloxone,⁴⁸ and naltrexone,⁴⁹ have been utilized as morphine receptor blockers (morphine antagonists), as an aid in the treatment of addicts, and to further the understanding of the morphine receptor site.⁴⁶ Seven morphine alkaloids have been utilized for relaxation studies, their structures are shown in Fig. 4.5. Codeine, heroin (diacetylmorphine), and nalorphine are simple derivatives of morphine with the same framework structure, whereas thebaine, naloxone, and naltrexone have both substituent and structural differences.

These molecules are quite rigid, and have a T-shaped structure. They tumble approximately isotropically in solution, and can be reliably modelled, so $^1\text{H-R}_1$ values can be calculated. Since the crystal structures of morphine,⁵⁰ codeine,⁵¹ heroin,⁵² and naloxone⁵³ have been published, the crystal coordinate method of calculation was used.

No high-field ^1H nmr studies of morphine alkaloids have been reported in the literature. A certain number of assignments in the low field region of morphine alkaloids spectra have been made at 60- and 100-MHz,⁵²⁻⁵⁵ but with the greatly increased dispersion and resolution available



	R_1	R_2
<u>morphine</u>	H	H
<u>codeine</u>	CH_3	H
<u>heroin</u>	Ac	Ac

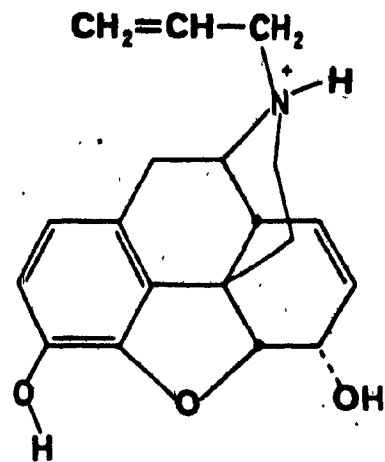
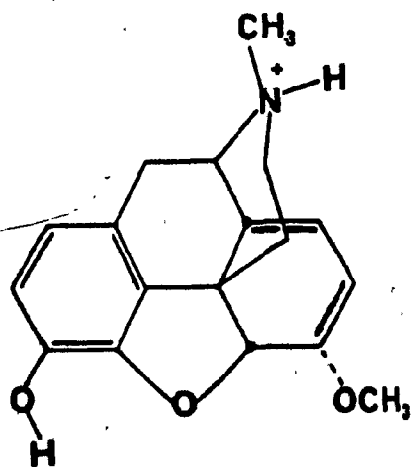
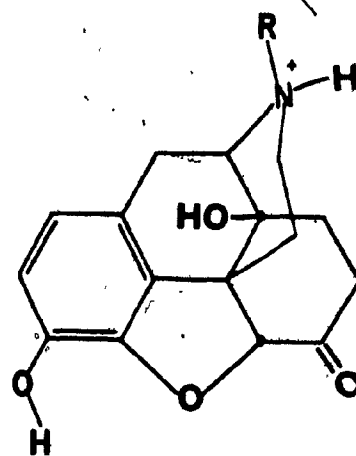
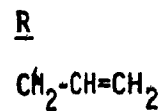
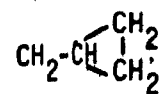
nalorphinethebaineNaloxoneNaltrexone

Fig. 4.5 Structures of the morphine alkaloids.

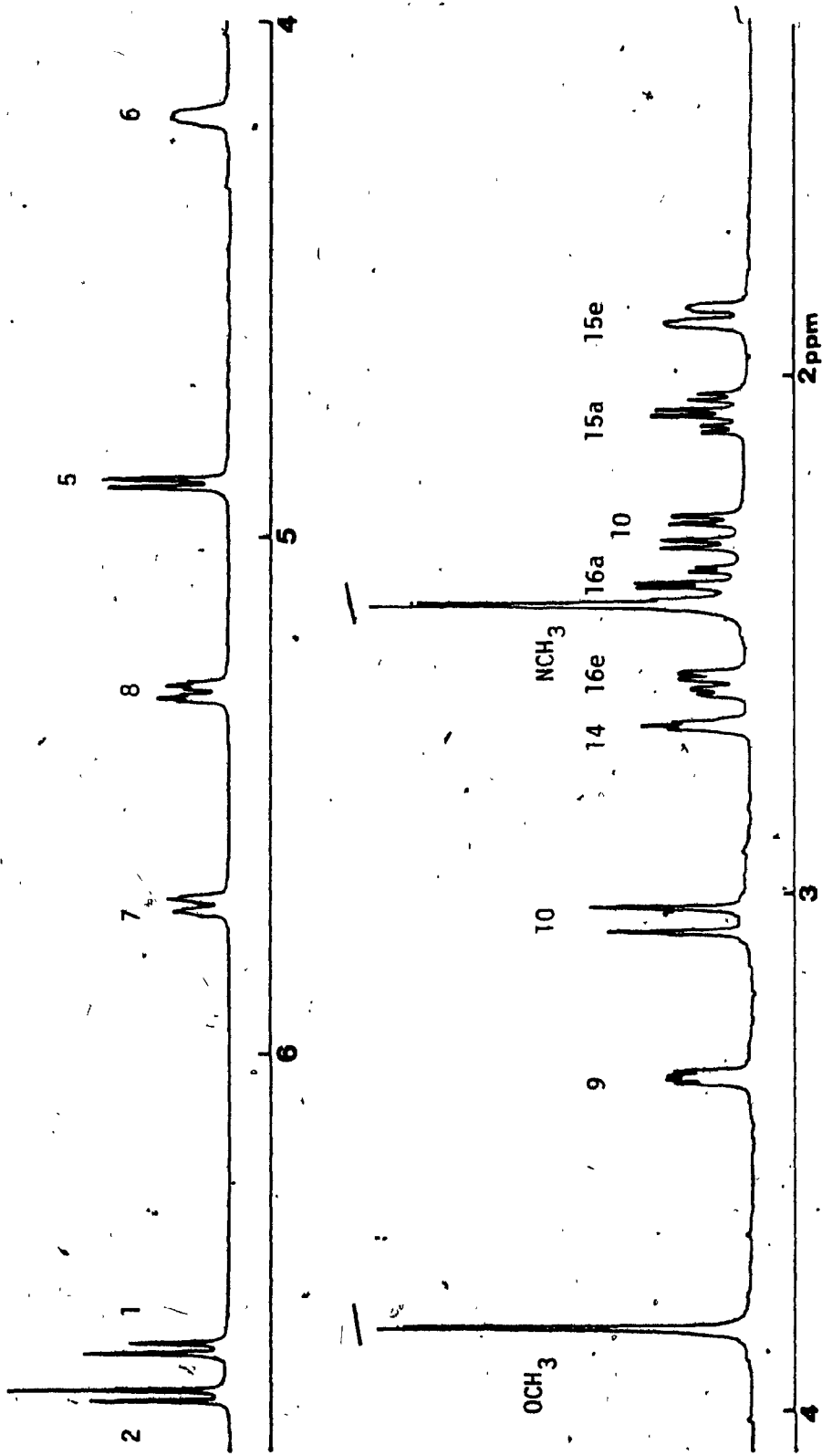


Fig. 4.6 400 MHz ¹H nmr spectrum of codeine, 0.1 M CDCl₃.

on a modern 400 MHz spectrometer, it was decided to assign all resonances from first principles. The 400 MHz ^1H spectrum of codeine is shown in Fig. 4.6. The assignments of resonances (Table 4.6) in all compounds were made in a similar manner, so only the parent compound, morphine, will be discussed in full detail.

4.5.1. Preliminary Assignment of the 400 MHz ^1H Spectrum of Morphine

Several resonances were easily assignable upon inspection of the spectra of the sulfate or HCl salts in DMSO-d_6 or D_2O solution. The methyl resonance was assigned to the large singlet integrating to three protons at 2.6 ppm. The resonances of 3-OH, 6-OH, and NH protons were assigned by consideration of chemical shifts, line-widths, and the disappearance of these signals in all D_2O spectra (exchange of deuterium with the solvent). The inability to completely dry a sample of the sulfate salt led to broad peaks for these resonances in DMSO-d_6 solution, but sharp signals could be obtained from a dried sample of the HCl salt. The assignments were: 11.4 ppm- quaternary R_3NH^+ , 9.0 ppm- phenolic OH, 4.1 ppm- aliphatic OH.

The low field AB quartet near 6.5 ppm could be assigned to the aromatic protons H1 and H2, on the basis of chemical shift and magnetic isolation- only one major coupling constant and very slow relaxation ($0.89\text{-}1.05\text{ s}^{-1}$, several measurements). H2 was expected to resonate at

Table 4.6 ¹H Chemical Shifts of Some Morphine Alkaloids

	<u>H</u>	<u>morphine</u>	<u>nalorphine</u>	<u>codeine</u>	<u>heroin</u>	<u>thebaine</u>	<u>nalozone</u>	<u>naltrexone</u>
1	6.45	6.52	6.71	6.44	6.70	6.63	6.61	
2	6.58	6.67	6.86	6.57	6.83	6.72	6.71	
3-OR	9.0 (H)	3.72 (Me)	2.24 (Ac)	9.04 (H)	3.58 (Me)	9.54 (H)	9.55 (H)	
5	5.12	4.76	5.20	4.82	5.44	5.04	5.05	
6	4.82	4.44	5.17	4.12	-	-	-	
6-OR	4.11 (H)	- (H)	2.05 (Ac)	5.1 (H)	3.74 (Me)	-	-	
7ax	5.65	5.59	5.65	5.64	5.24	3.01	3.04	
7eq	-	5.25	5.52	5.30	5.92	2.11	2.12	
8ax	-	-	-	-	-	1.48	1.51	
8eq	-	-	-	-	-	2.00	2.04	
9	4.06	3.69	4.14	4.09	4.43	3.67	4.02	
10a	2.71	2.52	2.78	2.68	3.65	2.92	3.01	
10b	3.18	3.08	3.30	3.19	3.65	3.37	3.34	
14-R	3.07 (H)	2.87 (H)	2.99 (H)	3.25 (H)	-	6.99 (OH)	7.11 (OH)	
15ax	2.35	2.22	2.41	2.35	2.42	2.69	2.70	
15eq	1.90	1.74	1.87	1.92	1.80	1.51	1.48	
16ax	2.8	2.55	3.38	2.77	3.18	2.50	2.46	
16eq	3.18	2.85	3.24	3.25	3.18	3.14	3.08	
N-CH ₃	2.81	2.62	2.82	3.25	2.79	-	-	
17	-	-	-	3.88	-	4.20	3.34	
17	-	-	-	3.88	-	3.79	2.92	
18	-	-	-	6.13	-	5.95	1.01	
19	-	-	-	5.50 (t)	-	5.52 (t)	0.68	
19	-	-	-	5.57 (c)	-	5.63 (c)	0.54	
20	-	-	-	-	-	-	0.60	
20	-	-	-	-	-	-	0.40	

1. All values measured from 0.1M DMSO-d₆ solutions of the HCl sats, except for codeine, which was as the phosphate salt.

2. Values in ppm from internal TMS, with a precision of ±0.01 ppm.

higher field due to a strong upfield shift from the ortho hydroxyl group (C3). The detection of some small coupling in the high field doublet in a resolution enhanced (gaussian multiplication⁶⁶) spectrum was, therefore, somewhat difficult to rationalize (this coupling did not disappear in D₂O). This coupling was most likely ortho benzylic coupling* between H1 and the C10 protons, so the relative assignments were tentatively switched.

The rest of the proton signals, in the more crowded region (1.5 to 6.0 ppm) of the spectrum, were categorized according to their relaxation rates (Table 4.6). Methine resonances relaxed in the range 0.9-2.8 s⁻¹, whereas methylene protons relaxed in the range 4.3-5.0 s⁻¹. The methine resonances between 3.5 and 5.8 ppm were assigned to H5, H6, H7, H8, and H9, on the basis of chemical shift, thus, H14 was the high field methine proton (2.8 ppm). C10 and C16 are both adjacent to the N atom, so the high field methylene protons (1.8 and 2.2 ppm) were assigned to C15.

4.5.2. Refinement of Assignments and Structural Inferences

The assignments were further refined by consideration of the magnitude of spin-spin coupling constants and standard decoupling experiments which will be only briefly summarized. C10 methylene protons could be distinguished from C16 methylenes by their mutual coupling constant and coupling to a methine proton, at 3.71 ppm, which had to be H9.

* For a recent discussion see Ref. 58.

A tentative relative assignment of 10a versus 10b was made with the aid of molecular models and consideration of the dependence of vicinal coupling on dihedral angle.⁵⁹ In the same manner, tentative assignments for the C15 and C16 methylene protons were made presuming a large coupling constant for $^3J_{aa}$, a small value for $^3J_{ae}$, and an intermediate value for $^3J_{ee}$.

H5 was differentiated from other methine protons by the presence of only one major (to H6) and one minor (to H7) coupling constant. Decoupling H5 identified H6. H9 had been identified by its appreciable coupling to H10a. The large coupling between protons with shifts at 5.25 and 5.60 ppm was characteristic of the cis vinyl protons at C7 and C8. Tentative identification of H7 was possible through its coupling to H5.

Using these assignments, relaxation pathways and R_1 values were calculated using the crystal coordinate method and compared to the observed values (Table 4.7). The agreement (Table 4.8) is excellent, thereby confirming assignments. Note that R_1 values allow for a clear differentiation between H7 and H8 ($R_{1H7} \ll R_{1H8}$), and H15a and H15e ($R_{1H15a} > R_{1H15e}$). The only protons whose assignments were not established by their R_1 values were the diastereomeric methylene pairs at C10 and C16.

For the differentiation of H10a from H10b, and H16a from H16e, it was necessary to experimentally characterize specific relaxation pathways through the use of nOe

Table 4.7

H	Normalized R ₁ Values of Morphine Alkaloids						
	<u>morphine</u>	<u>nalorphine</u>	<u>codeine</u>	<u>heroin</u>	<u>thebaine</u>	<u>nalozone</u>	<u>naltrexone</u>
1	.21	.20	.21	.20	.18	.20	.19
2	.21	.19	.21	.13	.19	.21	.19
3-OR	-	(.22(H))	.24(Me)	.25(AC)	.23(Me)	.26(H)	.25(H)
5	.38	.36	.39	.32	.18	.19	.19
6	.40	1.07	.42	.29	-	-	-
6-OR	-	.27(H)	-	.25(AC)	.42(Me)	-	-
7ax	.21	.20	.21	.19	.25	.88	1.00
7eq	-	-	-	-	-	.83	.78
8ax	.31	.29	.31	.30	.26	.88	.82
8eq	-	-	-	-	-	1.00	.93
9	.64	.54	.69	.65	.68	.65	.70
10a	(4.33)	(4.62)	(3.85)	(4.62)	(5.32)	(4.45)	(4.95)
10b	1.07	1.20	1.12	1.00	1.08	1.07	1.08
14-R	.64 ⁺ (H)	.42(H)	.62(H)	.50 ⁺ (H)	-	.29(OH)	.29(OH)
15ax	1.14	1.07	1.20	1.07	1.00	.94	.93
15eq	1.00	.94	.97	1.00	.87	.88	.88
16ax	1.00 ⁺	1.07	1.12	.83 ⁺	1.00	.94	.93
16eq	1.10	1.07	1.20	1.07	1.08	1.15	.88
N-CH ₃	.80	.80	.80	.65	.63	-	-
17	-	1.11*	-	-	-	1.15	1.08
18	-	1.11*	-	-	-	1.07	1.00
19	-	.31	-	-	-	.31	.48
19	-	.42(t)	-	-	-	.44(t)	.7*
19	-	.47(c)	-	-	-	.48(c)	.7*
20	-	-	-	-	-	-	.74
20	-	-	-	-	-	-	.78

1. All values measured from 0.1 M DMSO-d₆ solutions and normalized to the R₁ (s⁻¹) of H10a, given in parentheses ().

"+" = overlap problem, "*" = tight coupling, t = trans, c = cis.

Table 4.8

Comparison of Calculated¹ and Observed² R₁ Values in Morphine Alkaloids

H	morphine		codeine		heroin		naloxone	
	Expt.	Calc.	Expt.	Calc.	Expt.	Calc.	Expt.	Calc.
1	.21	.26	.18	.19	.17	.19	.18	.17
2	.21	.22	.18	.17	.10	.10	.18	.14
5	.38	.41	.37	.17	.30	.38	.17	.22
6	.40	.42	.40	.38	.27	.27	-	-
7ax	.22	.24	.18	.23	.17	.21	.88	.86
7eq	-	-	-	-	-	-	.83	.85
8ax	.31	.28	.28	.30	.28	.33	.88	.90
8eq	.64	.56	.68	.56	.64	.61	1.00	.99
9	1.00	1.00	1.00	1.00	1.00	1.00	.64	.60
10a	1.07	1.06	1.13	1.00	1.00	1.00	1.00	1.00
10b	.50	.50	.64	.53	.60+	.48	1.08	1.21
14	1.14	1.16	1.21	1.14	1.07	1.17	.94	1.00
15ax	1.00	1.02	.97	1.01	1.00	1.02	.88	.91
15eq	1.10+	1.05	1.13	1.06	1.00+	1.08	1.16	1.15
16ax	1.10	1.12	1.21	1.11	1.07	1.16	.94	.93
16eq	-	-	-	-	-	-	1.08	1.10
17ax	-	-	-	-	-	-	1.16	1.35
17eq	-	-	-	-	-	-	-	-

1. R₁ calculations carried out on HP-1000 computer using program WCDRR. Inter-proton distances measured by computer (PDP-8) using NRC programs for X-ray crystallography to generate H atom coordinates. X-ray data from Refs. 51, 52, 53, and 54.

2. Observed R₁ values measured from 0.1 M DMSO-d₆ solutions of morphine-sulfate, codeine-phosphate, heroin-HCl, and naloxone-HCl. All values normalized to R₁ of H10a. "+" = overlap problem.

experiments. The calculations served as a guide for the selection of which NOE experiments would give the desired information. In Table 4.9, the results of a number of NOE difference experiments on morphine and codeine are given.

Table 4.9

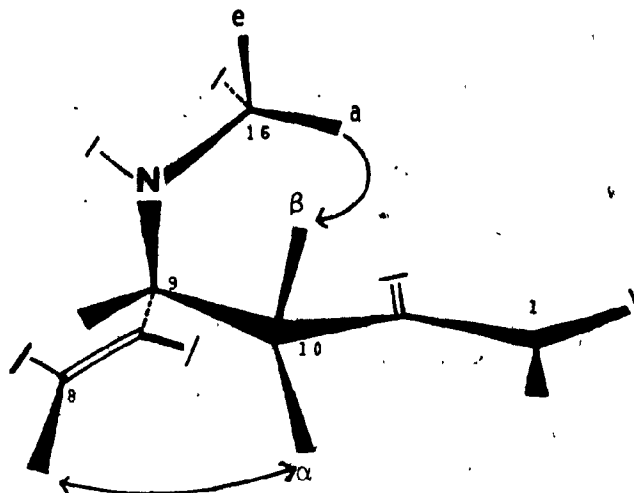
NOE Enhancements in Morphine and Codeine

<u>{ }^{1,2}</u>	<u>Key Enhancements³</u>	<u>Other Enhancements³</u>
1 ^m		2
2 ^m		1
5	14 ^m , 15a, 15e	6, 7 ^m
6	14	5, 7
8	6 ^m , 10a	5, 7, 9, 14
10a ^c	1, 8	10b, 9
10b		10a, N-CH ₃ ^c
14	5, 6	8, 9
15a	5, 14, 16e	15e
15e	5, 16e ^m	15a
16a ^c	10b	16e
16e	15a, 15e	16a

1. Experiments run at ambient temperature on 0.1M solutions of morphine-sulfate in DMSO-d₆ and codeine in CDCl₃.
2. Those experiments carried out on only one of the molecules are indicated by "m" for morphine, and "c" for codeine.
3. Enhancements observed for only one of the compounds are indicated by "m" and "c" as in 2.

The results of the NOE experiments confirmed all previously made assignments and differentiated the diastereotopic methylene protons at C10 and C16. Clear proof of the tentative assignments of H1 and H2 (based on the observation of benzylic coupling in the H1 resonance) was given by the enhancement of H1 upon saturation of H10a

or H10b. H10a was identified by its relaxation pathway with H8, whereas H10b could be distinguished on the basis of the nOe enhancement from H16a.



The $H10b \leftrightarrow H16a$ relaxation pathway served as an entry into the C15/C16 system of protons. Another key enhancement was observed from H15a to H14. These two relaxation pathways were actually sufficient data to assign all four resonances, but further corroborative evidence was obtained, as will be described below. With all resonances identified, it was possible to analyze coupling constants, and assign the full set of spectral parameters for morphine-sulfate in $DMSO-d_6$ (Table 4.10) and codeine in $CDCl_3$ (Table 4.11).

The relaxation pathways among the four C15/C16 protons are characteristic of relaxation in cyclohexane systems and deserve further discussion. The spatial relationship between the methylene protons on two adjacent C atoms in a cyclohexane ring (standard chair conformation) is given in the following diagram:

Table 4.10
Complete Assignment of ¹H Spectral Parameters of Morphine Sulfate

H	δ (ppm)	J (Hz)	i	1,10a	1,10b	0.2
1	6.405	1,2	= 8.0	1,10a	1,10b	0.2
2	6.510					
3OH	8.9					
5	4.736	5,6	= 6.2	5,7	= 1.0	
6	4.123	6,7	= 3	6,8	= 4.0	
6OH	5.0					
7	5.600	7,8	= 9.5	7,14	= 2.5	†
8	5.247	8,14	= 1.5			
9	3.707	9,10a	= 6.8	9,10b	< .1	9,14 = 3
10a	2.515	10a,10b	= 19.1			
10b	3.032					
14	2.772					
15a	2.157	15a,15e	= 13.0	15a,16a	= 13.0	15a,16e = 4.8
15e	1.765	15e,16a	< 0.2	15e,16e	= 2.0	
16a	2.608	16a,16e	= 13.0			
16e	2.886					
CH ₃	2.641					

1. All measurements made on 0.1 M solution in DMSO-d₆ at ambient probe temperature (20°C), with 0.1% TMS as internal reference.

2. The precision of measurement was ±0.003 ppm in chemical shifts (δ) and ±0.2 Hz in coupling constants (J), unless indicated by a smaller number of significant figures. The signs of the coupling constants have not been determined.

Table 1.11

Complete Assignment of ^1H Spectral Parameters of Codeine

H	δ (ppm)	J (Hz)	$1/10a$	1,10b	0.2
1	6.569	1,2	8.0		
2	6.664				
3-OMe	3.840				
5	4.895	5,6	6.5	5,7	= 1.0
6	4.194	6,7	3	6,8	= 1.7
6-OH	3.0				
7	5.712	7,8	10.0	7,14	= 2.2
8	5.298	8,14	3.7		
9	3.351	9,10a	6.3	9,10b	< 0.2
10a	2.295	10a,10b	19.0		9,14 = 3.5
10b	3.070				
14	2.670				
15a	2.065	15a,15e	13.0	15a,16a	= 12.1
15e	1.878	15e,16a	3.6	15e,16e	= 5.2
16a	2.400	16a,16e	12.3		
16e	2.599				
N-CH ₃	2.451				

1. All measurements made on 0.1 M solution in CDCl_3 at ambient probe temperature (20°C), with 0.1% TMS as internal reference.

2. The precision of measurement was ± 0.003 ppm in chemical shift (δ) and ± 0.2 Hz in coupling constants (J), unless indicated by a smaller number of significant figures. The signs of the coupling constants have not been determined.



(V)

The arrows and labels indicate the relaxation pathways in this system. Upon consideration of these pathways, it is clear that axial protons can be distinguished from equatorial protons by the number of intermediate vicinal pathways. With respect to the nOe characterization of relaxation pathways, this implies that the observation of enhancements of both vicinal protons identifies the saturated resonance as the equatorial methylene, since the axial proton is too far from the adjacent axial proton to cause an appreciable enhancement. In this manner, i.e., from the enhancements of both H15a and H15e, it was possible to identify the H16e resonance in morphine alkaloids. The lack of enhancements of H15e in the {H16a} experiment indicates that the spatial geometry in ring E is not exactly the same as in cyclohexane, in agreement with the spin-spin coupling constant data (Tables 4.10 and 4.11). Nonetheless, the assignment of H16e through its relaxation pathways is unambiguous.

Another important feature of relaxation pathway analysis is demonstrated by the nOe experiments involving H1, H10a, and H10b. To simplify this discussion, it is

necessary to recall some of the basic principles of relaxation, given in Chapter 2. First, the strength of the dipolar interaction between two protons is dependent on the inter-nuclear separation. Second, the rate of dipolar relaxation of any proton, A, is dependent on the sum total of all available dipolar interactions. This implies that the relative contributions of a relaxation pathway between two protons A and B is not necessarily the same for both, since the total of all pathways for proton A is not necessarily the same as the total for B. Experimentally, this means that the Overhauser effect will not necessarily be of the same magnitude in both directions along a relaxation pathway. The uni-directionally observed relaxation pathway from the C10 protons to H1 is a good example. H10a and H10b have several very efficient relaxation pathways (eg. $H10a \leftrightarrow H10b$, $H10a \leftrightarrow 9$, $H10b \leftrightarrow H16a$) available, so the relaxation contributions from H1 are relatively small. The very same relaxation pathways are very important for the relaxation of H1, because H1 has only one additional relaxation pathway (to H2) available. Even though the relaxation interactions involve the same two protons, the relative contributions to the overall relaxation rate are drastically different, thus, significant enhancement of H1 occurs upon saturation of H10a or H10b, but no enhancement of C10 protons is observed when H1 is saturated.

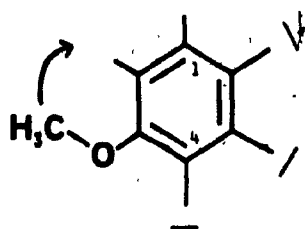
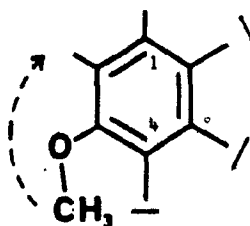
From nOe characterization of specific relaxation pathways in morphine and codeine, it was also possible to infer certain features of the molecular geometry. The principal points of information can be summarized in the following:

1. The relaxation pathway between H6 and H14 indicates that ring D is in a boat conformation.
2. Experimentally observed relaxation pathways between H5, H6, H14, and H9 prove that these protons are all situated on the same face of the molecule, allowing for the determination of relative stereochemistry at all four positions.
3. Inter-ring nOe enhancements (eg. $H_{10} \leftrightarrow H_1$, $H_8 \leftrightarrow H_{10a}$) indicate the close proximity of protons that appear to be rather distant in a standard two-dimensional diagram. These enhancements are instrumental in the determination of ring conformations, and in general, help to guide in the selection of appropriate molecular modelling schemes.

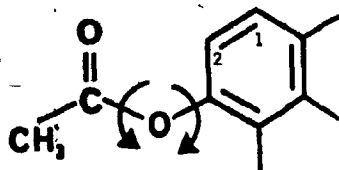
4.5.3. Conformational Preferences of Methoxy Groups

The conformation of the methoxy groups of codeine and thebaine, and of the O-acetyl groups in diacetylmorphine (heroin) can be investigated by relaxation pathway analysis of $^1H-R_1$ values. Only a summary of results will be presented here because the methodology has already been described in section 4.4.2 for quinine and quinidine.

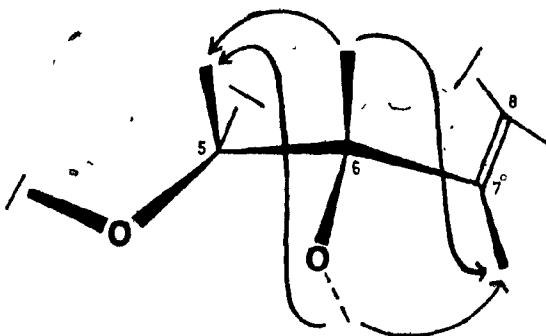
For an O-CH₃ group at C3 in morphine, calculations predict that a 2-trans orientation would result in H2 having a significantly lower R_1 value than H1, whereas for a 2-cis orientation, the R_1 values would be approximately equal. The observed R_1 values of H2 in codeine and thebaine were essentially equivalent to the H1 value, indicating a clear preference for the 2-cis orientation.

2-cis2-trans

Along these same lines, the reduction (35%) in the normalized R_1 value of H2 in heroin, relative to the other morphine alkaloids, in addition to the substantially slower relaxation of H2 relative to H1 (0.62 s^{-1} vs. 0.92 s^{-1} , respectively), indicated that the acetyl methyl group is at some distance from H2. In the solid state,⁵² the 3(O-acetyl) group of heroin adopts a 2-cis orientation, but with the carbonyl oxygen in plane and facing H2, and the methyl group turned away. Such a conformation is compatible with the $^1\text{H-R}_1$ data in solution, though an appreciable amount of motional freedom about the three single bonds is to be expected for such a functionality in solution.

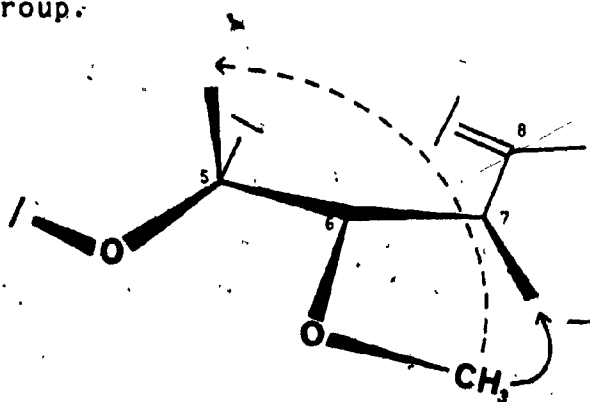


The conformational preference of 6-OCH₃ in thebaine has also been determined. In morphine, approximately 50% (by calculation) of both H5 and H7 relaxation comes from H6 and 6(OH). Comparing the experimental R₁ values of H5 and H7



morphine

in thebaine to those in morphine, a very substantial decrease in H5 (50%) and a significant increase in H7 (>25%) is observed. These data have been interpreted in the following manner; H5 has lost all contributions from the C6 proton or substituent, whereas H7 has acquired a more efficient relaxation pathway. Such trends are only consistent with a strong 7-cis conformational preference for the 6-OCH₃ group.



thebaine

4.6 Tropane Alkaloids

Tropane alkaloids, found in a variety of plants, are best known for their potent activity in the central nervous system.⁶⁰ Significant structural similarity with acetylcholine has led researchers to propose that pharmacologically, these compounds function as antagonists, binding to the same muscarinic receptor as acetylcholine.⁶¹ ^1H spin-lattice relaxation has been studied in four tropane alkaloids—tropine, atropine, scopolamine, and cocaine (Fig. 4.7).

Conformational studies of the piperidine ring and the orientation of the N-Me substituent in tropanes were subjects of considerable controversy in the early 1960's.^{60,62} It is now clear that the piperidine ring is in a distorted chair conformation and that the methyl group is syn to the ethano bridge in tropine, atropine, and cocaine, but anti in scopolamine.⁶³ These determinations were made on the basis of ^1H and ^{13}C studies of standard nmr parameters.

In a recent paper by Avdovich and Neville,⁶³ ^{13}C data from a number of sources have been consolidated and experimentally reexamined. The determination of solution structure of the four isomeric cocaines by ^{13}C and ^1H nmr analysis has been reported by Coleman and coworkers.⁶⁴ Using a method of analyzing ^1H chemical shifts in terms of ring currents, Feeney and coworkers⁶⁵ have proposed assignments and solution structures for atropine and scopolamine in aqueous solution. There are no reports of relaxation data from these tropane alkaloids in the literature.

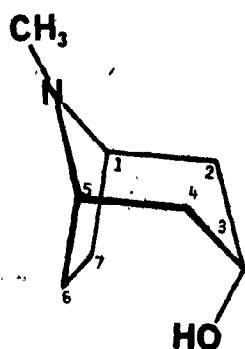
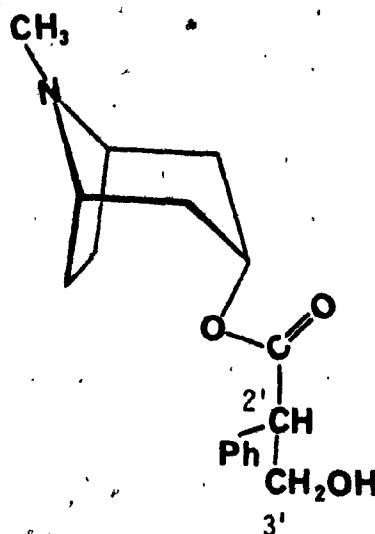
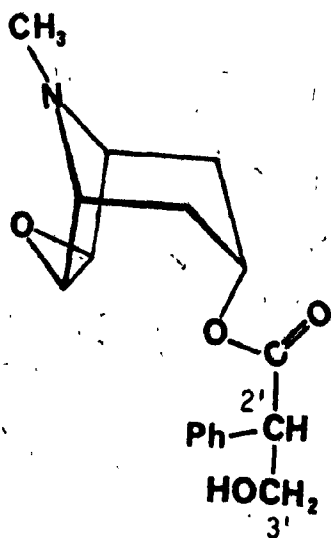
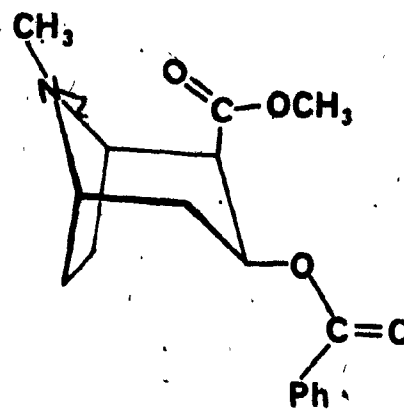
tropineatropinescopolaminecocaine

Fig. 4.7 Structures of the tropane alkaloids.

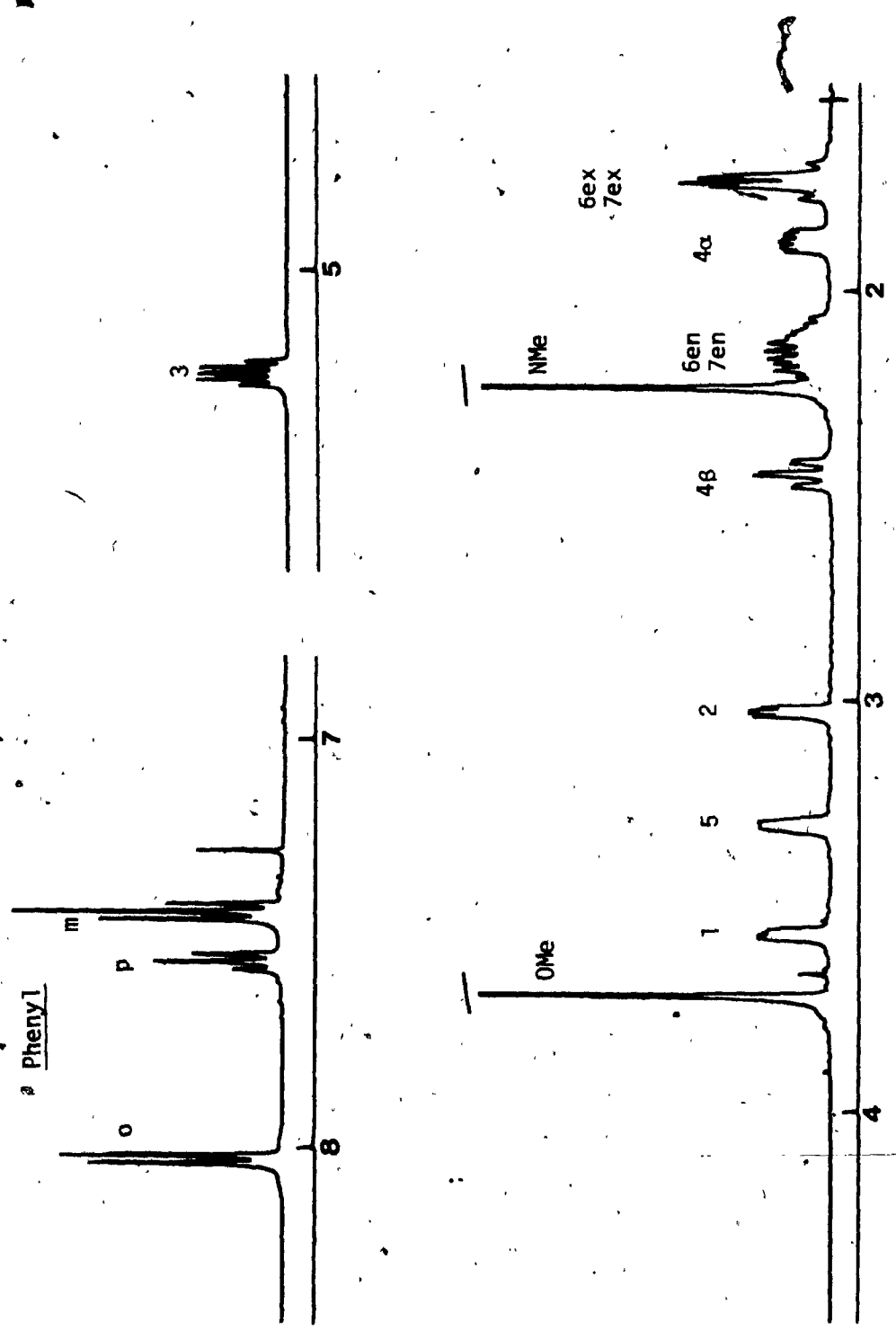


Fig. 4.8 400 MHz ¹H nmr spectrum of cocaine, 0.1 M CDCl₃.

^1H nmr studies at 400 MHz offer a significant improvement in spectral dispersion over the previous nmr studies of tropane alkaloids (250, 270 MHz), so all assignments have been reexamined (Table 4.12). The 400 MHz ^1H spectrum of cocaine is shown in Fig. 4.8. Though relaxation rates have been measured for all four compounds (Table 4.13), only one of these, scopolamine, will be examined in detail. Complete relaxation pathway analysis for this compound, through nOed experiments and calculations, was carried out to aid in the analysis of the structural features characterized by the relaxation parameters.

4.6.1 Tropine

Tropine is an achiral molecule, since the nuclei are symmetrically disposed with respect to a plane of symmetry through C3 and the N atom, and bisecting the C6-C7 bond. The symmetrically disposed nuclei are magnetically equivalent, so only eight resonances are present in the nmr spectrum. The assignment of resonances was made on the basis of relative chemical shifts and spin-spin couplings. The NCH_3 resonance was easily assigned to the large singlet integrating to three protons at 2.26 ppm. H3 could be assigned by its downfield shift (at ~ 4 ppm) caused by the geminal hydroxy substituent. The H1/H5 signal is shifted downfield (at ~ 3 ppm) because these protons are bound to C atoms α to N. The C2/C4 equatorial protons (at ~ 1.8 ppm) were differentiated from their axial partners by the very

Table 4.12

Chemical Shifts of some Tropane Alkaloids

	<u>tropine</u>	<u>atropine</u>	<u>scopolamine</u>	<u>cocaine</u>
1	3.08	2.91	2.97	3.56
2ax	2.10	2.02	2.02	-
2eq	1.67	1.47	1.33	3.02
3	4.03	5.02	5.02	5.25
4ax	2.10	2.10	2.11	2.44
4eq	1.67	1.68	1.58	1.87
5	3.08	3.03	3.11	3.30
6ex	2.0	1.86	-	1.72 ²
6en	2.0	1.74	3.38	2.14 ²
7ex	2.0	1.68	-	1.72 ²
7en	2.0	1.17	2.66	2.14 ²
N-CH ₃	2.26	2.19	2.45	2.23
2'	-	3.82	3.75	3.72(Ac)
3'a	-	3.79	3.81	-
3'b	-	4.16	4.17	-
Ph-o	-	7.29	6.72	8.03
-m	-	7.37	7.35	7.42
-p	-	7.35	7.30	7.54

1. All values measured from 0.1 M CDCl₃ solutions of free base at ambient probe temperature. The precision of measurement is ± 0.01 ppm or better.

2. The assignment of protons in the ABCD system of C6 and C7 is only tentative due to the extremely tight coupling.

Table 4.13

Normalized R₁ Values of some Tropane Alkaloids

	<u>tropine</u>	<u>atropine</u>	<u>scopolamine</u>	<u>cocaine</u>
1	.61	.45	.40	.53
2ax	1.11	1.05	1.12	-
2eq	1.00	1.00	1.02	.43
3	.64	.35	.43	.64
4ax	1.11	1.05	1.09	1.00
4eq	(0.64)	(1.73)	(1.69)	(1.28)
5	.61	.45	.40	.56
6ex	1.07	.94	-	1.36 ²
6en	1.02	.91	.27	1.36 ²
7ex	1.07	.94	-	1.36 ²
7en	1.02	.91	.27	1.36 ²
N-CH ₃	.96	.70	.60	.90
2'	-	.41	.33	.36(Ac)
3'a	-	.65	.69	-
3'b	-	.75	.73	-
Ph-o	-	.27	.28	.22
-m	-	.24	.23	.29
-p	-	.24	.22	.27

1. All values measured from 0.1 M CDCl₃ solutions of free base at ambient probe temperature by the null-point method and normalized to H4eq, whose observed R₁ value is indicated in parentheses ().

2. The assignment of protons in the ABCD system of C6 and C7 is only tentative due to the extremely tight coupling.

small vicinal coupling constants observed to H3, and H1 or H5. In the crowded region of the spectrum at 2.1 ppm, the 2a/4a protons could be identified by decoupling experiments. The C6 and C7 protons were assigned to the complicated multiplet that remained.

The results of relaxation experiments and calculations made by the Dreiding molecular model method are given in Table 4.14. There is general agreement between observed and calculated values, indicating that the molecule has been properly modelled, that assignments are correct, and that tumbling is essentially isotropic. Relaxation pathways have, therefore, been properly assigned, at least in a qualitative sense. These calculations will serve as a basis for R_1 analysis in the other molecules which have substitution on the tropane ring.

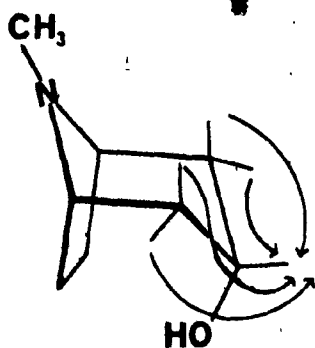
Table 4.14

Comparison of Calculated and Observed R_1 Values in Tropine¹

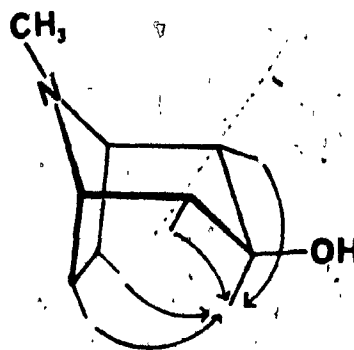
<u>H</u>	<u>R_1</u>	
	<u>Observed</u>	<u>Calculated</u>
1,5	0.47	0.41
2ax,4ax	1.04	0.95
2eq,4eq	1.00	1.00
3eq	0.50	0.59
6en,7en	0.9	0.95
6ex,7ex	1.0	0.96
3ax	0.50	0.77

¹. Observed values determined by null-point method, calculated values from the Dreiding molecular model method, and normalized to H2eq,4eq.

Note that the calculations clearly indicate that the R_1 value for H3 is consistent only with an equatorial position for this proton. A significantly higher R_1 value would be expected if H3 were axial, because two additional efficient relaxation pathways, to H6en and H7en, would be available.



H3-equatorial



H3-axial

(X)

4.6.2. Atropine

As mentioned previously, a 270 MHz ^1H nmr study of atropine has been reported,⁶⁵ but details on specific assignments were not given, so it was necessary to reexamine all spectral parameters. The NCH_3 and H3 resonances were easily assigned using the same reasoning as for the tropine assignments. In the aromatic region, assignments were possible upon inspection of relative intensities, multiplicities, and coupling constants, in a resolution enhanced (gaussian multiplication⁶⁶) spectrum. The assignment of all other protons required more detailed analysis.

Methylene and methine protons were classified by R_1 's (Table 4.13). Methylenes relaxed in the range $1.1-1.9 \text{ s}^{-1}$, whereas methines relaxed in the range $0.6-0.8 \text{ s}^{-1}$. The ABX $2',3'$ system of the tropic acid moiety was completely assigned by computer simulation, as shown in Fig. 4.9. An interesting and rather unusual aspect of this system is that the AB part of the spectrum was due to tight coupling between $H_{3'a}$ and $H_{2'}$, not between the geminal pair at $3'$. Atropine is a chiral molecule, so resonances in the tropane ring show significant non-equivalence at 400 MHz. Decoupling experiments were sufficient to give the proton connectivities around the tropane ring: $7 \leftrightarrow 1 \leftrightarrow 2 \leftrightarrow 3 \leftrightarrow 4 \leftrightarrow 5 \leftrightarrow 6$. It is the spatial positioning of the tropic acid moiety which gives rise to the large degree of non-equivalence, but unless information can be obtained about the relative positioning of the two parts of the molecule, the absolute assignments relative to the symmetry plane in the tropane ring cannot be determined. Feeney and coworkers⁶⁵ have utilized a method of analyzing chemical shifts on the basis of ring currents, which allows for the assignment of tropane ring ^1H resonances in atropine and scopolamine. Since there was no alternative method available to verify their assignments, they were assumed to be correct.

In addition to their use for assignment purposes, R_1 values (Table 4.13) for atropine can be analyzed for structural information concerning both the tropane ring and the tropic acid moiety. Since the structures of atropine

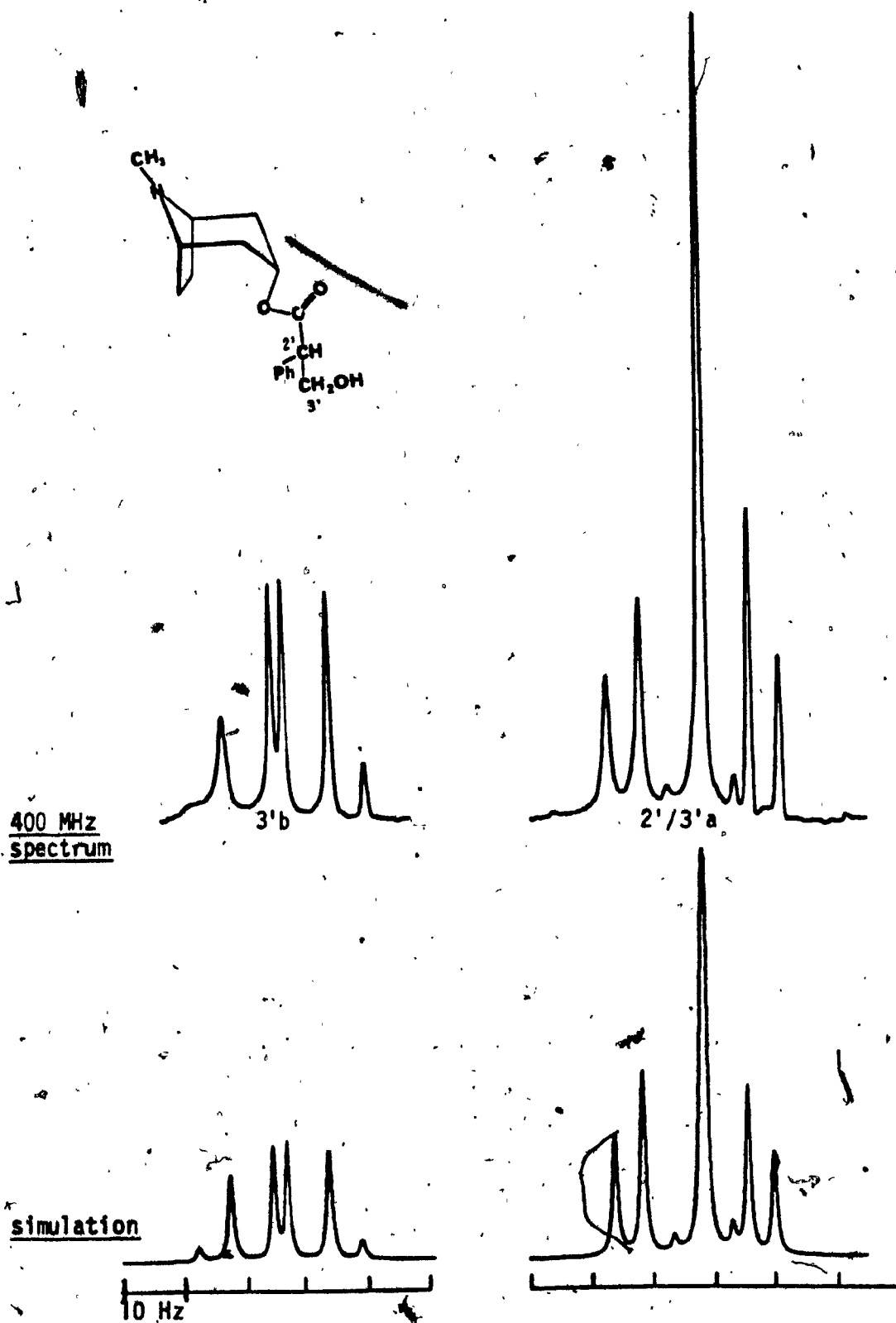


Fig. 4.9 400 MHz ^1H nmr spectrum of the tropic acid ester moiety of atropine, 0.1 M CDCl_3 .

and scopolamine are very similar, and the methodology for analysis is the same, a detailed discussion of atropine data will not be presented. The in-depth discussion will be based on scopolamine because a detailed experimental analysis of relaxation pathways has been carried out for this molecule. Most of the structural information drawn from the scopolamine relaxation data would be equally valid for atropine.

4.6.3. Scopolamine

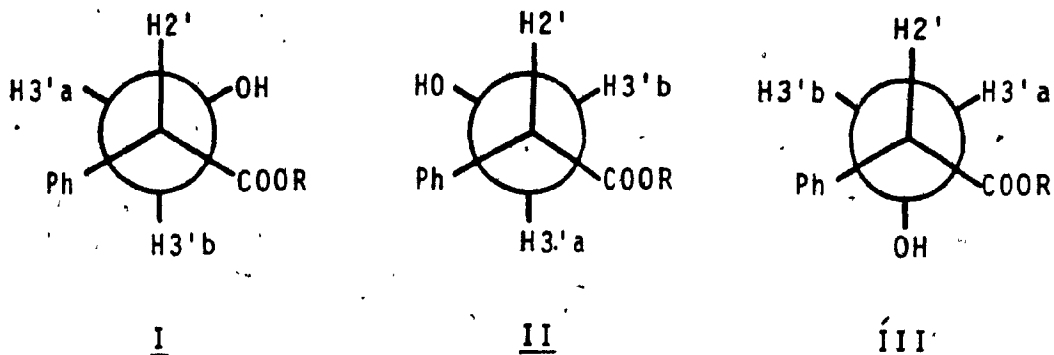
The 400 MHz ^1H spectrum of scopolamine free base in CDCl_3 solution has been completely assigned using standard methods and relaxation data. A complete list of chemical shifts and coupling constants is given in Table 4.15. Feeney and coworkers⁶⁵ have reported ^1H assignments at 270 MHz for scopolamine-HBr in D_2O solution. Our studies are in agreement, except for the relative assignments of the diastereotopic methylene protons at C2 and C4. The relaxation data (Table 4.13) data were instrumental in making these, and other key assignments.

It was possible to differentiate the diastereotopic protons at both C2 and C4 on the basis of R_1 values. Calculations predict that the axial proton will relax nearly 10% faster than the equatorial proton, and this is observed experimentally. The major portion of this differential arises from the flattening of the tropane ring in the C2-C3-C4 region of scopolamine,^{61,65} such that the

H2a \leftrightarrow H3 and H4a \leftrightarrow H3 relaxation pathways are much more efficient than the typical vicinal pathways in a standard chair conformation. A smaller part of this differential can be attributed to the 1,3-trans diaxial interaction between H2a and H4a, a relaxation pathway that has been well-characterized in carbohydrates⁴ and steroids.¹⁰ Finally, the relaxation rates of H2' and the 3' protons were also necessary to make the assignment of the AB portion of the ABX system in the tropic acid moiety, ~~to~~ H2' and H3'a.

The R_1 values of protons in the tropic acid portion of the molecule must reflect the rotameric equilibrium along the C2'-C3' bond. In such systems, relaxation is analyzed by assuming that the R_1 value is composed of the weighted average of relaxation rates in the different conformations. The relative populations of the three available conformations can be calculated by analysis of coupling constants. Such calculations have been carried out for tropic acid and derivatives,⁶⁷ and for aqueous solutions of scopolamine and atropine salts.⁶⁵ The relevant coupling constants measured for scopolamine ($J_{2',3'a} = 8.9$ Hz and $J_{2',3'b} = 5.2$ Hz, free-base, 0.1 M CDCl_3) were quite close to those reported for tropic acid methyl ester⁶⁷ (9.00 Hz and 5.30 Hz, respectively), whereas those for atropine (8.0 and 4.5 Hz, respectively) were lower than any other previously reported values for a tropic acid ester.⁶⁷

The three available staggered conformations for tropic acid derivatives can be represented in Newman projection:



Values of 12.1 Hz for anti vicinal coupling and 2.3 Hz for gauche coupling can be used in the following expressions⁶⁵ to determine the relative populations- P_I , P_{II} , and P_{III} :

$$(4.1) P_I + P_{II} + P_{III} = 1$$

$$J_{AX} = 5.2 = 2.3(P_I) + 12.1(P_{II}) + 2.3(P_{III})$$

$$J_{BX} = 8.9 = 12.1(P_I) + 2.3(P_{II}) + 2.3(P_{III})$$

The fractional populations of I, II, and III, respectively, are .67, .30, and .03 for scopolamine, and .58, .22, and .19 for atropine. R_1 values can be calculated using the expected relaxation vectors and the appropriate weighting for each conformation. By simple inspection of the diagrams above, a qualitative evaluation of relaxation contributions from H_2' to the H_3' protons is possible. In III, the contributions

from H2' to the 3' protons are clearly equivalent, whereas in I, the H2' contribution is greater for H3'a than H3'b and in II greater for H3'b than H3'a. Since the average population is heavily weighted to I in both atropine and scopolamine, it is predicted that H3'a should relax faster than H3'b. The observed R_1 values, however, follow an opposite trend (Table 4.13), indicating that a change in assignment may be necessary. Several other factors would have to be considered before such a change could be made. An analysis of cross-correlation in this system is required, since H3'a is somewhat tightly coupled to the more slowly relaxing H2' ($J/\Delta\delta = .23$). In addition, it is very likely that relaxation contributions from phenyl ring protons play a significant role in determining the relative R_1 values of H3'a and H3'b. These relaxation pathways will be further examined with respect to the R_1 values in the phenyl ring, and nOe data.

In a mono-substituted benzene, the ortho protons relax more slowly than the meta and para protons unless there are benzylic protons on the substituent. Clearly, there is only one adjacent relaxation pathway for an ortho proton, but two for the meta and para protons. The ortho protons in atropine, however, relax at the same rate as the meta and para protons, and in scopolamine, significantly faster. These elevated rates can be attributed to significant contributions from benzylic protons H2', H3'a, and H3'b.

Inspection of the diagrams describing the tropic acid conformation and subsequently, molecular models, suggest that the higher relaxation rate of ortho protons in scopolamine relative to atropine can be correlated to the greater preference for conformation I in scopolamine. In this conformation, the phenyl group is gauche to both 3' protons, hence, more efficient relaxation of ortho protons is expected than in either II or III, where the phenyl ring is gauche to only one 3' proton. The relatively lower normalized R_1 value in atropine reflects the higher population of the less relaxation efficient conformers, II and III. The expected relaxation pathway in the reverse direction, from the ortho protons to H3'a and H3'b, is also affected by relative populations, and must play a significant role in determining the relative values of R_1 for the 3' protons. Additional insights into relaxation in this system will be provided by the nOe data.

Specific spin-lattice relaxation pathways in tropane alkaloids were experimentally characterized by measurement of nOe enhancements (by the difference method) in scopolamine. The results of these experiments are given in Table 4.16. Analysis of relaxation pathways in terms of their structural implications was made with the aid of calculations (Dreiding molecular model method). The two parts of the molecule are isolated in terms of relaxation interactions, so each could be analyzed separately.

Table 4.16

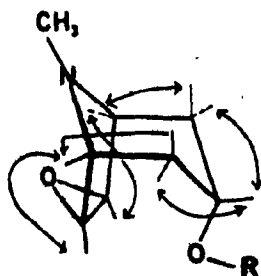
Nuclear Overhauser Effect Enhancements in Scopolamine¹

<u>{ }²</u>	<u>Key enhancements</u>	<u>Other Enhancements</u>
1	7	
2a	1	2e, 3
2e	1, 7	2a, 3
3	2a > 2e, 4a > 4e	
4a	5	4e, 3
4e	5,6	4a, 3
5	6	
6	5	7
7	1	6
2'	o-Ph	3'b
3'a	o-Ph	3'b
3'b	o-Ph	2', 3'a
CH ₃		1, 5

1. Measurements on 0.1 M solution in CDCl₃ at ambient temperature. o-Ph = ortho phenyl protons.

2. Irradiated proton.

In the tropane ring, relaxation pathways can be used to trace connectivities as had been carried out through decoupling experiments: 1 ↔ 2 ↔ 3 ↔ 4 ↔ 5. Note that in scopolamine, where there is only very small vinylic coupling to H6 and H7, the nOe experiments give not only the above mentioned connectivities, but also 5 ↔ 6 and 1 ↔ 7, completing the circle around the tropane ring:



Corroborative evidence for the H6, H7 assignment was also available from the enhancement of the signal from these protons in the {H4e} and {H2e} experiments. The presence of significant relaxation pathways between protons at C2 and C7, and C6 and C4 is exclusive to H6en \leftrightarrow H4e and H7en \leftrightarrow H2e, thus, the nOe data allow for the determination of stereochemistry at C6 and C7 (since the C6 and C7 protons are endo, the epoxide must be exo), and assignment of the diastereotopic C2 and C4 methylene protons. The differentiation of these methylene protons was also possible from the {H3} experiment. Calculations predicted that for H3 equatorial in a partially flattened tropane ring conformation, the relaxation pathway to the axial C2 and C4 protons should be greater than the corresponding pathways to the equatorial protons. The observed enhancements of H2a and H4a were three times as large as the H2e and H4e enhancements,* giving unambiguous proof that the previous assignments of these diastereomeric methylene protons⁶⁵ were incorrect.

* Such quantitative comparison of enhancements is only possible within a single experiment, and only if relaxation rates for the protons being compared are similar. Comparison of enhancements observed in separate experiments is not possible due to the use of sub-saturating power levels, short irradiation periods, etc.

With respect to the relaxation pathways in the tropic acid moiety, it has already been mentioned that the contributions of H2' to the relaxation of H3'a and H3'b are not expected to be equivalent. In addition, from nOe experiments, it was observed that the relaxation pathways from H2', H3'a, and H3'b to the ortho phenyl protons were not equivalent. Analysis of relaxation is severely complicated by the rotameric isomerism about the C2'-C3' bond but, in addition, the analysis of relaxation pathways involving the phenyl ring protons is further complicated by the rotational freedom of the phenyl ring. Interestingly, the crystal⁶¹ and solution⁶⁵ structures both indicate that the phenyl ring is tucked under the tropane ring, however, phenyl rotation in solution is not hindered on the nmr time scale, as indicated by the equivalence of the two ortho and two meta protons. Only single time averaged relaxation parameters are measurable, so, even though the contributions from the 2' and 3' protons may be very different for the two different ortho protons, the relaxation data are unable to differentiate between the two, because of the rapid exchange of relative positions. The presence of specific dipolar interactions is clearly indicated by the large nOe enhancements of the o-phenyl proton resonance upon pre-saturation of H2' (14%), H3'a (6%), and H3'b (4%), but detailed interpretation of such data are not possible.

Note that these enhancement magnitudes are given only to show that they are significant, and can not be compared to one another. Characterization of the specific relaxation pathways could in principle, be carried out by R_1 and nOe measurements at low temperature, providing that the phenyl rotation could be "frozen out".

In summary, the nOe evidence leads to a complete set of assignments of all resonances and unambiguously corroborates that the diastereotopic C2 and C4 methylene protons had been incorrectly assigned in previous studies.⁶⁵ The relaxation data were also used to infer structural information concerning the flattening of the piperidine ring in the tropane moiety, and to identify, in a non-specific manner, the existence of relaxation pathways between H2', H3'a, H3'b, and the ortho phenyl protons.

4.6.4. Cocaine

Partial assignments of 1H nmr parameters for cocaine in $CDCl_3$ solution have been reported at 250 MHz.⁶⁴ Our studies at 400 MHz (Table 4.12) agree with the previous assignments, except for the magnitudes of the various coupling constants in the H4a resonance. Carroll et al.⁶⁴ have assigned the value of the geminal coupling constant as 12.9 Hz and the vicinal coupling to H5 as 1.8 Hz, whereas we find that these values are 11.5 and 2.8 Hz, respectively. These differences may be attributable to differences in concentration, 0.05 M at 250 MHz versus 0.1 M at 400 MHz, or temperature effects.

As in previous studies, attempts at assigning C6 and C7 proton resonances were not undertaken, since discrete R_1 values cannot be measured in this very tightly coupled system (the effects of cross-correlation are significant).

The ^1H - R_1 values measured for cocaine (Table 4.13) were initially used to distinguish resonances. Methylene protons relaxed in the range 1.3 - 2.1 s^{-1} , aliphatic methines in the range 0.66 - 0.99 s^{-1} , and aromatic methines in the range 0.34 - 0.45 s^{-1} . The difference in the R_1 values of the N-Me (1.39 s^{-1}) and the O-Me (0.55 s^{-1}) groups is very significant, indicating a rather substantial difference in their steric environments.

Other important structural features which are reflected in the R_1 values of cocaine can be best interpreted by comparison of the corresponding values in other tropane alkaloids. The relaxation of H3 is appreciably faster in cocaine than in scopolamine or atropine, even though one of the significant relaxation pathways (to H2a or H2e) has been lost due to the substitution of a carbomethoxy group at C2. Calculations predicted that a reduction of 28% in the R_1 of H3, for C2 substitution at the axial position, and 19% for the equatorial position. An increase in the R_1 value of H3 could only be accounted for by a difference in the C3 stereochemistry. Faster relaxation is predicted for H3 in the axial position due to the additional efficient relaxation pathways available to H6en and H7en, as has been discussed above for tropine (see diagram (X)).

There is good agreement between the calculated (60%) and observed (50%) increase in the R_1 of H3, if the C2 substituent is in the axial position. These data confirm both C2 (β) and C3 (β) stereochemistry, in agreement with a crystal structure determination⁶⁸ and previous nmr studies.⁶⁴

The R_1 of H4a is smaller than that of H4e in cocaine, the opposite trend from that observed in the other tropane alkaloids. This reduction is mostly due to the loss of the relaxation pathway to H3, and to a much lesser extent, to the loss of the H2a contribution. The lower R_1 value for H1 relative to H5 results from the loss of the efficient relaxation pathway to H2a. Since calculations showed that the H5 relaxation pathway to the C2 axial proton is much more efficient than the pathway to the equatorial proton, the significant reduction observed in the R_1 of H5 corroborates the C2 stereochemistry--H2 is equatorial, the COOMe substituent is axial.

Finally, recall that the R_1 values for the o-phenyl protons in atropine and scopolamine were substantially larger than expected due to the presence of efficient relaxation pathways to benzylic protons. In cocaine, where there are no benzylic protons (benzoxy group instead of tropic acid ester), the R_1 values follow the expected trend for a simple mono-substituted benzene: para \sim meta > ortho.

4.7. Conclusion

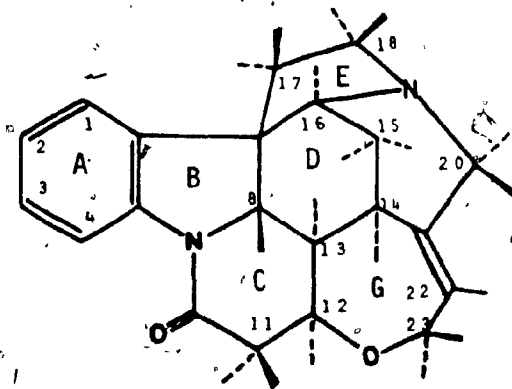
^1H - R_1 values provide an efficient method for the categorization of the spectral resonances into three groups: methylene protons relax rapidly; aromatic methine protons relax slowly; aliphatic methine protons relax in an intermediate range. When combined with simple mathematical modelling of relaxation pathways, relaxation parameters (R_1 and NOe enhancements) can provide insights into specific details of molecular structure. The accuracy of the model can be determined from the quality of the fit of calculated and observed values. The application of spin-lattice relaxation parameters to the assignment of high field ^1H spectra and the determination of molecular geometry and stereochemistry of alkaloids has been clearly demonstrated. Interestingly, for the alkaloids used in these studies, the solution and solid-state structures showed a great degree of similarity, since the relaxation data determined in solution could be accurately modelled using previously reported crystal structures.

Chapter 5

APPLICATION OF ^1H SPIN-LATTICE RELAXATION RATE MEASUREMENTS TO THE DETERMINATION OF STRUCTURE AND STEREOCHEMISTRY OF SOME STRYCHNOS ALKALOIDS

5.1. Introduction

^1H spin-lattice relaxation rate measurements have been used to examine the structure and stereochemistry of strychnos alkaloids- brucine, 16-hydroxystrychnine, 18-oxostrychnine, and five sulfonic acid derivatives of the parent compound, strychnine (I),* and brucine.



(I)

Initially, chemical shift assignments were made by comparison to published data on strychnine.⁶⁷ However, after preliminary analysis of ^1H -R₁ values, some anomalies in the published assignments became apparent.**

* The conventional structure used here for strychnine represents the enantiomer of the natural material.

** Tavernier and coworkers⁶⁸ reported that the geminal coupling constant for the C17 protons had been incorrectly assigned in the literature.⁶⁷

As a result, it was decided that a re-evaluation of the ^1H nmr spectrum of strychnine was necessary. From a detailed experimental study and mathematical simulation of relaxation pathways in strychnine, all resonances were assigned in an unambiguous manner. The in-depth analysis of relaxation in strychnine was then used to aid in the structure determination of the strychnine derivatives.

The relaxation expressions presented in Chapter 2 should be a good approximation for proton spin-lattice relaxation in strychnine and the derivatives studied here, since these molecules are quite rigid. It was, therefore, possible to utilize the relaxation pathway analysis technique for solution structure determination of strychnos alkaloids. In addition, calculation of relaxation pathways (Dreiding molecular model method) could be carried out in a straight forward manner. Verification of the structural assignments could then be achieved by comparing experimental and calculated R_1 values of protons in the immediate vicinity of the sites of substitution.

Since replacement of a hydrogen atom by a substituent changes the moments of inertia of the molecule, there are corresponding differences in correlation times for tumbling (t_c) which affect the measured R_1 values. For this reason, and since experimental conditions may vary from one experiment to another, normalization (see section 9.3) of the R_1 values was necessary before inter-comparisons could be made. The normalized R_1 values of strychnine,

18-oxostrychnine, 16-hydroxystrychnine, and brucine could be compared directly (Table 5.3), but comparisons between strychnine and the sulfonic acids were avoided because strychnine is insufficiently soluble in the common solvent, D_2O , utilized for study of the sulfonic acids. Since the sites of substitution in the sulfonic acids were in different parts of the molecule, and there were no instances where the same relaxation pathway was affected in two different sulfonic acids, it was possible to determine the effects of substitution on specific R_1 values by inter-comparison among the various isomers (Table 5.4).

5.2. A Partial Reassignment of the 1H NMR Spectrum of Strychnine

The previous assignments of the 1H nmr spectrum of strychnine were made at 250 MHz using a combination of aromatic-solvent-induced chemical shift changes, selective deuteration, double resonance techniques, and computer simulation of spectra.⁶⁷ Interpretation of the 1H spectrum of strychnine (Fig. 5.1) in the present study was facilitated by the greater chemical shift dispersion at 400 MHz. After preliminary analysis of the 1H - R_1 values of the strychnine sulfonic acids, a comparison of the experimental and calculated 1H - R_1 values of strychnine suggested that the stereochemical assignments of the geminal proton pairs at positions 15, 18, and 20 should be reversed.

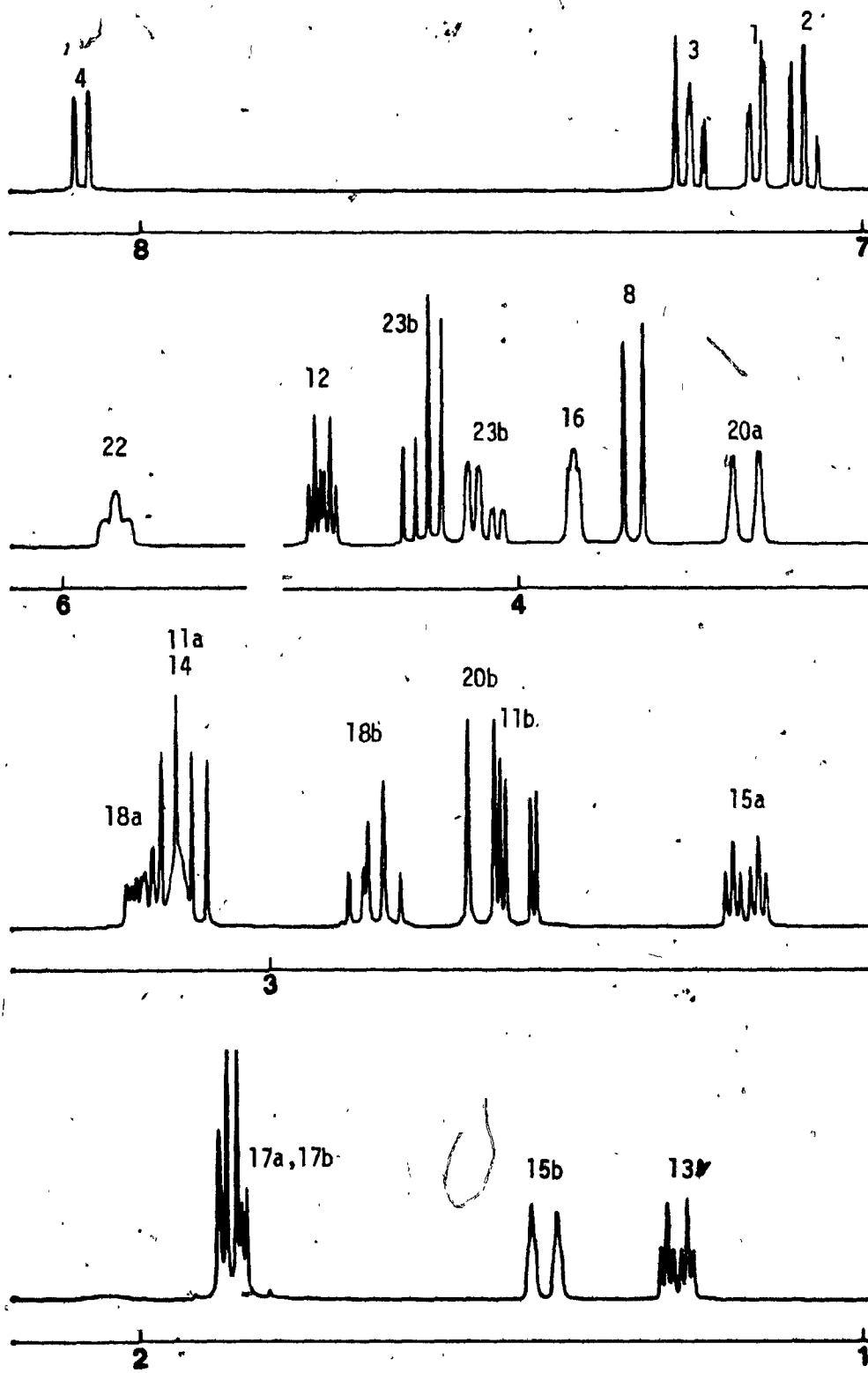


Fig. 5.1 400 MHz ^1H nmr spectrum of strychnine, 0.1 M CDCl_3 .

Relaxation pathway analysis was carried out in order to establish characteristic relaxation pathways for each proton of interest. Although both $^1\text{H-R}_1$ and nOe experiments were used in checking the ^1H chemical shift assignments of strychnine, the nOe data proved more definitive. The following discussion, therefore, centers on the nOe experiments. At least one key enhancement could be identified for all protons irradiated except H12 (Table 5.1). A key enhancement is defined here as:

1. An nOe enhancement which serves to identify either the irradiated or enhanced resonance.
2. An nOe enhancement which identifies a unique relaxation pathway having implications concerning the overall molecular structure.

The final assignments were checked by computer simulation of portions of the spectrum.

The signals due to the isolated C20 methylene group, adjacent to nitrogen, were originally assigned⁶⁷ as the simple AB pattern (with some long range coupling) at 3.70 and 2.72 ppm. The C15 proton signals (1.46 and 2.36 ppm) were assigned by comparison with the spectrum of 11a, 11b, 16-d₃-strychnine.⁶⁷ These assignments have recently been confirmed by 2D hetero- and homo-correlation methods.⁶⁹ Although there is no question as to the assignment of these four signals to the C20 and C15 protons, respectively, the problem of the stereochemistry of the assignments was not satisfactorily resolved.

Table 5.1

NOE Enhancements Determined for Strychnine
by the Difference Technique

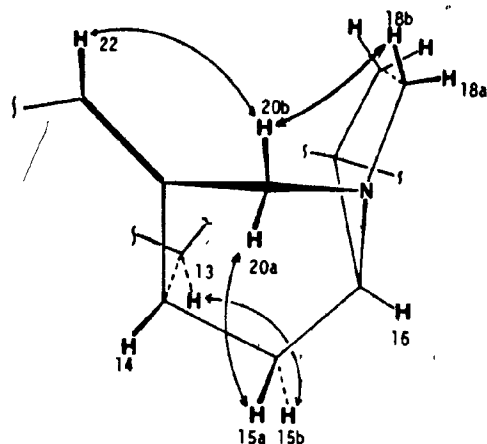
{ }	Key	Other	Negative ²
1	16, 17a, ^d 2 ^d		
12		13, 11b, 11a, 14	
13	15b	8, 12, 14	15a
14	23a	13, 15a, 15b, 12, 22	23b
15a	20a	15b, 16, 14	13
15b	13	15a, 16, 14	20a, 8
16	1	15a, 15b, 17a ^d	2
17a ³	1	17b, ^d 16, 18a	
17b ³	8	17a, ^d 18b	
18a	16 ^c	18b, 17a ^d	8
18b	8, 20b, 22	18a, 17b ^d	
20a	15a ^c	20b	15b, 22
20b	22, 18b ^d	20a	
22	20b, 23b, 18b ^c	8 ^c	20a
23a	12, 14	23b, 22	
23b	22	23a	

1. Spectra were determined at 400 MHz at ambient temperature (about 20°C) on non-degassed 0.1 M solutions in CDCl₃ and DMSO-d₆. Except for cases where overlap of signals in one solvent (eg. H17a and H17b in CDCl₃) prevented individual measurements, noe enhancements were observed in both solvents. "c" = CDCl₃ only, "d" = DMSO-d₆ only. { } = irradiated proton.

2. Negative enhancements arise from the three-spin effect³⁵ and depend on the choice of experimental conditions.

3. In CDCl₃ solution there is only a very small difference in H17a and H17b chemical shifts, so the enhancements were measured in a single experiment.

The key relaxation pathways for the protons at the 15 and 20 positions are indicated on partial structure II:



(II)

Saturation of the downfield (3.70 ppm) H20 signal produced an nOe at the downfield (2.36 ppm) H15 signal. Based on calculated nOe values, it is clear that the only significant relaxation pathway for one of the C20 protons with one of the C15 protons is between H20a and H15a. Saturation at 2.36 ppm gave the expected enhancement to the signal at 3.70 ppm, further corroborating the assignment. For additional proof, the other C20 proton, H20b, was identified by key nOe enhancements to and from H18b (2.87 ppm) and the vinylic proton, H22. Since the assignment of H22 is unambiguous, the above experiments verify the assignments of both H18b and H20b. In addition, H15b (1.46 ppm) was characterized by enhancements to and from H13 (unambiguously identified previously^{67,69}). A selected number of the nOe experiments are shown in Fig. 5.2.

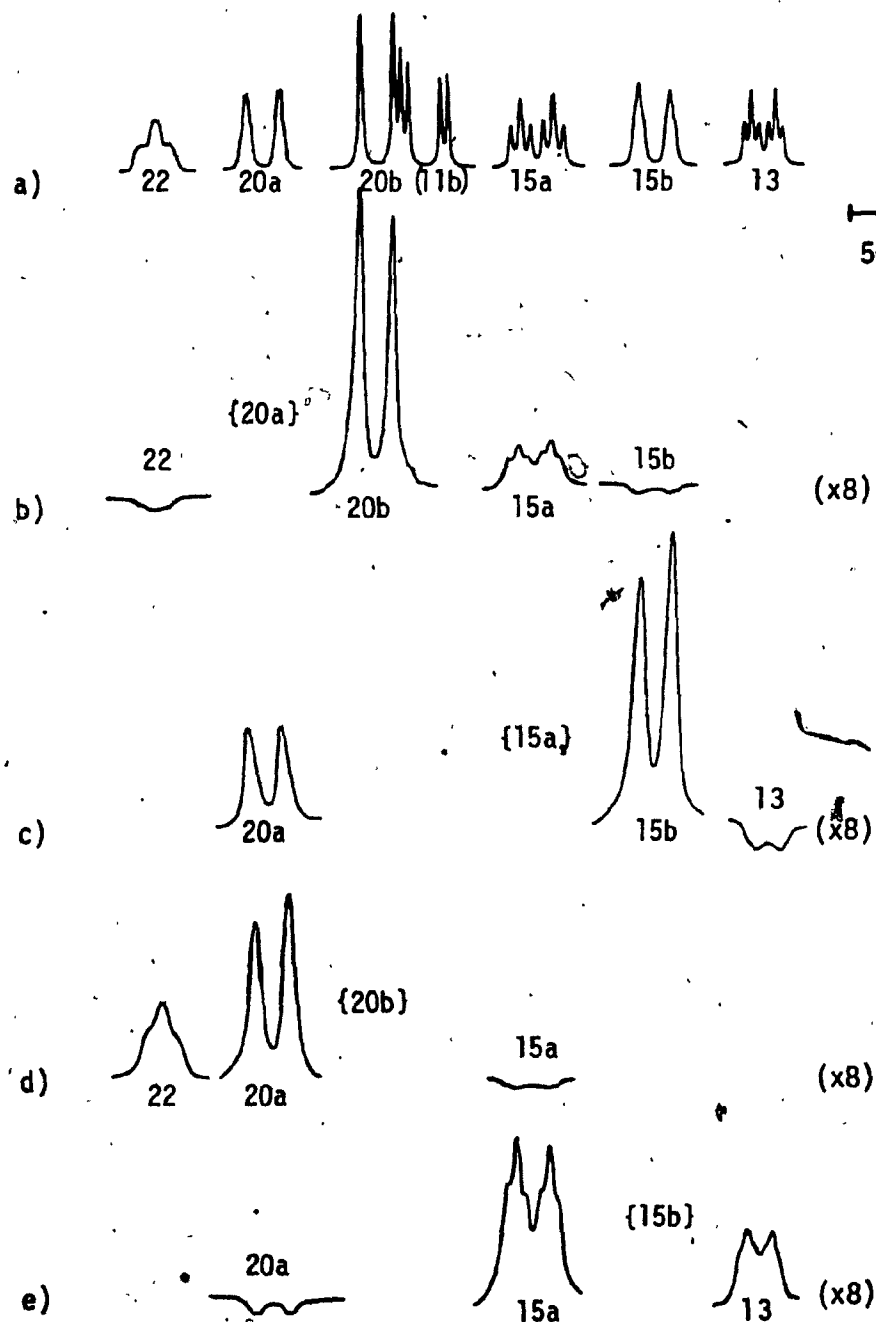
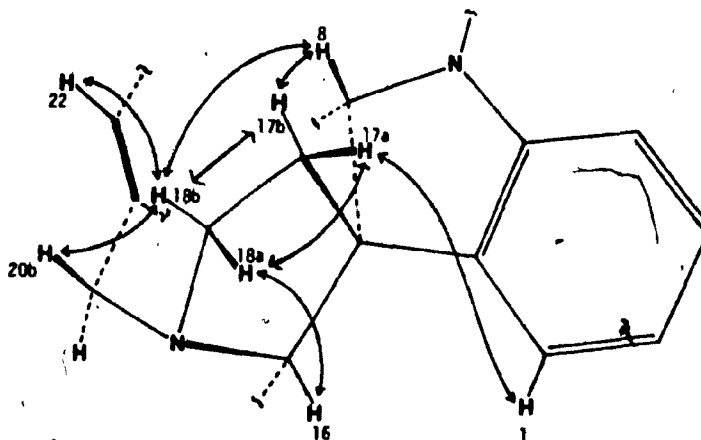


Fig. 5.2. NOe difference spectra to determine the assignments of diastereotopic methylene protons at C15 and C20 in strychnine (0.1 M CDCl_3): a) normal spectrum, b)-e) nOeds.

The nuclear Overhauser effects to and from H20b and H18b served as an entry into the ABMX system of protons 17a, 17b, 18a, and 18b. This spin system was initially analyzed from spectra of a DMSO-d₆ solution because, in this solvent, the four signals were more clearly separated and the C17 protons were less tightly coupled than in CDCl₃ solution. Calculations predicted that these protons could be differentiated by their nOe enhancements, as shown in the partial structure, III:



(III)

Experimental results verify that H18b has effective relaxation pathways to H8, H22, and H20b, whereas H18a has an effective pathway to H16. The C17 protons were distinguished by large key enhancements between H17a and H1, and between H17b and H8. Pertinent nOed experiments are shown for both DMSO-d₆ (Fig. 5.3) and CDCl₃ (Fig. 5.4) solutions.

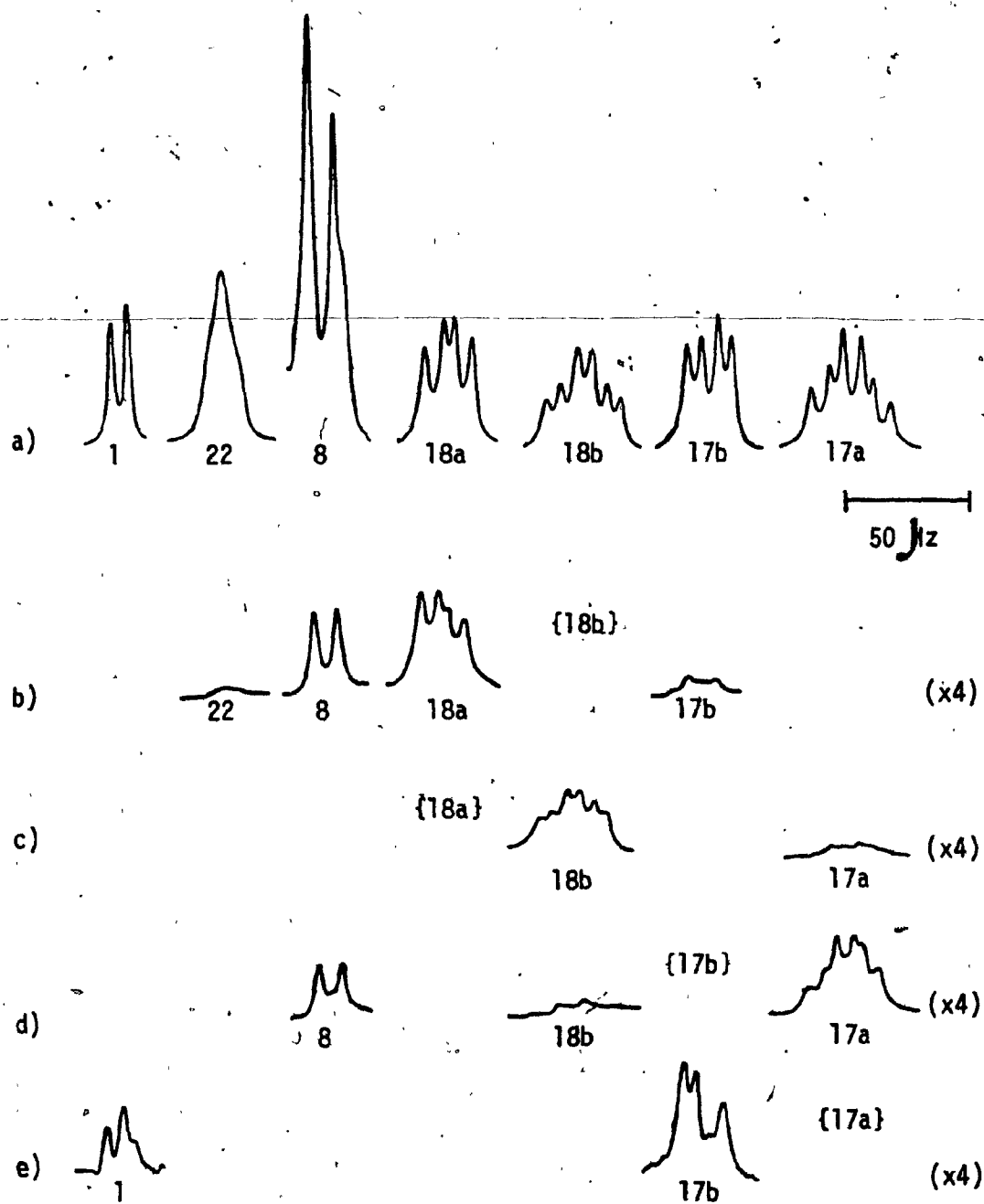


Fig. 5.3 NOe difference spectra to determine the assignments of diastereotopic methylene protons at C17 and C18 in strychnine (0.1 M DMSO- d_6): a) normal spectrum b)-e) nOeds.

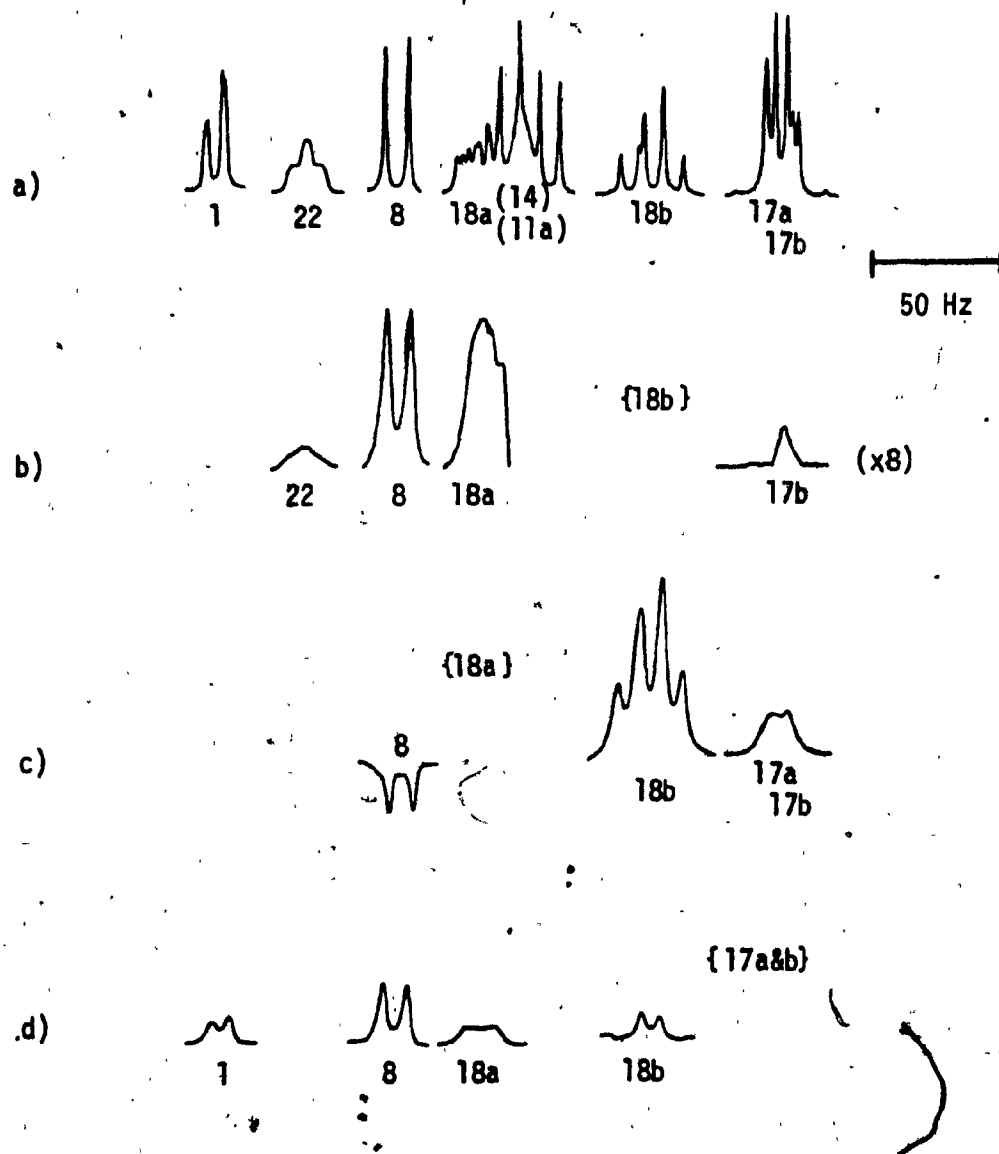


Fig. 5.4 NOE difference spectra to determine the assignments of diastereotopic methylene protons at C17 and C18 in strychnine (0.1 M CDCl₃): a) normal spectrum, b)-d) nOeds.

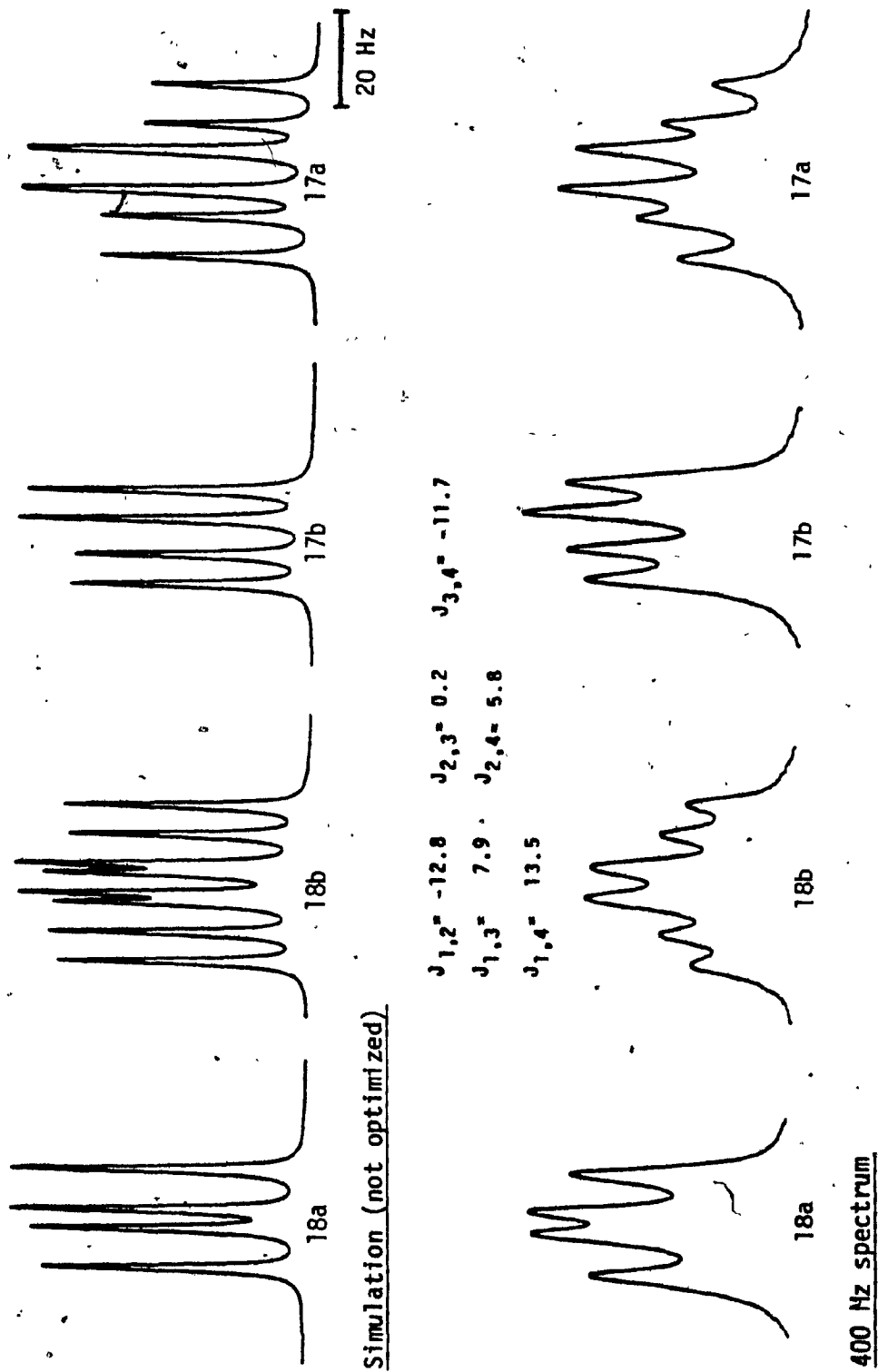


Fig. 5.5 Assignment of the ABMX spin system in ring E of strychnine, 0.1 M DMSO-d₆ solution.

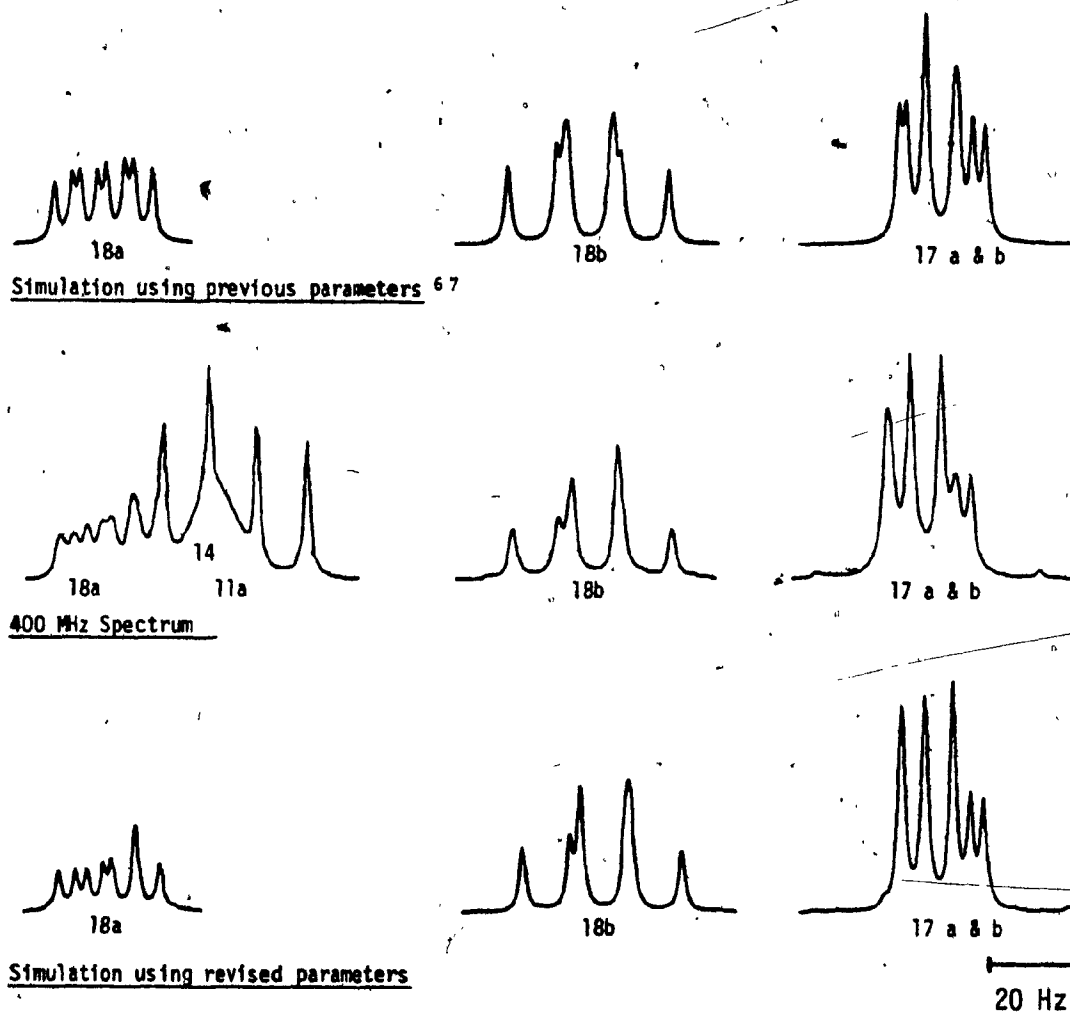
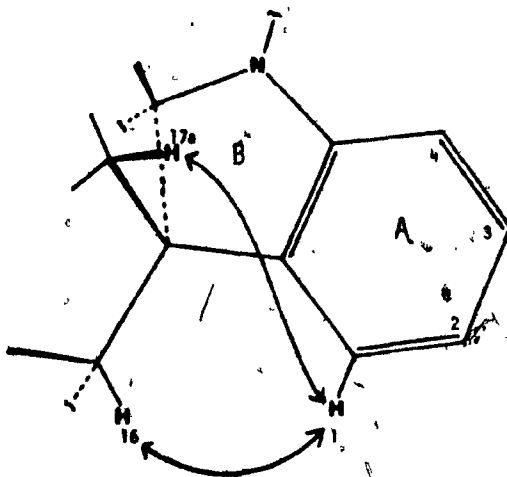


Fig. 5.6 Assignment of the ABMX spin system in ring E of strychnine, 0.1 M CDCl_3 solution.

Attempted computer simulation (LAOCOON III⁷⁰) of the ring E ABMX system (in DMSO-d₆ solution) failed to produce a reasonable fit, when a coupling constant of 0.2 Hz was utilized for the geminal pair at C17 as had been previously reported.⁶⁷ When the simulation was repeated, starting from a more normal⁷¹ value of -13 Hz for $^2J_{17a,17b}$, the calculation rapidly converged to an excellent fit to the experimental spectrum (Fig. 5.5).

The information obtained from the DMSO-d₆ spectrum was then correlated with the CDCl₃ spectrum. The relative ¹H-R₁ values and the nOe enhancements (Fig. 5.3) for the C18 gem protons were measured giving an unambiguous assignment of the signals. With CDCl₃ assignments of H18a and H18b and coupling constant data from the DMSO-d₆ spectrum, LAOCOON III simulation yielded an excellent fit to the experimental spectrum (Fig. 5.6). The set of corrected assignments of chemical shifts and coupling constants is given in Table 5.2.

The existence of an efficient inter-ring relaxation pathway between the aromatic ring proton, H1, and H17a provides structural information about the strychnine molecular framework. The close proximity of H17a on the bridging ring D is partially responsible for the observation that H1, on the apparently isolated aromatic system, relaxes much faster than the corresponding proton at position 4, and even faster than H2 and H3, which have two, as opposed to one, adjacent neighbors on the ring, IV.



(IV)

There is also an efficient inter-ring relaxation pathway between H1 and H16. It should be noted that the usual two-dimensional representation of the strychnine structure gives a misleading impression of the relative placement of H1 with respect to H16 and H17a.

A final point of interest concerns the coupling (0.9 Hz) between the vinylic proton, H22, and the C20 proton with a signal at 3.70 ppm, originally assigned to H20b.⁶⁷ The dihedral angle between H20b and the plane of the double bond is very close to 0° . The presence of any measurable coupling between H22 and H20b would, therefore, be unusual.⁷² When the stereochemistry of the original assignments at C20 was reversed, this coupling constant no longer appeared to be anomalous. The dihedral angle between H20a and the plane of the double bond is about 100° , so a small (<3 Hz), but significant coupling is to be expected.⁷²

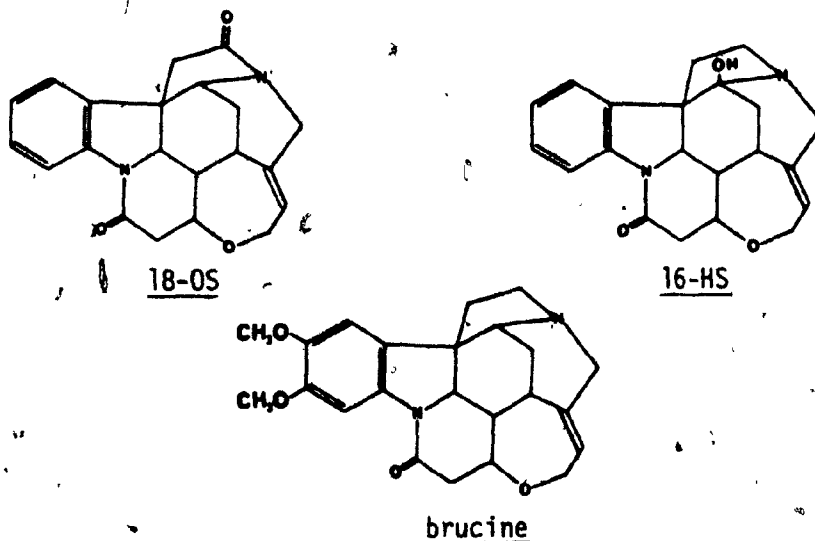
Table 5.2
 Revised ¹H Chemical Shifts and Coupling Constants for Strychnine¹

Proton	δ^2	Coupling constants, J (Hz) ³			
15a	2.36	15a,15b = -14.5	15a,16 = 4.9	15a,14 = 4.0	
15b	1.46	15b,16 = 2.0	15b,14 = 1.0		
17a	1.88	17a,17b = -15.5	17a,18a = 8.4	17a,18b = 11.7	
17b	1.89	17b,18a = 0.1	17b,18b = 6.9		
18a	3.19	18a,18b = -10.2			
18b	2.87				
20a	3.70	20a,20b = -14.7	20a,22 = 0.9		
20b	2.72				

1. The remaining assignments were in agreement with those in Ref. 67. Chemical shifts and coupling constants for the 17 and 18 protons were determined by spectral simulation, using a modified version of the program LAOCOON III (see Ref. 70). The other values were measured directly from the spectrum.
2. Measured from a 0.1 M CDCl₃ solution with δ values reported in ppm from 0.1% internal TMS.
3. Negative signs were assumed for geminal coupling constants.

5.3. 18-Oxostrychnine, 16-Hydroxystrychnine, and Brucine

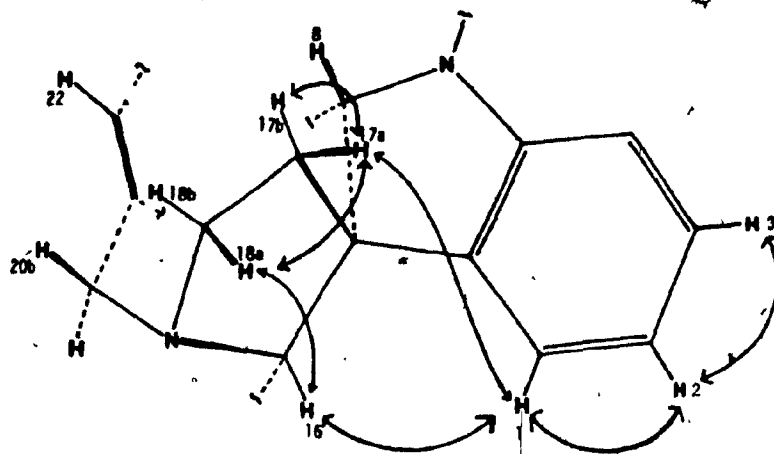
The sites of substitution in 18-oxostrychnine (18-OS), 16-hydroxystrychnine (16-HS), and brucine could be inferred



from characteristic differences in the CDCl_3 400 MHz ^1H spectra, relative to strychnine. In 18-OS, only C17 and C18 protons were perturbed, whereas in 16-HS, the H16 signal disappeared and the C15 protons were slightly affected. These spectral changes have been previously observed in 18-OS and a strychnine derivative with H16 replaced by deuterium,^{67,73} though some of the reported assignments were incorrect. Assignments were corrected on the basis of the studies of strychnine, described in the previous section of this chapter. In CDCl_3 , other than the simplification in the aromatic region to just two singlets, and the addition of the two methoxy group singlets around 4 ppm, the spectrum of brucine is nearly superimposable with that of strychnine. Relaxation pathway

analysis was carried out on all of these compounds, solely from $^1\text{H-R}_1$ data (Table 5.3), to verify the sites of substitution and to demonstrate the viability of this technique for structural analysis of strychnine derivatives.

For 16-HS, the lack of significant changes in the ^1H spectrum indicates that the basic structure of the molecule had not been altered. The only $^1\text{H-R}_1$ value which appeared to be affected (relative to strychnine) was that of H1. Calculations indicated that there were only three major contributors to H1 relaxation, H2, H16 and H17a, so the substituent had to be located at one of these positions, VI.



(VI)

Nearly 50% of H3 relaxation is attributable to dipolar interactions with H2, so substitution at C2 could be ruled out because the R_1 value of H3 was unaffected. The lack of an effect on the R_1 of geminal partner H17b, ruled out substitution at 17a. H16 appeared to be the only logical choice. No other significant effects on R_1 values had been

Table 5.3

Normalized R_1 Values of Strychnine Alkaloids^{1,2}

H	strychnine	brucine	16-HS	18-OS
1	.63	.72 [+15%]	.48 [-25%]	.7 ⁺
2	.47	.84 (OMe)	.48	.50 ⁺
3	.47	.71 (OMe)	.48	.5
4	.29	.38 [+30%]	.30	.31 [-30%]
8	.74 ⁺	.81 ⁺	.81	.52 [-30%]
11a	1.2	1.29	1.29	1.45
11b	1.20	1.4	1.26	1.45
12	(1.15)	(1.71)	(1.20)	(1.05)
13	.96 ⁺	.92 ⁺	.91	.90
14	.9	.9	.89	.91
15a	2.09	2.08	2.00	2.12
15b	1.92	1.93	1.83	2.03
16	.90	1.01	-	.79
17a	1.64*	1.62*	1.61	1.30 [-20%]
17b	1.64*	1.62*	1.66	1.34 [-20%]
18a	1.64 ⁺	1.62 ⁺	1.63	-
18b	1.8	1.9	2.0 ⁺	-
20a	1.59	1.62	1.68 ⁺	1.67
20b	1.55	1.56	1.7 ⁺	1.55 [-00%]
.22	.62	.60	.61	.57 [-10%]
23a	1.7*	1.6*	1.7*	1.8*
23b	1.2*	1.4*	1.4*	1.4*

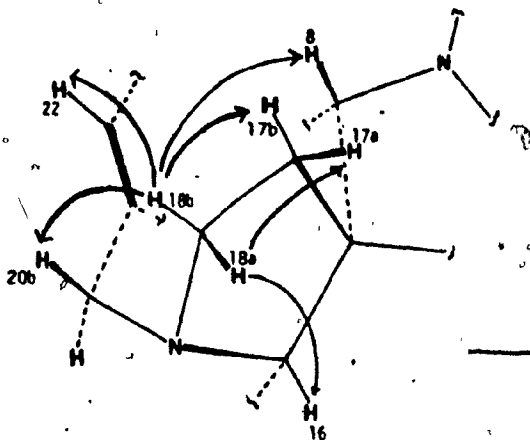
1. All values measured from 0.1 M $CDCl_3$ solutions at 293°K, and normalized to the R_1 value (s^{-1}) of H12, given in parentheses ().

2. The observed R_1 differentials relative to strychnine are given in brackets []. "*" = tight coupling, "+" = overlapped resonances.

observed,* as predicted by the calculations, because H16 has a relatively isolated location. The site of substitution had, therefore, been uniquely characterized and unambiguous assignment was possible.

The analysis of relaxation data for 18-OS was more complicated than that of 16-HS, since there is a much larger perturbation of the basic strychnine structure. The formation of a lactam function in ring E (at positions C18 and N19), implies a change in the rigid molecular framework. R_1 effects would, therefore, be expected not only from the loss of H18a and H18b, but also from changes in the relative proximities of ring E, and possibly, ring F protons.

Initial analysis of relaxation data was carried out by calculation of the effects on ^1H - R_1 values, upon removal of H18a and H18b. Significant (>10%) effects were predicted for H8, 16, H17a, H17b, H20b, and H22:



(VII)

* The significant difference in the R_1 values of H23b, relative to strychnine, is attributable to changes in cross-correlation effects due to tight-coupling to H23a.

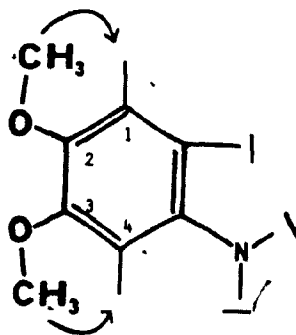
The agreement between these calculated and observed values was excellent. In addition, significant reductions, which were not predicted, were observed in the in the R_1 values of H1 and H16. These effects were rationalized using the following logic:

1. For the R_1 of H8 to have been affected, there could only have been substitution at positions 11b, 17b, or 18b, as indicated by the calculated relaxation pathways.
2. Reductions in the R_1 of H20b and H22 were only compatible with substitution at H18b.
3. No other protons in the vicinity of H11b including H11a) were affected, so this possibility could be ruled out.
4. The two anomalous R_1 effects, a larger than predicted (-7%) reduction in the R_1 of H16 and reduction in the R_1 of H1, are both attributable to a change in the relative distances to H17a, in response to structural changes induced in ring E.

The model chosen for interpretation of the relaxation data was, therefore, completely consistent, and the site of substitution (C18) was unambiguously confirmed.

The similarity of the 400 MHz ^1H spectrum of strychnine and brucine indicates that the substitution of methoxy groups at C2 and C3 does not affect the structure of the rest of the molecule. A great similarity in $^1\text{H-R}_1$ values for all, except ring A protons is experimentally observed (Table 5.3), further corroborating that the basic atomic framework is not perturbed. Following the previously developed logic (section 4.4.1) for determining methoxy group conformation from $^1\text{H-R}_1$ values of adjacent protons, it was possible

to determine the preferred orientations of the 2-OMe and 3-OMe groups. On the basis of potential adverse steric interactions, orientations 1-cis and 4-cis are predicted to be the most stable for 2-OMe and 3-OMe, respectively:



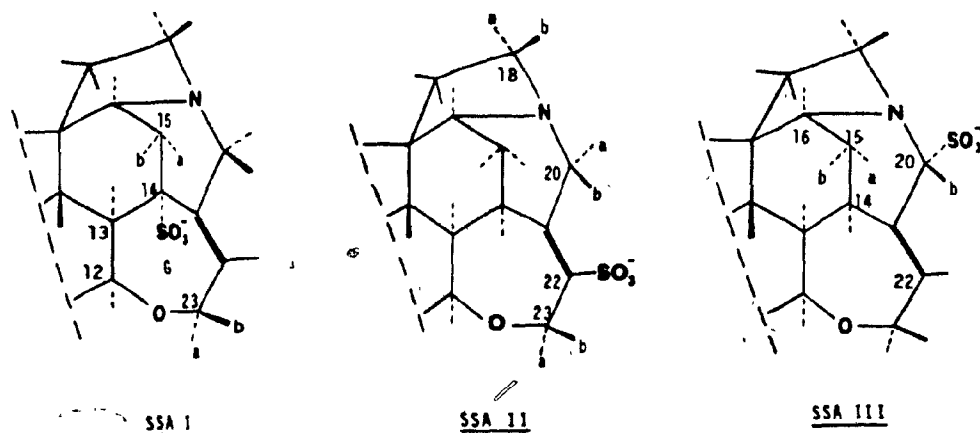
This hypothesis has been confirmed for model dimethoxy benzenes in a number of different studies.⁷⁴⁻⁷⁶ The elevated R_1 values of H1 and H4, relative to those in strychnine (Table 5.3) indicate that the same orientations which are preferred in the models are also preferred in brucine. For example, upon substitution at C2, the principle relaxation pathway for H1 (to the adjacent proton, H2) is lost, so an increase in the R_1 of H1 is only possible if the methyl protons of the 2-OMe group are in close proximity to H1. The 1-cis and 4-cis orientation must be preferred for the methoxy groups at C2 and C3, respectively. Note that, as for strychnine, H1 and H4 can be distinguished on the basis of the higher R_1 value for H1 (due to efficient relaxation pathways to H16 and H17a). The methoxy resonances can be identified by a single nOe experiment; the saturation of one of the methoxy signals will cause an enhancement of only the adjacent ring proton: H1 \leftarrow {2-OMe}, H4 \leftarrow {3-OMe}.

5.4 Strychnine Sulfonic Acids

In 1908-1909, Leuchs and Schneider⁷⁷ obtained three mono sulfonic acids (designated SSA-I, -II, and -III) on work-up of the solution obtained by bubbling sulfur dioxide through a warm aqueous solution of strychnine containing suspended manganese dioxide. A similar series of isomeric brucine sulfonic acids were also synthesized by this same method (designated BSA-I, -III, -IV). Although Leuchs and his collaborators continued to study these sulfonic acids for more than 30 years,⁷⁸ little became known of their structures, other than that SSA-I was not sulfonated on the aromatic ring or at the 11-position, until further studies were undertaken by Edward and coworkers.⁷⁹

On repeating Leuchs' procedures, the same six strychnine and brucine sulfonic acids were isolated: X-ray crystallographic analysis of a sample of SSA-I obtained at this time showed it to have the sulfonic acid group located at the allylic 14-position.⁸⁰ In addition, a comparison of optical rotations and pK_{BH^+} measurements suggested that SSA-I and BSA-I, SSA-III and BSA-III, and SSA-II and BSA-IV were structural analogues.⁷⁹

On the basis of pH measurements, ¹³C nmr spectra, and chemical arguments, the sulfonic acid groups in SSA-II and SSA-III (and by analogy, BSA-IV and BSA-III) were assigned to the vinylic 22-position, and the allylic 20-position, respectively.⁷⁹ The stereochemistry of substitution at position-20 in SSA-III was not established. To gain



(IX)

further insight into the structures of the sulfonic acid derivatives, a study of their ^1H spin-lattice relaxation rates was undertaken. Since its structure was already known, SSA-I was used in this study as a model compound, to evaluate the viability of the $^1\text{H-R}_1$ method for sulfonic acid derivatives of strychnine.

Proton chemical shift assignments for the sulfonic acids were made initially by comparing the 400 MHz ^1H spectra with the spectrum of strychnine in DMSO-d_6 and CDCl_3 , using the revised assignments (Table 5.2). NOed experiments and computer simulations were required to analyze the spectrum of SSA-III. Since the SSA and BSA structures were so similar, their spectra nearly superimposable, and $^1\text{H-R}_1$ values nearly identical (within experimental error), the discussion of results will be focussed on the SSA compounds, though BSA data are also reported here (Table 5.4). The conclusions drawn from the SSA data are equally valid for the BSA analogues, in all cases.

Table 5.4

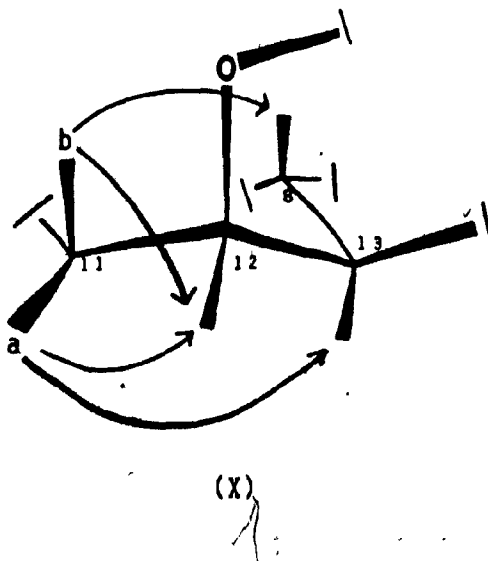
Normalized R_1 Values of the Sulfonic Acid Derivatives

<u>Proton</u>	<u>SSA-I²</u>	<u>BSA-I²</u>	<u>SSA-II²</u>	<u>BSA-IV²</u>	<u>SSA-III</u>
1	.63	.81	.70	.82	.70
2	.48	.90(OMe)	.53	.93(OMe)	.53
3	.50	.76(OMe)	.55	.82(OMe)	.52
4	.33	.48	.34	.49	.38
8	.78 [#]	.83 [#]	.82 [#]	.86 [#]	.89
11a	-	-	-	-	1.7
11b	-	-	-	-	1.7
12	.64 [#]	.69 [#]	.89 [#]	.93 [#]	1.3
13	.76	.81	1.1	1.4	1.1
14	- [#]	- [#]	1.22	1.2	1.1
15a	2.3	2.2	2.6	2.4	2.0
15b	2.2	2.2	2.6	2.4	2.5
16	(1.88)	(1.81)	(1.98)	(1.71)	(1.98)
17a	2.1	2.1	2.0	2.0	1.9
17b	2.2	2.2	2.1	2.1	2.2
18a	2.0	1.9	2.0	1.9	1.8
18b	2.4	2.3	2.4	2.2	2.0
20a	2.1	1.9	2.0	1.9	- [#]
20b	2.2	2.0	1.88	1.7	.58
22	.90	.95	- [#]	- [#]	.91
23a	- ⁺	- ⁺	2.1	1.9	2.0
23b	1.7	1.7	- ⁺	- ⁺	1.7

1. R_1 values from 0.1 M D₂O solutions at ambient temperature and normalized to H16, whose R_1 is given in parentheses ().
 "#" = site of substitution, "+", = R_1 not measurable.

2. One drop of NaOD solution was added to increase solubility. C11 protons were deuterated in these compounds, so certain R_1 values, indicated by "#", were reduced.

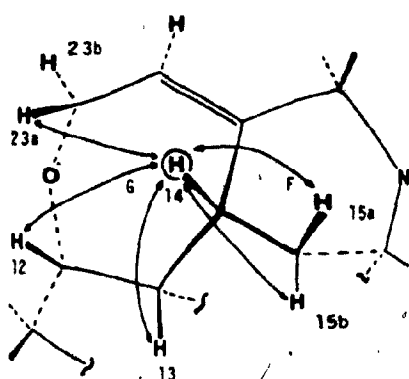
Since SSA-I and SSA-II were sparingly soluble in D_2O , it proved necessary to add a drop of NaOD solution to improve their solubility. This created a complication in that the hydrogen atoms at position 11 are acidic, and were replaced by deuterium. Reductions in the R_1 values of H8, H12, and H13 (X) of these compounds were expected, because deuterium has only about 6.3% of the relaxation efficiency of protium.¹⁶ These factors were easily accounted for in the calculations.



5.4.1. Strychnine Sulfonic Acid I

The site of substitution (C14) of SSA-I may be inferred from the disappearance of the 1H signal (3.14 ppm) attributed to H14 in strychnine,^{*} and the resulting change in the appearance of the multiplets arising from protons coupled to H14 (i.e. H13, H15a, H15b). Calculation of the effect of replacement of H14 on R_1 values of neighboring protons predicted reductions in the R_1 of H12, H13, H15a, and H15b, XI:

^{*} In $DMSO-d_6$ solution containing one drop of 40% DCl/D_2O .



R_1^{12-14}	=	11%
R_1^{13-14}	=	20%
R_1^{15a-14}	=	10%
R_1^{15b-14}	=	7%
R_1^{23a-14}	=	10%

(XI)

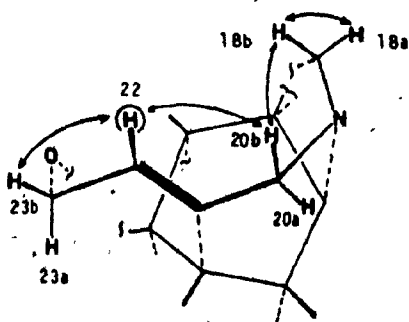
A significant effect on the R_1 value of H23a was also predicted, but was not measurable for experimental reasons.** Analysis of the R_1 value of H12 is complicated by the effect of deuteration at 11a and 11b, but the magnitude of this influence could be established by comparing the H12 R_1 values (Table 5.4) of SSA-II (deuterated) and SSA-III (non-deuterated). The difference in H12 R_1 values of SSA-II and SSA-I could then be attributed to the effect of substitution at position 14. On comparing the other R_1 values of SSA-I with those of SSA-II, the reductions predicted by the calculations were apparent. A large decrease in the R_1 value of H13 and smaller decreases in

** In SSA-I, the H23a signal is in close proximity to the residual HOD signal of the solvent, and a reliable R_1 value could not be obtained. The spread of saturation power from solvent suppression has the effect of reducing the intensity of the H23a signal and making the apparent R_1 value larger. The same problem arises for the H23b signal of SSA-II.

the R_1 values of H15a and H15b were observed (Table 5.4). This unique combination of effects on measured R_1 values is in complete agreement with the assignment of position 14 as the site of substitution.^{79,80}

5.4.2. Strychnine sulfonic acid II

Initial verification of the site of substitution in SSA-II was provided by the disappearance of the characteristic H22 vinyl proton signal (5.90 ppm) of strychnine,^{*} accompanied by only minor changes in the appearance of other signals. The only R_1 value showing a significant reduction was that of H20b (Table 5.4). Calculations identified H20a, H18b, and H22 as the major contributors to the relaxation of H20b:



R_1	H20b + 22	=	16%
R_1	H20b + 18b	=	16%
R_1	H23b + 22	=	13%
R_1	H18a + 18b	=	74%

(XII)

thereby establishing three possible sites of substitution. H22 was the logical choice because substitution at 20a would reduce the R_1 of H20b to a much greater extent than had been

* See footnote on p. 176.

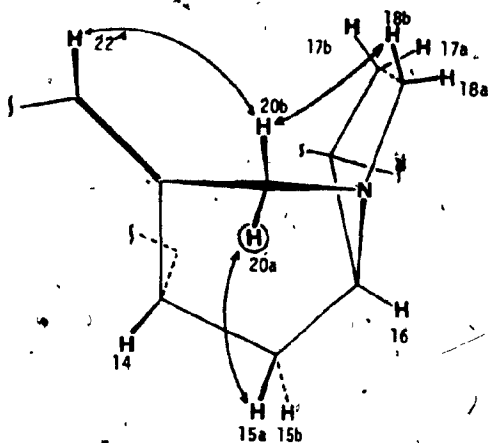
observed, and substitution at 18b would cause substantial R_1 effects on other protons, in particular H18a and H8. Calculation of the effect on other protons from replacement of H22 predicted significant decreases in R_1 values only for H20b and H23b, XI. For practical reasons,* an R_1 value for H23b could not be measured, but there was agreement between the calculated and observed influences on H20b. Hence, for this molecule, the R_1 evidence clearly indicated that substitution had occurred at position 22.

5.4.3. Strychnine sulfonic acid III

The site of substitution (C20) of SSA-III could be inferred from the ^1H spectrum, the only two substantial differences with respect to the spectrum of strychnine being the loss of the AB pattern of the H20 signals (3.70 and 2.72 ppm)* and the appearance of a sharp singlet, shifted significantly downfield (6.0 ppm). The loss of two signals from the spectrum without significant effects on coupling constants directly implied that substitution had occurred at position 20, since this is the only site with magnetically isolated (i.e. with no vicinal coupling constants) geminal protons. The large downfield shift of the remaining proton signal is consistent with a geminal relationship with the sulfonic acid substituent. The assignment was in agreement with the previous studies on SSA-III.⁷⁹

* See footnote on p. 176.

An efficient means of determining the stereochemistry at C20 is to evaluate the relaxation pathways of the remaining proton. The most important pathways available to H20a and H20b are summarized in XIII:



$$\begin{aligned} R_1 15a + 20a &= 16\% \\ R_1 22 + 20b &= 41\% \\ R_1 18b + 20b &= 14\% \end{aligned}$$

(XIII)

Calculation of the effects on the R_1 values of neighboring protons for substitution at 20a indicated significant reductions in the R_1 values of H20b and H15a. The corresponding calculation for substitution at 20b indicated significant reductions in the R_1 values of H20a, H18b, and H22. A clear distinction between the possibilities should, therefore, be possible.

Close inspection of the spectrum of SSA-III indicated that changes in the magnitudes of the coupling constants of the 17 and 18 protons are induced by substitution, implying a change in the geometry of ring E, and possible changes in the efficiencies of the relaxation pathways for H18b.

Together with an observed reduction in the normalized R_1 of H18b there were corresponding changes in the relative

R_1 values of H17a, H17b, and H18a (Table 5.4). This complication led to uncertainty in the prediction of the relaxation contribution from H20b, so that the R_1 value of H18b could not be used as a basis of the assignment. Since there was no spectral evidence of a conformational change affecting any other protons, a distinction between the two sites of substitution, 20a and 20b, was made on the basis of the R_1 values of H15a and H22.

Comparison of the R_1 values (Table 5.4) of SSA-III with SSA-I and SSA-II showed that the relative R_1 value of H22 was unchanged, but that of H15a was reduced. The reduction in the R_1 value of H15a relative to that of its geminal neighbor, H15b, is a good indication that H15a has been substantially affected. Consistency in the R_1 values of H14 and H16 suggested that there was no significant change in ring geometry affecting H15a and H15b. It is clear, therefore, that the site of substitution in SSA-III is 20a.

To substantiate this assignment, the nOe difference spectrum was measured for saturation of the remaining H20 resonance. This experiment was ideal from a practical standpoint, since the signal was completely isolated from the rest of the spectrum, and from a theoretical standpoint since the specific relaxation pathways of this proton could be characterized. A large enhancement was seen for H22, and a small enhancement for H18b (Fig. 5.7). These nOe enhancements establish that the irradiated signal was a proton at position 20b, thereby confirming that the site of substitution in SSA-III is 20a.

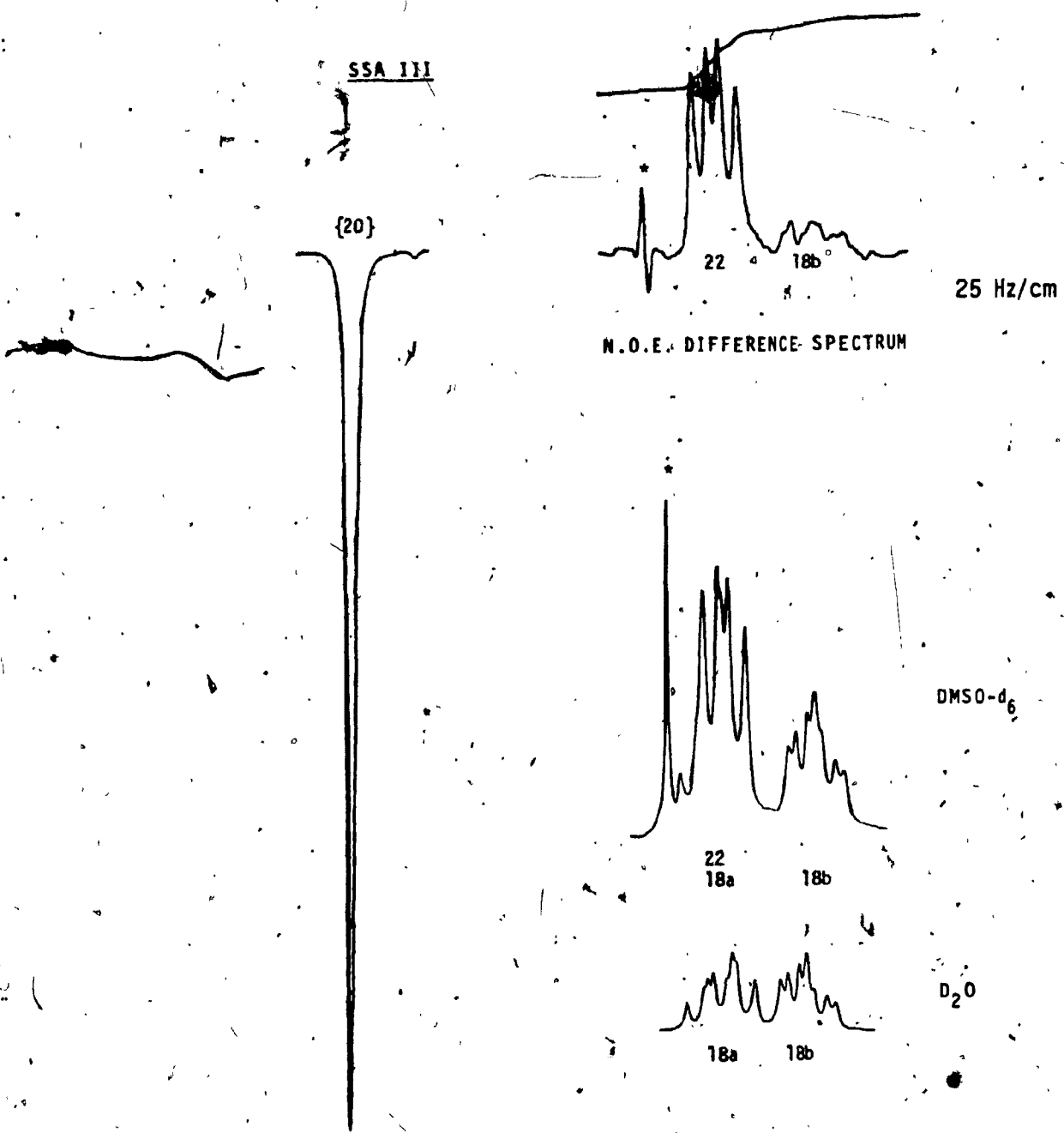


Fig. 5.7 Determination of C20 stereochemistry in SSA III by a nOe difference experiment.

5.5. Conclusion

¹H Relaxation pathway analysis in strychnine, using NOE experiments, was utilized to correct the chemical shift assignments of the diastereotopic methylene pairs at C15, C17, C18, and C20, and coupling constant assignments in the ABMX system of C17 and C18 protons. For the three strychnos alkaloids- 16-HS, 18-OX, and brucine, it has been shown that the set of observed effects on ¹H-R₁ values uniquely identifies the site of structural perturbation. This allows for an unambiguous confirmation of the structures of 16-HS and 18-OS, and for the determination of the methoxy group conformations in brucine. Using the same methodology, proposed sites of substitution for the strychnine and brucine sulfonic acids have been verified, and the previously undetermined stereochemistry of SSA-III (and by analogy BSA-III) has been established. These results are clear evidence that relaxation pathway analysis can be successfully applied for solution structure determination of complex alkaloids.

Chapter 6

APPLICATION OF ^1H RELAXATION PATHWAY ANALYSIS TO THE DETERMINATION OF THE STRUCTURE AND STEREOCHEMISTRY OF SOME 7-HYDROXYINDENE DIMERS

6.1 Introduction

Application of the relaxation pathway analysis technique will be demonstrated by the determination of the solution structure of a series of methyl-substituted 7-hydroxyindene dimers, 1-6 (Fig. 6.1).

One of these compounds, 5, was originally obtained as a mixture with its C-3 epimer, together with the expected tertiary alcohol, on the treatment of 3,4-dimethyl-7-hydroxyindan-1-one with methylmagnesium iodide. The structure of 5 was initially assigned⁸¹ on the basis of its 60 MHz ^1H nmr spectrum, and was confirmed by an X-ray diffraction study of its 6-bromo derivative.⁸² Subsequent investigation resulted in the synthesis and isolation of the remaining compounds.⁸³ In general, the dimers were prepared by treatment of the relevant indene in chloroform with 0.5% trifluoroacetic acid. Of the tetramethyl dimers, 1 and 2, prepared from 7-hydroxy-1,4-dimethyl-1-indene, 1 was the kinetic product, and 2 the thermodynamic product of the dimerization reaction. 1 and 2 were readily separated by chromatography. The hexamethyl dimers, 3-6, prepared from 7-hydroxy-1,3,4-trimethyl-1-indene, were obtained as the kinetic product, 3, and the successive isomerization products on longer acid treatment, 4, 5, and 6. Fractional crystallization was employed to separate 4 from 3, and 6 from 5.

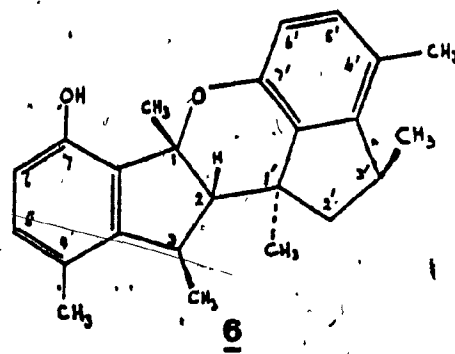
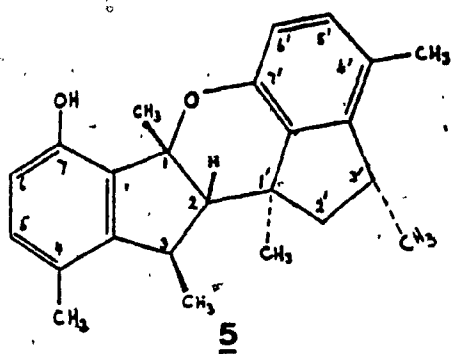
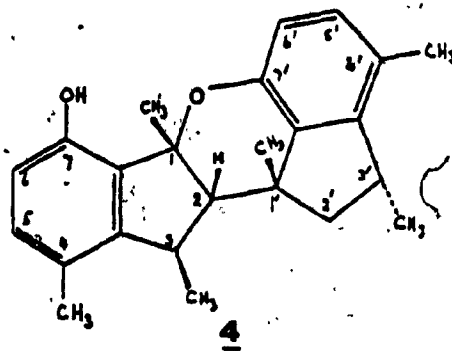
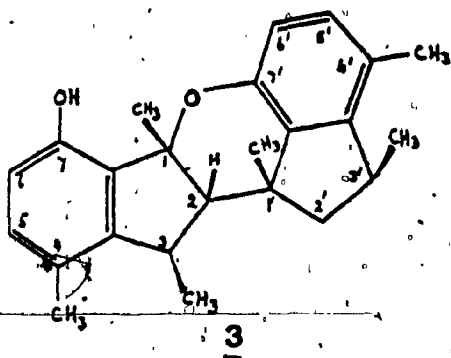
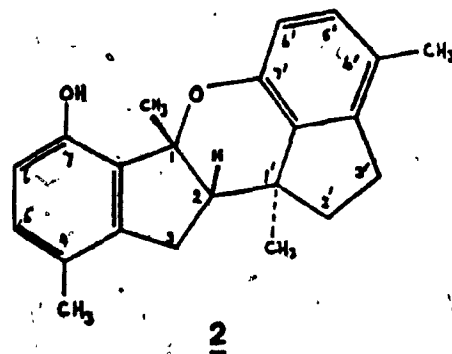
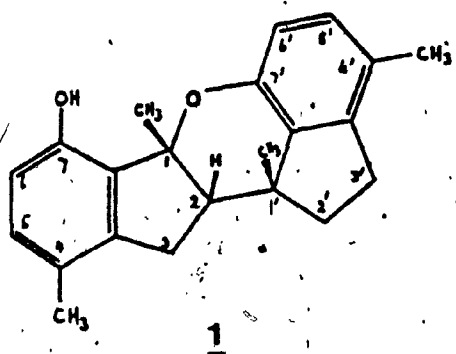


Fig. 6.1 Structures of the 7-hydroxyindene dimers.

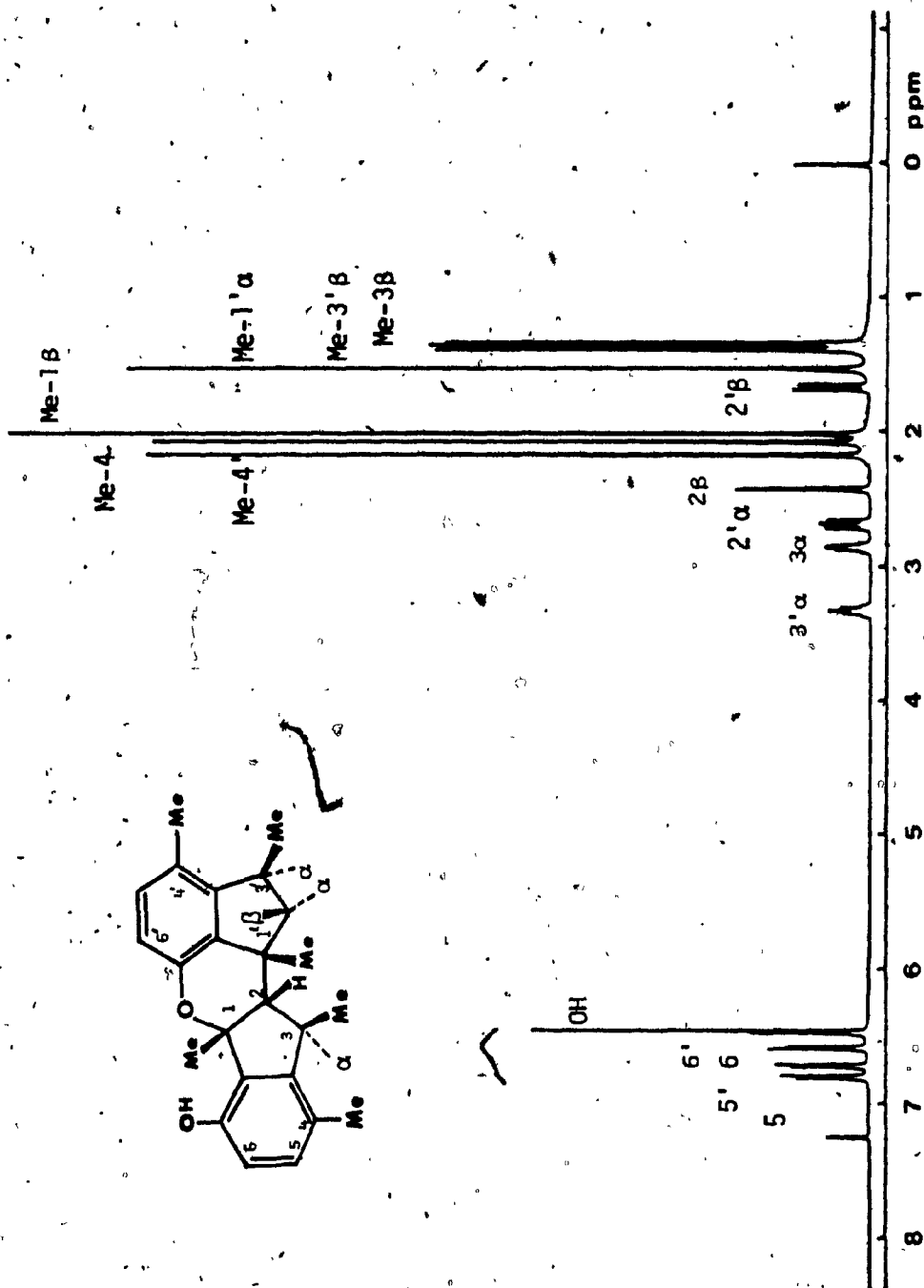


Fig. 6.2 400 MHz ^1H nmr spectrum of 7-hydroxyindene dimer **5**, 0.1 M CDCl_3 .

Preliminary stereochemical assignments were made largely on the basis of the ^{13}C nmr spectra, by considering the effects of adding methyl groups, e.g. γ -gauche and δ -synaxial effects. The ^{13}C chemical shift assignments had been made by comparison of the two series (tetra- and hexa-methyl), in experiments on samples in which the 1-methyl of the hydroxy-indene was enriched in ^{13}C , and by the analysis of spectra of mixed dimers in which an n-butyl group was substituted for the 1-methyl group in one half of the dimer. The assignments were in complete agreement with the X-ray crystallographic analysis of 3, and have been verified by the present study.

The dimeric nature of these compounds creates difficulties in the application of standard ^1H nmr techniques to their unambiguous structure determination. In particular, the assignment of ^1H chemical shifts to corresponding protons in each half of the dimer is difficult because of the very slight differences in shielding. High field ^1H spectra (eg. Fig. 6.2) were necessary to provide sufficient chemical shift dispersion to resolve all of the signals, while relaxation pathway analysis was critical for complete chemical shift assignment, and for the stereochemical assignments at the chiral centres. Complete analysis of the spectral parameters of all ^1H signals, including differentiation of all methylene signals and identification of stereochemistry at all (three or five) chiral centres, has been achieved. The solution structure and stereochemistry of 5, as determined by relaxation pathway analysis, was completely consistent with the X-ray crystallographic studies.⁸²

Table 6.1

7-Hydroxyindene Dimer ¹H Chemical Shifts¹

proton	Chemical shift (ppm)					
	1 ^c	2 ^t	3 ^c	4 ^o	5 ^c	6 ^t
Me-1B	1.99	1.57	2.01	2.01	1.63	1.70
H-2B	2.97	2.38	2.42	2.43	1.91	2.03
H-3A	2.90	2.90	2.85	3.07	3.36	3.36
H-3B	2.52	3.02	-	-	-	-
Me-3B	-	-	1.35	1.36	1.34	1.37
Me-4	2.03	2.21	2.08	2.11	2.27	2.26
H-5	6.83	6.96	6.80	6.82	6.98	6.97
H-6	6.58	6.69	6.58	6.59	6.71	6.71
OH-7	6.14	6.80	6.46	6.47	6.74	6.74
Me-1'A	1.40	-	1.53	1.35	-	-
B	-	0.71	-	-	0.92	0.73
H-2'A	2.20	2.14	2.68	1.85	1.87	2.38
H-2'B	1.97	1.88	1.67	2.21	2.29	1.54
H-3'A	2.78	2.93	3.32	-	-	3.48
Me-3'A	-	-	-	1.33	1.32	-
H-3'B	2.96	2.80	-	3.51	3.36	-
Me-3'B	-	-	1.39	-	-	1.40
Me-4'	2.13	2.22	2.17	2.20	2.26	2.31
H-5'	6.76	6.92	6.72	6.72	6.92	6.89
H-6'	6.51	6.70	6.47	6.48	6.71	6.68

1. All values given in ppm from TMS, and measured in 0.1 M CDCl₃ solution at ambient probe temperature.

2. Cis- and trans-fusion of rings B and C are indicated by "c" and "t", respectively.

A = lower face, B = upper face.

6.2. Results and Discussion

The strategy adopted in this study was to first carry out analysis of chemical shifts (Table 6.1) and $^1\text{H-R}_1$ measurements (Table 6.2) to develop a working model of the structures, then to use a number of NOED measurements (Table 6.3) to identify specific relaxation pathways to finalize the spectral and structural assignments.

6.2.1. Summary of $^1\text{H-R}_1$ Data

R_1 measurements provided a fast, efficient aid to the assignment of proton chemical shifts. The relatively isolated, and hence slowly relaxing, OH and aromatic protons have the lowest R_1 values (0.3-0.4 and 0.3-0.5 s^{-1} , respectively). The other methine protons relax more efficiently since they have a larger number of near neighbours (R_1 values of 0.7-1.0 s^{-1}). Due to their close proximity, the methylene protons relax each other very efficiently, and have higher R_1 values (1.1-2.0 s^{-1}). The aryl methyl groups, which are relatively free to rotate about the C- CH_3 bond axis, have R_1 values of 0.7-1.0 s^{-1} . In contrast, the alkyl methyl groups, whose rotation is evidently more restricted in these compounds, relax more efficiently, with R_1 values of 1.3-2.1 s^{-1} .

Table 6.2

7-Hydroxy Indene Dimer $^1\text{H-R}_1$ Values¹

Proton	R_1 (s^{-1}) ²					
	1	2	3	4	5	6
Me-1B	1.28	1.98	1.52	1.57	1.99	2.01
H-2B	0.97	0.92	0.90	0.92	0.99	0.99
H-3A	1.33	1.71	0.92	0.96	0.98	1.02
H-3B	1.37	1.64	-	-	-	-
Me-3B	-	-	1.36	1.42	1.48	1.43
Me-4	0.68	0.72	0.80	0.80	0.84	0.83
H-5	0.368	0.389	0.409	0.436	0.449	0.451
H-6	0.326	0.333	0.334	0.364	0.386	0.376
OH-7	0.341	0.311	0.38*	0.43*	0.374	0.380
Me-1'A	1.82	-	1.87	1.87*	-	-
B	-	1.95	-	-	1.81	2.12
H-2'A	1.67	1.70	2.16	2.11	1.82	1.88
H-2'B	1.61	1.79	1.70	1.64	2.11	2.00
H-3'A	1.48	1.68	0.71	-	-	0.82
Me-3'A	-	-	-	1.40	1.45	-
H-3'B	1.19*	1.60	-	0.69	0.80	-
Me-3'B	-	-	1.32	-	-	1.58
Me-4'	0.69	0.83	0.76	0.86	0.98	1.02
H-5'	0.379	0.437	0.412	0.458	0.512	0.528
H-6'	0.342	0.401	0.373	0.408	0.453	0.460

1. Measured from 0.1 M CDCl_3 solutions at ambient probe temperature. A = lower face, B = upper face.

2. R_1 values calculated by two-parameter non-linear regression analysis, except where overlap problems were prohibitive and the null-point method was utilized as indicated by "*".

6.2.2. Stereochemical Determinations

Differentiation of methine from methylene protons at C2, C3, C2', and C3' was easily made by consideration of $^1\text{H-R}_1$ values (Table 6.2), since methylene protons in these compounds; generally relax about twice as fast as the methine protons. Tentative assignments were made by consideration of chemical shifts and coupling constants. The stereochemistry at positions 2, 3, 1', 2', and 3' was then determined relative to that of the methyl group at position 1 (designated as being located on the upper (beta) face of the molecule⁸²), by complete relaxation pathway analysis using nOe experiments (Table 6.3). In all cases, H2 was on the same (beta) side of the molecule as Me-1, as evidenced by the substantial nOe enhancements between the two (Figs. 6.3, 6.4). In a similar manner, the relative stereochemistry at position 1' could be determined by the magnitudes of the nOe enhancements between Me-1' and H2 β . A large nOe established the ring fusion as cis (compounds 1, 3, and 4, Fig. 6.3); a small nOe, determined under similar conditions, established the ring fusion as trans (compounds 2, 5, and 6, Fig. 6.4). The proton or methyl group in the β -position at C3 was clearly distinguished from the α -position substituent by significant nOe enhancements to and from H2 β (Fig. 6.5). For all hexamethyl dimers, the 3-methyl group was identified as having β stereochemistry.

Table 6.3

NOE Enhancements Providing Stereochemical Information

<u>Saturated Proton</u>	<u>Observed enhancements²</u>
<u>Cis-fused Dimers (1, 3, 4)</u>	
Me-1B	2(B), OH-7, Me-1'(B)
H-2B	3(B), Me-1(B), Me-1'(B)
H-3A	3(B), 2'(A), Me-4
H-3B	3(A), 2(B)
Me-1'B	2(B), 2'(B), Me-1(B)
H-2'A	2'(B), 3'(A), 3(A), 3(B)
H-2'B	2'(A), 3'(B), 2(B), Me-1'(B)
H-3'A	3'(B), 2'(A), Me-4'
H-3'B	3'(A), 2'(B), Me-4'
<u>Trans-fused Dimers (2, 5, 6)</u>	
Me-1B	2(B), OH-7, 3(B)
H-2B	3(B), 2'(B), Me-1(B)
H-3A	3(B), 2'(A), Me-1'(A), Me-4
H-3B	3(A), 2(B), 3'(B)
Me-1'A	3(A), 2'(A), 3'(A)
H-2'A	2'(B), 3'(A), 3(A), Me-1'(A)
H-2'B	2'(A), 3'(B), 2(B), 3(B)
H-3'A	3'(B), 2'(A), Me-1'(A), Me-4'
H-3'B	3'(A), 2'(B), Me-4'

1. Measured on 0.1 M CDCl₃ solutions at ambient probe temperature. A = lower face, B = upper face.

2. Substituents at 3 and 3' differ among the six compounds, so enhancements are identified by position only.

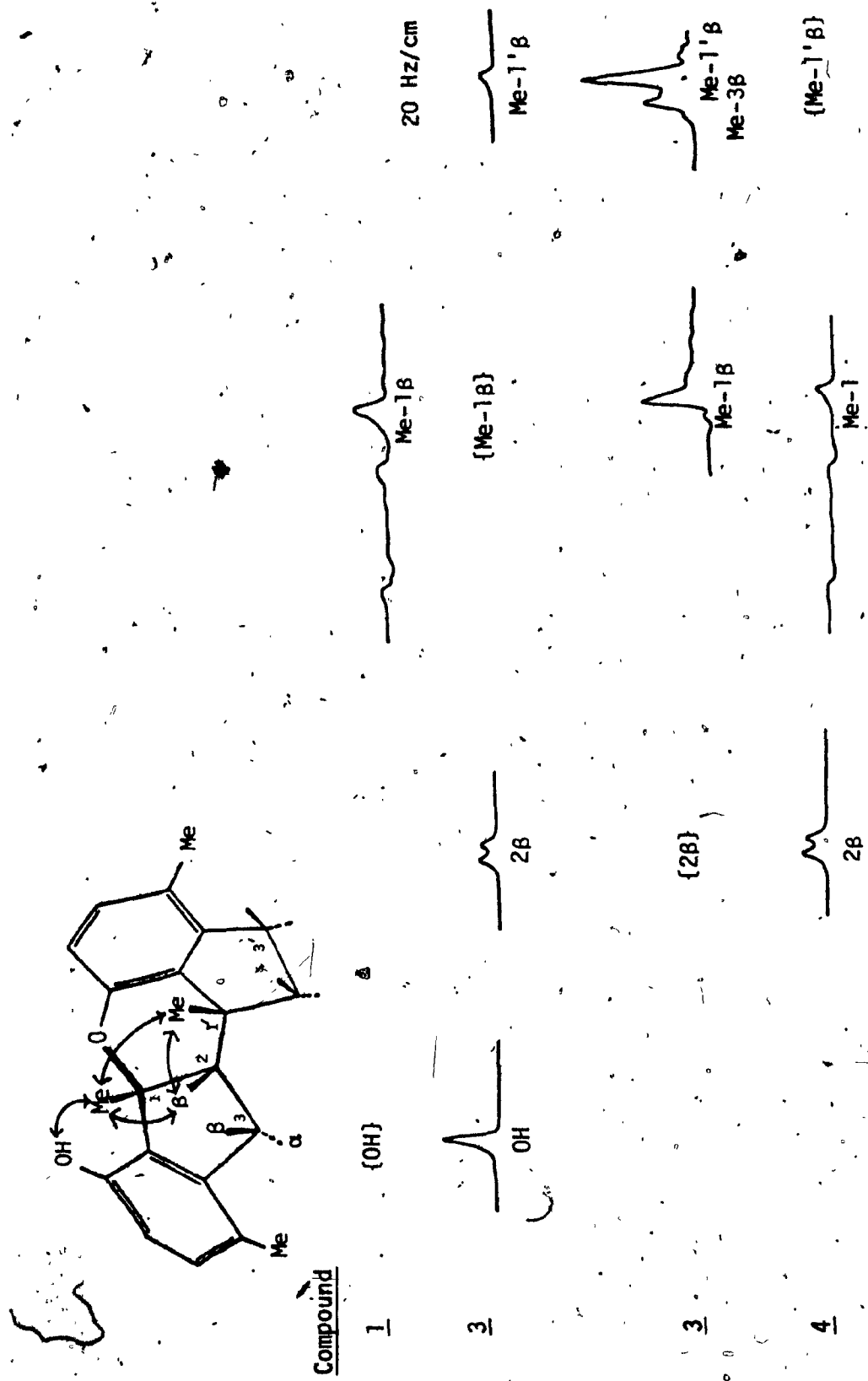


Fig. 6.3 NMR difference spectra to determine ring fusion- cis-fused dimers

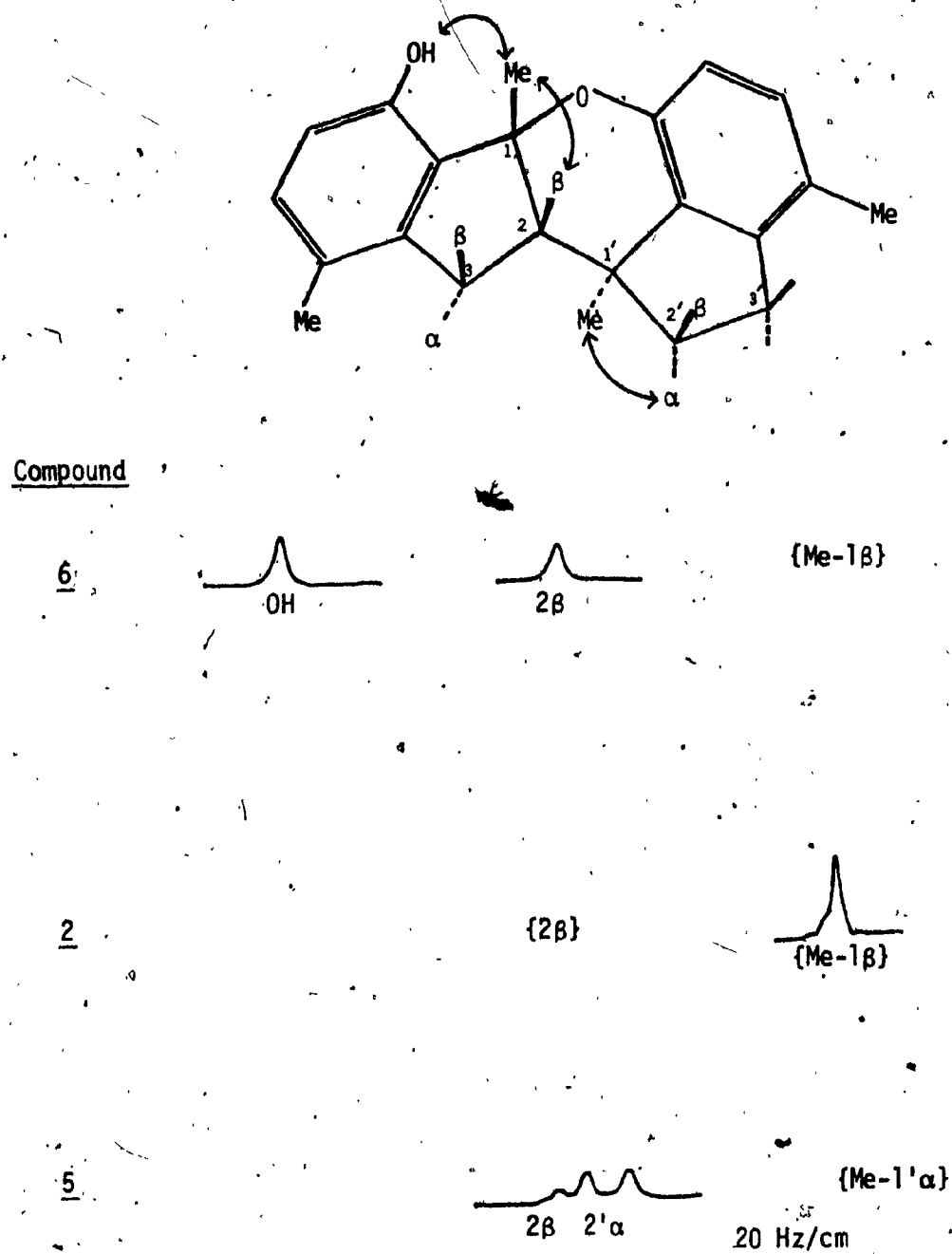


Fig. 6.4 NOe difference spectra to determine ring fusion-trans-fused dimers.

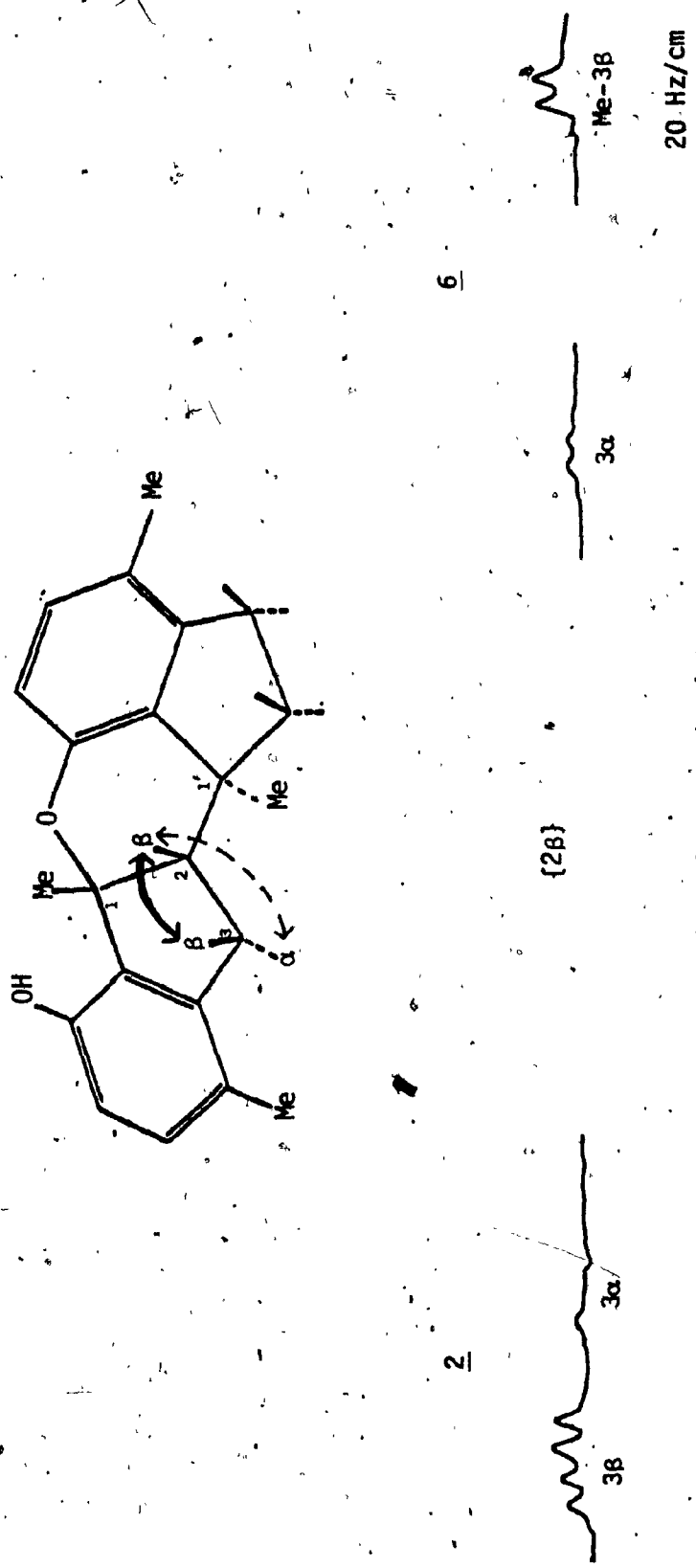


Fig. 6.5 NOe difference spectra to determine C3 stereochemistry.

The assignments at C2' and C3' were carried out in a similar manner, but required more careful consideration of the relaxation data and close inspection of molecular models. For the compounds which have trans-fusion of rings B and C (2, 5, and 6), the relaxation pathway between Me-1' α and the C2' proton on the same side of the molecule (Fig. 6.6) serves to distinguish between the two C2' protons. The relative magnitude of the the nOe enhancement to and from the C2' substituents and the previously assigned C3 substituents corroborates these assignments. The assignments at C3' were then made by relaying stereochemical assignments at C2' through the relative magnitudes of nOe enhancements (large values for adjacent substituents on the same face of the molecule, Fig. 6.6).

For compounds with cis-fusion of rings B and C (1, 3, and 4), the relaxation pathway between Me-1' β and the C2' protons (Fig. 6.7) clearly differentiates between the two protons. In these molecules, there is also a significant nOe between the substituents in the α -positions of C3 and C2', verifying the assignment and reflecting the folded geometry of the molecules. The assignments at C3' were made by relaying the stereochemistry established at C2', as explained above for the trans-fused dimers, through the magnitudes of the nOe enhancements (Fig. 6.7).

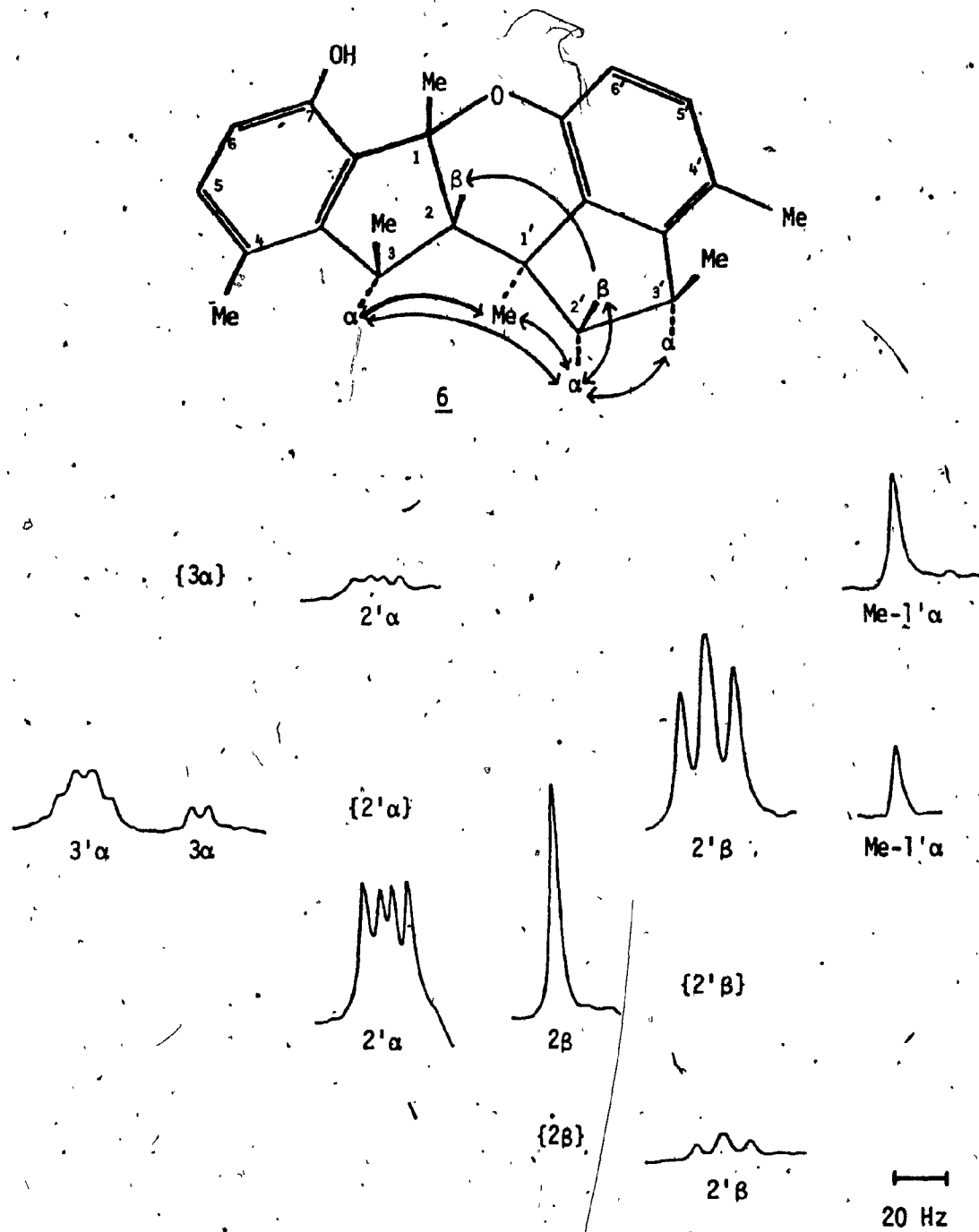
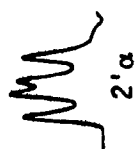
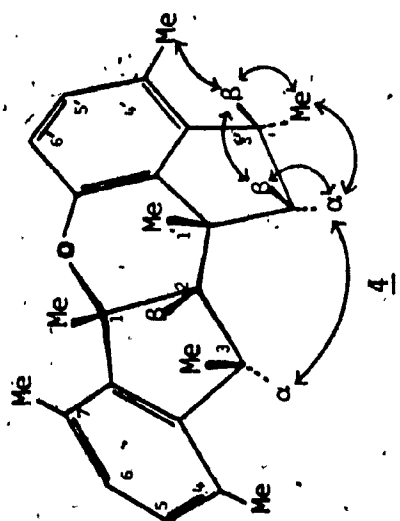


Fig. 6.6 NOe difference spectra to determine C2' and C3' stereochemistry-trans-fused dimers.



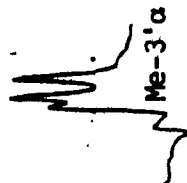
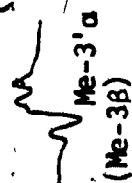
{2' α }



{Me-4'
SOFT}



{3 α }



{3' β }



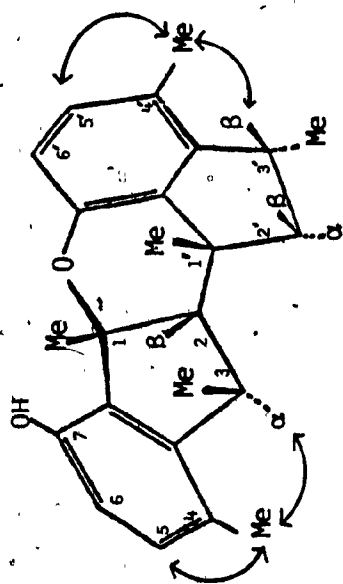
20 Hz

Fig. 6.7 NOe difference spectra to determine C2' and C3' stereochemistry- cis-fused dimers.

6.2.3. Assignments in Aromatic Rings

The signals (400 MHz) arising from ring A protons could be distinguished from the corresponding ring E signals by a combination of chemical shift arguments, double resonance, and, in particular, by relaxation pathway analysis. The hydroxyl proton signals were readily identified as the slowly relaxing singlets at 6.1-6.8 ppm. H5 may be distinguished from H6, and H5' from H6', on the basis of the shielding effect of the ortho oxygen substituent (7-OH and 7'-OR), and the higher relaxation rate (10-20%) of the 5 and 5' protons resulting from relaxation contributions from the adjacent 4 and 4' methyl groups.

A definitive distinction between the ring A and ring E aromatic signals was established by identification, through NOE experiments, of consecutive relaxation pathways originating on the previously assigned C3 and C3' protons (Fig. 6.8). Saturation of H3 α gave an enhancement of Me-4, while saturation of H3' α and/or H3' β gave an enhancement of Me-4' (Fig. 6.8). Since the chemical shifts of the two methyl resonances were very different ($\Delta\delta = 0.2$ ppm), these NOE enhancements gave the methyl assignments unambiguously. The H5 and H5' resonances could then be assigned from the NOE enhancements observed upon saturation of Me-4 and Me-4', respectively (Fig. 6.8). The completion of the aromatic

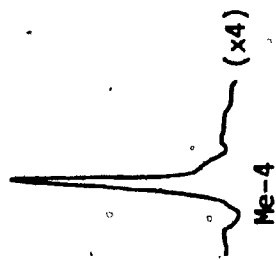


4

{Me-4}



{3 α }



{Me-4'}



{3'B}



Fig. 6.8. NOe difference spectra to determine aromatic ring assignments.

proton relaxation sequences to 6 and 6' protons:



was trivial, hence, chemical shifts of all aromatic resonances were assigned.

With this information, the structural analysis was complete, and the full set of assignments of the nmr parameters could be made. These were refined by computer simulation when necessary, and are listed in Table 6.1.

6.3. Conclusion

By utilizing the relaxation pathway analysis technique outlined in Chapter 2, it was possible to assign all the signals in the ^1H nmr spectrum of the six 7-hydroxyindene dimers, including the diastereotopic methylene protons. In addition, by careful analysis of nOe enhancements with the aid of molecular models, it was possible to determine ring fusion, and to assign the stereochemistry at all three or five chiral centres. These studies demonstrate the great power of the relaxation pathway technique for the analysis of the solution structure of organic molecules.

Chapter 7

STERIC EFFECTS ON ^1H SPIN-LATTICE RELAXATION OF METHYL GROUPS

7.1. Introduction

Most relaxation studies have involved the analysis of R_1 values of methine or methylene groups, whereas methyl rates have been only rarely utilized. The principal reason for this omission is that methyl relaxation is complicated by the internal methyl rotation which is superimposed on the overall tumbling of the molecule. There is no simple way to explicitly model the motion of the methyl relaxation vectors, thus the R_1 values have proven to be much more difficult to analyze. Although there has been a considerable amount of theoretical work on various aspects of methyl relaxation (eg. Refs. 84-90), most experimental studies have been focussed on quantitative determination of methyl rotation barriers from ^{13}C - R_1 measurements.* In the course of ^1H - R_1 studies undertaken by this laboratory, however, a significant dynamic range of methyl group R_1 values has been observed, eg. in 1-aryl-4,4-dimethyl-2-imidazolin-5-ones,⁹¹ di- and tri-methyl 7-hydroxyindene dimers,⁹² and steroids.¹⁰

No comprehensive examination of substituent steric influences on methyl ^1H - R_1 values has been reported in the literature, so a broadly based study of these effects has been undertaken. Results are reported here for simple model systems. The immediate goal of this research was to observe

* An excellent review on this subject is given in Ref. 12.

the sensitivity of methyl ^1H - R_1 values to specific steric interactions, while the long term goal was to determine the potential of using these values as probes of molecular structure in solution, as is now possible with methine and methylene proton R_1 's.

In order to evaluate the usefulness of methyl relaxation rates measured under routine experimental conditions, non-degassed 0.1 M solutions in deuterated solvents were employed. Under these conditions, the spin-lattice relaxation of methyl protons is dominated by dipolar relaxation (R_{1d}) to other protons in the molecule, and spin-rotation. There is also a contribution from paramagnetic dipolar relaxation to dissolved oxygen (R_{10}) (see Chapters 2 and 3). The approximate equivalence of the oxygen contribution to relaxation of all of the protons in a molecule has been verified in studies of a selected number of the model compounds discussed below. Relative methyl R_1 values in non-degassed samples will, therefore, reflect the differences in R_{1sr} and R_{1d} terms.

The spin-rotation relaxation contribution for a methyl group is given by the following:⁹³

$$(2) R_{1sr} = K * T * I_m * (2c_{\perp}^2 + c_{\parallel}^2) * t_{sr}$$

where K is a series of constants, T is temperature, I_m is the moment of inertia of the methyl group, c_{\perp} and c_{\parallel} are components of the spin-rotation interaction tensor, and t_{sr} is the spin-rotation correlation time. Note that t_{sr}

is different from the dipolar t_c , in particular, the dependence on methyl rotation rate of t_{sr} is opposite to that of t_c . For the purposes of these studies, the fact that the efficiency of the spin-rotation relaxation mechanism will increase the faster the methyl group rotates, is of utmost importance. For greater detail, the reader is referred to an excellent discussion by Green and Powles.⁹⁴

The dipolar relaxation contribution for a proton j , has already been given in Chapter 2, and can be reformulated:

$$(2) R_{1dj} = K \left[\sum_i \left(\frac{1}{r_{ij}} \right)^6 t_{cij} \right]$$

K , r_{ij} , and t_c have all been previously defined. The t_c term in (2) depends on both the overall rate of tumbling and any internal motions in the molecule, thus, the efficiency of dipolar relaxation will decrease as the rate of methyl group rotation increases. Note that the dependence of the dipolar relaxation rate on methyl rotation is opposite to that for the spin-rotation mechanism.

Interpretation of methyl R_{1d} values is invariably facilitated by the efficient "internal" dipolar relaxation resulting from the close proximity of the three methyl protons. Calculations based on simple mathematical models of dipolar relaxation predict that external dipolar contributions to methyl R_{1d} values are practically non-existent for ^{13}C , and are rarely as large as 10% for ^1H . This latter prediction has been verified for a few representative

compounds in this study, by measurements of $^1\text{H}\{-^1\text{H}\}$ NOE enhancements; no significant enhancements of methyl groups were observed. In a study of 3,5-dichlorotoluene, the external dipolar contribution to methyl group relaxation from the adjacent ring protons was reported to be less than 3%.⁹⁵ Since there are only very small "external" contributions to the methyl relaxation, and since the basic structure of the group is invariant, it is evident that differences in methyl R_{1d} values can only result from differences in motion. This implies that if the internal motion (methyl rotation) can be separated from the overall tumbling, then steric influences on the methyl R_{1d} can be determined.

The separation of the overall tumbling effects from internal motion for different methyl groups is possible in an isotropically-tumbling molecule which has several non-equivalent methyl groups. In such a molecule, the contributions of the overall tumbling to t_c are equal, so any differences in methyl R_{1d} values are directly attributable to influences on the rate of methyl rotation. In attempting to make similar comparisons between different molecules, the relaxation data must be normalized in order to eliminate the influence of different tumbling rates and experimental conditions. Differences in normalized methyl R_{1d} values can be attributed to factors affecting the rates of methyl rotation, as long as the overall tumbling motions of the molecules being compared are similar. Normalized comparisons are, therefore, valid between all isotropically

tumbling molecules or between anisotropically tumbling molecules whose anisotropies are the same (molecules whose structures are very similar). In this study, comparisons of normalized methyl $^1\text{H-R}_1$ values have been made between ortho- and meta-positioned methyl groups in a single molecule, or in pairs of isomerically related molecules. In non-aromatic molecules, the comparisons are made between methyl groups that are interacting sterically with a specific structural feature in the molecule, and another methyl group either in the same molecule or in a structural isomer. The observed differences in R_1 values have been attributed to the steric influence of the substituent in the ortho isomer.*

With both R_{1sr} and R_{1d} dependent on methyl rotation rates, it follows that variation in observed $^1\text{H-R}_1$ values for different methyl groups should also depend on the relative rates of rotation. The rate of rotation of a methyl group is usually determined by its steric environment, so the R_1 value should be sensitive to the details of molecular structure. The interpretation of these values must be made carefully, since the two relaxation mechanisms that are operative have opposite response to changes in methyl rotation rates.

* The effect of various substituents on methyl rotational barriers has been loosely correlated to electronic effects in some p-toluenes.⁹⁶

In order to properly interpret the overall methyl R_1 values, the relative contributions of the two competing mechanisms must be determined. Since the two mechanisms have an opposite dependence on temperature, it is possible to determine which term is dominant in a particular range by studying the temperature dependence of the R_1 value (eg. Refs. 97, 98). Another method involves ^1H - R_1 and $-n\text{Oe}$ measurements of selectively mono- and di-deuterated methyl groups.⁹⁵ By this method, the spin-rotation contribution to the ^1H - R_1 of the freely rotating methyl group was found to be 26%, in 3,5-dichlorotoluene at 300°K.⁹⁵ At a single temperature there is no simple and efficient way in which to quantitatively measure the relative contributions by proton experiments, but the corresponding ^{13}C data can be easily obtained by measuring methyl ^{13}C - $\{^1\text{H}\}$ $n\text{Oe}$ enhancements. Since ^{13}C relaxation, under conditions of broadband proton decoupling, is dominated by dipolar interactions to the directly attached protons, the $n\text{Oe}$ experiment is a direct method of measuring the magnitude of the dipolar contribution. The residual relaxation is attributable to spin-rotation. Following the changes in the dipolar and the spin-rotation contributions to methyl ^{13}C - R_1 values gives information about the relative rates of rotation of various methyl groups. In addition, it is possible to calculate the methyl group rotational barrier, using equation (2.35). The information derived from the ^{13}C experiments can then be correlated to the ^1H data, and used as an aid in the interpretation of the steric influences on methyl ^1H - R_1 values.

A final point, which must be considered in any study of methyl relaxation, is that relaxation is complicated by the presence of cross-correlation (eg. Ref. 98). In the triply degenerate methyl spin-system there are two components of magnetization, a quartet and a doublet state, which have separate spectral parameters (eg. line-widths, R_1 values, and in certain cases, resonant frequencies).⁸⁹ This can result in bi-exponential decay in the relaxation recovery curve used to determine R_1 . We have observed spectral asymmetries for methyl groups in several of our compounds during relaxation experiments. Haslinger and Lynden-Bell⁸⁸ were able to identify the separate R_1 components by analyzing the spectral asymmetries in the vicinity of the null-point of a typical inversion-recovery sequence. As pointed out by Werbelow,⁸⁹ for molecules tumbling in the extreme narrowing limit, the second, narrower component of methyl magnetization is usually quite weak; the total spectral intensity and, therefore, R_1 values are dominated by the broader, primary component. By working with data in the initial-slope region of the recovery curve,² where the effects of the dipolar cross-correlations for methyl groups have been shown to be negligible,⁹⁸ the R_1 data can be accurately characterized by a single exponential. All R_1 values reported here have been determined from data within the initial-slope region.*

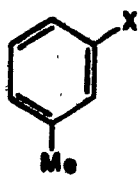
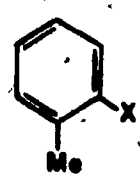
* See the Experimental (Chapter 9) for greater detail.

7.2. Methyl Group Relaxation in Substituted Aromatic Compounds

In planar aromatic compounds with a methyl group and a bulky adjacent substituent, the methyl group is believed to adopt a minimum energy conformation with two hydrogen atoms facing the substituent and out of the ring plane, and the third proton lying away from the substituent and in the ring plane; the methyl group has a three-fold (degenerate) rotational axis. When two similar flanking substituents are present, this minimal energy conformation is not attainable for steric reasons; the methyl group has a six-fold rotational axis, with ground state conformations of higher energy. As a result, barriers to rotation are larger for methyl groups with three-fold axes, the methyl groups with adjacent substituents experience hindered rotation.¹⁰⁰

7.2.1 Summary of Results

The compounds used in this study are shown in Fig. 7.1. Ring proton chemical shifts and coupling constants were analyzed by spectral simulation where necessary, so that all assignments could be made and appropriate R_1 values could be used for normalization. Methyl assignments in compounds with more than one methyl group were made by comparison to the corresponding mono-methyl derivatives and by consideration of substituent induced effects on chemical shift. ^1H Assignments for toluenes¹⁰¹ and methyl-naphthalenes¹⁰² have been reported in the literature.

		
Meta "Free"	Ortho "Hindered"	X
<u>1</u>	<u>2</u>	F
<u>3</u>	<u>4</u>	Cl
<u>5</u>	<u>6</u>	Br
<u>7</u>	<u>8</u>	I
<u>9</u>	<u>10</u>	CH ₃
<u>11</u>	<u>12</u>	C ₂ H ₅
<u>13</u>	<u>14</u>	OCH ₃
<u>15</u>	<u>16</u>	SCH ₃
<u>17</u>	<u>18</u>	NO ₂
<u>19</u>	<u>20</u>	NH ₂

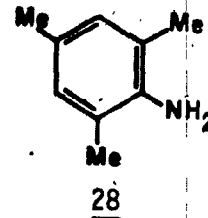
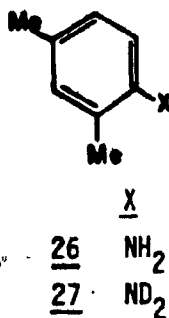
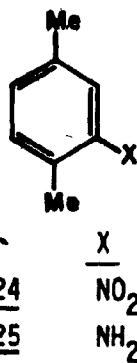
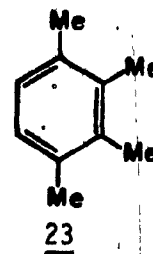
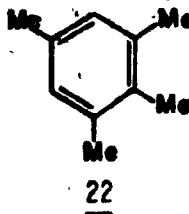
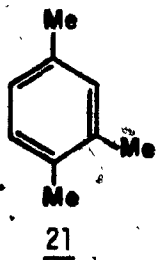
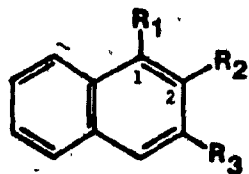


Fig. 7.1a Structures of the planar aromatic compounds.



	R ₁	R ₂	R ₃
<u>29</u>	H	CH ₃	H
<u>30</u>	CH ₃	H	H
<u>31</u>	CH ₃	H	CH ₃

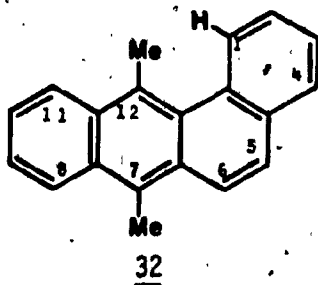


Fig. 7.1b Structures of the planar aromatic compounds.

The assignments for 1,3-dimethylnaphthalene, 31, and 7,12-dimethylbenz[*a*]anthracene, 32, were verified by ^1H -(^1H) NOe experiments.

Normalized methyl R_1 values for ortho (with the steric effect) and meta (without the steric effect) mono-substituted toluenes are given in the first part of Table 7.1. ^1H - R_1 data for a selected number of benzene derivatives containing both types of methyl groups, and for two larger aromatic systems are also given in this table. The range of R_1 values observed for freely rotating methyl groups was 0.242-0.398 s^{-1} , whereas the corresponding range for hindered methyls was 0.252-0.467 s^{-1} . These ranges exclude the values for 32, where the magnitude and dynamic range of R_1 values was by far the greatest- $R_1(\text{Me-7})$ was 0.564 s^{-1} and $R_1(\text{Me-12})$ was 1.58 s^{-1} .

In Table 7.2 are found the results of ^{13}C relaxation experiments for a representative number of compounds (7/8, 22, 11/12, 13/14, 24, 25, 26). The magnitude and dynamic range of R_1 values were much smaller than for ^1H data- a range of 0.093-0.120 s^{-1} for freely rotating methyl groups, and 0.089-0.179 s^{-1} for hindered methyls. NOe enhancements were quite consistent for unhindered methyls, 0.83-1.06, but varied considerably for hindered methyls 1.46-1.99. ^{13}C relaxation of freely rotating methyl groups was about 50% dipolar and 50% via spin-rotation, whereas dipolar interactions dominated (80-100%) the relaxation of all hindered methyls. The R_{1d} values calculated from these data were

Table 7.1

Normalized Methyl R₁ Values- Substituted Aromatic Compounds

<u>Entry</u>		<u>Subst.</u>	<u>Normalized R₁ Value</u>	
			<u>Free</u>	<u>Hindered</u>
<u>Toluenes</u>				
1,	2	F	1.32	1.30
3,	4	Cl	1.36	1.32
5,	6	Br	1.36	1.32
7,	8	I	1.36	1.39
9,	10	CH ₃	1.33	1.30
11,	12	C ₂ H ₅	1.30	1.29
13,	14	OCH ₃	1.37	1.34
15,	16	SCH ₃	1.32	1.36
17,	18	NO ₂	1.30	1.43
19,	20	NH ₂	1.33	1.63
<u>Xylenes</u>				
21		CH ₃	1.38	1.43 (1) ³ 1.46 (2) ³
22		CH ₃	1.51 (2) 1.44 (5)	1.59
23		CH ₃	1.27	1.59
24		NO ₂	1.37	1.43
25		NH ₂	1.42	1.69
26		NH ₂	1.43	1.66
27		ND ₂	1.44	1.64
28		NH ₂	1.47	1.82
<u>Larger Aromatics</u>				
29,	30	Naphth.	1.41	1.71
31		Naphth.	1.44	1.79
32		Benza.	1.55	4.33

1. Experiments carried out on 0.1 M CDCl₃ solutions at ambient probe temperature (292°K on the average). Average of at least two separate measurements.

2. R₁ values normalized to a ring proton not adjacent to the substituent.

3. Tentative assignments.

4. Naphth. = naphthalene, Benza. = Benz[a]anthracene.

Table 7.2
 $^{13}\text{C-R}_1$ and $-\text{NOE}$ Values of Substituted Aromatic Compounds¹

Entry	Free		Hindered	
	R_1 (s^{-1})	n	R_{1d} (s^{-1})	n
7/8	.112	1.0	.06	1.8
11/12	.109	.9	.05	1.5
13/14	.105	.9	.05	1.6
22 (Me-2) ₂	.093	1.1	.05	1.7
(Me-2) ₂	.09	.9	.04	1.8
(Me-5) ₂	.129	1.0	.06	
(Me-5) ₂	.09	1.0	.04	
24	.120	1.0	.06	1.8
25	.119	1.0	.06	2.0
26	.113	.8	.05	1.9
32 ³	.15	2.0	.15	2.0
33 ²	.08	.8	.04	1.8

1. Measurements on 1.0 M CDCl_3 solutions with 1W broadband proton decoupling at ambient probe temperature ($\sim 302^\circ\text{K}$).

2. Taken from Ref. 108, neat sample run at 306°K . Compound 33 is 1,2,3-trimethylbenzene.

3. Taken from Ref. 28, saturated in CS_2 , run at 306°K .

Table 7.3

Methyl Group Diffusion Constants and Rotational Barriers
for Substituted Aromatic Compounds¹

Ent.	Sub.	Free				Hindered			
		Jump		Stoch.		Jump		Stoch.	
		D _i	V	D _i	V	D _i	V	D _i	V
7/82	I	220	0.8	320	0.6	52	1.7	35	2.0
7/83		220	0.8	320	0.6	55	1.7	37	2.0
7/83						40	1.9	26	2.1
11/12	Et	250	0.8	370	0.5	120	1.2	88	1.3
13/142	OMe	410	0.5	610	0.2	91	1.2	65	1.6
13/142		410	0.5	610	0.2				
22 (2)	Me	340	0.6	500	0.3	42	1.8	28	2.1
(5)		100	1.3	150	1.1				
24	NO ₂	100	1.3	150	1.1	40	1.9	27	2.2
25	NH ₂	180	1.0	260	0.7	19	2.3	12	2.6
26		110	1.2	160	1.0	28	2.1	17	2.4
32 ⁴	H		>2.4						<0.4

1. D_i is given in units of (s X 10⁻¹¹), V in kcal/mole.

2. Anisotropic motion calculation assuming rigid ellipsoid model.

3. Anisotropic motion calculation assuming rigid ellipsoid model and off principal-axis methyl rotation (α = 60°). See text for details.

4. Taken from Ref. 25. See text for details of structure.

consistently in the range $0.05\text{-}0.06\text{ s}^{-1}$ for unhindered methyls, but varied from $0.07\text{-}0.18\text{ s}^{-1}$ for hindered methyls.

The corresponding values of methyl rotation rates and rotational barriers are given in Table 7.3. These derived values consistently indicate that the rate of rotation was faster and rotational barrier smaller for meta-positioned methyls. The range of rotation barriers of the unhindered methyls was $0.5\text{-}1.6\text{ kcal/mole}$ (methyl jump, 6-fold rotational barrier) and $0.2\text{-}1.3\text{ kcal/mole}$ (stochastic diffusion), whereas the corresponding ranges for the hindered methyls was $1.2\text{-}2.3\text{ kcal/mole}$ (methyl jump, 3-fold barrier), and $1.4\text{-}2.6\text{ kcal/mole}$ (stochastic diffusion). These results are in agreement with determinations of methyl rotation barriers by micro-wave spectroscopy for cis- and trans-propenes, where the barriers were found to differ by approximately 0.75 kcal/mole .¹⁰³ The best agreement with microwave data is obtained by using a 3-fold methyl jump model in the high barrier regime and the stochastic diffusion model in the low barrier regime.

Both the stochastic diffusion and methyl-jump models have been utilized to calculate rotational barriers, because there is no clear-cut evidence in the literature for favoring one over the other. One author has mentioned a practical guideline of 1.4 kcal/mole ,¹⁰⁴ below which stochastic diffusion is preferred, above which the jump model is preferred. Unfortunately, the reasons for this guideline are given no experimental or theoretical basis, so calculations have been carried out using both models for

methyl rotation.* In only a few cases have the results of the two models been compared,^{96,104-106} but since there are very little data available on rotational barriers measured by other techniques, there are no reliable means for judging which method gives more accurate results. Though most authors have reported no consistent trends, in one published study,¹⁰⁵ it was stated that stochastic diffusion gave consistently higher rotation barriers. Studies on the wide range of methyl groups reported here, show that this is only true for unhindered methyl groups. The trend of relative values depends on whether methyl rotation is hindered or not. The stochastic diffusion model was found to give consistently lower rotational barriers than the three-fold jump model for hindered methyls, but consistently higher barriers relative to the six-fold jump model for unhindered methyls. The observed differences reported both in the literature, and in the studies described here, varied from -0.2 to 0.2 kcal/mole.¹² These differences are on the order of the error in the calculated barrier. For the purposes of the studies discussed here, it was only necessary to compare rotational barriers for hindered and freely-rotating methyl groups in the same [or very similar] molecule[s]. By working in this manner, the systematic errors due to differences in experimental conditions, etc., are minimized, and qualitative conclusions can be safely drawn from the ¹³C data.

* Ref. 12 is invaluable for making a rapid comparison of the range of results reported in the literature.

7.2.2. Methyl Relaxation in Benzene Derivatives

For compounds 1-16, and 21 in Table 7.1, the methyl $^1\text{H-R}_1$ values are approximately the same for the methyls adjacent to the substituent, and those which are "freely" rotating. This apparent lack of $^1\text{H-R}_1$ sensitivity was further investigated by analysis of ^{13}C relaxation. For all molecules studied, there was a significantly greater $^{13}\text{C}-\{^1\text{H}\} \text{ nOe}^5$ and larger rotational barriers for the methyl group adjacent to the substituent (hindered methyl). Our measurements are in agreement with the $^{13}\text{C-R}_1$ and nOe measurements of methyl-substituted toluenes carried out by Grant and coworkers.^{107,108} A few selected examples from their work are included in Table 2. The nOe data imply that ^{13}C dipolar relaxation is substantially greater for all methyls adjacent to a substituent, and the calculated rates of the internal (methyl rotation) diffusion constants and methyl rotational barriers, are clear indication that methyl rotation is hindered, hence, in those molecules where the difference in the observable $^{13}\text{C-R}_1$ value between a hindered and a freely rotating methyl is negligible, the increase in R_{1d} must be coincidentally equivalent to the decrease in R_{1sr} (also associated with the slower methyl rotation). It is reasonable to assume that ^1H and ^{13}C data can be correlated, certainly methyl diffusion constants and barriers to rotation can, so the lack of sensitivity in the

methyl $^1\text{H-R}_1$ value to certain steric interactions can be attributed to the coincidental equivalence but opposite sign of the changes in R_{1d} and R_{1sr} , as observed in the ^{13}C data.

For 17-20, 22, 23, and 25-28, methyl $^1\text{H-R}_1$ values were significantly greater (9-25%) for the hindered methyl. In these molecules, the ^{13}C data indicate that the increase in R_{1d} is larger than the decrease in R_{1sr} , resulting in the methyl $^1\text{H-R}_1$ exhibiting sensitivity to the steric influence. It is evident from a consideration of the R_1 data on benzene derivatives 1-28 that the sensitivity of the methyl $^1\text{H-R}_1$ to steric factors depends on the "effective" size of the adjacent substituent.

The term "effective" is of key importance, because structural deformation or conformational preference may lead to a considerable variation in the steric hindrance expected from a substituent. The role of structural deformation in determining rotational barriers is demonstrated in the methyl $^1\text{H-R}_1$ values of the methyl benzene derivatives (9/10, 21, 22, 23). In 9 and 10, and in 21, the difference in free and hindered methyl R_1 's is negligible, and in 22, at the limit of sensitivity (~10%). In 23, the large differential (25%) is the result of the extreme amount of crowding of methyl groups. These results can be rationalized in the following manner.

With two, and to some extent three, adjacent methyl groups, in-plane distortion of bond angles reduces steric strain. Though out-of-plane distortions have also been detected in the crystal state for such molecules, these deformations are usually much smaller than the in-plane distortions.¹⁰⁹ In 23, where there are four adjacent methyls, bond angle distortion appears to no longer be sufficient to significantly reduce the adverse steric interactions.

In o-xylene, 10, the methyl groups each bend away from each other, so steric strain is somewhat reduced. In 1,2,3,5-tetramethylbenzene, 22, Me-1 and Me-3 bend in opposite directions from Me-2. Me-2, however, retains "normal" geometry, so the Me-1/Me-3 to Me-2 contact is somewhat shorter than in 10. The steric hindrance to Me-1 rotation is correspondingly greater in 22 than in 10, and is reflected by the larger $^1\text{H-R}_1$ differential between hindered and free methyl groups. The effect on Me-2 rotation (in 22) will be somewhat more complex since both low and high energy states are destabilized. Clearly, the "inner" Me-2 has a small six-fold barrier, as indicated by its low $^1\text{H-R}_1$ value. In 1,2,3,4-tetramethylbenzene, 23, Me-1 and Me-2 bend in the opposite direction from Me-3 and Me-4. This means that the "outer" methyls (Me-1 and Me-4) have an even shorter contact with the "inner" methyls than in 22, so steric hindrance is expected to be greater, and is observed in the significantly higher R_1 value of the hindered.

methyls. The "inner" methyls in 23 will also be more severely crowded, but the effect on rotational barrier is similar to that on Me-2 in 22, namely, a decrease in the rotational barrier. Interestingly, the differences between "inner" and "outer" methyl groups indicate that there is no gear effect,¹¹⁰ in these methyl benzenes. The absence of a gear effect in methyl tryptycenes has also been proposed on the basis of $^1\text{H-R}_1$ studies of methyl rotation barriers in the solid state.¹¹¹

A reduction in "effective" size due to conformational preference is demonstrated in nitrobenzenes 18 and 24, which have ortho-substituted methyl groups. In nitrobenzene, the nitro group favors a conformation coplanar with the aromatic ring^{112,113} to maximize orbital overlap. In compounds with an adjacent substituent, experimental evidence indicates that the nitro group rotates away from the favored conformation.^{112,113} A compromise, preferred conformation with a dihedral angle in the range $20-30^\circ$ to the aromatic ring plane has been proposed for molecules with an adjacent methyl group.¹¹² The resultant steric interaction is considerably reduced relative to the coplanar conformation. The observed differential in $^1\text{H-R}_1$ values of 17/18 (10%) and 24 (4%), is at the limit of detectability of this technique, hence, much less than expected if the nitro group remained in a coplanar conformation.

7.2.3. Verification of the Steric Effect in Methylanilines

The most substantial differential in the methyl $^1\text{H-R}_1$ values of mono-substituted toluenes was observed for the toluidine isomers 19 and 20, hence, relaxation of methyl groups adjacent to amino functions* was further investigated in dimethylanilines 25-28.

Relaxation calculations, carried out assuming a completely static spatial relationship between amino and methyl protons, suggested that the larger methyl $^1\text{H-R}_1$ values could possibly be due to relaxation to an amino proton(s). This relaxation pathway was found not to be significant from measurements of the $^1\text{H-R}_1$ values of the N,N-deuterated analog, 27. In addition, an nOe difference experiment was carried out to measure the enhancement of the methyl group upon irradiation of the amino protons. The observed enhancement was very small, less than 3%. There is a full $^{13}\text{C}\{-^1\text{H}\}$ nOe ($n = 2.0$) for the methyl carbons which are adjacent to the amine substituent, but a much smaller nOe ($n = 1.0$) for the "freely" rotating methyl carbons, indicating that the hindered methyl is rotating more slowly (see the rotation barriers in Table 7.3), hence, dipolar

* The amino group electronically favors a conformation where the amino protons are coplanar with the aromatic ring^{112,114} but which maximizes the steric interaction in the adjacent position. In molecules with an adjacent methyl group, the balance of electronic stabilization and steric destabilization appears to result in a conformation with a high degree of steric interaction, to which the $^1\text{H-R}_1$ is quite sensitive.

relaxation is more efficient. From these experiments, it was possible to conclude that the $^1\text{H-R}_1$ differential was due to the steric influence of the substituent.

7.2.4. Methyl Relaxation in Other Aromatic Systems.

A significant and consistent difference in methyl $^1\text{H-R}_1$ values in the A and B positions has been observed in methyl-naphthalenes 29-31 (Table 7.1). The lack of a significant nOe enhancement of methyl-1 in 31, upon pre-saturation of either H2 or H8, indicated that the R_1 effect was not due to an increase in external dipolar contributions, but to a change in methyl rotation rate. The $^1\text{H-R}_1$ value of H8, in both 30 and 31, is 20% larger than the other ring protons, and the $^1\text{H-}[^1\text{H}]$ nOe enhancement of H8 is substantially larger than that of H2, upon pre-saturation of methyl-1. These differences in relaxation parameters reflect the differences in distances to the methyl group; H8 (peri) is closer to Me-1 than H2 (vicinal).^{*} These data verify that the observed differential in the methyl $^1\text{H-R}_1$ values is attributable to a steric influence.

^{*} This can be observed by inspecting molecular models, and has been verified by X-ray and neutron diffraction studies of a number of naphthalenes and related compounds.¹¹⁵

The most substantial steric effect on a methyl $^1\text{H-R}_1$ value in this study has been observed in 7,12-dimethyl benz[*a*]anthracene, 32. If complete planarity were assumed, methyl-12 and H1 would be located only 0.4 \AA from each other.²⁸ Though the non-planarity of this system is well documented,¹¹⁶ the structural deformation is not sufficient to completely nullify the adverse steric interaction, as indicated by the very high barrier to rotation that has been measured by $^{13}\text{C-R}_1$ analysis.²⁸ Since the methyl rotation rate is very slow, t_c is very large, and a correspondingly high $^1\text{H-R}_1$ is expected and observed, for Me-12, relative to Me-7 (Table 7.1). To verify that the large methyl-12 R_1 was due to motional effects, and not due to relaxation to H1, a measure of the nOe enhancement of methyl-12 upon saturation of H1 was made, and was found to be less than 3%. The elevated $^1\text{H-R}_1$ value for H1, and the large nOe enhancement observed upon saturation of methyl-12, gave further evidence of the close proximity of H1 and methyl-12. The nearly threefold dynamic range of methyl $^1\text{H-R}_1$ values in 32 indicates a substantial steric influence on methyl relaxation.

7.3. Methyl Relaxation in Non-planar Aliphatic Systems

As part of the overall strategy of research into the steric effects on methyl relaxation, an investigation of the steric effects of geminal substituents on methyl group $^1\text{H-R}_1$ values was in order. A number of relatively high $^1\text{H-R}_1$ values had been observed for gem dimethyl groups in previous $^1\text{H-R}_1$ studies by this laboratory.^{11,91} These observations gave an indication that the steric effect from a geminal substituent may be significant. Further investigation to fully characterize such interactions is clearly warranted, and is a logical extension of studies of steric effects from adjacent substituents. A description of preliminary investigations is given here.

In one previous study by this laboratory,¹¹ methyl $^1\text{H-R}_1$ values in steroids were correlated to the number and relative locations of 1,3-diaxial interactions. This study demonstrated that methyl $^1\text{H-R}_1$ values could be interpreted in a manner similar to the previously reported ^{13}C relaxation analysis,¹⁰⁰ where differences in R_1 values were rationalized in terms of steric effects on methyl rotation rates. It was, therefore, necessary to consider both the effects of the gem substituent and any 1,3-diaxial interactions. To this end, it was decided to examine some simple model compounds, where such effects might be separable. Conformationally biased 1-substituted-4-t-butylcyclohexanes and some 1,3-dioxane analogues (Fig. 7.2) were chosen because the number and the magnitude of 1,3-diaxial interactions with the axial methyl

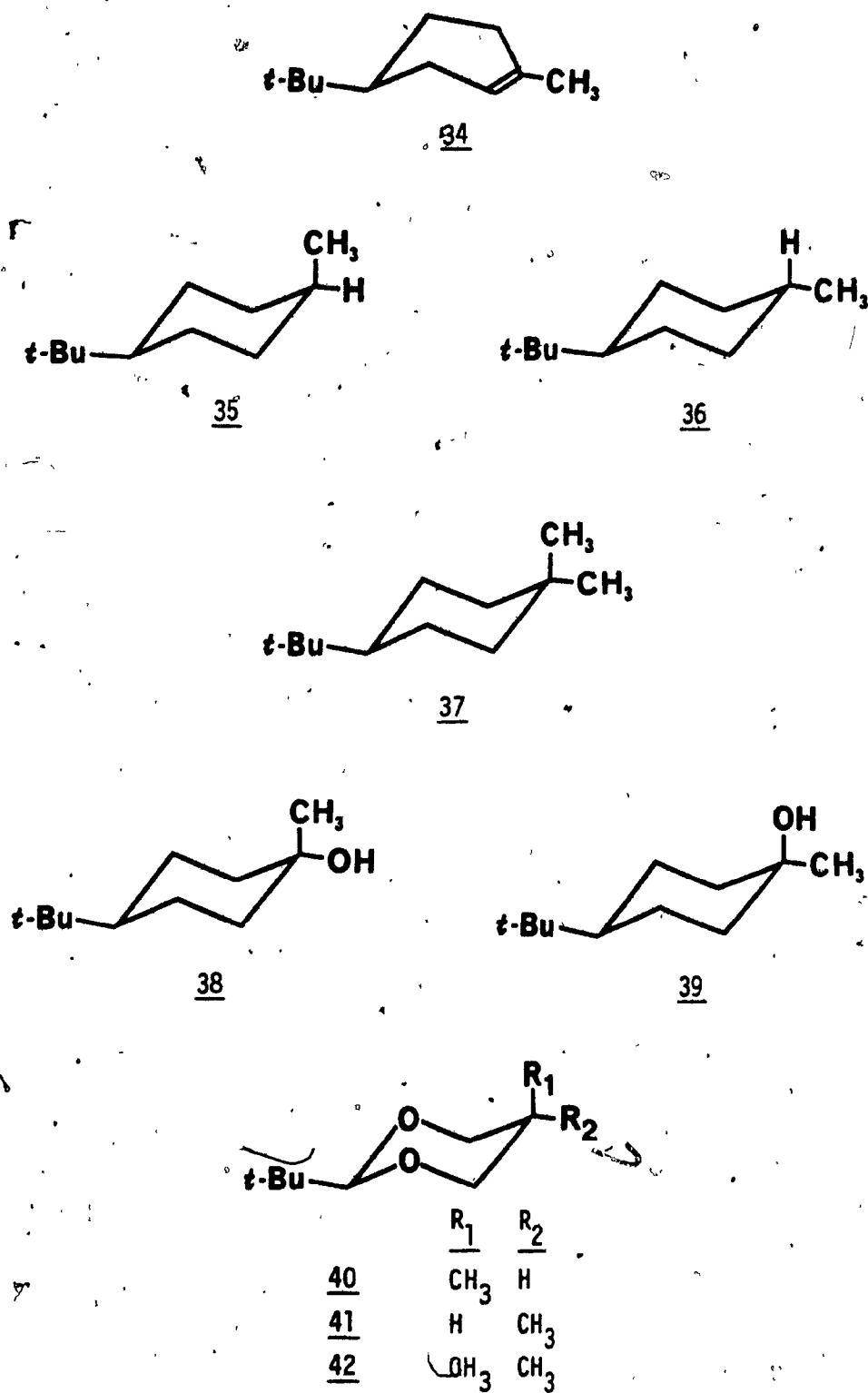


Fig. 7.2 Structures of the non-planar aliphatic compounds.

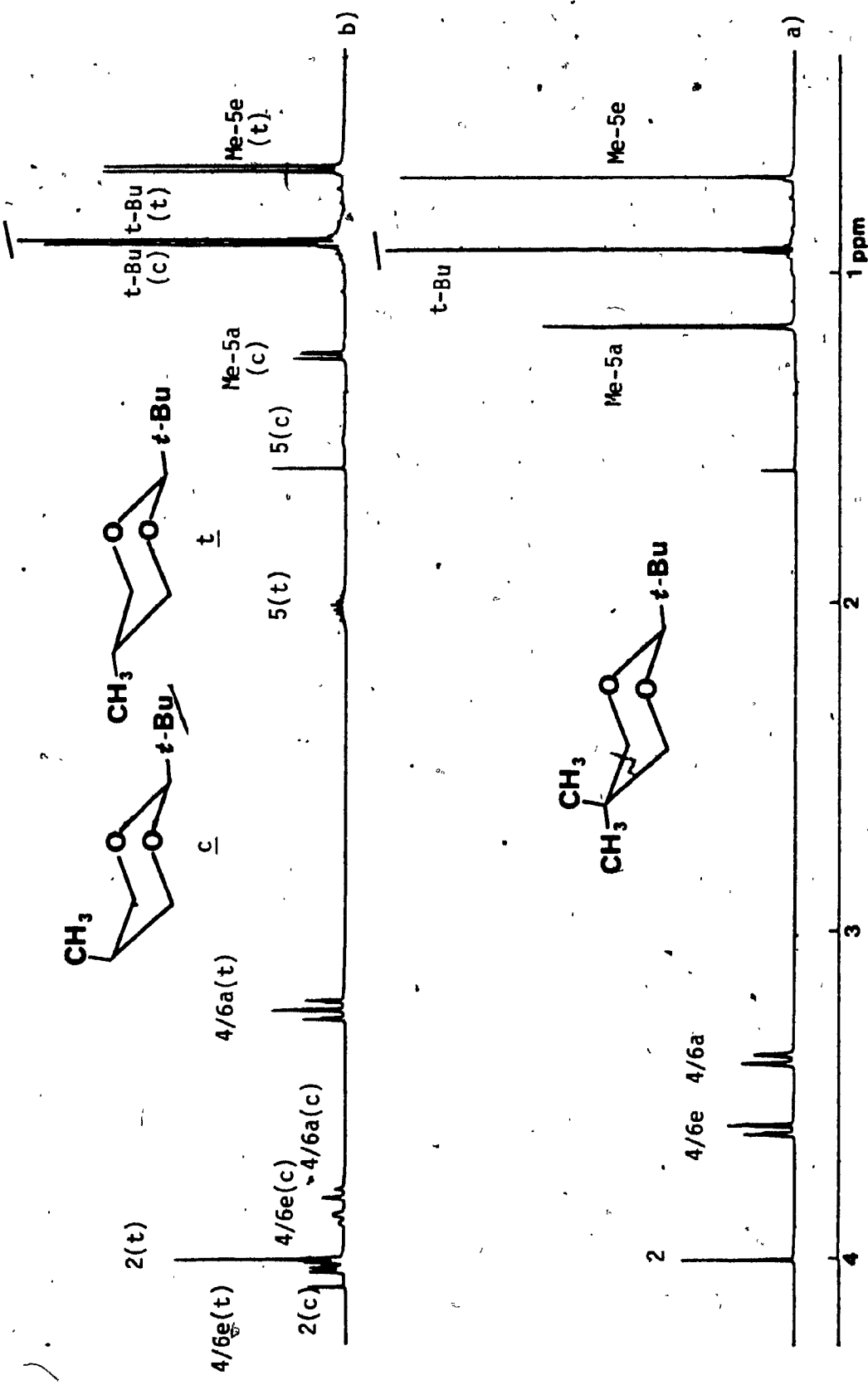


Fig. 7.3 400 MHz ¹H nmr spectra of 2-t-butyl-1,3-dioxanes, 0.1 M CDCl₃: a) 5,5-dimethyl, b) cis- and trans-5-methyl.

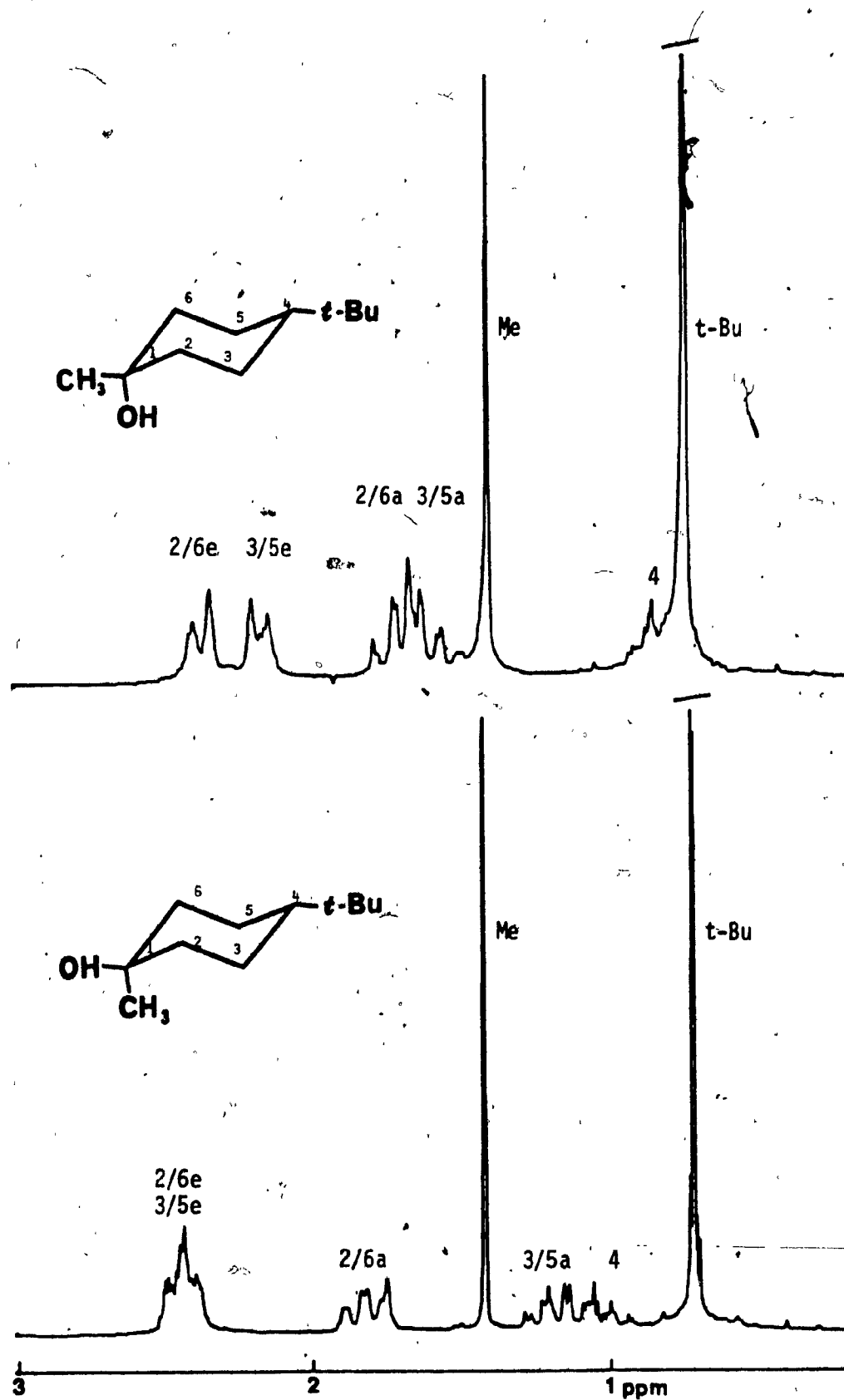
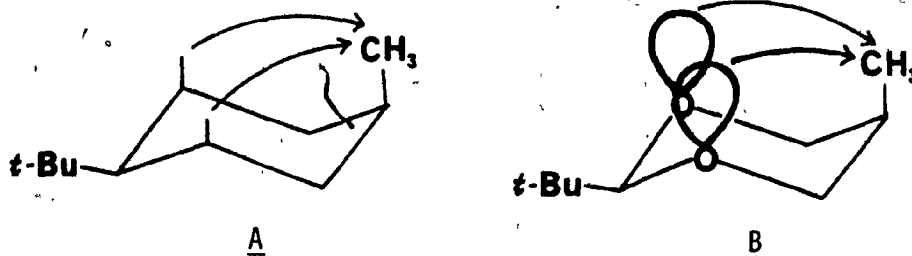


Fig. 7.4 400 MHz ^1H nmr spectrum of *cis*- and *trans*-4-*t*-butyl-1-methylcyclohexanol, 0.1 M CDCl_3 .

groups would be kept to a minimum. The 1,3-dioxanes were selected to complement the studies of the cyclohexane derivatives because these compounds have very similar structures, they are readily available (see Chapter 9), and their ^1H nmr spectra are simple and well dispersed (Fig 7.3) relative to corresponding cyclohexane analogues (Fig. 7.4). In addition, a contrast between cyclohexane and 1,3-dioxane analogues would allow for a determination of the relative magnitudes of 1,3-diaxial proton (A- cyclohexanes) and the 1,3-lone-pair electron (B- 1,3-dioxanes) interactions with axial methyl groups.



In the 1-cyclohexene derivative, 34, there is no geminal substituent, but in all other derivatives, an increasingly larger geminal interaction is expected ($\text{H} < \text{OH} < \text{CH}_3$). Note that in all mono-methyl derivatives, there are two isomers possible, denoted as cis and trans. Since the bulky t-butyl group will invariably occupy an equatorial position to

minimize steric interactions in the ring, the cis compounds (35; 36,* 40) have an axial methyl group, and the trans isomers (36, 39,* 41) an equatorial methyl. 1,3-diaxial interactions may affect the relaxation of an axial methyl group, so the identification of the steric effects must be made separately for axial and equatorial methyls. For example, the axial methyl group in gem-dimethyl derivative, 37, must be contrasted to the methyl group of the cis mono-methyl compound, 35, whereas the equatorial methyl of 37 must be compared to the trans mono-methyl compound, 36, in order to determine the effects of a geminal methyl group. Comparisons to compounds 34 and 38/39, allow for characterization of the relative strengths of the steric effects from other geminal substituents. Results from 1,3-dioxane derivatives, 40-42, were expected to closely parallel those from cyclohexane analogues. Finally, a determination of the relative strengths of the 1,3-diaxial (both protons and electron lone-pairs) and geminal interactions was expected from the comparison of corresponding $^1\text{H-R}_1$ values for axial and equatorial methyl groups.

Partial ^1H nmr assignments for 4-t-butyl-1,1-dimethylcyclohexane¹¹⁷ and all 1,3-dioxanes¹¹⁸ used in these studies have been reported in the literature. All other assignments were made by the standard methods. In Table 7.4, the results of $^1\text{H-R}_1$ studies on model cyclohexane and 1,3-dioxane systems are given. The ranges of R_1 values observed for these

* Note that 38 is, in fact, the trans-cyclohexanol and 39, the cis isomer. Abnormal nomenclature is utilized here to accentuate the position of the methyl group of interest.

compounds were 0.49-0.63 s⁻¹ for t-butyls, 0.44-0.64 s⁻¹ for axial methyls, and 0.44-0.63 s⁻¹ for equatorial methyls. It is obvious from inspection of Table 7.4 that methyl ¹H-R₁ values of these model compounds were very insensitive to the steric effects from both the geminal and 1,3-diaxial interactions. This lack of sensitivity is somewhat surprising in light of the past results.

Table 7.4

Normalized Methyl ¹H-R₁ Values
Conformationally Biased Cyclohexanes and 1,3-Dioxanes

<u>Entry</u>	<u>Normalized R₁ Value¹</u>		
	<u>Axial-Me</u>	<u>Equatorial-Me</u>	<u>t-Butyl (s⁻¹)</u>
34	-	.78	(.56)
35 ³	.94 ⁿ	-	(.5 ^{n,*})
36 ³	-	1.1	(.49)
37	.94	1 ^{n,*}	(.49)
38	.90	-	(.63)
39	-	.88	(.61)
40 ³	1.02	-	(.52)
41 ³	-	1.02	(.52)
42	1.05	1.03	(.62)

1. Measured from 0.1 M CDCl₃ solutions at ambient probe temperature (292^oK on the average). Methyl R₁ values are normalized to the t-butyl R₁ in parenthesis ().
2. R₁'s determined by two-parameter, non-linear regression analysis unless specified by "n", which indicates that the R₁ value could only be determined by the null-point method.
* = accurate R₁ was not measurable due to overlap.
3. Measured from a mixture of cis and trans isomers.

For the cyclohexane derivatives, there were severe problems concerning the lack of chemical shift dispersion in the spectra. For example, in 37, the t-butyl and the equatorial methyl were almost completely overlapped in CDCl_3 , $\text{CDCl}_3 + \text{C}_6\text{D}_6$, and $\text{CDCl}_3 + (\text{CD}_3)_2\text{CO}$ solution. The larger t-butyl group swamped the methyl group, so it was impossible to measure an accurate R_1 for the methyl. In addition, in any compound with a t-butyl group, there is a dynamic range problem due to the presence of a sharp t-butyl singlet of 9H intensity. This greatly reduces the accuracy of R_1 measurements of low intensity resonances (eg. multiplet resonances), and prevented a possible corroborative analysis of ring proton ^1H - R_1 values. Being fully aware of these adverse factors before carrying out the experiments, the final results were, nonetheless, very disappointing. Certainly the lack of consistent trends in the data was not expected.

In an attempt to gain further insight into the ^1H - R_1 results, ^{13}C relaxation experiments on the 1,3-dioxane derivatives were undertaken. The methodology for the ^{13}C studies parallels that utilized for the planar aromatic systems described in the previous section. 1,3-Dioxanes were chosen on the basis of chemical shift dispersion and simplicity in their ^{13}C spectra. In addition, there were not sufficient quantities of the cyclohexane derivatives to carry out a ^{13}C analysis. The values measured for ^{13}C relaxation parameters are listed in Table 7.5. The t-butyl R_1 values were in the range $0.376\text{--}0.410 \text{ s}^{-1}$, whereas ring

methyls ranged from 0.282-0.403 s⁻¹. The ¹³C-¹H NOE values, 1.8-2.0, indicate the dominance of the dipolar mechanism.

Results of the ¹³C experiments are given in Table 7.5. These data are consistent in demonstrating sensitivity to the steric interactions described above. There was a significant (>10% in both 1-methyl and 1,1-dimethyl derivatives) differential in the R₁ values of axial and equatorial methyl groups which can be correlated to the slower methyl rotation that arises from 1,3-diaxial interactions with oxygen lone-pair electrons. There is also a significant (>10% for the equatorial methyl and 7% for the axial) differential between the corresponding mono-methyl and gem-dimethyl methyl ¹³C-R₁ values, which demonstrates sensitivity to the geminal steric interaction. The data given here, though only on a limited number of compounds, indicate that 1,3-diaxial interactions are of the same order of magnitude as the interaction with a geminal methyl group.

Table 7.5

Normalized ¹³C-R₁ and -NOE Values of Some 1,3-Dioxanes¹

Entry	Axial Methyl			Equatorial Methyl		
	R ₁	n	R _{1d}	R ₁	n	R _{1d}
40	1.27	1.8	1.2	-	-	-
41	-	-	-	1.12	1.8	1.0
42	1.36	1.8	1.2	1.23	1.8	1.1

1. Measured from 1.0 M CDCl₃ solutions with 1 W broadband proton decoupling at ambient temperature (302°K). R₁ values are normalized to C-2/4.

The results of the ^{13}C relaxation data make the results of ^1H data appear even more puzzling, particularly in light of the previous success in analyzing the ^1H and ^{13}C methyl relaxation data from steroids. At the present time, there is no satisfactory explanation of the lack of sensitivity in the $^1\text{H-R}_1$ values of these model compounds. Suffice it to say that this subject requires a more detailed investigation.

7.4. Conclusion

It is clear from the data presented in this study that methyl $^1\text{H-R}_1$ values can be sensitive to steric influences in model systems. In simple toluene and xylene derivatives, for certain substituents there is a reduction in the $R_{1\text{sr}}$ contribution and an offsetting increase in $R_{1\text{d}}$, thus little effect is observed on the overall R_1 of a methyl group in an adjacent position. In such instances, the determination of $R_{1\text{d}}$ and $R_{1\text{sr}}$ contributions is necessary to completely characterize the effect of the substituent. For larger substituents, and in molecules with sterically-crowded frameworks, a direct effect on the $^1\text{H-R}_1$ is observed, and can be correlated to the strength of the steric interaction. The lack of sensitivity in some model (non-planar) cyclohexanes and 1,3-dioxanes was not expected, and requires more thorough investigation.

For most molecules in this study, methyl ^1H - and ^{13}C - R_1 values measured for the same compound followed similar trends. The facility with which the contributions to methyl relaxation can be separated is a distinct advantage for ^{13}C measurements, particularly if quantitative information is required (eg. calculation of methyl rotational barriers). ^{13}C - R_1 experiments are, however, limited by the much lower relative sensitivity and longer relaxation times of the ^{13}C nucleus. Further experimental characterization of methyl ^1H - R_1 values in a wide range of molecules can now be carried out using the results reported here as a guide for interpretation of relaxation data in more complex compounds.

Chapter 8

SUMMARY

The overall strategy of research in this laboratory on spin-lattice relaxation has been to demonstrate, to the practising chemist, the great value of ^1H spin-lattice relaxation parameters for the determination of structure and stereochemistry of organic molecules. For most molecules, ^1H - and ^{13}C - R_1 values measured for the same compound will follow similar trends. The facility with which the various contributions to relaxation can be separated is a distinct advantage for ^{13}C measurements, for example, if R_1 data are required for a quantitative analysis of methyl rotation. ^{13}C - R_1 experiments are, however, limited by the low sensitivity and long relaxation times of the ^{13}C nucleus. Accurate ^1H - R_1 values can be obtained extremely rapidly, even on sub-milligram quantities, thus, for qualitative studies to probe molecular structure, it would be highly desirable to utilize these more efficient measurements.

^1H -nOe measurements, obtained in the difference mode, require a considerably greater amount of time to set-up and acquire than the ^1H - R_1 experiments, but can also be carried out on small quantities. They offer the advantage of giving information on specific pairwise dipolar interactions. Since relaxation parameters provide spatial information that cannot be obtained from the standard chemical shift and spin-spin coupling constants, ^1H - R_1 and -nOe measurements are rapidly becoming standard tools for structural analysis by nmr.

In this thesis, a conscious effort has been made to present the theory (Chapter 2) and practice (Chapter 3) of nmr measurement of ^1H spin-lattice relaxation in an illustrative manner. A clear understanding of relaxation theory is required to fully comprehend the utility of the R_1 and nOe values, however, a rigorous mathematical treatment is often too complicated to improve the comprehensibility of the subject. As a result, an attempt has been made here to give a thorough treatment, but without complete mathematical derivation, in terms that can be easily understood by the practising chemist.

Now that $^1\text{H-R}_1$ ¹¹ and $-nOe$ ^{23,33} experiments can be carried out in a routine manner, it is particularly important to demonstrate the generality of these techniques for structural analysis. To this end, the studies described in Chapters 4-6 demonstrate the potential of ^1H relaxation parameters for structural analysis of alkaloids (Chapters 4 and 5) and of some synthetic products (Chapter 6). The author feels that the relaxation pathway analysis technique, developed in these chapters, is a useful conceptual approach, accentuating the sensitivity of relaxation parameters to local environment (molecular geometry) and clarifying the relationship between the R_1 and nOe measurements. From the survey studies published here on alkaloids and elsewhere on steroids,¹⁰ it is clear that systematic investigations of spin-lattice relaxation in other types of natural products are warranted, and should prove to be an interesting and rewarding area of future nmr studies.

The introduction of the relaxation pathway analysis technique is particularly relevant at this time, in light of the rapid growth in application of the ^1H -nOed experiment to structural analysis in a wide variety of compounds.* With a more general realization of the potential for characterizing specific relaxation pathways via the nOe, the utility of the R_1 experiment for rapid structural analysis is being somewhat overlooked. As described in section 2.5 and demonstrated in Chapters 4 and 5, ^1H - R_1 values often supply sufficient information for the determination of molecular structure and stereochemistry. Since ^1H - R_1 values can be obtained more rapidly (and with greater accuracy and precision) than a set of nOe enhancements, it is strongly advised to attempt the structural analysis from the R_1 data (in conjunction with some form of molecular modelling), before resorting to the more time-consuming nOe measurements. The greater sensitivity of the nOed experiment can then be utilized in an efficient manner, by selecting only those experiments involving the specific relaxation pathways of interest.

There is a second, more fundamental reason that the ^1H - R_1 values should be measured before attempting nOe experiments. Since the nOe is a function of the sum total of all available relaxation pathways to a particular proton, as well as the particular pathway being observed, it is necessary to evaluate the relative relaxation rates of the

* Nmr double resonance difference spectroscopy has been recently reviewed by Sanders and Merish in Ref. 23.

protons under study before attempting to interpret NOE enhancements. Erroneous conclusions have been published in the literature (see Refs. 40 and 41), though discussion of this subject in a recent review article by Sanders and Merish,²³ should be of help in this area in the future.

Investigations into determining the potential for methyl group R_1 values as probes of molecular structure in solution have been described in Chapter 7. The results on model planar systems demonstrate unequivocally that steric interactions can play a major role in determining $^1\text{H}-R_1$ values. Steric interactions from an adjacent position have been shown to be dependent on the "effective" size of the substituent. This work must be extended beyond the stage of model systems to include molecules of greater complexity. In the investigation of the effect of geminal steric interactions, the results on conformationally-biased cyclohexanes and 1,3-dioxanes were inconclusive. The lack of consistency in the ^1H and ^{13}C data was particularly puzzling, though the ^1H data are somewhat more suspect for experimental reasons. In addition, the apparent observation of geminal steric effects in methyl $^1\text{H}-R_1$ values in previous studies by this laboratory,⁹¹ indicate that this subject requires a more detailed examination. ^{13}C experiments on the cyclohexane models would help to clarify the situation, as well as an attempt at finding suitable solvent conditions (mixtures of two or more solvents) where all ^1H signals of interest

would be well dispersed, so that reliable $^1\text{H-R}_1$ values could be measured. Studies of other conformationally rigid aliphatic ring systems could be used as a complement or alternative to the present studies. The bicyclo [2.2.1] system in molecules such as camphor appears to be an ideal choice.

Finally, another closely-related subject of interest and a potential new source of relaxation data, is the contribution of methyl protons to the relaxation of other protons in the molecule. The "centroid model"¹¹⁹ has proven to be useful in a very qualitative sense,* but this approximation takes no account of the differences in methyl rotation rates. John and McClung have derived expressions for the R_1 of a nucleus experiencing intra-molecular dipolar interactions which are modulated by internal motion.¹²⁰ They have shown that modulation of the internuclear distance can give rise to substantial effects on the nuclear R_1 in certain molecular geometries. In the model toluene derivatives studied here, differentials in the methyl group contributions to ring proton relaxation have been observed, suggesting a correlation between methyl $^1\text{H-R}_1$ and relaxation contribution. More detailed study was hindered by the undetermined contributions from cross-correlation effects in these semi-tightly coupled spin systems.

1. The "centroid model"¹²⁰ assumes that the relaxation contribution from a methyl group is equivalent to the contribution of a single proton located at the centroid of the CH_3 pyramid.

Further investigation is warranted, in light of the growing popularity of using $^1\text{H-R}_1$ ⁹ and $-\text{nOed}^{23}$ experiments for structural analysis, the application to increasingly more difficult problems, and the corresponding need to utilize all conceivable relaxation sources for obtaining the desired structural information.

Chapter 9

EXPERIMENTAL

9.1. Materials

The compounds used for studies described in this thesis were obtained from commercial sources, as gifts, or were prepared by simple synthetic schemes, as will be outlined below. The identity of all compounds was routinely verified by boiling or melting points, and by 60-MHz (Varian T-60) or 400-MHz (Bruker WH-400) nmr. Deuterated solvents were purchased from Merck, Sharp, and Dohme, Canada.

9.1.1. Benzene Derivatives

All methyl-substituted toluenes, anilines, halotoluenes and naphthalenes, as well as o- and m-nitrotoluene and 7,12-dimethylbenz[a] anthracene were commercially available (Aldrich Chemical Co.). The solid compounds had satisfactory melting points and were used without further purification. Liquid compounds were routinely purified by distillation, just prior to use.

The preparation of o- and m-methylanisole (11, 12) and o- and m-methylthioanisole (13, 14), was carried out by methylation of the corresponding cresol or thiocresol (Aldrich), using standard methods.^{121,122} The compounds were identified by b.p., and the disappearance of the OH or SH signal (integrating to one proton) and the appearance of the O- or S-methyl signal (integrating to three protons) in the nmr spectra (Table 9.1).

Table 9.1.

Physical Properties of Methyl-anisoles and -thioanisoles

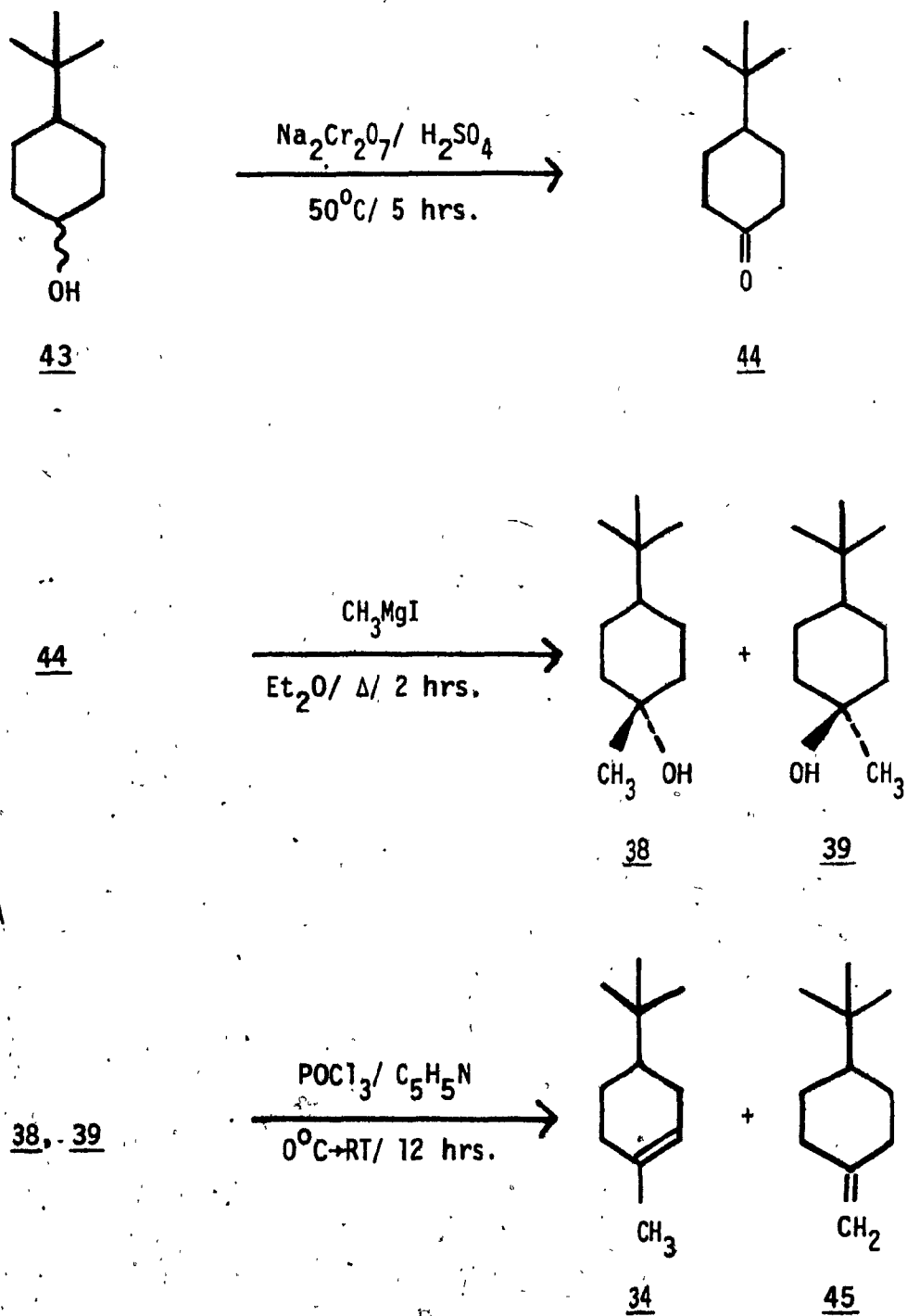
<u>Entry</u>	<u>B.P.</u> <u>(°C)</u>	<u>Lit.</u> ¹ <u>(°C)</u>	<u>Ref.</u>	<u>O(S)-Me²</u> <u>(ppm)</u>	<u>O(S)-H²</u> <u>(ppm)</u> _c
11	168-170	170-172	123	3.73	6.20
12	172-174	175-176	123	3.68	6.39
13	203-204	104 (34)	124	2.36	3.08
14	210-212	110-112(31)	122	2.34	3.27

1. Boiling points measured in-vacuo, with pressures given in parentheses ().

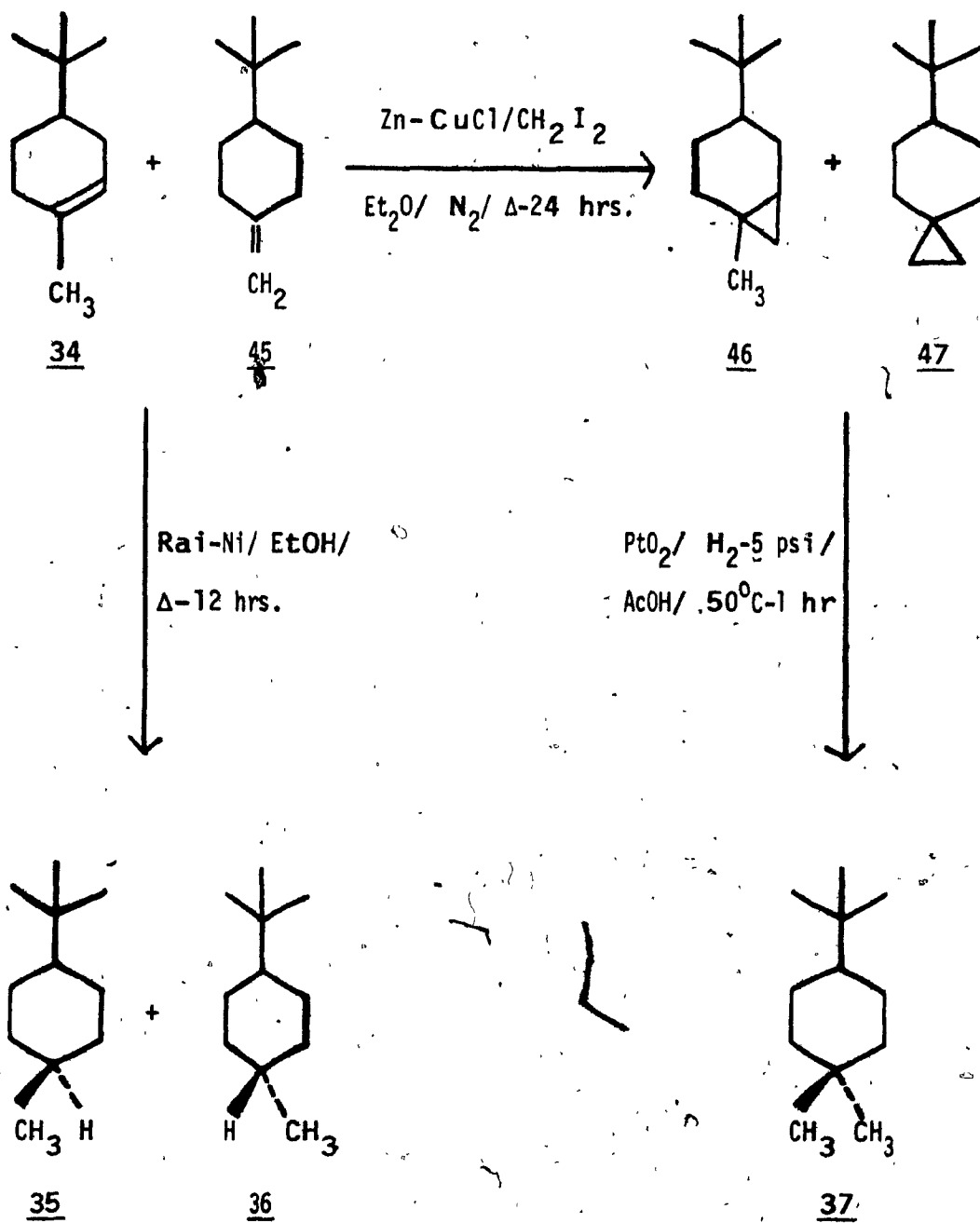
2. 60-MHz nmr spectra, samples of 50 mg in CCl₄ with 1% TMS for referencing.

N,N-Dideutero-2,4-dimethylaniline, 25, was prepared from 2,4-dimethylaniline by acid catalyzed deuterium exchange in D₂O. The product was identified by the disappearance of the NH₂ signal in the nmr spectrum. 2-Nitro-p-xylene, 22, was prepared by standard mixed acid (H₂SO₄/HNO₃) nitration of p-xylene. The product was identified by b.p. 235-237°C (239.5-241°C)¹²⁵ and by the characteristic signals in the nmr spectrum (50 mg in CCl₄ + 1% TMS: H-3, d, 7.69 ppm; Me-1, s, 2.51 ppm).

Scheme I



Scheme I (cont.)



9.1.2. Preparation of 4-t-Butylcyclohexanes

The preparation of the six conformationally-biased cyclohexanes was designed to give all the desired products from a single starting material, 4-t-butylcyclohexanol, 43. Scheme 1 outlines the synthetic steps to each of the products, physical properties are summarized in Table 9.2.

In the first step, the alcohol was oxidized to the corresponding cyclohexanone with chromic acid,¹²⁶ which upon treatment with the Grignard reagent,¹²⁶ methylmagnesiumiodide, gave a mixture of cis- and trans-4-t-butyl-1-methylcyclohexanol, 38 and 39. A portion of this mixture was separated by column chromatography on silica gel using 1:1 benzene:ether as eluant.¹²⁶ The unpurified mixture of isomers was dehydrated to give the corresponding cyclohexene, 34, using POCl_3 in dry pyridine. A 7:1 mixture of endocyclic to exocyclic (45) olefin was formed, as reported in the literature.¹²⁷ The sample used for nmr studies was enriched to about 95% exo-olefin by fractional distillation. The olefin mixture was directly hydrogenalized with Raney nickel in abs. ethanol, to give a mixture of cis- and trans-1-t-butyl-4-methylcyclohexane, 35 and 36. $^1\text{H-NMR}$ measurements were carried out directly on the mixture of isomers.

The dimethyl cyclohexane, 37, was prepared in two steps from the olefin mixture. A modified Simmons-Smith reaction using CuI as catalyst,¹²⁸ gave the corresponding cyclopropane derivatives (shown in Scheme 1) in about 50%

yield (estimated by nmr). The reaction mixture was then treated a second time under identical conditions, and the yield improved to 70% (estimated by nmr). The presence of desired products was clearly identified by the high-field signals (0.1-0.4 and 0.5-0.9 ppm) in the ^1H nmr spectrum, and corroborated by mass spectrometry ($m/z = 166$). The unreacted starting material could also be identified in the nmr spectrum, from the characteristic vinyl signal at 5.35 ppm (see Table 9.2). Hydrogenation of the product mixture with PtO_2 catalyst under 5 psi of H_2 * in acetic acid,¹²⁹ gave approximately 70% of the desired product, 1-t-butyl-4,4-dimethylcyclohexane, 37, as estimated by gas chromatography (GC). The remaining 30% of product was identified as the mono-methyl derivatives, 35 and 36, from retention times in the GC analysis. Compound 37 was purified by preparative GC, and identified by its mass spectrum ($m/z = 168$, characteristic peaks at 153, 111, 57).

The reaction sequence from the cyclohexanol starting material, 43, to the olefin mixture, 34/45, was repeated, and the final two steps in the preparation of 37 was carried out by Mr. Paolo Bouca under the author's direction.

* The author is indebted to Ayerst Laboratories for supplying facilities to carry out this hydrogenation.

Table 9.2

Physical Properties of t-Butylcyclohexane Derivatives

Entry	Yield (%)	M.P./B.P. ¹ (°C)	Lit. (°C)	Spectral Data ²	Ref.
44	80	47-49	51.8-52	IR: 1688 (C=O)	126
38/39	99	55-56	57-58	IR: 3420 (OH)	126
38		95-96	97.8	NMR: 0.865 (t-bu), 1.210 (Me)	126
39		67-68	71	NMR: 0.868 (t-bu), 1.200 (Me)	126
34/45	76	58(4)	70-71(7)	NMR: 0.535 (vinyl), 1.62 (Me)	127
34				NMR: 0.456 (vinyl)	
45					
35	-3	-3		NMR: 0.85 (t-bu), 0.794 (Me)	
36				NMR: 0.85 (t-bu), 0.931 (Me)	
46/47	67	68-70(10)	-4	NMR: 0.1-0.4 (propyl), 0.5-0.9 (propyl)	-4
37	78	-3		NMR: 0.811 (t-bu), 0.813 (eq-Me), 0.848 (ax-Me)	117, 130 130

1. Pressure indicated in parentheses () for boiling points measured in-vacuo.

2. IR data on CHCl₃ solutions, given in units of cm⁻¹.
Nmr data from 0.1 M CDCl₃ solutions, given in ppm downfield from 0.1% internal TMS.

3. Reaction carried out on very small quantity.

4. New compound. Mass spectrum: m/z = 166, characteristic peaks at 151, 109, 57.

9.1.3. Preparation of 2-t-Butyl-1,3-Dioxanes

5,5-Dimethyl-2-t-butyl-1,3-dioxane, 40, and a 1:3 mixture of cis- and trans-5-methyl-2-t-butyl-1,3-dioxane, 40 and 41, were prepared by the standard acid-catalyzed condensation of the appropriate diol and carbonyl compound, as reported by Eliel.¹¹⁸ The starting materials dimethyl-1,3-propanediol and 2,2-dimethylpropanal, were commercially available (Aldrich). 2-Methyl-1,3-propanediol was prepared by LiAlH_4 reduction of diethyl methylmalonate in >95% yield (b.p. 112-115°C (20mm), (lit. 111-114°C (17mm))¹²³; nmr, 40 mgs in CDCl_3 + 1 TMS: d, 3H, 0.77 ppm; m, 1H, 1.75 ppm; m, 4H, 3.55 ppm; broad s, 2H, 4.02 ppm). All products were isolated in high yield and were identified by 400 MHz nmr (Table 9.3), and boiling or melting point (42: 74%, m.p. 57-58°C (lit. 72%, 58-58.5°C)¹¹⁸; 40/41: 70%, b.p. 162-167°C (lit. 85%, 162-166°C)¹¹⁸).

Table 9.3

Chemical Shifts of Methyl-substituted 2-t-Butyl-1,3-Dioxanes

<u>Proton</u>	<u>5,5-dimethyl (ppm)</u>	<u>cis-5-methyl (ppm)</u>	<u>trans-5-methyl (ppm)</u>
2-ax	4.00	4.09	4.01
2-eq (t-bu)	0.93	0.92	0.90
4,6-ax	3.60	3.81	3.25
4,6-eq	3.39	3.89	4.03
5-ax	1.16 (Me)	1.25 (Me)	2.02 (H)
5-eq	0.70 (Me)	1.52 (H)	0.68 (Me)

1. 400 MHz nmr spectra of 0.1M CDCl_3 solutions referenced to 0.1% internal TMS.

9.1.4. Alkaloids and 7-Hydroxyindene Dimers

Tropine, atropine-sulfate, brucine, strychnine, and the four cinchona alkaloids were obtained from commercial sources (Aldrich, Sigma). Strychnine derivatives were obtained through a collaboration with Dr. J.T. Edward of McGill University. The preparation of these compounds has been described elsewhere.^{79, 131, 132} Morphine alkaloid and cocaine-HCl studies were made in collaboration with the Center for the Study of Drug Dependence, Psychology Department, Concordia University. Scopolamine was a gift from Dr. R.K. Ibrahim, Biology and Chemistry Departments, Concordia University. The 7-hydroxyindene dimers were obtained from the laboratory of Dr. B.R. Davis, Chemistry Department, University of Auckland, New Zealand. Their preparation is to be described elsewhere.¹³³

All alkaloids were dried overnight *in-vacuo* over P_2O_5 or fresh Drierite. Temperatures of 40-120°C were required to ensure that all water of crystallization was removed.

For many of the alkaloids, it was extremely beneficial for assignment purposes, to study solvent shifts in the nmr spectra. For this reason, and since most compounds were obtained as salts of the free-base which were not soluble in non-polar solvents of interest, certain alkaloid salts were treated with aq. 5% $NaHCO_3$, then concentrated aq. NaOH, until the free-base had completely precipitated.

9.2. NMR Sample Preparation

For acquisition of all ^1H spectra, the required amount of compound to make a 0.1 M solution was dissolved in 0.4-0.5 ml of deuterated solvent, and filtered through sintered glass, glass wool, or cotton, into a 5 mm tube. For the control experiments to determine the contribution to R_1 from dissolved atmospheric oxygen, degassing was carried out by subjecting the sample to five freeze-pump-thaw cycles, then sealing off the tube under vacuum. Water-soluble alkaloid salts which had been previously oven-dried in-vacuo were prepared in 99.5% DMSO-d_6 or 99.8% D_2O , while all other samples were dissolved in 99.8% CDCl_3 or, only if necessary, in DMSO-d_6 .

All samples for ^{13}C experiments were prepared in the same manner as the samples for ^1H studies, except that the solutions were made up to 1.0 M in 2.0 ml of CDCl_3 . These samples were not degassed, since $^{13}\text{C-R}_{1d}$ values were significantly larger than the oxygen contribution.¹³⁴ Corroborative evidence for not degassing was provided by the observation of full 200% $^{13}\text{C-}\{^1\text{H}\}$ NOE enhancements of all protonated ring carbons in all molecules studied.

9.3. NMR Measurements

The 400 MHz ^1H spectra were obtained on a Bruker WH-400 nmr spectrometer (at the Montreal Regional Centre for High Field NMR) equipped with an Aspect 2000 computer and two Diablo hard disk drives. This instrument provides for complete computer control of the receiver, pulse transmitter, and decoupler, and automated multi-step experiments.

All $^1\text{H-R}_1$ data were obtained by the standard inversion-recovery pulse sequence.¹ The partially relaxed spectra were obtained by Fourier transformation of the stored free induction decays (fids), after applying a standard exponential multiplication corresponding to 1-2 X (Hz/pt.) Hz of line-broadening. A constant phase correction was made to all spectra just before either stackplotting to determine null-points or obtaining a computer listing of all peak heights for a regression analysis of the data. Two-parameter, non-linear regression analysis was applied to all the $^1\text{H-R}_1$ data, using a standard program, NLNRX,* on an HP-1000 computer. The peak heights of all multiplet resonances were co-added by computer to obtain a value for the total magnetization of the resonance. These values were then utilized, along with their corresponding t values, to determine R_1 's.

In a typical $^1\text{H-R}_1$ experiment, eight scans from a 0.1 M solution were acquired into 16K data blocks over a spectral window of 4000 Hz. The 90° pulse width on the WH-400 was 6.2-7.0 μs . A pre-equilibration period of $5X T_1$ of the

* NLNRX was written by Dr. L.D. Colebrook

slowest relaxing proton in the molecule was allowed before the acquisition of each scan. A minimum of fifteen different experiments were run, while ensuring that at least eight data points for t less than the null-point of the fastest relaxing proton in the molecule could be obtained.

To compare data from different molecules, the R_1 values were normalized. This procedure accounts for changes in operating conditions, and differences in tumbling rates (caused by the differences in molecular size and shape). For example, an aromatic ring proton situated such that the two adjacent positions are occupied by protons, is an ideal choice for normalization. Relaxation for such a proton is dominated (>95%) by dipolar interactions with the two near neighbors. The R_1 values of such protons in different molecules will be independent of structural variations in the other parts of the molecule because inter-proton distances in the rigid, planar aromatic rings will not vary by much. Since the principal relaxation vectors are invariant, the R_1 values must vary only in response to differences in t_c , thereby accounting for differences in tumbling or operating conditions.

NOed experiments were acquired under complete computer control of decoupler power and frequency, and with variable irradiation periods, thereby tailoring each experiment to the protons of interest. Separate disk storage of each enhanced and control spectrum maximized the flexibility in data processing. The high stability of the superconducting magnet

allows for the acquisition of up to eight different difference spectra, using a single control, thereby significantly increasing the efficiency of the experiment.

The procedure for obtaining the nOe spectrum consists of saturating a particular resonance for a period of time equal to 1-5 times its T_1 value, then applying an observation pulse while sending the saturating field far off-resonance, and detecting the signal. The first few (2-4) transients were not stored as the system reached a steady state. The process was repeated until eight scans had been stored on disk. The decoupler frequency and power were then reset for a different resonance (or far from all resonances for the control experiment), and the cycle repeated. The entire process is supercycled until sufficient S/N has been acquired. This requires between 80 and 1200 scans/experiment, depending on the experimental conditions, the magnitudes of the enhancements, and the desired precision in the measurements.

The difference spectra are obtained by subtracting the control fid from the fid containing the nOe information, after applying an exponential multiplication corresponding to 0.8-1.5 Hz of line-broadening to both fids. The line-broadening has the effect of reducing the resolution, but considerably improves the quality of the subtraction, particularly for tall sharp lines. If the multiplet splittings in the spectrum are of interest, a second difference spectrum can be obtained with a considerably smaller amount of line-broadening. A more elegant, but considerably more complex

correction, SUDSY, can be implemented to improve the quality of subtraction without affecting resolution.¹³⁵ The difference fids are Fourier transformed and phase corrected, resulting in a spectrum which contains the irradiated proton(s) fully inverted, and those signals that have been enhanced in an upright position. The intensities of the enhanced signals can be integrated against the irradiated proton, or more precisely, relative to the enhanced signal in the control spectrum.

¹³C spectra were measured at 20.13 MHz on a Bruker WP-80SY spectrometer, equipped with an Aspect 2000 computer and a CDC-CMD32 hard disk drive. Typically, 80 scans from a 1.0M solution were acquired over 4000 Hz into a 16K data block, with 1 W of broadband proton decoupling. The 90° pulse width was 7.0-7.2 μs. The classical inversion-recovery pulse sequence¹ was utilized for ¹³C-R₁ measurements, using the same conditions as mentioned above for the selection of t values and the pre-equilibration period. A total of 80 scans were collected for each experiment (t value) using the ¹H procedure (eight scans/ experiment) and supercycling ten times. All ¹³C-R₁ data were calculated by three-parameter, non-linear regression analysis directly on the Aspect 2000.

The ¹³C-{¹H} NOe enhancements were measured by the standard gated decoupling method¹³⁶ with the following two refinements. To minimize decoupler heating effects, the decoupler was not gated off, but was placed far off-resonance (>20 KHz) and shifted from broadband to single frequency

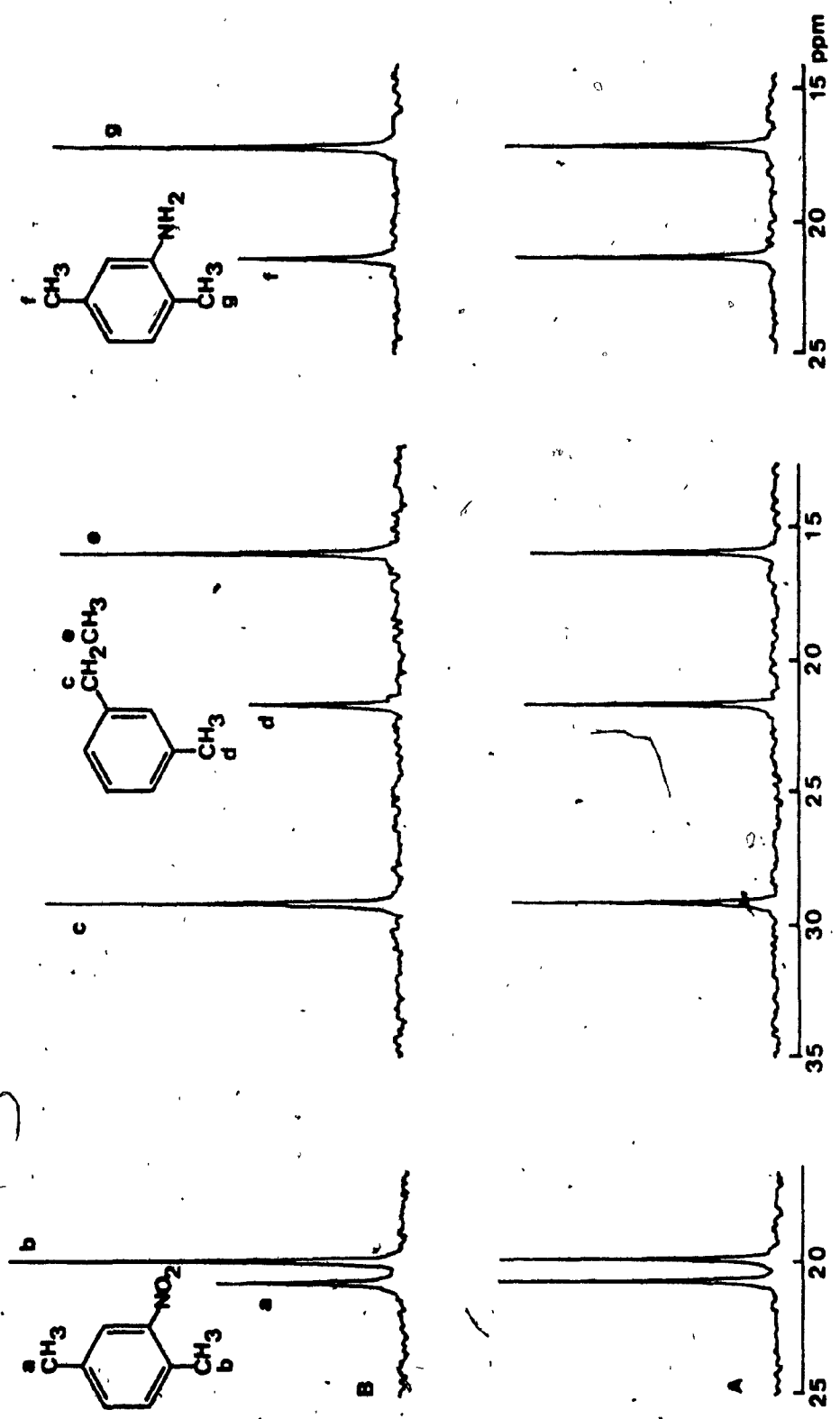


Fig. 9.1 20 MHz ^{13}C nOed spectra of methyl carbons. All experiments on 1.0 M CDCl_3 solutions. A) spectra with no nOe, B) nOe difference spectra.

irradiation. Fids corresponding to broadband proton irradiation were acquired alternately (after suitable pre-equilibration) and stored separately on disk. This reduces the effect of instrumental drift over the long periods of data acquisition (typically 20 hrs.) required for high quality spectra.

In a typical experiment, for $5X T_1$ of the slowest relaxing carbon, 1 W of broadband decoupling was applied in the 1H spectrum. The decoupler power was then increased to 3 W as a 90° observe pulse was applied and the signal detected. This procedure was repeated twelve times, the first four cycles for establishing a steady-state, the last eight stored on disk. The twelve cycles were then repeated, except that during the saturation period the decoupler was set to single frequency irradiation, far off-resonance (>20 KHz). The nOe and control spectra were alternately acquired in this manner, until sufficient S/N had been obtained (typically, 400-800 scans for high quality measurements). Since the ^{13}C signals were well dispersed and the enhancements were invariably quite large (100-200%), it was not necessary to utilize difference techniques to increase sensitivity. The difference technique did, however, allow for a rapid distinction of those resonances which are not relaxing strictly via the dipolar mechanism, for example, rapidly rotating methyl groups (see Fig. 9.1).

REFERENCES

1. R.L. Vold, J.S. Waugh, M.P. Klein, D.E. Phelps, *J. Chem. Phys.* 48, 3831 (1968).
2. R. Freeman, S. Wittekoek, R.R. Ernst, *J. Chem. Phys.* 52, 1529 (1970).
3. C.W.M. Grant, Ph.D. Thesis, University of British Columbia, 1972.
4. L.D. Hall, *Chem. Soc. Rev.* 4, 401 (1975); L.D. Hall, C.M. Preston, *Carb. Res.* 49, 3 (1976).
5. J.H. Noggle, R.E. Schirmer, "The Nuclear Overhauser Effect", Academic Press, New York (1971).
6. R. Richarz, K. Wuthrich, *J. Magn. Reson.* 30, 147 (1978); G.E. Chapman, B.D. Ambercrombie, P.D. Cary, E.M. Bradbury, *J. Magn. Reson.* 31, 459 (1979); R.E. Hurd, B.R. Reid, *Biochem.* 18, 4017 (1979); P.J. Cayle, J.P. Albrand, J. Feeney, G.C.K. Roberts, E.A. Piper, A.S.V. Burgen, *Biochem.* 18, 3886 (1979); M. Kuo, W. Gibbons, *J. Biol. Chem.* 254, 6278 (1979).
7. N. Bloembergen, E.M. Purcell, R.V. Pound, *Nature* 160, 475 (1947); N. Bloembergen, E.M. Purcell, R.V. Pound, *Phys. Rev.* 73, 679 (1948).
8. I. Solomon, *Phys. Rev.* 99, 559 (1955).
9. L.D. Colebrook, L.D. Hall, Tetrahedron Reports, manuscript in preparation.
10. L.D. Colebrook, L.D. Hall, *Org. Magn. Res.*, in press.
11. L.D. Colebrook, L.D. Hall, *Can. J. Chem.* 58, 2106 (1980).
12. J.B. Lambert, R.J. Nienhuis, J.W. Keepers, *Angew. Chem. Int. Ed. Engl.* 20, 487 (1981).
13. A. Carrington, A.D. McLachlan, "Introduction to Magnetic Resonance", Harper & Row, New York (1967).
14. L.G. Werbelow, D.M. Grant, *J. Chem. Phys.* 63, 544 (1975).
15. L.G. Werbelow, D.M. Grant, *Adv. Magn. Res.* 9, 189 (1977). 189 (1977).
16. K.F. Wong, Ph.D. Thesis, University of British Columbia.

17. R.L. Vold, R.R. Vold, Prog. Nucl. Magn. Reson. Spectrosc. 12, 79 (1978).
18. A. Abragam, "Principles of Magnetic Resonance", Oxford University Press, London (1961).
19. W.T. Huntress, Jr., J. Chem. Phys. 48, 3524 (1968); W.T. Huntress, Jr., Advan. Magn. Reson. 4, 2 (1970).
20. D.E. Woessner, J. Chem. Phys. 37, 647 (1962).
21. R. Freeman, S. Wittekoek, "Proc. of the Fifteenth Colloque AMPERE", September, 1968, North Holland Publ., Amsterdam (1969), p. 205.; R. Freeman, S. Wittekoek, J. Magn. Reson. 1:2, 238 (1969).
22. L.D. Hall, K.F. Wong, H.W. Hill, J. Chem. Soc., Chem. Commun., 951 (1979).
23. J.K.M. Sanders, J.D. Merish, Prog. Nucl. Magn. Reson., in press.
24. N. Platzner, Org. Magn. Reson. 11:7, 349 (1978).
25. J.B. Lambert, R.J. Nienhuis, R.B. Finzel, J. Phys. Chem. 85, 1170 (1981).
26. D.E. Woessner, B. Snowden, G.H. Meyer, J. Chem. Phys. 50, 719 (1969).
27. A. Ericsson, J. Kowalewski, T. Liljefors, P. Stilbs, J. Magn. Reson. 38, 9 (1980).
28. K.H. Ladner, D.K. Dalling, D.M. Grant, J. Phys. Chem. 80, 1783 (1976).
29. M.L. Martin, J.-J. Delpuech, G.J. Martin, "Practical NMR Spectroscopy", Heyden and Son Ltd., London (1980), Chap. 7.
30. R. Freeman, M.L. Levitt, J. Magn. Reson. 33, 473 (1979).
31. T.K. Leipert, D.W. Marquardt, J. Magn. Reson. 24, 181 (1976).
32. M.L. Martin, J.-J. Delpuech, G.J. Martin, op. cit., p. 267.
33. J.K.M. Sanders, L.D. Hall, J. Amer. Chem Soc. 102:18, 5703 (1980).
34. J.K.M. Sanders, J.C. Waterton, and I.S.J. Denniss, J. Chem. Soc. PI, 1150 (1978).
35. J. Merish and J.K.M. Sanders, Org. Magn. Reson. 18, 122 (1982).

36. R.B. Turner, R.B. Woodward, "The Cinchona Alkaloids", in "The Alkaloids", R.H.F. Manske and H.L. Holmes, eds., Academic Press, New York (1950), Vol. 1, p. 1; M.R. Uskokovic, G. Grethe, "The Cinchona Alkaloids", ibid., (1973), Vol. 14, p. 181.
37. T. Balzas, E. Herman, J. Atkinson, J. Pharm. Sci. 67, 1355 (1978).
38. J.D. Mersh, J.K.M. Sanders, Tett. Lett. 22:40, 4029 (1981).
39. A. Makriyannis, S. Fesik, J. Amer. Chem. Soc. 104:23, 6462 (1982).
40. L.I. Kruse, J.K. Cha, J. Chem. Soc., Chem. Comm., 1329 (1982).
41. J.D. Mersh, J.K.M. Sanders, S.A. Matlin, J. Chem. Soc., Chem. Comm., 306 (1983).
42. M.J. Aroney, M.G. Cornfield, R.J.W. Le Fevre, J. Chem. Soc., 2954 (1964).
43. N.L. Allinger, J.L. Maul, M.J. Hickey, J. Org. Chem. 36, 2747 (1971).
44. W.J. Chazin, L.D. Colebrook, unpublished results.
45. R. Doherty, N.R. Benson, M. Maienthal, J. Stewart, J. Pharm Sci. 67, 1698 (1978).
46. J. Wasacz, Amer. Sci. 69, 318 (1981).
47. J. Weijlard, A. Erickson, J. Am. Chem. Soc. 64, 869 (1942).
48. A.G. Gilman, L.S. Goodman, A. Gilman, "Goodman and Gilman's- The pharmacological Basis of Therapeutics", Macmillan Publ. Co., Inc., New York (1980), p. 521-5.
49. W. Martin, D. Jasinski, P. Mansky, Arch. Gen. Psychiatry 28, 784 (1973).
50. L. Gilbert, Acta Cryst. B29, 1630 (1973).
51. G. Kartha, F.R. Ahmed, W.H. Barnes, Acta Cryst. 15, 326 (1962).
52. D. Canfield, J. Barrick, B.C. Giessen, Acta Cryst. B35, B35, 2806 (1979); B37, 1800 (1981).
53. I. Karle, Acta Cryst. B30, 1682 (1974).

54. A.E. Jacobson, H.J.C. Yeh, L.J. Sargent, *Org. Magn. Reson.* 4, 875 (1972).
55. M. Takeda, H. Inoue, H. Kugita, *Tetrahed.* 25:9, 1839 (1969).
56. T.J. Batterham, K.H. Bell, U. Weiss, *Aust. J. Chem.* 18, 1799 (1965).
57. S. Okuda, S. Yamaguchi, Y. Kawazoe, K. Tsuda, *Chem. Pharm. Bull.* 12, 104 (1964).
58. M. Barfield, C.J. Fallick, K. Hata, S. Sternhell, P.W. Westerman, *J. Amer. Chem. Soc.* 105:8, 2178 (1983).
59. L.M. Jackman, S. Sternhell, "Applications of Nuclear Magnetic Resonance Spectroscopy in Organic Chemistry", 2nd edn., Pergamon Press, London (1969), p. 280-298.
60. H.L. Holmes, "The Tropane Alkaloids", in "The Alkaloids", R.H.L. Manske and H.L. Holmes, eds., Academic Press, New York (1950), Vol. 1, p. 272; G. Fodor, "The Tropane Alkaloids", *ibid.* (1960), Vol. 6, p. 145; *ibid.* (1967), Vol. 9, p. 269; *ibid.* (1971), Vol. 13, p. ; R.L. Clarke, "The Tropane Alkaloids", *ibid.* (1977), Vol. 16, p. 83.
61. P.J. Pauling, T.J. Pechter, *J. Chem. Soc., Chem. Comm.*, 1001 (1969); P.J. Pauling, T.J. Pechter, *Nature* 228, 673 (1970).
62. R.J. Bishop, G. Fodor, A.R. Katritzky, F. Soti, L.E. Sutton, E.J. Swinbourne, *J. Chem. Soc. (C)*, 74 (1966).
63. H.W. Avdovich, G.A. Neville, *Can. J. Spectrosc.* 28:1, 1 (1983).
64. F.I. Carroll, M.L. Coleman, A.H. Lewin, *J. Org. Chem.* 47:1, 13 (1982).
65. J. Feeney, R. Foster, E.A. Piper, *J. Chem. Soc. P II*, 2016 (1977).
66. A.G. Ferrige, J.C. Lindon, *J. Magn. Reson.* 31, 337 (1978).
67. V.S. Dimitrov, S.L. Spasov, T.Z. Radeva, J.A. Ladd, *J. Molec. Struct.* 27, 167 (1975).
68. E.J. Gabe, W.H. Barnes, *Acta Crystallogr.* B16, 796 (1963).
67. J.C. Carter, G.W. Luther, T.C. Long, *J. Magn. Reson.* 15, 122 (1974).

68. D. Tavernier, M.J.O. Anteunis, M.J.G. Tits, L.J.G. Angenot, *Bull. Soc. Chim. Belg.* 87:9, 595 (1978).
69. S. Wehrli, Personal communication.
70. S. Castellano, A.A. Bothner-By, *J. Chem. Phys.* 41, 3863 (1964).
71. L.M. Jackman and S. Sternhell, "Applications of Nuclear Magnetic Resonance Spectroscopy", 2nd. ed, Pergamon Press, London (1969), p. 270-277.
72. L.M. Jackman and S. Sternhell, *op. cit.*, p. 316.
73. J.C. Carter, G.W. Luther, T.C. Long, *J. Magn. Reson.* 15, 132 (1974).
74. W. Kitching, I de Jonge, W. Adcock, A.N. Abeywickrema, *Org. Magn. Reson.* 14:6, 502 (1980).
75. G.M. Anderson, P.A. Kollman, L.N. Domelsmith, K. Makriyanis, J.J. Knittel, *J. Amer. Chem. Soc.* 101, 2344 (1979).
76. A. Makriyanis, J.J. Knittel, *Tetrahedron Lett.*, 2573 (1979).
77. H. Leuchs, W. Schneider. *Ber.* 41, 4393 (1908); *Ber.* 42, 2681 (1909).
78. H. Leuchs and H.G. Bött. *Ber.* 73, 855 (1940), and references therein.
79. J.T. Edward, P.G. Farrell, S.A. Samad, R. Wojtowski, S.C. Wong, *Can. J. Chem.* 58, 2380 (1980).
80. D.S. Sake Gouda, L. Cartz, S. Natarajan, *Acta Crystallograph.* B29, 2760 (1973).
81. B.R. Davis, I.R.N. McCormick, *J. Chem. Soc. P1*, 3001 (1979).
82. A.W. King, L.J. McDonald, J.M. Waters, T.N. Waters, *Cryst. Struct. Comm.* 3, 681 (1974).
83. S. Johnson, Ph.D. Thesis, University of Auckland.
84. L.G. Werbelow, A.G. Marshall, *J. Magn. Reson.* 11, 299 (1973).
85. L.G. Werbelow, D.M. Grant, *J. Magn. Reson.* 20, 554 (1975).

86. L.G. Werbelow, D.M. Grant, *Adv. Magn. Reson.* 9, 189 (1977).
87. G. Matson, *J. Chem. Phys.* 67, 5152 (1977).
88. E. Haslinger, R.M. Lynden-Bell, *J. Magn. Reson.* 31, 33 (1978).
89. L.G. Werbelow, *J. Magn. Reson.* 34, 439 (1979).
90. L.G. Werbelow, A. Thevand, G. Pouzard, *J. Chem. Soc. Faraday Trans. II* 75, 971 (1979).
91. J.M. Navarre, L.D. Colebrook, L.D. Hall, *Org. Magn. Reson.* 14:5, 410 (1980).
92. W.J. Chazin, L.D. Colebrook, submitted to *Can. J. Chem.*
93. C. Deverell, *Mol. Phys.* 18:3, 319 (1970).
94. D.K. Green, J.G. Powles, *Proc. Phys. Soc.* 85, 87 (1965).
95. R. Rowan, P. Mazzocchi, C. Kanagy, M. Regan, *J. Magn. Reson.* 39, 27 (1980).
96. J.B. Lambert, R.J. Nienhuis, *J. Am. Chem. Soc.* 102:22, 6659 (1980).
97. W.M. Bovee, J. Smidt, *Molec. Phys.* 26, 1133 (1973).
98. W.M. Bovee, J. Smidt, *Molec. Phys.* 28, 1617 (1974).
99. J.D. Cutnell, J.A. Glasel, *J. Am. Chem. Soc.* 98:1, 264 (1976).
100. F.W. Wehrli, T. Wirthlin, "Interpretation of Carbon-13 NMR Spectra", Heyden and Son, Ltd., London (1976), p. 245.
101. O. Yamamoto, K. Hayamizu, K. Sekine, S. Funahira, *Analyt. Chem.* 44:11, 1796 (1972).
102. N.K. Wilson, J.B. Stothers, *J. Magn. Reson.* 15, 31 (1974).
103. J. Dale, *Tetrahedron* 22, 3373 (1966); R.G. Ford, *J. Molec. Spectrosc.* 49, 117 (1974).
104. J.W. Blunt, J.B. Stothers, *J. Magn. Reson.* 27, 117 (1974).
105. D.E. Axelson, C.E. Holloway, *Can. J. Chem.* 54, 2820 (1976).

106. J. Kowalewski, A. Ericsson, *J. Phys. Chem.* 83, 2044 (1979).
107. K. Kuhlmann, D.M. Grant, *J. Chem. Phys.* 55:6, 2998 (1971).
108. T. Alger, D.M. Grant, R. Harris, *J. Chem. Phys.* 76:2, 281 (1972).
109. W.C. Hamilton, J.W. Edwards, A. Tripe, J.J. Rush, *Discuss. Faraday Soc.* 48, 192 (1969); C.H. Stam, *Acta Crystallogr.* B28, 2630 (1972); E. Prince, L.W. Schroeder, J.J. Rush, *Acta Crystallogr.* B29, 184 (1973).
110. C. Roussel, M. Chanon, J. Metzger, *Tetrahedron Lett.*, 1861 (1971).
111. F. Imashiro, K. Takegoshi, S. Okazawa, J. Furukawa, T. Terao, A. Saika, *J. Chem. Phys.* 78:3, 1104 (1983).
112. B.M. Wepster, "Electronic Spectra and Chemical Data", in "Steric Effects in Conjugated Systems", G.W. Gray, ed., Butterworths Scientific Publications, London (1958), p. 82.
113. J. Trotter, *Can. J. Chem.* 37, 1487 (1959); J. Trotter, *Acta Crystallogr.* 12, 884 (1959).
114. D. Lister, J. Tyler, *J. Chem. Soc., Chem. Commun.*, 152 (1966); M. Dewar, Y. Takeuchi, *J. Am. Chem. Soc.* 89:2, 390 (1967); V. Sahini, J. Weinberg, *Rev. Roum. Chim.* 18:9, 1493 (1973); J.W. Smith, "Dipole Moment Evidence Regarding Steric Effects in Aromatic Molecules", in "Steric Effects in Conjugated Systems", *op. cit.*, p. 141.
115. M.B. Jameson, B.R. Penfold, *J. Chem. Soc.*, 528 (1965); A. Bilmenti, *Acta Crystallogr.* 18, 647 (1965); G. Ferraris, D.W. Jones, T. Yerkess, K.D. Bartle, *J. Chem. Soc., P II*, 1628 (1972); D. Bright, I.E. Maxwell, J. de Boer, *J. Chem. Soc., P II*, 1861 (1973).
116. D. Sayre, P.H. Friedlander, *Nature* 187, 139 (1960); J.P. Glusker, H.L. Carrell, D.E. Zacharias, R.G. Harvey, *Cancer Biochem. Biophys.* 1, 43 (1974).
117. P.J. Peeby, S. Sternhell, *Aust. J. Chem.* 23:5, 1005 (1970).
118. E.L. Eliel, M.C. Knoeber, *J. Am. Chem. Soc.* 90:13, 3344 (1968).

119. B. Honig, B. Hudson, B.D. Sykes, M. Karplus, Proc. Nat. Acad. Sci. US 68, 1289 (1971); R. Rowan, J.A. McCammon, B.D. Sykes, J. Am. Chem. Soc. 96, 4773 (1974); R. Rowan, A. Warshel, B.D. Sykes, M. Karplus, Biochem. 13, 970 (1974).
120. B.K. John, R.E.D. McClung, J. Magn. Reson. 50, 267 (1982).
121. D. Boyd, D. Hardy, J. Chem. Soc., 637 (1928).
122. D.S. Tarbell, D.K. Fukushima, J. Am. Chem. Soc. 68, 1548 (1946).
123. Aldrich Catalog Handbook of Fine Chemicals, 1982.
124. Sadtler Index of Standard Spectra.
125. Handbook of Chemistry and Physics, 55th Edn., CRC Press, Cleveland, Ohio, (1974).
126. W.J. Houlihan, J. Org. Chem. 27, 3860 (1962).
127. B. Cross, G.H. Whitham, J. Chem. Soc., 3892 (1960).
128. J.T. Harrison, R.J. Rawson, J. Org. Chem. 35:6, 2057 (1970).
129. J-F. Sauvage, R.H. Baker, A.S. Hussey, J. Am. Chem. Soc. 82, 6090 (1960); B. Rickborn, J. H-H. Chen, J. Org. Chem. 32, 3576 (1967).
130. M.T. Reetz, J. Westerman, R. Steinbaeh, Angew. Chem. 92:11, 931 (1980).
131. P.J. Scheuer, J. Am. Chem. Soc. 82, 193 (1960).
132. A.S. Bailey, R. Robinson, J. Chem. Soc., 703 (1948).
133. W.J. Chazin, L.D. Colebrook, B.R. Davis, I.R.N. McCormick, S.J. Johnson, submitted to Can. J. Chem.
134. J.R. Lyerla, Jr., G.C. Levy, in "Topics in Carbon-13 NMR Spectroscopy", G.C. Levy, ed., Wiley-Interscience, New York (1974), Vol. 1, p. 106; G.C. Levy, J.D. Cargioli, F.A.L. Anet, J. Am. Chem. Soc. 95, 1527 (1973).
135. J.D. Mersh, J.K.M. Sanders, J. Magn. Reson. 50, 289 (1982).
136. R. Freeman, H.D.W. Hill, R. Kapstein, J. Magn. Reson. 7, 327 (1972).

